

Washington University in St. Louis

Washington University Open Scholarship

Arts & Sciences Electronic Theses and
Dissertations

Arts & Sciences

Spring 5-15-2019

Oxidative C–C and C–Heteroatom Reactivity of High-Valent Nickel Complexes

Sofia Marie Smith

Washington University in St. Louis

Follow this and additional works at: https://openscholarship.wustl.edu/art_sci_etds

 Part of the [Inorganic Chemistry Commons](#)

Recommended Citation

Smith, Sofia Marie, "Oxidative C–C and C–Heteroatom Reactivity of High-Valent Nickel Complexes" (2019). *Arts & Sciences Electronic Theses and Dissertations*. 1833.
https://openscholarship.wustl.edu/art_sci_etds/1833

This Dissertation is brought to you for free and open access by the Arts & Sciences at Washington University Open Scholarship. It has been accepted for inclusion in Arts & Sciences Electronic Theses and Dissertations by an authorized administrator of Washington University Open Scholarship. For more information, please contact digital@wumail.wustl.edu.

WASHINGTON UNIVERSITY IN ST. LOUIS

Department of Chemistry

Dissertation Examination Committee:

Liviu M. Mirica, Chair

Kevin D. Moeller, Co-Chair

John R. Bleeke

Sophia E. Hayes

Nigam P. Rath

Oxidative C–C and C–Heteroatom Reactivity of High-Valent Nickel Complexes

by

Sofia M. Smith

A dissertation presented to
The Graduate School
of Washington University in
partial fulfillment of the
requirements for the degree
of Doctor of Philosophy

May 2019

St. Louis, Missouri

© 2019, Sofia M. Smith

Table of Contents

List of Figures	v
List of Tables	xi
List of Schemes	xvi
Acknowledgements	xx
Abstract	xxiii
Chapter 1: High-Valent Organometallic Nickel Complexes and Their Reactivity	1
1.1 Introduction	2
1.2 Organometallic Ni ^{III} Complexes	3
1.3 Organometallic Ni ^{IV} Complexes	18
1.4 Other High-Valent Ni Complexes	25
1.4.1 Ni ^{III} Structures	25
1.4.2 Ni ^{IV} Structures	26
1.5 Conclusion and Outlook	28
1.6 Acknowledgements	30
1.7 References	30
Chapter 2: High-Valent Organometallic Nickel Species Relevant to Carbon-Carbon Bond Formation Reactions.....	39
2.1 Introduction	40
2.2 Experimental Section	41
2.2.1 Synthesis of the Nickel Complexes.....	41
2.2.2 Reactivity Studies.....	46
2.2.3 Physical Measurements	49
2.3 Results and Discussion.....	51
2.3.1 Synthesis and Characterization of Ni ^{II/III} Complexes.....	51
2.3.2 C–C Bond Formation Reactivity of (R ^N 4)Ni ^{II} Me ₂ Complexes.....	56
2.3.3 Catalytic Reactivity of (R ^N 4)Ni ^{II} Br ₂ Complexes.....	61
2.4 Conclusion	61
2.5 Acknowledgements	62
2.6 References	62
Chapter 3: Aerobic C–C and C–O Bond Formation Reactions Mediated by High-Valent Organometallic Nickel Species.....	67
3.1 Introduction	68
3.2 Experimental Section	69
3.2.1 Synthesis of the Nickel Complexes.....	69
3.2.2 Reactivity Studies.....	73

3.2.3	Physical Measurements	74
3.3	Results and Discussion.....	76
3.3.1	Synthesis and Characterization of Ni ^{II/III} Complexes	76
3.3.2	C–C Bond Formation Reactivity of (^R N ₄)Ni ^{II} (cycloneophyl) Complexes	80
3.4	Conclusion	86
3.5	Acknowledgements	86
3.6	References	86
Chapter 4: Synthesis and Characterization of (^RMe₂TACN)Ni(cycloneophyl) Complexes and Their Reactivity.....		93
4.1	Introduction	94
4.2	Experimental Section	95
4.2.1	Synthesis of the Ligands and Nickel Complexes	96
4.2.2	Reactivity Studies.....	97
4.2.3	Physical Measurements	98
4.3	Results and Discussion.....	100
4.3.1	Synthesis and Characterization of Ni ^{II/III} Complexes.....	100
4.3.2	C–C Bond Formation Reactivity of (^R Me ₂ TACN)Ni ^{II} (cycloneophyl) Complexes	104
4.4	Conclusion	105
4.5	Acknowledgements	106
4.6	References	106
Chapter 5: Catalytic Oxidation Studies for Unactivated Alkanes Using Hypohalites as the Oxidant.....		113
5.1	Introduction	114
5.2	Experimental Section	114
5.2.1	General Catalytic Procedure for Unactivated Alkanes.....	115
5.2.2	Kinetic Isotope Effect Procedures.....	117
5.2.3	Physical Measurements	118
5.3	Results and Discussion.....	118
5.3.1	Optimization of the Catalytic Chlorination Reaction.....	118
5.3.2	Substrate Scope	125
5.3.3	Kinetic Isotope Effect Determination.....	128
5.4	Conclusion	130
5.5	Acknowledgements	131
5.6	References	131
Chapter 6: Catalytic Hydroxylation Studies using <i>m</i>CPBA as the Oxidant		137
6.1	Introduction	138
6.2	Experimental Section	139
6.2.1	General Catalytic Procedure for Unactivated Alkanes.....	140

6.2.2 Physical Measurements	140
6.3 Results and Discussion.....	141
6.3.1 Optimization of the Catalytic Hydroxylation Reaction.....	141
6.3.2 Hydroxylation of <i>tert</i> -Butylcyclohexane.....	143
6.4 Conclusion	145
6.5 Acknowledgements	145
6.6 References	146
Chapter 7: Future Directions.....	153
7.1 A New (^{TsMe} 2TACN)NiMe ₂ Complex and its Reactivity	154
7.2 A New (^{iPr} 3TACN)Ni(cycloneophyl) Complex.....	156
7.3 Reductive Dimerization of Alkyl Halides.....	158
7.4 References	160
Appendix A: Select NMR Spectra of Ligands and Metal Complexes	162
Appendix B: Select Cyclic Voltammetry (CV) Spectra	183
Appendix C: Select Ultraviolet-Visible Spectroscopy (UV-Vis) Spectra.....	192
Appendix D: Supplemental Reactivity Data.....	195
Appendix E: Supplemental Kumada Cross-Coupling Reactions Data.....	209
Appendix F: Supplemental Cryo-ESI-MS Data	222
Appendix G: X-ray Crystal Structure Data	230

List of Figures

Figure 1.1	Other observed Ni ^{III} complexes.	26
Figure 1.2	Other observed Ni ^{IV} complexes.	28
Figure 2.1	Proton (left) and carbon (right) structural assignments from NMR experiments for (T ^s MeN ₄)Ni ^{II} Me ₂	43
Figure 2.2	Proton (left) and carbon (right) structural assignments from NMR experiments for (T ^s N ₄)Ni ^{II} Me ₂	45
Figure 2.3	Ligands used for stabilizing high-valent nickel complexes.	51
Figure 2.4	ORTEP representation of 2 (left) and 3 (right), with 50% probability thermal ellipsoids. Selected bond distances (Å), 2 : Ni1-C1, 1.934; Ni1-C2, 1.923; Ni1-N1, 1.976; Ni1-N2, 1.971 3 : Ni1-C8, 1.929; Ni1-C8_i, 1.929; Ni1-N1, 1.974; Ni1-N1_i, 1.974.	53
Figure 2.5	CV of 2 (left) in 0.1 M <i>n</i> Bu ₄ NPF ₆ / MeCN at RT (100 mV/s scan rate). Redox potential: E _(Ni^{III}) = -890 mV and CV of 3 (right) in 0.1 M <i>n</i> Bu ₄ NPF ₆ /MeCN at RT (100 mV/s scan rate). Redox potential: E _(Ni^{III}) = -430 mV.	53
Figure 2.6	ORTEP representation of 2 ⁺ (left) and 3 ⁺ _{decomposition} (right) with 50% probability thermal ellipsoids. Selected bond distances (Å), 2 ⁺ : Ni1-C1, 1.932; Ni1-C2, 1.925; Ni1-N1, 1.968; Ni1-N2, 1.965; Ni1-N3, 2.145; Ni1-N4, 2.456 3 ⁺ _{decomposition} : Ni1-O1, 2.081; Ni1-O2, 1.977; Ni1-N1, 1.908; Ni1-N2, 2.03; Ni1-N3, 2.25; Ni1-N4, 2.29.	54
Figure 2.7	Experimental (1:3 THF:MeTHF, 77K) and simulated EPR spectra of 2 ⁺ (left) using the following parameters: g _x = 2.270 (A _x = 12.0 G), g _y = 2.243 (A _y = 12.0 G), g _z = 2.011 (A _z (N) = 17.5 G and A _z (N) = 5.8 G). Experimental (1:3 MeCN:PrCN, 77K) and simulated EPR spectra of 2 ⁺ (right) using the following parameters: g _x = 2.222, g _y = 2.202, g _z = 2.012 (A _z (2N) = 15.0 G).	55
Figure 2.8	Experimental (1:3 MeCN:PrCN, 77K) and simulated EPR spectra of 3 ⁺ using the following parameters: g _x = 2.365, g _y = 2.304, g _z = 2.002 (A _z (2N) = 9.0 G).	56
Figure 3.1	Proton structural assignments from NMR experiments for (MeN ₄)Ni ^{II} (cycloneophyl).	70
Figure 3.2	Proton (left) and carbon (right) structural assignments from NMR experiments for (T ^s MeN ₄)Ni ^{II} (cycloneophyl).	71

Figure 3.3	Proton (left) and carbon (right) structural assignments from NMR experiments for $(^{Ts}N_4)Ni^{II}(\text{cycloneophyl})$	72
Figure 3.4	Proton (left) and carbon (right) structural assignments from NMR experiments for $(^{tBu}N_4)Ni^{II}(\text{cycloneophyl})$	73
Figure 3.5	ORTEP representation of 2^+ (left) and 3^+ (right) with 50% probability thermal ellipsoids. Selected bond distances (Å), 2^+ : Ni1-C1, 1.938; Ni1-C4, 1.938; Ni1-N1, 2.182; Ni1-N2, 1.867; Ni1-N3, 2.199; Ni1-N4, 2.253; 3^+ : Ni1-C1, 1.933; Ni1-C8, 1.982; Ni1-N1, 1.993; Ni1-N2, 2.010; Ni1-N3, 2.360; Ni1-N4, 2.436.	79
Figure 3.6	Experimental (1:3 MeCN:PrCN, 77K) and simulated EPR spectra of 2^+ (left) using the following parameters: $g_x=2.277$, $g_y=2.235$, $g_z=2.009$ ($A_z(N)=18.0$ G). Experimental (1:3 MeCN:PrCN, 77K) and simulated EPR spectra of 3^+ (middle) using the following parameters for sim 1: $g_x=2.409$, $g_y=2.318$, $g_z=2.000$ ($A_z(2N)=8.0$ G) and sim 2: $g_x=2.253$, $g_y=2.220$, $g_z=2.010$ ($A_z(N)=18.0$ G). Simulation 1 and 2 were added in a 19:1 ratio respectively to simulate the experimental spectra properly. Experimental (1:3 MeCN:PrCN, 77K) and simulated EPR spectra of 4^+ (right) using the following parameters: $g_x=2.345$, $g_y=2.273$, $g_z=2.006$ ($A_z(2N)=11.0$ G)	80
Figure 3.7	Cryo-ESI-MS spectra and simulations showing the isotopic patterns of cationic Ni^{III} and Ni^{IV} intermediates found during the oxidation of 2 with O_2 in 10% H_2O /acetone at -80 °C. From left to right: A , $[(^{TsMe}N_4)Ni^{IV}(\text{cycloneophyl})(OOH)]^+$ m/z 631.1843 (transient species), B , $[(^{TsMe}N_4)Ni^{IV}(\text{cycloneophyl})(OH)]^+$ m/z 615.1940 (transient species) and C , $[(^{TsMe}N_4)Ni^{III}(-CH_2CMe_2-o-C_6H_4-O)]^+$ m/z 614.1862 (persistent species).....	84
Figure 4.1	ORTEP representation of 2 (left) and 3 (right), with 50% probability thermal ellipsoids. Selected bond distances (Å), 2 : Ni1a-C1a, 1.909; Ni1a-C8a, 1.935; Ni1a-N1a, 2.052; Ni1a-N2a, 2.055 3 : Ni1a-C1a, 1.920; Ni1a-C8a, 1.944; Ni1a-N1a, 2.077; Ni1a-N2a, 2.075.....	101
Figure 4.2	CV of 2 (left) in 0.1 M $nBu_4NPF_6/MeCN$ at RT (100 mV/s scan rate). Redox potential: $E_{(Ni^{III})}=-1025$ mV and CV of 3 (right) in 0.1 M $nBu_4NPF_6/MeCN$ at RT (100 mV/s scan rate). Redox potential: $E_{(Ni^{III})}=-490$ mV.	102
Figure 4.3	Experimental (1:3 THF:MeTHF, 77K) and simulated EPR spectra of 2^+ (left) using the following parameters: $g_x=2.311$, $g_y=2.267$, $g_z=2.011$ ($A_z(N)=17.0$ G). Experimental (1:3 MeCN:PrCN, 77K) and simulated EPR spectra of 3^+ (right) using the following parameters: $g_x=2.327$, $g_y=2.257$, $g_z=2.012$ ($A_z(N)=17.0$ G and ($A_z(P)=10$ G).	103

Figure 7.1	CV of 1 in 0.1 M <i>n</i> Bu ₄ NPF ₆ / MeCN at RT (100 mV/s scan rate). Redox potentials: E _(Ni^{III/II}) = -330 mV and E _(Ni^{IV/III}) = 620 mV.	155
Figure 7.2	Experimental (1:3 THF:MeTHF, 77K) and simulated EPR spectra of 1 ⁺ using the following parameters: g _x = 2.070, g _y = 2.055, g _z = 2.274.....	155
Figure 7.3	ORTEP representation of 2 (left) with 50% probability thermal ellipsoids. Selected bond distances (Å), 2 : Ni1-C1, 1.933; Ni1-C2, 1.919; Ni1-N1, 2.102; Ni1-N2, 2.098, and CV of 2 (right) 0.1 M <i>n</i> Bu ₄ NPF ₆ / MeCN at RT (100 mV/s scan rate). Redox potentials: E(Ni ^{III/II}) = -450 mV and E(Ni ^{IV/III}) = -10 mV vs. Fc/Fc ⁺	157
Figure 7.4	Experimental (1:3 THF:MeTHF, 77K) and simulated EPR spectra of 2 ⁺ using the following parameters (left): g _x = 2.353, g _y = 2.297, g _z = 2.007 (A _z (N) = 16.5 G) and experimental (1:3 MeCN:PrCN, 77K) and simulated EPR spectra of 2 ⁺ using the following parameters (right): g _x = 2.353, g _y = 2.297, g _z = 2.007 (A _z (2N) = 17.0 G).	158
Figure A1.	¹ H NMR spectrum of (T ^s MeN ₄)Ni ^{II} Me ₂ in THF-d ₈ (300 MHz). Peaks marked with an asterisk correspond to a trace amount of solvent (THF-d ₈ , THF and pentane).	163
Figure A2.	APT spectrum of (T ^s MeN ₄)Ni ^{II} Me ₂ in THF-d ₈ (500 MHz). Peaks marked with an asterisk correspond to a trace amount of solvent (THF-d ₈ and THF).	163
Figure A3.	² H NMR spectrum of (T ^s MeN ₄)Ni ^{II} (CD ₃) ₂ in MeCN with benzene-d ₆ as standard (500 MHz). Peaks marked with an asterisk correspond to a trace amount of solvent (benzene-d ₆ and MeCN).	164
Figure A4.	¹ H NMR spectrum of (T ^s N ₄)Ni ^{II} Me ₂ in THF-d ₈ (500 MHz). Peaks marked with an asterisk correspond to a trace amount of solvent (THF-d ₈ , THF and diethyl ether).	164
Figure A5.	¹³ C NMR spectrum of (T ^s N ₄)Ni ^{II} Me ₂ in THF-d ₈ (500 MHz). Peaks marked with an asterisk correspond to a trace amount of solvent (THF-d ₈).	165
Figure A6.	¹ H NMR spectrum of (MeN ₄)Ni ^{II} (cycloneophyl) in MeCN-d ₃ (300 MHz). Peaks marked with an asterisk correspond to a trace amount of solvent (MeCN-d ₃ and diethyl ether).	165
Figure A7.	¹ H NMR spectrum of (T ^s MeN ₄)Ni ^{II} (cycloneophyl) in THF-d ₈ (600 MHz). Peaks marked with an asterisk correspond to a trace amount of solvent (THF-d ₈ , THF and pentane).	166

Figure A8.	^{13}C NMR spectrum of $(^{\text{T}^{\text{Me}}\text{N}4)\text{Ni}^{\text{II}}(\text{cycloneophyl})$ in THF- d_8 (600 MHz). Peaks marked with an asterisk correspond to a trace amount of solvent (THF- d_8 , THF and pentane).	166
Figure A9.	^1H - ^1H gCOSY spectrum of $(^{\text{T}^{\text{Me}}\text{N}4)\text{Ni}^{\text{II}}(\text{cycloneophyl})$ in THF- d_8 (600 MHz). 167	
Figure A10.	^1H - ^1H TOXY spectrum of $(^{\text{T}^{\text{Me}}\text{N}4)\text{Ni}^{\text{II}}(\text{cycloneophyl})$ in THF- d_8 (600 MHz)...167	
Figure A11.	^1H - ^1H NOESY spectrum of $(^{\text{T}^{\text{Me}}\text{N}4)\text{Ni}^{\text{II}}(\text{cycloneophyl})$ in THF- d_8 (600 MHz).	168
Figure A12.	^1H - ^{13}C HSQC spectrum of $(^{\text{T}^{\text{Me}}\text{N}4)\text{Ni}^{\text{II}}(\text{cycloneophyl})$ in THF- d_8 (600 MHz)..168	
Figure A13.	^1H - ^{13}C HMBC spectrum of $(^{\text{T}^{\text{Me}}\text{N}4)\text{Ni}^{\text{II}}(\text{cycloneophyl})$ in THF- d_8 (600 MHz).169	
Figure A14.	^1H NMR spectrum of $(^{\text{T}^{\text{s}}\text{N}4)\text{Ni}^{\text{II}}(\text{cycloneophyl})$ in THF- d_8 (500 MHz). Peaks marked with an asterisk correspond to a trace amount of solvent (THF- d_8 and pentane).....	169
Figure A15.	APT spectrum of $(^{\text{T}^{\text{s}}\text{N}4)\text{Ni}^{\text{II}}(\text{cycloneophyl})$ in THF- d_8 (500 MHz). Peaks marked with an asterisk correspond to a trace amount of solvent (THF- d_8 and pentane).	170
Figure A16.	^1H - ^1H gCOSY spectrum of $(^{\text{T}^{\text{s}}\text{N}4)\text{Ni}^{\text{II}}(\text{cycloneophyl})$ in THF- d_8 (500 MHz).....	170
Figure A17.	^1H - ^1H TOXY spectrum of $(^{\text{T}^{\text{s}}\text{N}4)\text{Ni}^{\text{II}}(\text{cycloneophyl})$ in THF- d_8 (500 MHz).	171
Figure A18.	^1H - ^{13}C HSQC spectrum of $(^{\text{T}^{\text{s}}\text{N}4)\text{Ni}^{\text{II}}(\text{cycloneophyl})$ in THF- d_8 (500 MHz).	171
Figure A19.	^1H - ^{13}C HMBC spectrum of $(^{\text{T}^{\text{s}}\text{N}4)\text{Ni}^{\text{II}}(\text{cycloneophyl})$ in THF- d_8 (500 MHz). ...	172
Figure A20.	^1H NMR spectrum of $(^{\text{t}^{\text{Bu}}\text{N}4)\text{Ni}^{\text{II}}(\text{cycloneophyl})$ in THF- d_8 (500 MHz). Peaks marked with an asterisk correspond to a trace amount of solvent (THF- d_8).	172
Figure A21.	APT spectrum of $(^{\text{t}^{\text{Bu}}\text{N}4)\text{Ni}^{\text{II}}(\text{cycloneophyl})$ in THF- d_8 (500 MHz). Peaks marked with an asterisk correspond to a trace amount of solvent (THF- d_8).	173
Figure A22.	^1H - ^1H gCOSY spectrum of $(^{\text{t}^{\text{Bu}}\text{N}4)\text{Ni}^{\text{II}}(\text{cycloneophyl})$ in THF- d_8 (500 MHz). ..	173
Figure A23.	^1H - ^1H TOXY spectrum of $(^{\text{t}^{\text{Bu}}\text{N}4)\text{Ni}^{\text{II}}(\text{cycloneophyl})$ in THF- d_8 (500 MHz). ...	174
Figure A24.	^1H - ^{13}C HSQC spectrum of $(^{\text{t}^{\text{Bu}}\text{N}4)\text{Ni}^{\text{II}}(\text{cycloneophyl})$ in THF- d_8 (500 MHz). ...	174
Figure A25.	^1H - ^{13}C HMBC spectrum of $(^{\text{t}^{\text{Bu}}\text{N}4)\text{Ni}^{\text{II}}(\text{cycloneophyl})$ in THF- d_8 (500 MHz). ..	175
Figure A26.	^1H NMR spectrum of $^{\text{T}^{\text{s}}\text{Me}2}\text{TACN}$ in THF- d_8 (500 MHz).	175

Figure A27.	APT spectrum of ^{TsMe2} TACN in THF-d ₈ (500 MHz).	176
Figure A28.	¹ H NMR spectrum of (^{TsMe2} TACN)Ni ^{II} (cycloneophyl) in THF-d ₈ (500 MHz). .	176
Figure A29.	APT spectrum of (^{TsMe2} TACN)Ni ^{II} (cycloneophyl) in THF-d ₈ (500 MHz).	177
Figure A30.	¹ H- ¹ H gCOSY spectrum of (^{TsMe2} TACN)Ni ^{II} (cycloneophyl) in THF-d ₈ (500 MHz).	177
Figure A31.	¹ H- ¹ H TOXY spectrum of (^{TsMe2} TACN)Ni ^{II} (cycloneophyl) in THF-d ₈ (500 MHz).	178
Figure A32.	¹ H- ¹³ C HMBC spectrum of (^{TsMe2} TACN)Ni ^{II} (cycloneophyl) in THF-d ₈ (500 MHz).	178
Figure A33.	¹ H NMR spectrum of ^{iPrMe2} TACN in THF-d ₈ (500 MHz).	179
Figure A34.	APT spectrum of ^{iPrMe2} TACN in THF-d ₈ (500 MHz).	179
Figure A35.	¹ H NMR spectrum of (^{iPrMe2} TACN)Ni ^{II} (cycloneophyl) in THF-d ₈ (500 MHz). .	180
Figure A36.	APT spectrum of (^{iPrMe2} TACN)Ni ^{II} (cycloneophyl) in THF-d ₈ (500 MHz).	180
Figure A37.	¹ H- ¹ H gCOSY spectrum of (^{iPrMe2} TACN)Ni ^{II} (cycloneophyl) in THF-d ₈ (500 MHz).	181
Figure A38.	¹ H- ¹ H TOXY spectrum of (^{iPrMe2} TACN)Ni ^{II} (cycloneophyl) in THF-d ₈ (500 MHz).	181
Figure A39.	¹ H- ¹³ C HMBC spectrum of (^{iPrMe2} TACN)Ni ^{II} (cycloneophyl) in THF-d ₈ (500 MHz).	182
Figure B1.	CVs of (^{TsMe} N ₄)Ni ^{II} Me ₂ in 0.1 M <i>n</i> Bu ₄ NPF ₆ /MeCN at RT, at 100 mV/s scan rate (left) and variable scan rates (right).	184
Figure B2.	CVs of (^{Ts} N ₄)Ni ^{II} Me ₂ in 0.1 M <i>n</i> Bu ₄ NPF ₆ /MeCN at RT, at 100 mV/s scan rate (left) and variable scan rates (right).	185
Figure B3.	CVs of (^{TsMe} N ₄)Ni ^{II} (cycloneophyl) in 0.1 M <i>n</i> Bu ₄ NPF ₆ /MeCN at RT, at 100 mV/s scan rate (left) and variable scan rates (right).	186
Figure B4.	CVs of (^{Ts} N ₄)Ni ^{II} (cycloneophyl) in 0.1 M <i>n</i> Bu ₄ NPF ₆ /MeCN at RT, at 100 mV/s scan rate (left) and variable scan rates (right).	187
Figure B5.	CVs of (^{tBu} N ₄)Ni ^{II} (cycloneophyl) in 0.1 M <i>n</i> Bu ₄ NPF ₆ /MeCN at RT, at 100 mV/s scan rate (left) and variable scan rates (right).	188

Figure B6.	CVs of (^{iPrMe2} TACN)Ni ^{II} (cycloneophyl) in 0.1 M <i>n</i> Bu ₄ NPF ₆ /MeCN at RT, at 100 mV/s scan rate (left) and variable scan rates (right).	189
Figure B7.	CVs of (^{TsMe2} TACN)Ni ^{II} (cycloneophyl) in 0.1 M <i>n</i> Bu ₄ NPF ₆ /MeCN at RT, at 100 mV/s scan rate (left) and variable scan rates (right).	190
Figure B8.	CVs of (^{iPr3} TACN)Ni ^{II} (cycloneophyl) in 0.1 M <i>n</i> Bu ₄ NPF ₆ /MeCN at RT, at 100 mV/s scan rate (left) and variable scan rates (right).	191
Figure C1.	UV-visible spectrum of (^{TsMe} N4)Ni ^{II} Me ₂ in THF (3.125*10 ⁻⁵ M).	193
Figure C2.	UV-visible spectrum of (^{TsMe} N4)Ni ^{II} (cycloneophyl) in THF (1.25*10 ⁻⁴ M).	193
Figure C3.	UV-visible spectrum of (^{TsMe} N4)Ni ^{III} (cycloneophyl) in THF (6.25*10 ⁻⁵ M).	194
Figure D1.	¹ H NMR of ½ equivalent of (^{TsMe} N4)NiMe ₂ and ½ equivalent of (^{TsMe} N4)Ni(CD ₃) ₂ plus one equivalent of ^{Ac} FcBF ₄ in MeCN-d ₃ . ² H NMR spectrum show of the two-hour time point. No cross-over product is visible (CD ₃ -CH ₃). Peaks marked with an asterisk correspond to a trace amount of solvent (MeCN-d ₃ , diethyl ether and 1,4-dioxane (3.60 ppm)).	206
Figure D2.	² H NMR of ½ equivalent of (^{TsMe} N4)NiMe ₂ and ½ equivalent of (^{TsMe} N4)Ni(CD ₃) ₂ plus one equivalent of ^{Ac} FcBF ₄ in acetonitrile. ² H NMR spectrum show of the 2-hour time point. No cross-over product is visible (CD ₃ -CH ₃).	207
Figure E1.	Representative GC chromatogram for the Kumada cross-coupling of <i>p</i> -iodotoluene with phenylMgBr catalyzed by 5 mol% (^{TsMe} N4)Ni ^{II} Br ₂ at one hour.	212
Figure E2.	Representative GC chromatogram for the Kumada cross-coupling of <i>p</i> -iodotoluene with hexylMgBr catalyzed by 5 mol% (^{TsMe} N4)Ni ^{II} Br ₂ at one hour.	215
Figure E3.	Representative GC chromatogram for the Kumada cross-coupling of 1-iodooctane with phenylMgBr catalyzed by 5 mol% (^{TsMe} N4)Ni ^{II} Br ₂ at one hour.	218
Figure E4.	Representative GC chromatogram for the Kumada cross-coupling of 1-iodooctane with hexylMgBr catalyzed by 5 mol% (^{TsMe} N4)Ni ^{II} Br ₂ at one hour.	221

List of Tables

Table 2.1	Kumada cross-Coupling reactions catalyzed by (^R N ₄)Ni ^{II} Br ₂	61
Table 3.1	Cyclic voltammetry (CV) data for (^R N ₄)Ni(cycloneophyl) complexes.	78
Table 3.2	Yields of the products from the reaction of (^R N ₄)Ni ^{II} (cycloneophyl) with a variety of oxidants.....	82
Table 4.1	Yields of the products from the reaction of (^{RMe2} TACN)Ni ^{II} (cycloneophyl) with a variety of oxidants in MeCN.....	105
Table 5.1	Optimization for a variety of solvents.	117
Table 5.2	Optimization for different reaction conditions.	120
Table 5.3	Optimization of the catalyst loading.	121
Table 5.4	Amount of substrate, oxidant and additive optimization.	122
Table 5.5	Ligand optimization.	123
Table 5.6	Metal salt optimization.	124
Table 5.7	Substrate scope investigation.....	126
Table 6.1	Optimization for a variety of solvents.	142
Table 6.2	Optimization for a variety of ligands.	143
Table 6.3	Oxidation of <i>tert</i> -butylcyclohexane with <i>m</i> CPBA.....	144
Table 7.1	Reductive dimerization of alkyl halides substrate scope.	159
Table D1.	Yields of the products upon oxidation of (^{Me} N ₄)Ni ^{II} Me ₂ with one equivalent of ^{Ac} FcBF ₄ in MeCN-d ₃ at 20 °C.	196
Table D2.	Yields of the products upon oxidation of (^{Me} N ₄)Ni ^{II} Me ₂ with two equivalents of ^{Ac} FcBF ₄ in MeCN-d ₃ at 20 °C.	196
Table D3.	Yields of the products upon oxidation of (^{TsMe} N ₄)Ni ^{II} Me ₂ with one equivalent of ^{Ac} FcBF ₄ in MeCN-d ₃ at 20 °C.	196
Table D4.	Yields of the products upon oxidation of (^{TsMe} N ₄)Ni ^{II} Me ₂ with two equivalents of ^{Ac} FcBF ₄ in MeCN-d ₃ at 20 °C.	197

Table D5.	Yields of the products upon oxidation of (^{Ts} N ₄)Ni ^{II} Me ₂ with one equivalent of ^{Ac} FcBF ₄ in MeCN-d ₃ at -20 °C.	197
Table D6.	Yields of the products upon oxidation of (^{Ts} N ₄)Ni ^{II} Me ₂ with two equivalents of ^{Ac} FcBF ₄ in MeCN-d ₃ at -20 °C.	197
Table D7.	Yields of the products upon oxidation of (^{TsMe2} TACN)Ni ^{II} Me ₂ with one equivalent of ^{Ac} FcBF ₄ in MeCN-d ₃ at -20 °C.....	198
Table D8.	Yields of the products upon oxidation of (^{TsMe2} TACN)Ni ^{II} Me ₂ with two equivalents of ^{Ac} FcBF ₄ in MeCN-d ₃ at -20 °C.	198
Table D9.	Yields of the products upon oxidation of (^{Me} N ₄)Ni ^{II} Me ₂ with O ₂ bubbled through a solution of MeCN-d ₃ for 5 min at 20 °C.....	198
Table D10.	Yields of the products upon oxidation of (^{TsMe} N ₄)Ni ^{II} Me ₂ with O ₂ bubbled through a solution of MeCN-d ₃ for 5 min at 20 °C.....	199
Table D11.	Yields of the products upon oxidation of (^{Ts} N ₄)Ni ^{II} Me ₂ with O ₂ bubbled through a solution of MeCN-d ₃ for 5 min at -20 °C.	199
Table D12.	Yields of the products upon oxidation of (^{Me} N ₄)Ni ^{II} Me ₂ with five equivalents of H ₂ O ₂ in MeCN-d ₃ at 20 °C.	200
Table D13.	Yields of the products upon oxidation of (^{TsMe} N ₄)Ni ^{II} Me ₂ with five equivalents of H ₂ O ₂ in MeCN-d ₃ at 20 °C.	200
Table D14.	Yields of the products upon oxidation of (^{Ts} N ₄)Ni ^{II} Me ₂ with five equivalents of H ₂ O ₂ in MeCN-d ₃ at -20 °C.....	200
Table D15.	Yields of the products upon oxidation of (^{Me} N ₄)Ni ^{II} Me ₂ with three equivalents of NFTPT in MeCN-d ₃ at 20 °C.	201
Table D16.	Yields of the products upon oxidation of (^{TsMe} N ₄)Ni ^{II} Me ₂ with three equivalents of NFTPT in MeCN-d ₃ at 20 °C.	201
Table D17.	Yields of the products upon oxidation of (^{Ts} N ₄)Ni ^{II} Me ₂ with three equivalents of NFTPT in MeCN-d ₃ at -20 °C.....	201
Table D18.	Yields of the products upon oxidation of (^{Me} N ₄)Ni ^{II} Me ₂ with one equivalent of PhI(OAc) ₂ in MeCN-d ₃ at 20 °C.....	202
Table D19.	Yields of the products upon oxidation of (^{TsMe} N ₄)Ni ^{II} Me ₂ with one equivalent of PhI(OAc) ₂ in MeCN-d ₃ at 20 °C.....	202

Table D20.	Yields of the products upon oxidation of (^{Ts} N4)Ni ^{II} Me ₂ with one equivalent of PhI(OAc) ₂ in MeCN-d ₃ at -20 °C.	202
Table D21.	Yields of the products upon oxidation of (^{Me} N4)Ni ^{II} Me ₂ with one equivalent of TDTT in MeCN-d ₃ at 20 °C.	203
Table D22.	Yields of the products upon oxidation of (^{TsMe} N4)Ni ^{II} Me ₂ with one equivalent of TDTT in MeCN-d ₃ at 20 °C.	203
Table D23.	Yields of the products upon oxidation of (^{Ts} N4)Ni ^{II} Me ₂ with one equivalent of TDTT in MeCN-d ₃ at -20 °C.	203
Table D24.	Yields of the products from the crossover experiments of (^{Me} N4)Ni ^{II} Me ₂ and (^{Me} N4)Ni ^{II} (CD ₃) ₂ with one equivalent of ^{Ac} FcBF ₄ in MeCN-d ₃ at 20 °C analyzed by ¹ H NMR.	204
Table D25.	Yields of the products from the crossover experiments of (^{Me} N4)Ni ^{II} Me ₂ and (^{Me} N4)Ni ^{II} (CD ₃) ₂ with two equivalents of ^{Ac} FcBF ₄ in MeCN-d ₃ at 20 °C analyzed by ¹ H NMR.	204
Table D26.	Yields of the products from the crossover experiments of (^{TsMe} N4)Ni ^{II} Me ₂ and (^{TsMe} N4)Ni ^{II} (CD ₃) ₂ with one equivalent of ^{Ac} FcBF ₄ in MeCN-d ₃ at 20 °C analyzed by ¹ H NMR.	205
Table D27.	Yields of the products from the crossover experiments of (^{TsMe} N4)Ni ^{II} Me ₂ and (^{TsMe} N4)Ni ^{II} (CD ₃) ₂ with two equivalents of ^{Ac} FcBF ₄ in MeCN-d ₃ at 20 °C analyzed by ¹ H NMR.	205
Table D28.	Yields of the products from the crossover experiments of (^{TsMe} N4)Ni ^{II} Me ₂ and (^{TsMe} N4)Ni ^{II} (CD ₃) ₂ with one equivalent of ^{Ac} FcBF ₄ in acetonitrile at 20 °C analyzed by ² H NMR.	207
Table D29.	Yields of the products from the crossover experiments of (^{Ts} N4)Ni ^{II} Me ₂ and (^{Ts} N4)Ni ^{II} (CD ₃) ₂ with one equivalent of ^{Ac} FcBF ₄ in MeCN-d ₃ at -20 °C analyzed by ¹ H NMR.	208
Table D30.	Yields of the products from the crossover experiments of (^{Ts} N4)Ni ^{II} Me ₂ and (^{Ts} N4)Ni ^{II} (CD ₃) ₂ with two equivalents of ^{Ac} FcBF ₄ in MeCN-d ₃ at -20 °C analyzed by ¹ H NMR.	208
Table E1.	Products and yields for the Kumada cross-coupling reaction of <i>p</i> -iodotoluene and phenylMgBr catalyzed by 5 mol % (^{Me} N4)Ni ^{II} Br ₂	210

Table E2.	Products and yields for the Kumada cross-coupling reaction of <i>p</i> -iodotoluene and phenylMgBr catalyzed by 5 mol % (^{TsMe} N4)Ni ^{II} Br ₂	211
Table E3.	Products and yields for the Kumada cross-coupling reaction of <i>p</i> -iodotoluene and phenylMgBr catalyzed by 5 mol % (^{Ts} N4)Ni ^{II} Br ₂	211
Table E4.	Products and yields from the Kumada cross-coupling reactions of <i>p</i> -iodotoluene and hexylMgBr catalyzed by 5 mol % (^{Me} N4)Ni ^{II} Br ₂	213
Table E5.	Products and yields from the Kumada cross-coupling reactions of <i>p</i> -iodotoluene and hexylMgBr catalyzed by 5 mol % (^{TsMe} N4)Ni ^{II} Br ₂	214
Table E6.	Products and yields from the Kumada cross-coupling reactions of <i>p</i> -iodotoluene and hexylMgBr catalyzed by 5 mol % (^{Ts} N4)Ni ^{II} Br ₂	214
Table E7.	Products and yields from the Kumada cross-coupling reactions of 1-iodooctane and phenylMgBr catalyzed by 5 mol % (^{Me} N4)Ni ^{II} Br ₂	216
Table E8.	Products and yields from the Kumada cross-coupling reactions of 1-iodooctane and phenylMgBr catalyzed by 5 mol % (^{TsMe} N4)Ni ^{II} Br ₂	217
Table E9.	Products and yields from the Kumada cross-coupling reactions of 1-iodooctane and phenylMgBr catalyzed by 5 mol % (^{Ts} N4)Ni ^{II} Br ₂	217
Table E10.	Products and yields from the Kumada cross-coupling reactions of 1-iodooctane and hexylMgBr catalyzed by 5 mol % (^{Me} N4)Ni ^{II} Br ₂	219
Table E11.	Products and yields from the Kumada cross-coupling reactions of 1-iodooctane and hexylMgBr catalyzed by 5 mol % (^{TsMe} N4)Ni ^{II} Br ₂	220
Table E12.	Products and yields from the Kumada cross-coupling reactions of 1-iodooctane and hexylMgBr catalyzed by 5 mol % (^{Ts} N4)Ni ^{II} Br ₂	220
Table F1.	Cryo-ESI-MS results for the oxidation of (^{Me} N4)Ni ^{II} (cycloneophyl).....	223
Table F2.	Cryo-ESI-MS results for the oxidation of (^{TsMe} N4)Ni ^{II} (cycloneophyl).....	225
Table F3.	Cryo-ESI-MS results for the oxidation of (^{Ts} N4)Ni ^{II} (cycloneophyl).....	228
Table G1.	ORTEP representation with 50% probability thermal ellipsoids.....	231
Table G2.	Crystal data and structure refinement for Im614. (^{TsMe} N4)Ni ^{II} Br ₂	235
Table G3.	Select bond lengths [Å] and angles [°] for Im614.....	236
Table G4.	Crystal data and structure refinement for Im9716. (^{TsMe} N4)Ni ^{II} Me ₂	237

Table G5.	Select bond lengths [\AA] and angles [$^{\circ}$] for lm9716.....	238
Table G6.	Crystal data and structure refinement for l13816_sq. ($^{\text{TsMe}}\text{N4}$)Ni ^{III} Me ₂ ⁺	239
Table G7.	Select bond lengths [\AA] and angles [$^{\circ}$] for l13816_sq.	240
Table G8.	Crystal data and structure refinement for lm9017. ($^{\text{TsMe}}\text{N4}$)Ni ^{III} (cycloneophyl) ⁺	241
Table G9.	Select bond lengths [\AA] and angles [$^{\circ}$] for lm9017.....	242
Table G10.	Crystal data and structure refinement for lm11317. ($^{\text{TsMe}}\text{N4}$)Ni ^{II} (MeCN) ₂ ²⁺	243
Table G11.	Select bond lengths [\AA] and angles [$^{\circ}$] for lm11317.....	245
Table G12.	Crystal data and structure refinement for lm2216. ($^{\text{Ts}}\text{N4}$)Ni ^{II} (acac) ⁺	246
Table G13.	Select bond lengths [\AA] and angles [$^{\circ}$] for lm2216.....	247
Table G14.	Crystal data and structure refinement for lm1016. ($^{\text{Ts}}\text{N4}$)Ni ^{II} Me ₂	248
Table G15.	Select bond lengths [\AA] and angles [$^{\circ}$] for lm1016.....	249
Table G16.	Crystal data and structure refinement for l15316_sq. ($^{\text{Ts}}\text{N4}$)Ni ^{III} (OH)(H ₂ O) ₂ ²⁺ ...	250
Table G17.	Select bond lengths [\AA] and angles [$^{\circ}$] for l15316_sq.	251
Table G18.	Crystal data and structure refinement for lm8417. ($^{\text{Ts}}\text{N4}$)Ni ^{III} (cycloneophyl) ⁺ ...	252
Table G19.	Select bond lengths [\AA] and angles [$^{\circ}$] for lm8417.....	253
Table G20.	Crystal data and structure refinement for lm2418. ($^{\text{tBu}}\text{N4}$)Ni ^{II} (cycloneophyl)....	254
Table G21.	Select bond lengths [\AA] and angles [$^{\circ}$] for lm2418.....	255
Table G22.	Crystal data and structure refinement for lm15218. ($^{\text{iPrMe}_2}\text{TACN}$)Ni ^{II} (cycloneophyl)	256
Table G23.	Select bond lengths [\AA] and angles [$^{\circ}$] for lm15218.....	257
Table G24.	Crystal data and structure refinement for l3118t5. ($^{\text{TsMe}_2}\text{TACN}$)Ni ^{II} (cycloneophyl)	258
Table G25.	Select bond lengths [\AA] and angles [$^{\circ}$] for l3118t5.....	259
Table G26.	Crystal data and structure refinement for lm20417. ($^{\text{Me}}\text{N4}$)Ni ^{II} (MeCN) ₂ ²⁺	260
Table G27.	Select bond lengths [\AA] and angles [$^{\circ}$] for lm20417.....	261

Table G28.	Crystal data and structure refinement for ($i\text{Pr}^3\text{TACN}$) Ni^{II} (cycloneophyl).....	263
Table G29.	Select bond lengths [\AA] and angles [$^\circ$] for ($i\text{Pr}^3\text{TACN}$) Ni^{II} (cycloneophyl).....	264

List of Schemes

Scheme 1.1	The first observed organometallic Ni ^{III} species by Kochi and co-workers in 1978.	3
Scheme 1.2	The first high-valent nickel organometallic complexes stabilized by the pincer ligand published by van Koten and co-workers and then later revisited by Zargarian and co-workers in 2018.	4
Scheme 1.3	The first isolated chiral Ni ^{III} organometallic complex stabilized by an amino-acid pincer ligand.	5
Scheme 1.4	Oxidatively-induced Ni ^{II} , stabilized by a 2,2'-bipyridyl ligand published in 1995 by Hillhouse and co-workers.	5
Scheme 1.5	Oxidatively-induced reaction of the dimeric seven-membered Ni(II) oxametallacycle.	6
Scheme 1.6	The reformation of aziridine by an oxidatively induced reductive elimination.	7
Scheme 1.7	N-X bond formation using trigonal planar terminal imido Ni ^{III} complex published by Warren and co-workers in 2005.	7
Scheme 1.8	Several phosphonite pincer Ni ^{III} complexes isolated by Zargarian and co-workers in 2007 and 2009, showing also the Kharasch addition reactivity.	8
Scheme 1.9	PCP pincer Ni ^{III} complexes stabilized in a trigonal bipyramidal geometry, isolated by Zargarian and co-workers in 2008.	8
Scheme 1.10	Hillhouse and co-workers isolated an alkyl and aryl-substituted Ni ^{III} imide complexes in 2011.	9
Scheme 1.11	One electron oxidation of the Ni ^{II} complex supported by a BOXAM ligand reported by Vicic and co-workers.	9
Scheme 1.12	Proposed five-coordinate Ni ^{III} complex stabilized by two CF ₃ ligands and a bulky terpyridine ligand.	10
Scheme 1.13	Synthesis of a Ni ^{III} alkyl species proceeding through a Ni ^I species stabilized by a bis-amido ligand framework.	10
Scheme 1.14	Synthesis and reactivity of the Ni ^{III} (aryl)halide and Ni ^{III} (aryl)alkyl complexes by Mirica and co-workers in 2014.	11

Scheme 1.15	Synthesis of stable bis(trifluoromethyl)nickel(III) complexes supported by a tetradentate pyridinophane ligand.....	12
Scheme 1.16	Synthesis of a several of Ni ^{III} complexes supported by a modified tetradentate pyridinophane ligand containing one phenyl group.....	12
Scheme 1.17	Oxidation of (tpy)Ni ^{II} (C ₄ F ₈) complex, leading to a stable Ni ^{III} complex reported by Vicic and co-workers in 2015.....	13
Scheme 1.18	Synthesis of a square pyramidal Ni ^{III} alkyl-complex and its reactivity.....	13
Scheme 1.19	N-N bond formation at Ni ^{III} dimer published by Diao and co-workers in 2016....	14
Scheme 1.20	Synthesis and reactivity of Ni ^{III} complexes stabilized by a modified tetradentate pyridinophane ligand.	14
Scheme 1.21	Synthesis and reactivity of the Ni ^{III} -dialkyl complex reported by Mirica and co-workers in 2016.....	15
Scheme 1.22	Catalytic oxidation of cyclohexane through a Ni ^{III} -OCl intermediate.....	16
Scheme 1.23	Alkyl-alkyl and alkyl-aryl C–C bond formation and trifluoromethylation using an isolated Ni ^{III} complex stabilized by scorpionate borate ligand and C(sp ²), C(sp ³), and CF ₃ ligands.	16
Scheme 1.24	C–Br bond formation using a Ni ^{III} dimer supported by carboxylate and benzoquinoline ligands.	17
Scheme 1.25	C–F bond formation with aryl Ni ^{III} fluoride complexes and active Ni ^{III} species observed published by Ritter and co-workers in 2017.....	18
Scheme 1.26	Formation of a quasi-tetrahedral Ni ^{IV} complex that leads to C–C bond formation published by Dimitrov and co-workers in 2003.	19
Scheme 1.27	Synthesis of a stable tetraalkyl Ni ^{IV} complex published by Turro and co-workers.	19
Scheme 1.28	Proposed nickel-catalyzed alkylation mechanism involving high-valent nickel intermediates by Chatani and co-workers.....	20
Scheme 1.29	C(sp ²)–C(sp ³) and C(sp ³)–X bond formation using isolated tris(2-pyridyl)methane Ni ^{IV} -cycloneophyl(CF ₃) complexes.....	21
Scheme 1.30	C(sp ³)–X bond formation using in-situ trispyrazolylborate Ni ^{IV} -cycloneophyl(CF ₃) complexes.	21

Scheme 1.31	Trifluoromethylation of different aryl substrates by using a trispyrazolylborate Ni ^{IV} -aryl(CF ₃) ₂ complexes.....	22
Scheme 1.32	Bromination of alkenes using an isolated Ni ^{IV} tribromide complex as a bromide transfer reagent.....	23
Scheme 1.33	Oxidatively induced C-H activation of bis(2-pyridyl)(2- ^R phenyl)-fluoromethane Ni-aryl(CF ₃) ₂ complexes.....	23
Scheme 1.34	Synthesis of (Me ₃ tacn)Ni(CH ₂ CMe ₂ - <i>o</i> -C ₆ H ₄) complexes with the corresponding reactivity.	24
Scheme 1.35	C-H bond activation and trifluoromethylation of 1,2-dichlorobenzene using isolated Ni ^{IV} complex supported by simple, monodentate ligands.....	25
Scheme 2.1	General reactivities studies.	47
Scheme 2.2	Crossover reactivity.	48
Scheme 2.3	Synthesis of (^R N ₄)NiMe ₂ complexes.....	52
Scheme 2.4	C–C bond formation reactivity of the (^R N ₄)Ni ^{II} Me ₂ complexes with ^{Ac} FcBF ₄	57
Scheme 2.5	Crossover reactivity studies of the (^R N ₄)Ni ^{II} Me ₂ complexes.	58
Scheme 2.6	Proposed mechanism for one-electron oxidation of (^{TsMe} N ₄)Ni ^{II} Me ₂ , 2	59
Scheme 2.7	C–C bond formation reactivity of the (^R N ₄)Ni ^{II} Me ₂ complexes with O ₂ and H ₂ O ₂	59
Scheme 2.8	C–C bond formation reactivity of the (^R N ₄)Ni ^{II} Me ₂ complexes with NFTPT, PhI(OAc) ₂ and TDDT.	60
Scheme 2.9	Kumada cross-coupling reactions catalyzed by (^R N ₄)Ni ^{II} Br ₂	61
Scheme 3.1	Synthesis of (^R N ₄)Ni(cycloneophyl) complexes.	77
Scheme 3.2	General reaction for the formation of the different oxidation products.....	82
Scheme 3.3	Proposed mechanism leading to C–C and C–O bond formation using complex 2 with O ₂ as the oxidant.	85
Scheme 4.1	Synthesis of (^{RMe2} TACN)Ni(cycloneophyl) complexes.	101
Scheme 4.2	General reaction for the formation of the different oxidation products.....	104
Scheme 5.1.	General reaction scheme for the chlorination of unactivated C–H bonds.	116

Scheme 5.2.	General reaction scheme for the bromination of unactivated C–H bonds.	117
Scheme 5.3	Optimization for a variety of solvents.	119
Scheme 5.4	Optimization for different reaction conditions.	120
Scheme 5.5	Optimization of the catalyst loading.	121
Scheme 5.6	Substrate, oxidant and additive optimization.	122
Scheme 5.7	Ligand optimization.	123
Scheme 5.8	Metal salt optimization.	124
Scheme 5.9	Proposed C–H chlorination mechanism.	129
Scheme 5.10	Alternative C–H chlorination mechanism.	130
Scheme 6.1	Optimization for a variety of solvents.	141
Scheme 6.2	Optimization for a variety of ligands.	143
Scheme 6.3	Oxidation of <i>tert</i> -butylcyclohexane with <i>m</i> CPBA.	144
Scheme 7.1	Synthesis of (^{TsMe2} TACN)NiMe ₂ complexes.	154
Scheme 7.2	C–C bond formation reactivity of the (^{TsMe2} TACN)Ni ^{II} Me ₂ complex with ^{Ac} FcBF ₄	156
Scheme 7.3	Synthesis of (^{iPr3} TACN)Ni(cycloneophyl) complexes.	157

Acknowledgments

At this time, I would like to thank several people for their support and guidance throughout my graduate studies. First, I would like to thank my advisor, Professor Liviu M. Mirica, for all his help, support, and guidance. I greatly appreciate everything he has done for me throughout my graduate studies.

I would also like to thank Professors Kevin D. Moeller and John R. Bleeke for being members of my annual committee. The insight and support you provided over the years have been invaluable. Additionally, I would like to thank Professors Sophia E Hayes and Nigam P. Rath for being members on my defense committee. I would like to acknowledge Professor Nigam P. Rath for his help and advice in the analysis of all the X-ray structures reported in this dissertation and obtained throughout my graduate studies. Furthermore, I would like to thank Professor Vladimir B. Birman for taking me in for my final undergraduate research internship for my B.A.Sc. Without him I wouldn't have been here today.

Thank you to the entire Mirica Group, present and past, for making this journey as painless as possible. You guys were always there if I needed to talk about research or anything else. I wish you success in the future. In addition, I would like to thank the entire chemistry department and administrative staff for their great guidance throughout the past few years.

I would like to thank the following institutions for the financial support during my graduate studies: The Department of Chemistry at Washington University in St. Louis, the Department of Energy (DE-FG02-11ER16256) and the National Science Foundation (CHE-1255424).

Many friends and acquaintances were made during my time here at Washington University in St. Louis. I want to thank all my friends from the newly funded ballroom dancing club and the PhD chemistry class of 2014, we were a small class but a great one.

Lastly, I would like to thank my family, to whom I dedicate this work. You have always been there for me with your love and support. I couldn't have asked for more dedicated parents always putting their children first. I will never be able to say thank you enough for everything you have done for me. A special thanks to my sister Sara to whom I can call day and night if I needed a pep talk or if it was just to say hi. The time zone difference didn't always make it easy, but we made it work.

Sofia M. Smith

Washington University in St. Louis

May 2019

Dedicated to my Family, I Love You.

ABSTRACT OF THE DISSERTATION

Oxidative C–C and C–Heteroatom Reactivity of High-Valent Nickel Complexes

by

Sofia M. Smith

Doctor of Philosophy in Chemistry

Washington University in St. Louis, 2019

Professor Liviu M. Mirica, Chair

Professor Kevin D. Moeller, Co-Chair

Nickel catalysts are commonly used for cross-coupling reactions such as Negishi, Kumada and Suzuki couplings. While Ni(0), Ni(I), and Ni(II) intermediates are most relevant in these transformations, Ni(III) and Ni(IV) species have also been recently proposed to play a role in catalysis. The formation of C–C and C–heteroatom bonds plays a fundamental role in organic transformations, and today cross-coupling reactions are one of the most powerful tools for the construction of new C–C bonds. However, limited examples exist of Ni-mediated C–heteroatom bond formation reactions, likely due to the difficulty of accessing high-valent organometallic Ni species that can undergo reductive elimination.

One way to expand our knowledge of these C–C and C–heteroatom atom bond formation reactions is to look at the stabilization and destabilization effects of the high-valent nickel complexes. Studying these effects will help us determine the most efficient way in performing C–C and C–heteroatom atom bond formation reactions. Tetradentate pyridinophane ligands have

been to stabilize uncommon high-valent organometallic nickel complexes. By varying the N-substituents, we are now able to probe the stabilization and destabilization effects that might play a crucial role in the C–C and C–heteroatom atom bond formation reactions.

A series of nickel complexes were synthesized to probe the C–C and C–heteroatom atom bond reactivity using the Ni-dimethyl and -metallacycle complexes. These complexes were fully characterized and their reactivity was tested. The oxidative reactivity was studied by looking at a variety of oxidants which include dioxygen and hydrogen peroxide to probe any C–O bond formation. Interestingly, while the oxidation of the Ni^{II} metallacycle complexes with various oxidants led to exclusive C–C bond formation in very good yields, the use of O₂ or H₂O₂ as oxidants led to appreciable amounts of C–O bond formation products, especially for an asymmetric pyridinophane ligand with one tosyl N-substituent. Moreover, cryo-ESI-MS studies strongly support the formation of several high-valent nickel species as key intermediates in this unprecedented aerobic Ni-mediated oxygenase-type chemistry.

Lastly, the tetradentate pyridinophane ligands were used in two catalytic oxidation reactions, a hydroxylation and a chlorination reaction for unactivated alkanes. These catalytic oxidation reactions use mild oxidants such as hypohalites which are commercially available. All these reactions could have important implications in organic transformations.

Chapter 1

High-Valent Organometallic Nickel Complexes and Their Reactivity

1.1 Introduction

Nickel (Ni) is commonly used as a catalyst for various cross-coupling reactions, including Negishi, Kumada, and Suzuki couplings. Although the 0, I, and II oxidation states of Ni are commonly involved in these catalytic transformations, recent studies show that the III and IV oxidation states of Ni also play a key role in organic transformations such as C–C and C–heteroatom bond formation reactions.

The first Ni^{III} and Ni^{IV} organometallic complexes were reported almost 40 years ago, yet those were unreactive. In the past decade reports of reactive organometallic Ni complexes have exploded. This chapter reports all these systems, with a focus on the more recent, reactive examples. Other high-valent, non-organometallic Ni complexes are not discussed in detail, unless they promote organic reactions.

In the past decade, many advances have been made in the synthesis of high-valent organometallic Ni complexes and the study of their reactivity and involvement in various organic transformations. In 2007, Zargarian isolated and probed the reactivity of a Ni^{III} organometallic complex, which promoted chlorination of alkenes through Kharasch addition. In 2014 and 2015 Mirica isolated an alkyl(halide) and alkyl-alkyl Ni^{III} species capable of mediating C–X and C–C bond formation after heating, respectively. Similar reactivity was observed by Sanford in 2015, but with an isolated Ni^{IV} species that promoted C–X and C(sp²)–C(sp³) bond formation. Reactivity studies of high-valent Ni has been on the rise. Other observed reactivity mediated by these high-valent Ni species include bromination of alkenes and trifluoromethylation of alkyl and aryl substrates. The once elusive and unreactive Ni^{III} and Ni^{IV} species are now promoting organic

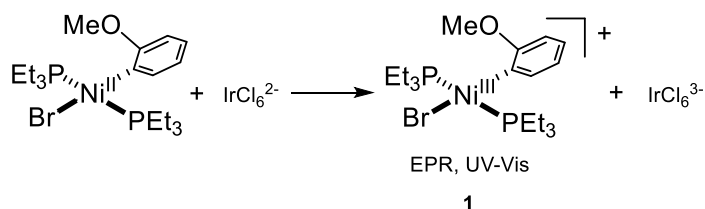
transformations normally proposed to be done by Ni^{0/II} intermediates. This opens a new path where Ni^{III/IV} could be accessed in a catalytic cycle during an organic transformation.

It is important to note that there are other high-valent Ni complexes that are not organometallic that could potentially provide information of the stability of these complexes in organic transformations. In this chapter we will present accomplishments made in the past 40 years involving organometallic Ni^{III} and Ni^{IV} complexes since they were first observed by Kochi in 1978 and Smart in 1982, respectively. Several other reviews on high-valent nickel chemistry are available as well.¹⁻⁵

1.2 Organometallic Ni^{III} Complexes

Kochi and co-workers published in 1978 the first organometallic Ni^{III}, **1**, species that was observed by EPR and UV-Vis (Scheme 1.1). Starting from the Ni^{II} precursor, sodium hexachloroiridate was added at -50 °C. A stable electronic spectrum with λ_{max} 410 nm and an EPR spectrum were immediately observed. After warming the solution to -18 °C, the EPR spectrum disappeared after approximately 20 minutes, which was associated with a reductive elimination from the paramagnetic species.⁶

Scheme 1.1 The first observed organometallic Ni^{III} species by Kochi and co-workers in 1978.

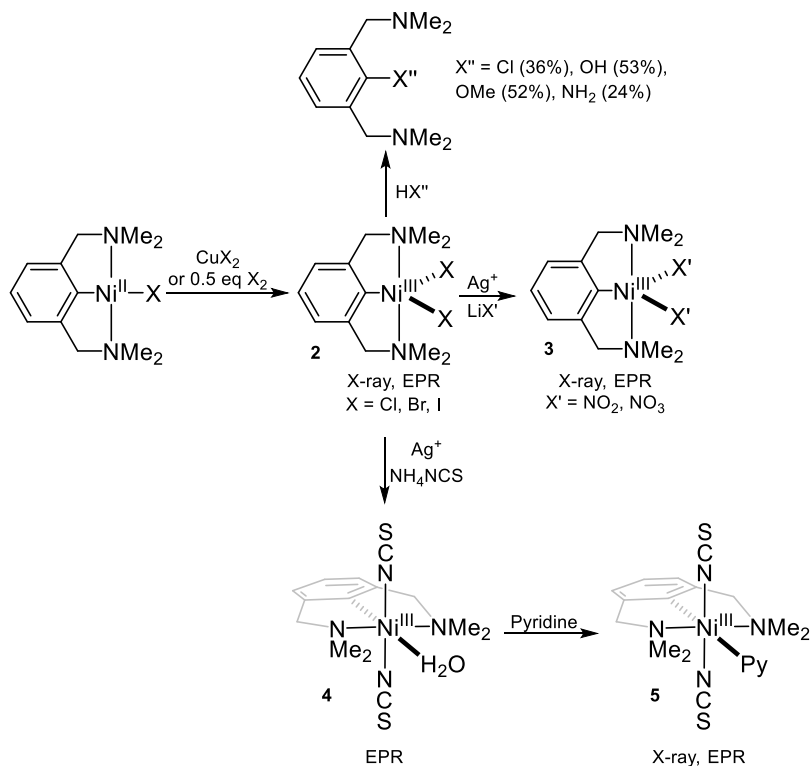


It was not until 1983 that van Koten and co-workers isolated the first high-valent nickel organometallic complex using the pincer ligand 1,1'-(1,3-phenylene)bis(N,N-

dimethylmethanamine) (NCN) (Scheme 1.2). The binding of the tridentate NCN pincer ligand and two anionic ligands yielded a stable trigonal bipyramidal Ni^{III}, **2**. The auxiliary ligands in the cis coordination sites could easily be interchanged with anionic halogens, nitrites/nitrates, **3**, or isothiocyanato ligands, **4** and **5**, yet the complexes were unusually stable and were only proposed as plausible intermediates in chlorination of alkenes with CCl₄ through Kharasch addition.⁷⁻¹¹

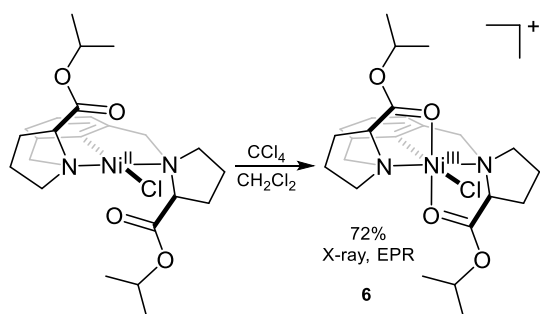
Zargarian and co-workers revisited **2** in 2018 and used the electrophilic nature of the ligand backbone to promote C–X formation with water, alcohols, amines, and strong acids under mild conditions. Although the reactions generating C–X products were not high yielding or selective, the reactivity observed for **2** was rare.¹²

Scheme 1.2 The first high-valent nickel organometallic complexes stabilized by the pincer ligand published by van Koten and co-workers and then later revisited by Zargarian and co-workers in 2018.



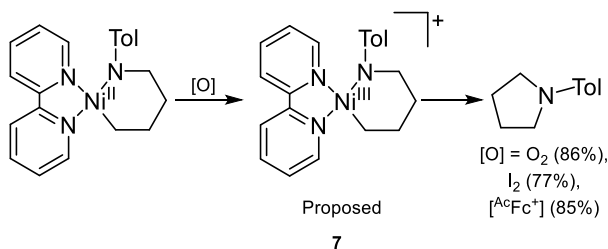
In 1995, van Koten and co-workers introduced a similar pincer complex to 1,1'-(1,3-phenylene)bis(*N,N*-dimethylmethanamine), but with amino acid derivatives. In contrast to their original NCN ligand, this proline-type NCN pincer ligand could coordinate to the Ni center in a tridentate or pentadentate fashion. In this case, the Ni^{III} complex **6** was stabilized in an octahedral geometry and could be isolated in a 72% yield (Scheme 1.3).¹³

Scheme 1.3 The first isolated chiral Ni^{III} organometallic complex stabilized by an amino-acid pincer ligand.



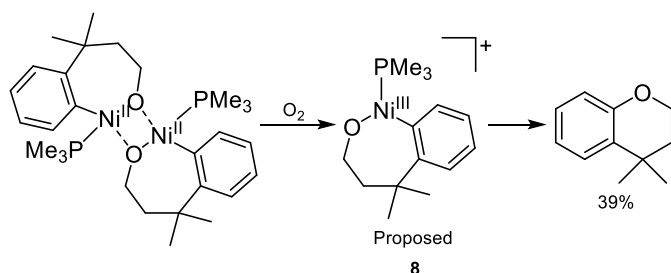
In 1995, Hillhouse and co-workers proposed a Ni^{III} intermediate, **7** after exposing the Ni^{II} precursor to either O₂ or I₂ at room temperature (Scheme 1.4). The reaction resulted in a clean formation of *N*-*p*-tolylpyrrolidine, 86% and 77% respectively, after a chromatographic workup. Moreover, the one electron oxidant acetyl ferrocenium tetrafluoroborate also cleanly converts the Ni^{II} to **7** (85%).¹⁴⁻¹⁵

Scheme 1.4 Oxidatively-induced Ni^{II}, stabilized by a 2,2'-bipyridyl ligand published in 1995 by Hillhouse and co-workers.



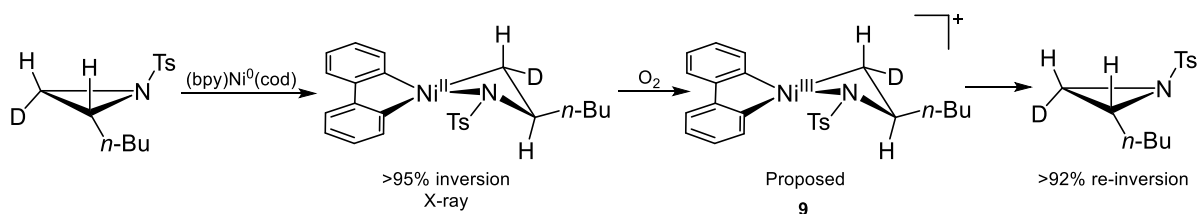
In 1997, Hillhouse and co-workers published the oxidatively-induced reaction of the dimeric seven-membered nickel(II) oxametallacycle. Starting with the dimeric Ni^{II}, O₂ was bubbled through a solution of benzene forming over the course of 72 hours at room temperature a new C–O bond (Scheme 1.5). Formation of the C–O bond occurs via an oxidatively-induced mechanism to form the proposed Ni^{III} intermediate, **8** followed by a reductive-elimination to give 4,4-dimethylchroman, in 39% isolated yield.¹⁴⁻¹⁵

Scheme 1.5 Oxidatively-induced reaction of the dimeric seven-membered Ni(II) oxametallacycle.



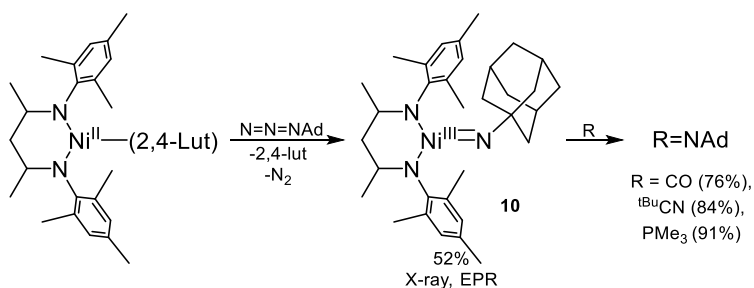
In 2002, Hillhouse and co-workers described a stereochemical synthesis of aziridine by an oxidatively induced reductive elimination from a Ni^{III} complex (Scheme 1.6). Reaction of *N*-tosylaziridine with a (bpy)Ni⁰(cod) results in the elimination of 1,5-cyclooctadiene and the oxidative addition of the aziridine, to give the azametallacyclobutane complex. The formation of the Ni^{II} complex results in only one regioisomer, with the oxidative addition occurring exclusively at the least-hindered C–N bond. Addition of dioxygen forms the proposed Ni^{III} complex **9** which then undergoes a reductive elimination with inversion of stereochemistry to reform the aziridine with 92% inversion by ¹H NMR.¹⁶

Scheme 1.6 The reformation of aziridine by an oxidatively induced reductive elimination.



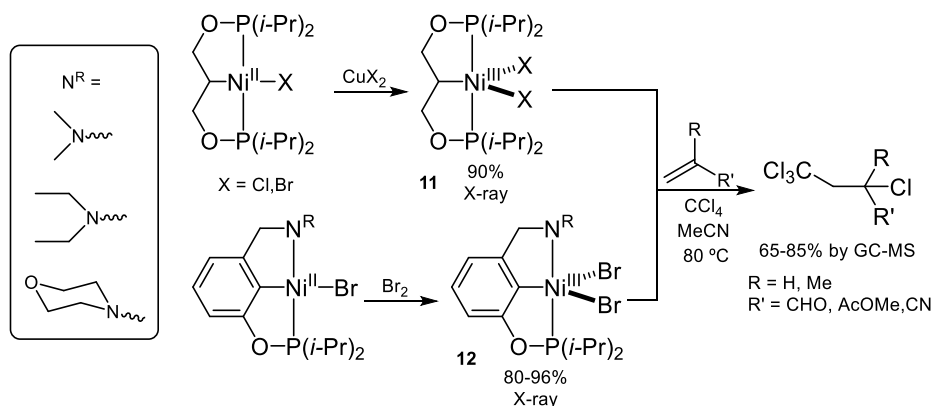
In 2005, Warren and co-workers isolated a trigonal planar Ni^{III} complex **10** stabilized by bidentate β -diketiminato-type ligand and an imidoadamantane nitrogen donor (Scheme 1.7). Reactivity of terminal imido complex with CO , CN^tBu , and PMe_3 resulted in OC-N , NC-N , and P-N bond formation in good yields (76%, 84%, and 91%).¹⁷

Scheme 1.7 N–X bond formation using trigonal planar terminal imido Ni^{III} complex published by Warren and co-workers in 2005.



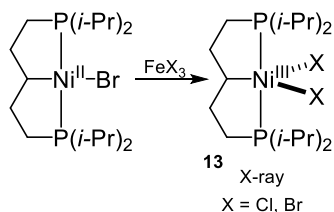
In 2007 and 2009, Zargarian and co-workers used the (1,3-bis((diisopropylphosphaneyl)oxy)propane) PCP-type phosphonite ligand and (1-(3-((diisopropylphosphaneyl)oxy)phenyl)-N,N-di N^{R} methanamine) PCN-type phosphonite pincer ligands to stabilize the Ni^{III} centers, complexes **11** and **12**, respectively (Scheme 1.8). Similar to the NCN Ni complexes from van Koten and co-workers, the PCP/PCN oxidized Ni species could promote C–Cl coupling of alkenes with CCl_4 through the Kharasch addition in good yields (60–85%).¹⁸⁻¹⁹

Scheme 1.8 Several phosphonite pincer Ni^{III} complexes isolated by Zargarian and co-workers in 2007 and 2009, showing also the Kharasch addition reactivity.



In 2008, Zargarian and co-workers used PCP pincer ligand 1,5-bis(diisopropylphosphaneyl)pentyl. In this case, the Ni^{III} center in complex **13** is stabilized with a trigonal bipyramidal geometry (Scheme 1.9). In contrast to their previously discussed PCP phosphonite ligands, the complex does not show reactivity at the isolated Ni^{III} oxidation state.²⁰

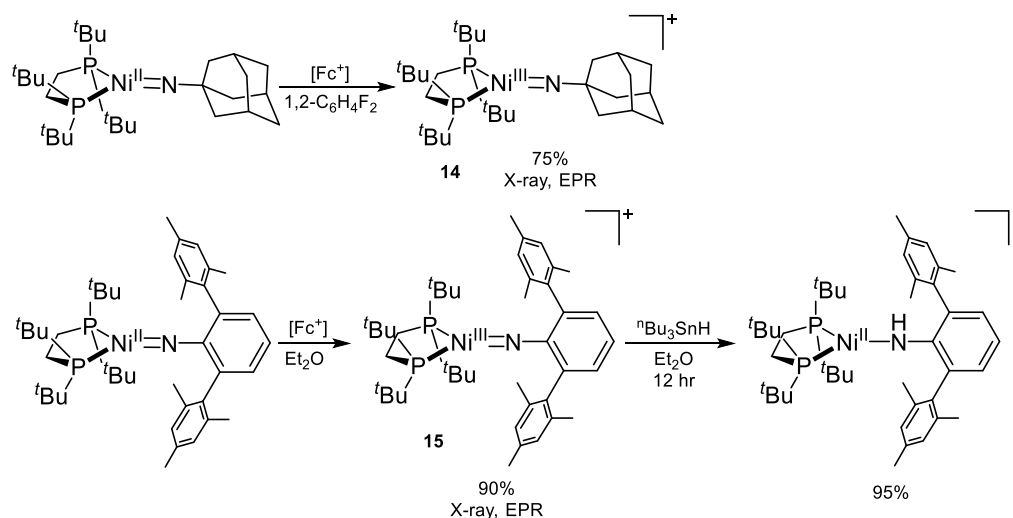
Scheme 1.9 PCP pincer Ni^{III} complexes stabilized in a trigonal bipyramidal geometry, isolated by Zargarian and co-workers in 2008.



Hillhouse and co-workers synthesized two Ni^{III} imides supported by 1,2-bis(di-tert-butylphosphino)ethane in 2011 (Scheme 1.10). The oxidation of the Ni^{II} complexes led to the formation of both aryl- and alkyl-substituted Ni^{III} imides. The aryl substituent was the bulky 2,6-dimesitylphenyl and the alkyl substituent was adamantane. Both Ni^{III} imide compounds showed analogous EPR spectra at low temperature but different variable-temperature magnetic properties. A low-spin/high-spin equilibrium was proposed to take place for the alkyl-substituted Ni^{III} imide

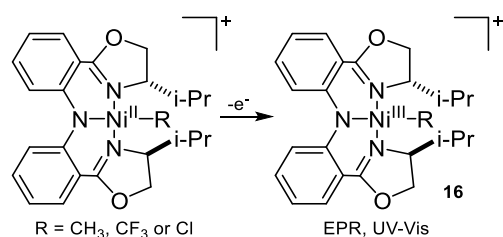
complex **14** to account for the difference. The aryl-substituted Ni^{III} imide, **15**, favors one rotamer because of the steric properties of the 2,6-dimesitylphenyl substituent. Complex **15** can undergo hydrogen atom abstraction resulting in the Ni^{II} complex with ⁿBu₃SnH (95%).²¹

Scheme 1.10 Hillhouse and co-workers isolated an alkyl and aryl-substituted Ni^{III} imide complexes in 2011.



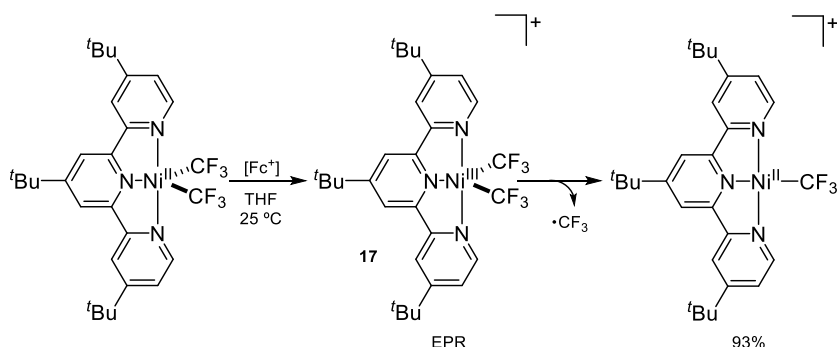
Vicic and co-workers reported in 2012 a one-electron oxidation of the Ni^{II} complex supported by a BOXAM ligand (BOXAM = bis((4-isopropyl-4,5-dihydrooxazol-2-yl)phenyl)amine) (Scheme 1.11). The Ni^{III} complexes, **16** were all characterized by EPR and UV-Vis. The redox behavior of these complexes strongly depends on the co-ligand (CH₃, CF₃ or Cl). The oxidation potential varies from -0.17 V for R = CH₃ to +0.43 V for R = CF₃.²²⁻²³

Scheme 1.11 One electron oxidation of the Ni^{II} complex supported by a BOXAM ligand reported by Vicic and co-workers.



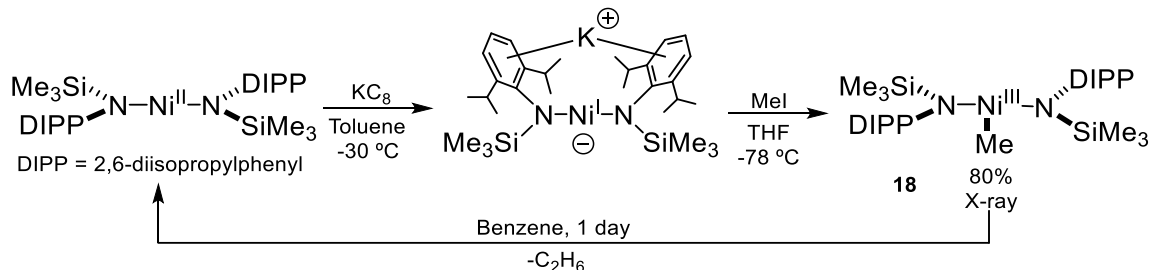
In 2013, Vicic and co-workers proposed a five-coordinate Ni^{III} complex supported by a terpyridine ligand and two fluoroalkyl ligands (Scheme 1.12). Ferrocenium hexafluorophosphate was used to oxidize the Ni^{II} complex to the proposed Ni^{III} complex **17**, but even upon rapid workup of the reaction mixture, one CF₃ group eliminated to form the new Ni^{II} complex. The last step might occur through a reductive homolysis of a trifluoromethyl radical from complex **17**.²⁴

Scheme 1.12 Proposed five-coordinate Ni^{III} complex stabilized by two CF₃ ligands and a bulky terpyridine ligand.



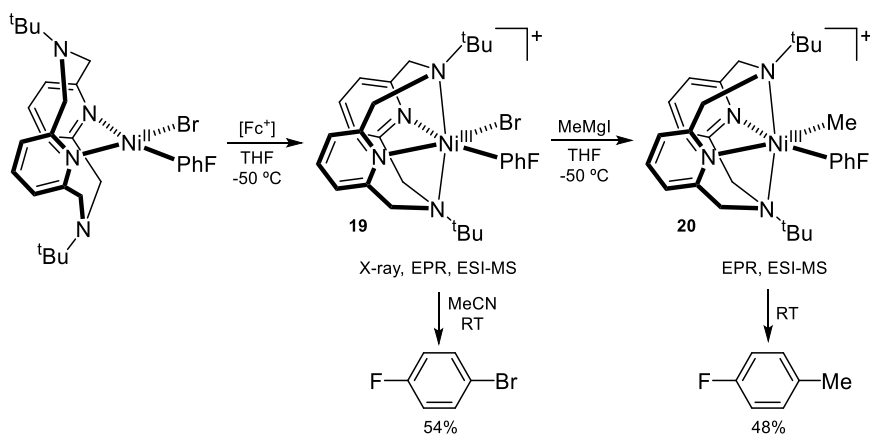
In 2013, Tilley and co-worker reported an isolable Ni^{III} alkyl species, complex **18** that has been prepared through a two-electron oxidative addition of methyl iodide to a Ni^I complex (80%) (Scheme 1.13). The bis-amido ligand framework is capable of supporting the nickel complexes in three different oxidation states. Complex **18** was thermally unstable and decomposed in one day in benzene into the Ni^{II} complex and ethene.²⁵⁻²⁶

Scheme 1.13 Synthesis of a Ni^{III} alkyl species proceeding through a Ni^I species stabilized by a bis-amido ligand framework.



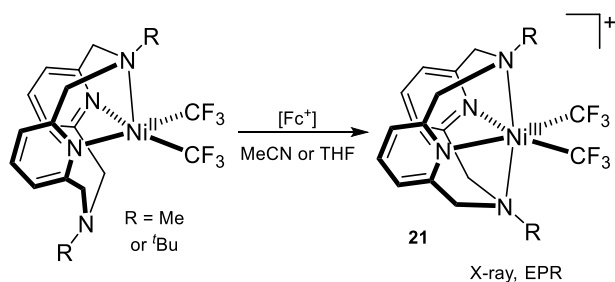
Mirica and co-workers published in 2014 a series of Ni^{III}(aryl)halide complexes stabilized by the tetradentate ligand *N,N'*-di-*tert*-butyl-2,11-diaza[3,3](2,6)pyridophane (Scheme 1.14). The Ni^{III}(aryl)halide complex **19** is stable at low temperature yet undergoes rapid C–halide bond formation at room temperature (54%). The Ni^{III}(aryl)halide complex also undergoes a rapid transmetalation reaction with Grignard reagents to yield a detectable Ni^{III}(aryl)alkyl complex **20**, followed by C–C bond formation at RT (48%).²⁷

Scheme 1.14 Synthesis and reactivity of the Ni^{III}(aryl)halide and Ni^{III}(aryl)alkyl complexes by Mirica and co-workers in 2014.



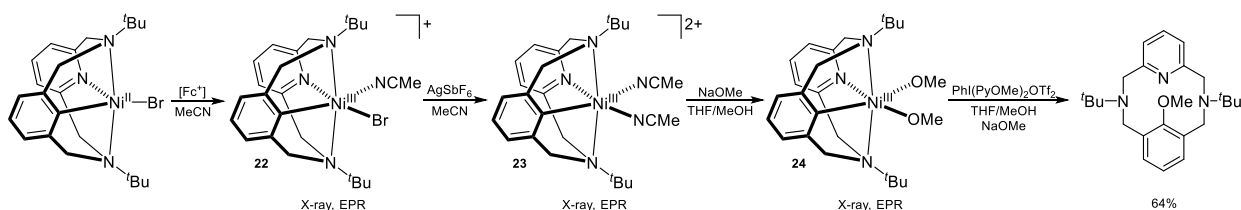
Mirica and co-workers published in 2015 the synthesis of two stable organometallic Ni^{III} complexes that contain two trifluoromethyl ligands and are supported by tetradentate N-donor ligands ^RN₄ (R = Me or *t*Bu) (Scheme 1.15). Interestingly, the corresponding Ni^{II} precursors undergo facile oxidation, including aerobic oxidation to generate the Ni^{III} complexes **21**. Unlike most other organometallic Ni^{III} complexes, complexes **21** are indefinitely stable at room temperature under N₂. Heating complexes **21** at 80 °C for 24 hours or photolysis with visible light at room temperature produces only trace amounts of the deposition products CF₃H and C₂F₆.²⁸

Scheme 1.15 Synthesis of stable bis(trifluoromethyl)nickel(III) complexes supported by a tetradentate pyridinophane ligand.



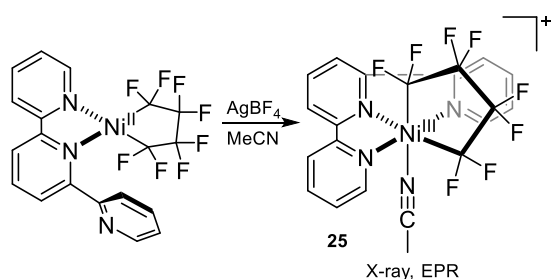
Mirica and co-workers reported in 2015 a synthesis of several Ni^{III} complexes supported by a modified tetradentate pyridinophane ligand containing one phenyl group (Scheme 1.16). Starting from the Ni^{II} precursor, one equivalent of oxidant is added to generate the Ni^{III}(MeCN)Br complex **22**. Subsequently, silver hexafluoroantimony was added to abstract the bromide and give the Ni^{III}-disolvento complex **23**, which is a room-temperature stable dicationic complex. The Ni^{III}-dimethoxide species **24**, can be synthesized and undergoes aryl methoxylation that is favored by addition of the PhI(PyOMe)₂OTf₂ oxidant, the possible formation of a Ni^{IV} intermediate can be invoked. Further studies show that when the oxidant is added, the proposed Ni^{IV} species is too unstable to observe and rapidly undergoes reductive elimination.²⁹

Scheme 1.16 Synthesis of a several of Ni^{III} complexes supported by a modified tetradentate pyridinophane ligand containing one phenyl group.



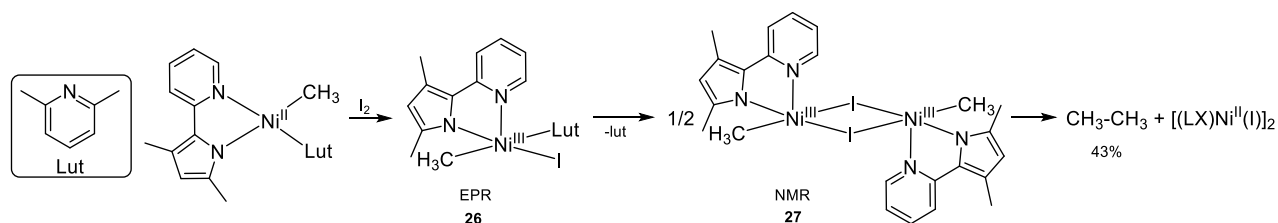
Vicic and co-workers reported the oxidation of $(\text{tpy})\text{Ni}^{\text{II}}(\text{C}_4\text{F}_8)$ (tpy = terpyridine) in 2015 by using the $[\text{C}_4\text{F}_8]$ ligand. The oxidation was performed with silver tetrafluoroborate to obtain the desired Ni^{III} complex **25** (Scheme 1.17). **25** has an octahedral nickel center where the terpyridine ligand binds in a κ^3 formation. The nickel-nitrogen bonds *trans* to the fluoroalkyl ligands were found to be much shorter than the nickel-nitrogen bonds that were *cis* to the fluoroalkyl groups by about 0.2 Å.³⁰

Scheme 1.17 Oxidation of $(\text{tpy})\text{Ni}^{\text{II}}(\text{C}_4\text{F}_8)$ complex, leading to a stable Ni^{III} complex reported by Vicic and co-workers in 2015.



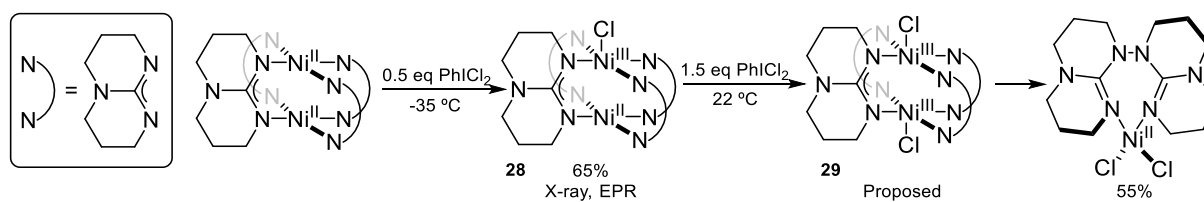
In 2016, Diao and co-workers proposed a square pyramidal Ni^{III} alkyl-complex **26** stabilized by bidentate, anionic ligand 3,5-dimethyl-2-(2-pyridyl)pyrrole. The unstable intermediate is thought to form an iodide bridged Ni^{III} dimer **27**, which undergoes rapid reductive elimination to form ethane in 43% yield (Scheme 1.18).³¹

Scheme 1.18 Synthesis of a square pyramidal Ni^{III} alkyl-complex and its reactivity.



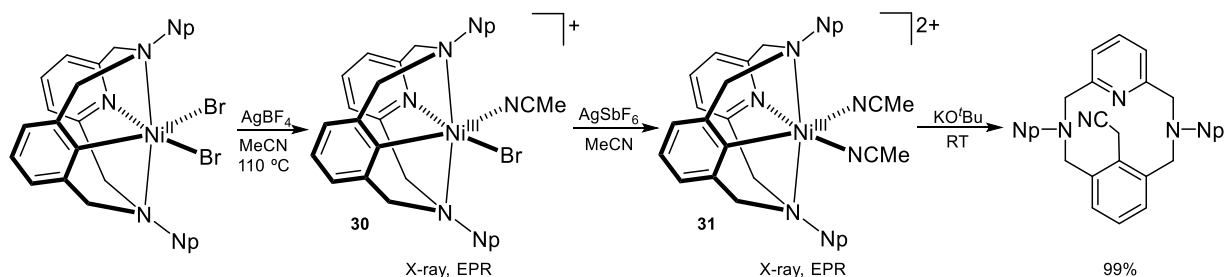
In 2016 Diao and co-workers presented a mixed valent Ni^{II}/Ni^{III} complex **28** stabilized by four triazabicyclodecene (TBD) nitrogen ligands. The Ni centers adopt a square planar and square pyramidal geometry, respectively. Attempts to oxidize **28** with 1.5 eq PhICl₂ did not produce the high-valent dimer complex **29**. However, the proposed intermediate **29** promotes ligand functionalization of two TBD ligands with N-N coupling, which is isolated as a new Ni^{II} complex in 55% yield (Scheme 1.19).³²

Scheme 1.19 N-N bond formation at Ni^{III} dimer published by Diao and co-workers in 2016.



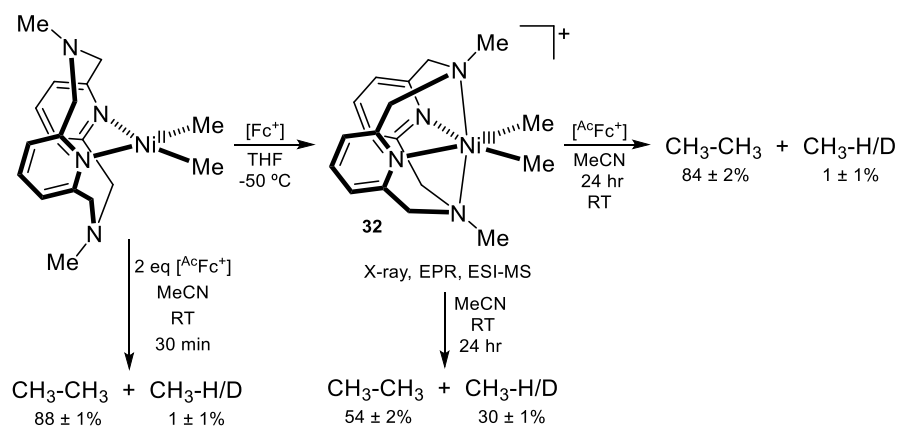
In 2016, Mirica and co-workers subsequently published a series of Ni^{III} complexes **30** and **31** that perform aromatic cyanoalkylation (Scheme 1.20). The synthesis of the Ni^{III} complexes is relatively similar to the paper published by Mirica et al. in 2015. The difference is that the axial nitrogens contain a neopentyl group instead of a *t*-butyl group. Base was added to the Ni^{III}-solvento complex **31** at room temperature to obtain the cyanoalkylated product. Regioselective α -cyanoalkylation was observed with various nitrile substrates to generate secondary and tertiary nitriles.³³

Scheme 1.20 Synthesis and reactivity of Ni^{III} complexes stabilized by a modified tetradentate pyridinophane ligand.



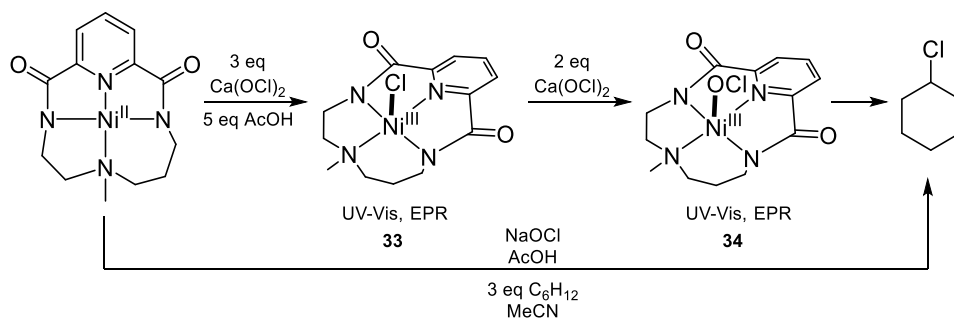
In 2016, Mirica and co-workers synthesized the first isolated Ni^{III}-dialkyl complex stabilized by the *N,N'*-dimethyl-2,11-diaz[3.3](2,6)pyridinophane ligand (Scheme 1.21). The Ni^{III} complex **32** was shown to generate ethane in 54% yield over 24 hours at room temperature. However, the addition of one equivalent of oxidant to the Ni^{III} complex **32** led to clean formation of ethane in 84% yield, while addition of two equivalent oxidant to the Ni^{II} precursor generated an almost quantitative amount of ethane within 30 min at room temperature (88%). These results suggest that access to a Ni^{IV} intermediate should lead to fast reductive elimination and C–C bond formation.³⁴

Scheme 1.21 Synthesis and reactivity of the Ni^{III}-dialkyl complex reported by Mirica and co-workers in 2016.



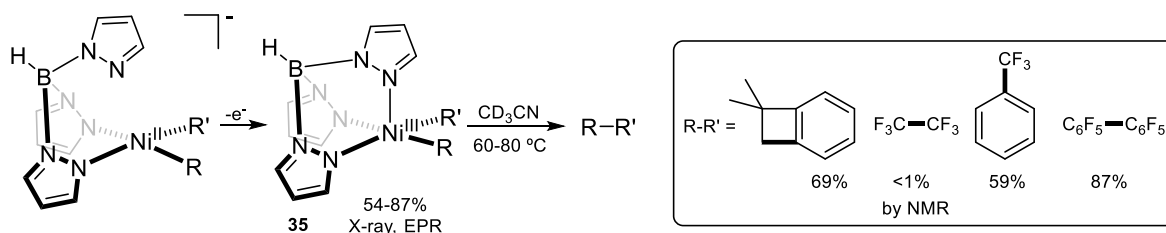
In 2016, Company and co-workers observed an active Ni^{III}-OCl intermediate stabilized by tetradentate macrocyclic ligand composed of two amidate, one pyridine, and one aliphatic amine groups (Scheme 1.22). Oxidation of the Ni^{II} complex by addition of 3 equivalents of Ca(OCl)₂ leads to the formation of square pyramidal complex **33**. However, 2 more equivalents of Ca(OCl)₂ lead to the formation of perchlorate Ni^{III} complex **34**, which is thought to be active intermediate in the catalytic oxidation of cyclohexane.³⁵

Scheme 1.22 Catalytic oxidation of cyclohexane through a Ni^{III}-OCl intermediate.



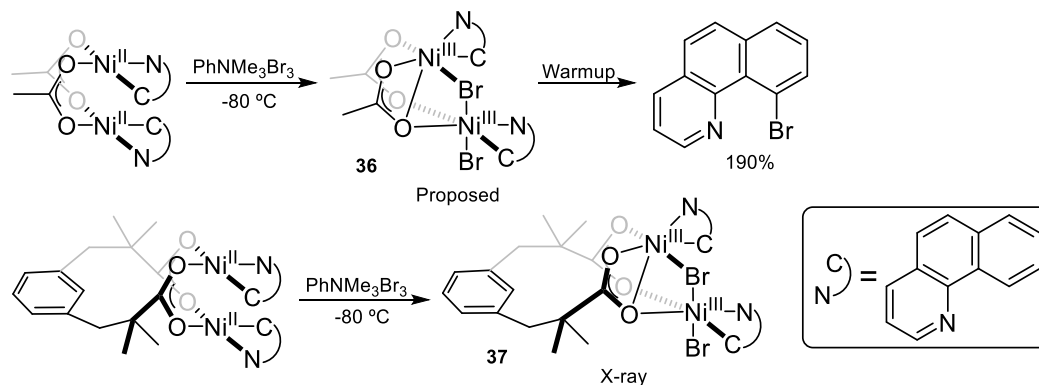
In 2016, Sanford and co-workers isolated a series of Ni^{III} complexes **35**, stabilized by tridentate trispyrazolylborate anionic ligand and different C(sp²), C(sp³), and CF₃ ligands. Upon heating at mild temperatures, these complexes undergo reductive elimination followed by C–C bond formation of the auxiliary ligands in moderate yields (Scheme 1.23).³⁶

Scheme 1.23 Alkyl-alkyl and alkyl-aryl C–C bond formation and trifluoromethylation using an isolated Ni^{III} complex stabilized by scorpionate borate ligand and C(sp²), C(sp³), and CF₃ ligands.



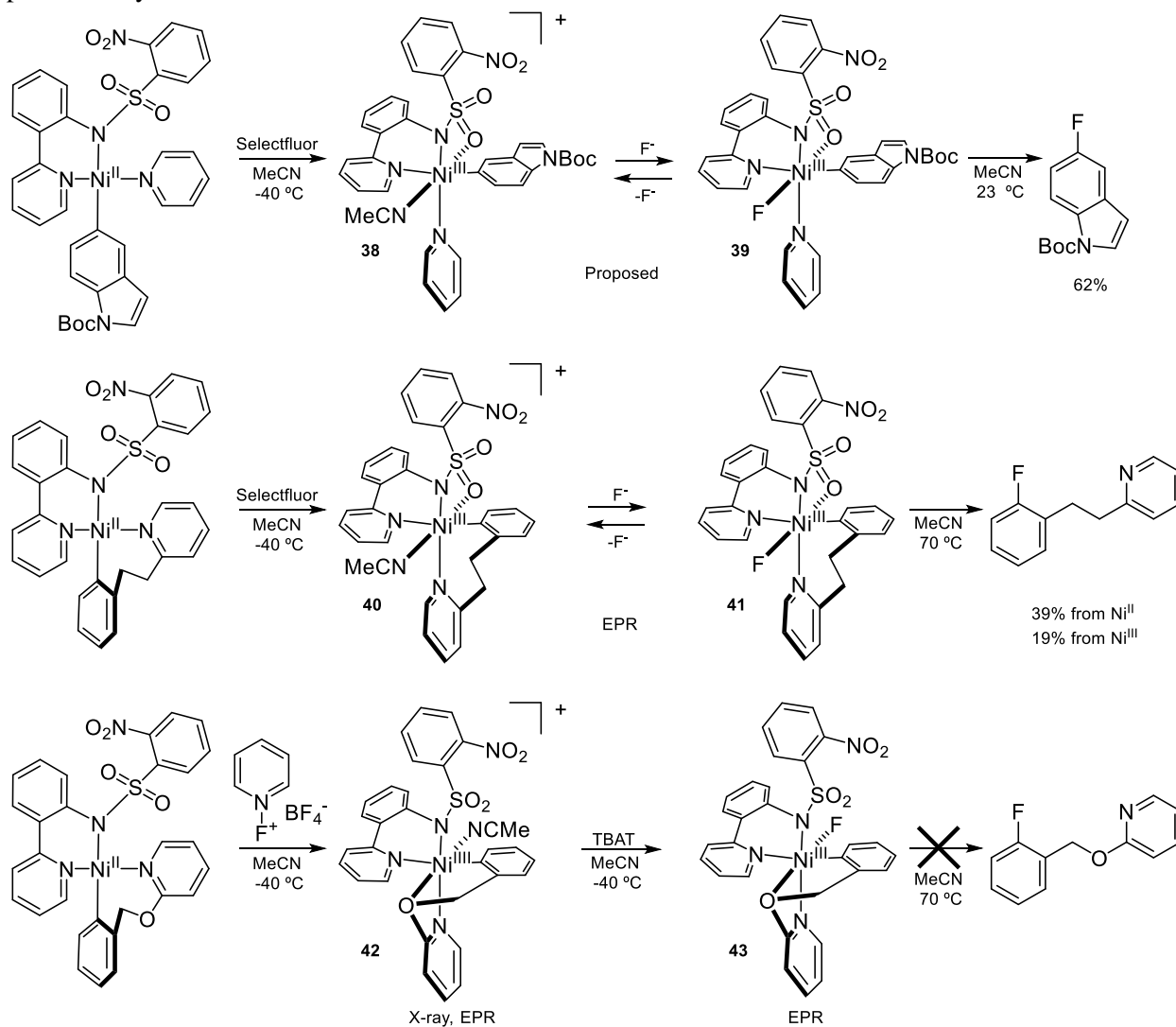
In 2017, Diao and co-workers observed two high-valent Ni^{III}/Ni^{III} dimers (Scheme 1.24) stabilized by benzoquinoline and carboxylate ligands. The Ni centers adopt a pseudo-octahedral structure and are bridged by a bromide atom. The warming of complex **36** leads to reductive elimination and C–Br bond formation of 10-bromobenzoquinoline in 190% yield. A stable Ni^{III}-Ni^{III} dimer **37** was confirmed by X-ray, however, no C–Br bond formation was observed.³⁷

Scheme 1.24 C–Br bond formation using a Ni^{III} dimer supported by carboxylate and benzoquinoline ligands.



In 2017, Ritter and co-workers showed C–F bond formation from aryl-Ni^{III} fluorides stabilized by bidentate ligand (2-(2-pyridinyl)phenyl-2-nitrobenzenesulfonamide) with an octahedral geometry (Scheme 1.25). Addition of selectfluor to complex the first two Ni^{II} complexes promotes C–F bond formation of corresponding products in 62% and 39% yield, respectively. The high-valent Ni complexes **38** and **39** could not be isolated but were proposed and in the case of **40** and **41** were detected by EPR. In contrast, oxidation of the last Ni^{II}, which contains a strong rigid coordinating oxygen atom within the aryl moiety, leads to the isolation of stable complex **42**. Although the Ni^{III}-F complex **43** was also detected by EPR, C–F bond formation was not detected.³⁸

Scheme 1.25 C–F bond formation with aryl Ni^{III} fluoride complexes and active Ni^{III} species observed published by Ritter and co-workers in 2017.

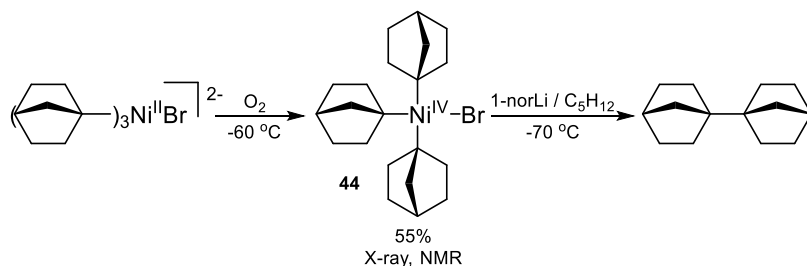


1.3 Organometallic Ni^{IV} Complexes

In 2003, Dimitrov and co-workers oxidized the starting material with air at -60 °C to give a quasi-tetrahedral Ni^{IV} complex **44** stabilized by four anionic ligands (three 1-norboryl ligands and halide atom) (Scheme 1.26). Addition of one extra equivalent of 1-norborylLi to **44**, attempting to remove the halide ligand to isolate a homoleptic Ni^{IV} complex was unsuccessful. However, this

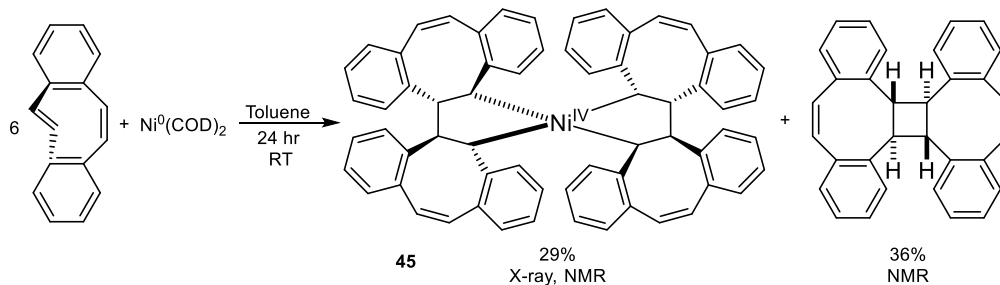
resulted in the detection of dinorbornane, obtained from C–C bond formation of two 1-norboryl ligands.³⁹

Scheme 1.26 Formation of a quasi-tetrahedral Ni^{IV} complex that leads to C–C bond formation published by Dimitrov and co-workers in 2003.



Turro and co-workers published in 2009 a stable tetraalkyl Ni^{IV} complex **45** stabilized by two (5Z,11E)-dibenzo[a,e]cyclooctatetraene in a distorted tetrahedral fashion (Scheme 1.27). Interestingly the high-valent Ni^{IV} complex doesn't exhibit any reactivity; the complex is air-stable and can be heated to above 290 °C before any decomposition is observed.⁴⁰

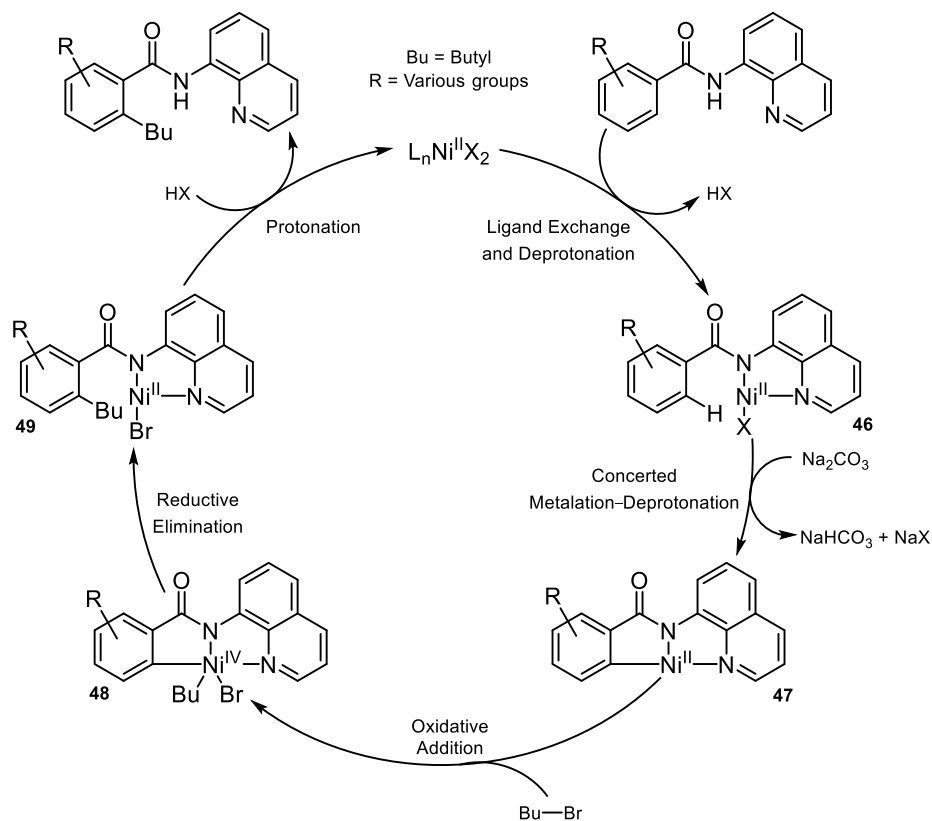
Scheme 1.27 Synthesis of a stable tetraalkyl Ni^{IV} complex published by Turro and co-workers.



It is important to mention that starting in 2013, Chatani and co-workers proposed a nickel-catalyzed alkylation and arylation mechanisms involving C–H bonds of benzamides and acrylamides. The proposed mechanism proposes that the first step is a ligand exchange followed by the coordination of the amide to the Ni center generating **46** and HX (Scheme 1.28). **47** forms probably via a concerted metalation-deprotonation mechanism, which then undergoes an oxidative

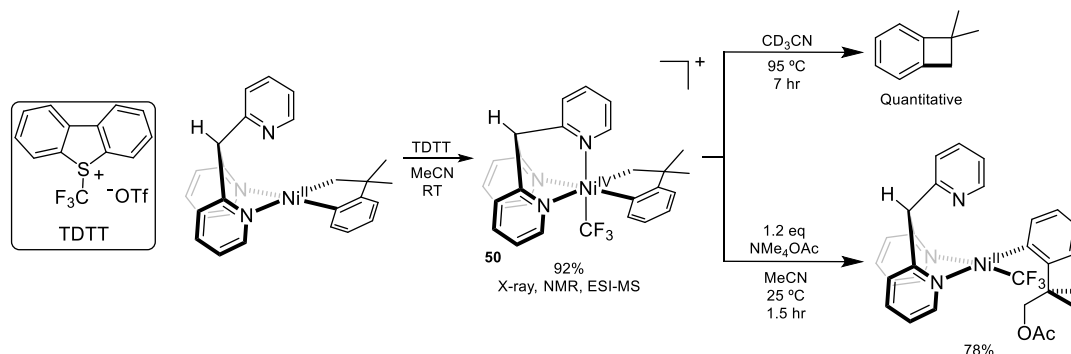
addition of butyl-bromide to generate **48**. The Ni^{IV} intermediate goes through a reductive elimination to form **49**, which then gets protonated to form the alkylation product and regenerate the Ni^{II} complex. The catalytic system takes advantage of chelation assistance by an 8-aminoquinoline moiety, which supports the nickel complex.⁴¹⁻⁴²

Scheme 1.28 Proposed nickel-catalyzed alkylation mechanism involving high-valent nickel intermediates by Chatani and co-workers.



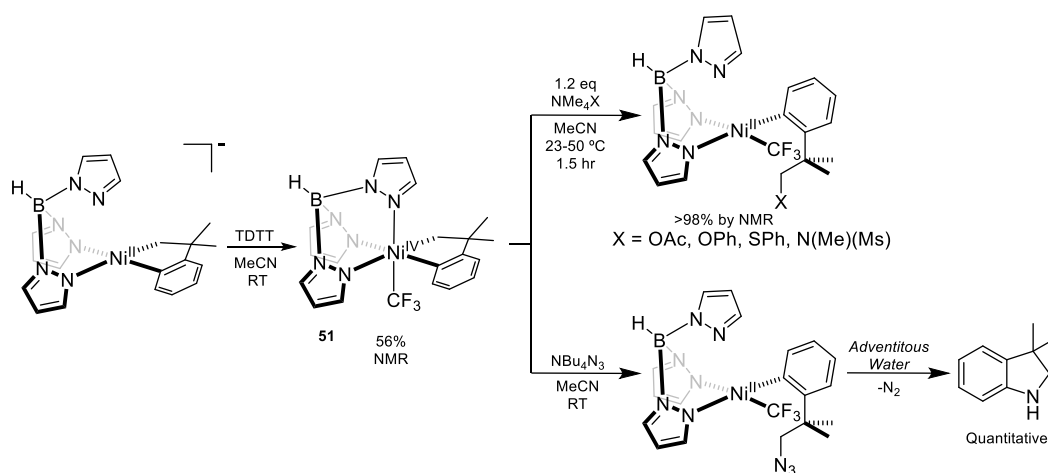
In 2015, Sanford and co-workers isolated an octahedral Ni^{IV} center stabilized by a neutral scorpionate tris(2-pyridyl)methane, cyclic alky/aryl C-donor ligand (-CH₂CMe₂-*o*-C₆H₄-) and anionic trifluoromethyl ligands, complex **50**. A quantitative amount of benzocyclobutane was detected upon heating of **50** for seven hours, indicating reductive elimination and C-C bond formation. On the other hand, addition of 1.2 equivalents of acetate resulted in C(sp³)-O bond formation in 78% yield (Scheme 1.29).

Scheme 1.29 C(sp²)-C(sp³) and C(sp³)-X bond formation using isolated tris(2-pyridyl)methane Ni^{IV}-cycloneophyl(CF₃) complexes.



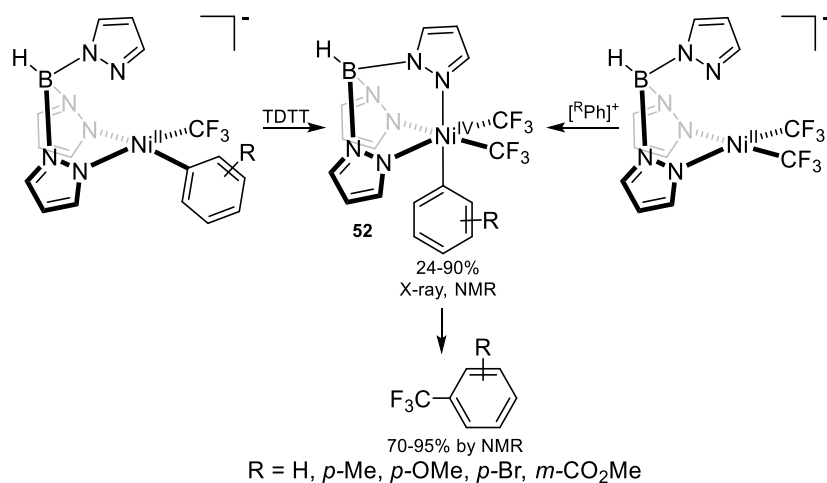
Similarly, the anionic scorpionate ligand, trispyrazolylborate also stabilizes a Ni^{IV} center complex **51**, but does not undergo reductive elimination of benzocyclobutane. Addition of 1.2 equivalents of different X nucleophiles also result in C(sp³)-X bond formation in 98% yields (Scheme 1.30). However, addition of nucleophilic azide results in the slow formation of indoline in quantitative yields after Ni^{II} is exposed to adventitious water.⁴³ In addition, the Ni^{III} and Ni^{IV} complexes supported by the trispyrazolylborate ligand were isolated in 2017 with different axial ligands.⁴⁴

Scheme 1.30 C(sp³)-X bond formation using in-situ trispyrazolylborate Ni^{IV}-cycloneophyl(CF₃) complexes.



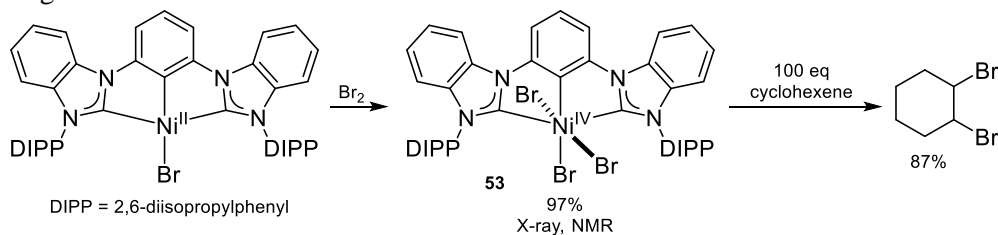
In 2015, Sanford and co-workers tested the reactivity of alkyl-aryl Ni^{IV} complexes **52** stabilized by tridentate trispyrazolylborate anionic ligand. Upon heating, these complexes undergo reductive elimination and trifluoroalkylation of aryl groups with different electronic properties (Scheme 1.31).⁴³

Scheme 1.31 Trifluoromethylation of different aryl substrates by using a trispyrazolylborate Ni^{IV}-aryl(CF₃)₂ complexes.



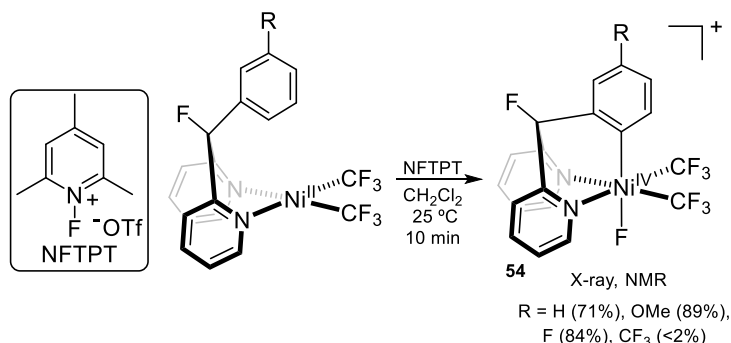
In 2016, Fout and co-workers isolated an octahedral Ni^{IV} structure, **53**, supported by anionic, tridentate bis(diisopropylphenyl-benzimidazol-2-ylidene)phenyl pincer ligand and three bromide anionic ligands. Complex **53** is obtained from the addition of Br₂ to its Ni^{II} counterpart. The complex was then used as a bromide transfer reagent for bromination of different organic substrates including styrene, cyclohexene, mesitylmagnesium bromide, and lithium hexamethyldisilazide in 50-87% yield (Scheme 1.32).⁴⁵

Scheme 1.32 Bromination of alkenes using an isolated Ni^{IV} tribromide complex as a bromide transfer reagent.



In 2017, Sanford and co-workers probed intramolecular C-H activation by using scorpionate ligand bis(2-pyridyl)(2-^Rphenyl)-fluoromethane as a model system. Oxidation of the Ni^{II} complex under mild conditions resulted in C_{ipso}-H activation of the aryl ring on the ligand. A range of bis(2-pyridyl)(2-^Rphenyl)-fluoromethaneNi^{IV}F(CF₃)₂ octahedral complexes, **54**, were isolated in good yields (Scheme 1.33).⁴⁶

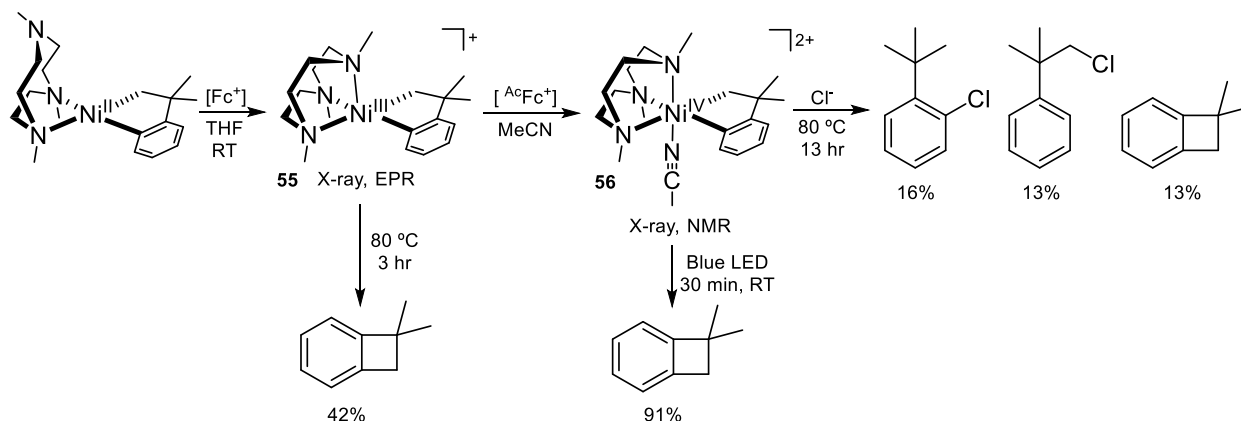
Scheme 1.33 Oxidatively induced C-H activation of bis(2-pyridyl)(2-^Rphenyl)-fluoromethane Ni-aryl(CF₃)₂ complexes.



Mirica and co-workers reported in 2017 the first organometallic nickel complexes supported by a triazacyclononane (Me₃tacn) and the cyclic alky/aryl C-donor ligand (-CH₂CMe₂-*o*-C₆H₄-) (Scheme 1.34). A combination of these two ligands allowed for the synthesis and isolation of the organometallic Ni^{III}, **55** and Ni^{IV}, **56** complexes. With these complexes in hand a variety of reactivity experiments was tested. Heating the Ni^{III} complex for three hours at 80 °C, 42% of C-C bond formation was observed. When performing the same reaction with the Ni^{IV}

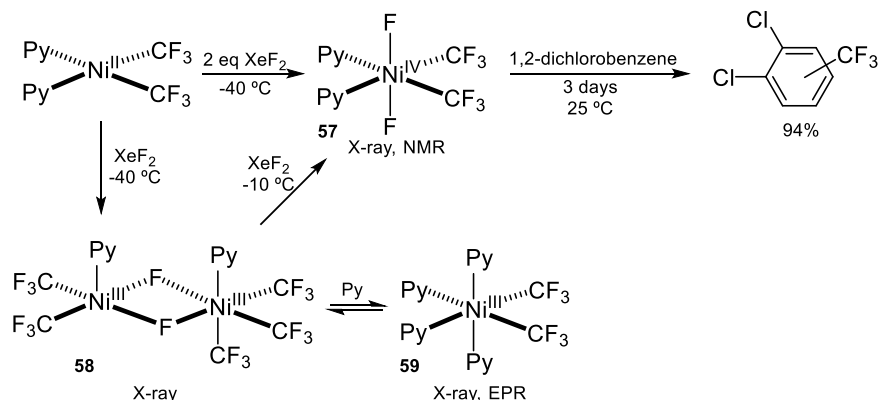
complex instead of the Ni^{III}, 34% of C–C bond formation was observed. Interestingly, shining a blue LED light on the Ni^{IV} complex leads to rapid C–C bond formation with yields up to 91%. Reactivity of the Ni^{IV} complex in the presence of a nucleophile leads to a decrease of C–C product and observation of 29% combined yield for C–heteroatom bond formation.⁴⁷

Scheme 1.34 Synthesis of (Me₃tacn)Ni(CH₂CMe₂-*o*-C₆H₄) complexes with the corresponding reactivity.



In 2017, Nebra and co-workers showed C–H bond activation and trifluoromethylation of arenes by using a stable octahedral Ni^{IV} complex supported by simple monodentate ligands. Addition of one equivalent of XeF₂ to the Ni^{II} results in the formation of monomeric and dimeric Ni^{III} species, complex **58** and **59**. The active Ni^{IV} species, **57**, was obtained by the addition of second equivalent of XeF₂; this complex can be used for trifluoromethylation of 1,2-dichlorobenzene in 94% yield (Scheme 1.35).⁴⁸

Scheme 1.35 C-H bond activation and trifluoromethylation of 1,2-dichlorobenzene using isolated Ni^{IV} complex supported by simple, monodentate ligands.



1.4 Other High-Valent Ni Complexes

1.4.1 Ni^{III} Structures

Other Ni^{III} complexes that were previously isolated (Figure 1.1). In 1982, Smart and co-workers isolated a Ni^{III}, decamethylnickelocene complex. Oxidation of the Ni^{II} complex with one equivalent of oxidant leads to the formation of cationic species **60**, which is supported by two pentamethylcyclopentadiene ligands.⁴⁹⁻⁵⁰ In 2006 and 2008, Liaw and co-workers isolated a high-valent Ni^{III} species, **61**, stabilized in a distorted trigonal bipyramidal fashion by a trianionic, tetradentate triphenylphosphine-type ligand with thiolate substituents.⁵¹⁻⁵² Using the same ligand framework, Lee and co-workers isolated the first high-valent nickel alkyl (**61**, R = ethyl or methyl) substituted complexes in 2010.⁵³ One year later, Kinoshita and co-workers obtained a high-valent halide bridged Ni^{III} dimer stabilized by tetradentate ligand tris (2-pyridylthio)methanide in 90% yield, **62**.⁵⁴ The dimer slowly transforms into mononuclear **63** (89%), which adopts a distorted trigonal bipyramidal geometry after the ligand isomerizes into bis(2-pyridylthio)(2-thiopyridinium)methyl in solution.⁵⁴ In 2012, although the complex was not isolated, Ray and co-workers observed a trigonal bipyramidal high-valent Ni^{III}-oxo species stabilized by tetradentate

ligand (tris[2-(N-tetramethylguanidyl)ethyl] amine) **64**.⁵⁵ In the same year, Patral and co-workers observed a high-valent Ni^{III} species stabilized in a distorted octahedral fashion by two tridentate ligands N-2-Methylthiophenyl-2'-pyridinecarboxamide, **65**.⁵⁶

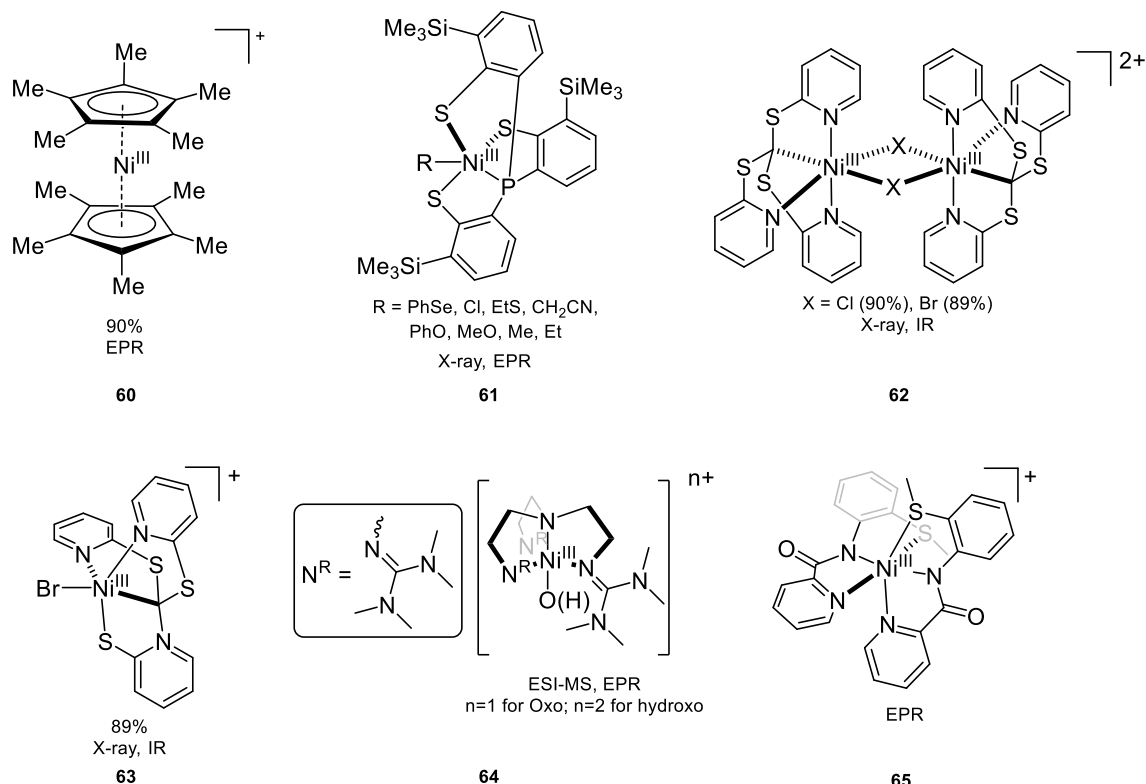


Figure 1.1 Other observed Ni^{III} complexes.

1.4.2 Ni^{IV} Structures

Other Ni^{IV} complexes that were previously isolated (Figure 1.2). Starting with complex **66**, Smart and co-workers published in 1982 an Ni^{IV} decamethylnickelocene complex. The complex was synthesized by oxidizing the Ni^{II} complex with two equivalents of oxidant. The complex is supported by a two pentamethylcyclopentadiene ligands.⁴⁹⁻⁵⁰ In 1994, Klein and co-workers published the first organometallic Ni^{IV} complex, **67**. Complex **67** is stabilized by a chelating acylphenolato dianion, a pair of trans trimethylphosphine, iodide and methyl ligand and adopts an

octahedral geometry.⁵⁷⁻⁵⁸ A few years later Klein and co-workers published in 1997 a new organometallic Ni^{IV} complex, **68**, which also adopted an octahedral geometry. Complex **68** is supported by a pair of trimethylphosphine and a pair of acylphenolate dianion ligands.⁵⁹ In 1995, Gould and co-workers isolated a high-valent Ni^{IV} species, **69**, stabilized in an octahedral fashion by two tridentate ligands, 2,6-diacetylpyridine dioxime.⁶⁰⁻⁶¹ The first silylnickel(IV) complex **70** was isolated in 1999 by Tanka and co-workers. Complex **70** was stabilized by a bis(dimethylphosphino)ethane and two 1,2-disilylbenzene ligands; the complex adopts an octahedral geometry.⁶² In 2004, Saigo and co-workers published a high-valent Ni^{IV} complex **71** which was similar to complex **70**. The big difference between these two complexes is that **71** adopts a distorted trigonal-bipyramidal orientation.⁶³ Ray and co-workers published in 2012 a trigonal bipyramidal high-valent Ni^{IV}-oxo species **72** stabilized by tetradentate ligand (tris[2-(N-tetramethylguanidyl)ethyl] amine) which was observed by ESI-MS.⁵⁵ Finally, the first Ni^{IV} dimer, **73**, was isolated by Browne and co-workers in 2017. The complex was generated by the reaction of its Ni^{II}-tris- μ -chloro bridging counterpart with NaOCl. The high-valent dinuclear Ni^{IV} complex was stabilized by two 1,4,7-trimethyl-1,4,7-triazacyclononane ligands and was bridged by a tris- μ -oxido structure.⁶⁴

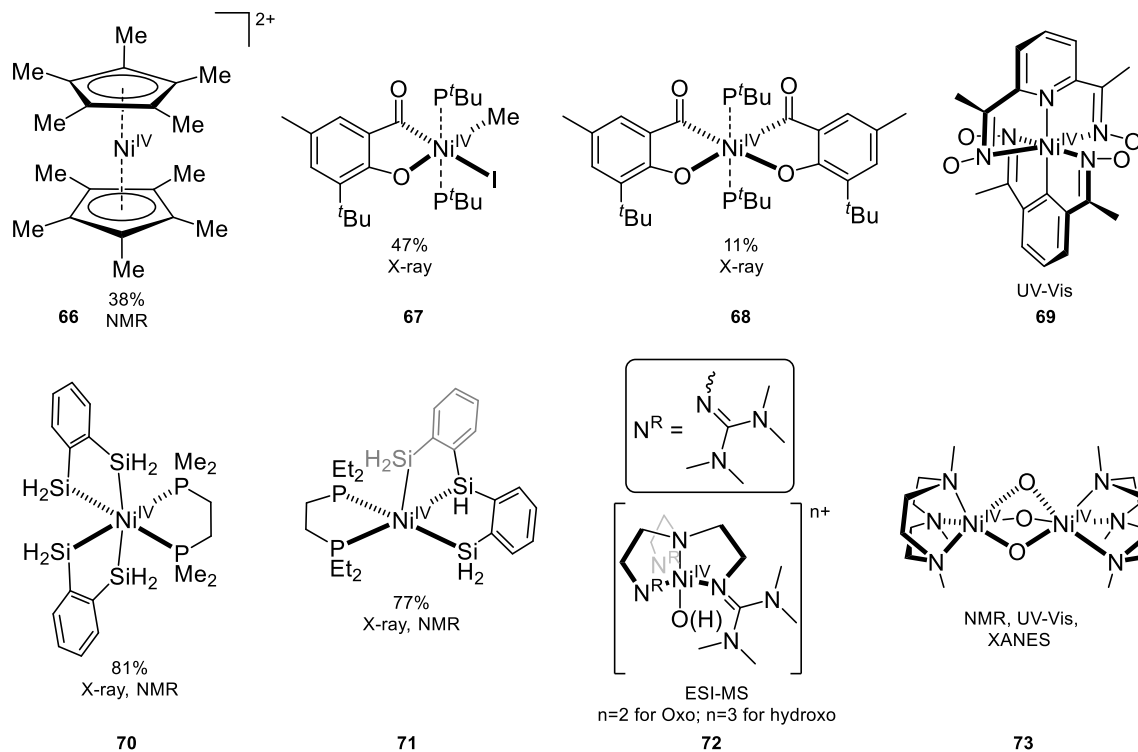


Figure 1.2 Other observed Ni^{IV} complexes.

1.5 Conclusion and Outlook

This chapter provided an overview of the organometallic chemistry of isolated Ni^{III} and Ni^{IV} complexes and the proposed involvement of Ni^{III} and Ni^{IV} intermediates in various organometallic transformations. The importance of high-valent nickel chemistry is to gain a better understanding of the catalytic cycles in order to employ more effective catalysts for a range of synthetically useful organic transformations such as C-H functionalization, transmetalation and C-C and C-heteroatom bond formation reactions at the Ni^{II} stage. Although most C-C and C-heteroatom coupling reactions that are catalyzed by nickel are mainly involved in a Ni^{0/II} oxidation-state change, the past decade has shown a growing amount of evidence for the participation of Ni^{III} and Ni^{IV} intermediates in the catalytic cycles.

The first mononuclear organometallic Ni^{III} complex was observed in 1978 but it wasn't until 1982 that a different high-valent organometallic Ni^{III} complex was isolated. No reactivity was shown for the first isolated Ni^{III} complex. Starting in 1995, more reactivity was being observed with the proposing Ni^{III} intermediates. Furthermore, mononuclear Ni^{III} intermediates have been observed during oxidatively induced C–C bond elimination from a Ni^{II} precursors. Additionally, the involvement of mononuclear Ni^{III} intermediates has been proposed in a wide range of C–C and C–heteroatom bond formation reactions.

The first isolated Ni^{IV} complex was in 1982 but it wasn't until 2003 when the first C–C bond formation reactivity from a high-valent Ni^{IV} organometallic complexes was observed. More proposed catalytic cycles involving Ni^{IV} intermediates have become more accepted recently. In addition, dinuclear Ni^{III} complexes that are not stabilized by a Ni–Ni bond and their role in catalytic processes have also been reported. Most importantly, the interconversion between Ni^{III} and Ni^{IV} complexes has been demonstrated, suggesting that it is not always possible to unambiguously confirm the oxidation state.

Finally, we envision that in the near future, the chemistry of the less-common oxidation states of Ni will lead to novel organometallic reactions that involve one and two-electron oxidation processes. This includes higher yielding C–C and C–heteroatom bond formation reactions and a better understanding of the catalytic cycles involving high-valent Ni species. More specifically, we anticipate the ability of Ni^{IV} complexes to engage in selective C(sp³) and C(sp²)–heteroatom coupling reactions. A key challenge for achieving this objective will be to define a class of oxidants and supporting ligands that selectively access the Ni^{IV} intermediate rather than the more common Ni^{III}. This should enable the design of catalytic sequences in which a Ni–carbon bond forming step is coupled with oxidation and C–heteroatom coupling via Ni^{II/IV} catalysis.

1.6 Acknowledgements

I would like to thank Leonel Griego in helping to write this chapter, with equal contribution by each author.

1.7 References

1. Hu, X., Nickel-catalyzed cross coupling of non-activated alkyl halides: a mechanistic perspective. *Chem. Sci.* **2011**, *2* (10), 1867.
2. Sivaramakrishna, A.; Clayton, H. S.; Muralikrishna, U., Synthesis, structure, chemistry, and applications of tetravalent nickel complexes. *J. Coord. Chem.* **2011**, *64* (8), 1309.
3. Vabre, B.; Spasyuk, D. M.; Zargarian, D., Impact of Backbone Substituents on POCOP-Ni Pincer Complexes: A Structural, Spectroscopic, and Electrochemical Study. *Organometallics* **2012**, *31* (24), 8561.
4. Zargarian, D.; Castonguay, A.; Spasyuk, D. M., ECE-Type Pincer Complexes of Nickel. *Top. Organomet. Chem.* **2013**, *40*, 131.
5. Silva, F. C. S. E.; Tierno, A. F.; Wengryniuk, S. E., Hypervalent Iodine Reagents in High Valent Transition Metal Chemistry. *Molecules* **2017**, *22* (5).
6. Tsou, T. T.; Kochi, J. K., Reductive Coupling of Organometals Induced by Oxidation - Detection of Metastable Paramagnetic Intermediates. *J. Am. Chem. Soc.* **1978**, *100* (5), 1634.
7. Grove, D. M.; van Koten, G.; Zoet, R.; Murrall, N. W.; Welch, A. J., Unique stable organometallic nickel(III) complexes; syntheses and the molecular structure of $[\text{Ni}[\text{C}_6\text{H}_3(\text{CH}_2\text{NMe}_2)_2\text{-}2,6]\text{I}_2]$. *J. Am. Chem. Soc.* **1983**, *105* (5), 1379.
8. Grove, D. M.; Van Koten, G.; Mul, P.; Van der Zeijden, A. A. H.; Terheijden, J.; Zoutberg, M. C.; Stam, C. H., Arylnickel(III) species containing nitrogen trioxide, nitrogen dioxide, and

thiocyanate ligands. ESR data and the x-ray crystal structure of hexacoordinate (pyridine)bis(thiocyanato)[o,o'-bis{(dimethylamino)methyl}phenyl]nickel(III). *Organometallics* **1986**, 5 (2), 322.

9. Grove, D. M.; Van Koten, G.; Mul, P.; Zoet, R.; Van der Linden, J. G. M.; Legters, J.; Schmitz, J. E. J.; Murrall, N. W.; Welch, A. J., Syntheses and characterization of unique organometallic nickel(III) aryl species. ESR and electrochemical studies and the x-ray molecular study of square-pyramidal $[\text{Ni}\{\text{C}_6\text{H}_3(\text{CH}_2\text{NMe}_2)_2\text{-o,o'}\}\text{I}_2]$. *Inorg. Chem.* **1988**, 27 (14), 2466.

10. Grove, D. M.; Vankoten, G.; Ubbels, H. J. C.; Zoet, R.; Spek, A. L., Organonickel(II) Complexes of the Terdentate Monoanionic Ligand-Omicron,Omicron'-Bis[(Dimethylamino)Methyl]Phenyl (N-C-N) - Syntheses and the X-Ray Crystal-Structure of the Stable Nickel(II) Formate $[\text{Ni}(\text{N-C-N})\text{O}_2\text{CH}]$. *Organometallics* **1984**, 3 (7), 1003.

11. van de Kuil, L. A.; Grove, D. M.; Gossage, R. A.; Zwikker, J. W.; Jenneskens, L. W.; Drenth, W.; van Koten, G., Mechanistic aspects of the Kharasch addition reaction catalyzed by organonickel(II) complexes containing the monoanionic terdentate arlydiamine ligand system $[\text{C}_6\text{H}_2(\text{CH}_2\text{NMe}_2)(2)\text{-}2,6\text{-R-}4]$. *Organometallics* **1997**, 16 (23), 4985.

12. Cloutier, J. P.; Zargarian, D., Functionalization of the Aryl Moiety in the Pincer Complex $(\text{NCN})(\text{NiBr}_2)\text{-Br-III}$: Insights on Ni-III-Promoted Carbon-Heteroatom Coupling. *Organometallics* **2018**, 37 (9), 1446.

13. van de Kuil, L. A.; Veldhuizen, Y. S. J.; Grove, D. M.; Zwikker, J. W.; Jenneskens, L. W.; Drenth, W.; Smeets, W. J. J.; Spek, A. L.; van Koten, G., A novel enantiopure proline-based organonickel(III) halide monocation with a pentadentate C,N₂,O₂-bonded bis(ortho-chelating) arlydiamine ligand. *J. Organomet. Chem.* **1995**, 488 (1-2), 191.

14. Koo, K.; Hillhouse, G. L., Carbon-Nitrogen Bond Formation by Reductive Elimination from Nickel(II) Amido Alkyl Complexes. *Organometallics* **1995**, *14* (9), 4421.
15. Han, R. Y.; Hillhouse, G. L., Carbon-oxygen reductive-elimination from nickel(II) oxametallacycles and factors that control formation of ether, aldehyde, alcohol, or ester products. *J. Am. Chem. Soc.* **1997**, *119* (34), 8135.
16. Lin, B. L.; Clough, C. R.; Hillhouse, G. L., Interactions of aziridines with nickel complexes: Oxidative-addition and reductive-elimination reactions that break and make C-N bonds. *J. Am. Chem. Soc.* **2002**, *124* (12), 2890.
17. Kogut, E.; Wiencko, H. L.; Zhang, L. B.; Cordeau, D. E.; Warren, T. H., A terminal Ni(III)-imide with diverse reactivity pathways. *J. Am. Chem. Soc.* **2005**, *127* (32), 11248.
18. Pandarus, V.; Zargarian, D., New pincer-type diphosphinito (POCOP) complexes of Ni(II) and Ni(III). *Chemical communications (Cambridge)* **2007**, (9), 978.
19. Spasyuk, D. M.; Zargarian, D.; van der Est, A., New POCN-Type Pincer Complexes of Nickel(II) and Nickel(III). *Organometallics* **2009**, *28* (22), 6531.
20. Castonguay, A.; Beauchamp, A. L.; Zargarian, D., Preparation and Reactivities of PCP-Type Pincer Complexes of Nickel. Impact of Different Ligand Skeletons and Phosphine Substituents. *Organometallics* **2008**, *27* (21), 5723.
21. Iluc, V. M.; Miller, A. J. M.; Anderson, J. S.; Monreal, M. J.; Mehn, M. P.; Hillhouse, G. L., Synthesis and Characterization of Three-Coordinate Ni(III)-Imide Complexes. *J. Am. Chem. Soc.* **2011**, *133* (33), 13055.
22. Jones, G. D.; McFarland, C.; Anderson, T. J.; Vicic, D. A., Analysis of key steps in the catalytic cross-coupling of alkyl electrophiles under Negishi-like conditions. *Chem. Comm.* **2005**, (33), 4211.

23. Klein, A.; Vivic, D. A.; Biewer, C.; Kieltsch, I.; Stirnat, K.; Hamacher, C., Oxidative Cleavage of CH₃ and CF₃ Radicals from BOXAM Nickel Complexes. *Organometallics* **2012**, *31* (15), 5334.
24. Zhang, C. P.; Wang, H.; Klein, A.; Biewer, C.; Stimat, K.; Yarnaguchi, Y.; Xu, L.; Gomez-Benitez, V.; Vivic, D. A., A Five-Coordinate Nickel(II) Fluoroalkyl Complex as a Precursor to a Spectroscopically Detectable Ni(III) Species. *J. Am. Chem. Soc.* **2013**, *135* (22), 8141.
25. Lipschutz, M. I.; Yang, X.; Chatterjee, R.; Tilley, T. D., A Structurally Rigid Bis(amido) Ligand Framework in Low-Coordinate Ni(I), Ni(II), and Ni(III) Analogues Provides Access to a Ni(III) Methyl Complex via Oxidative Addition. *J. Am. Chem. Soc.* **2013**, *135*, 15298.
26. Lipschutz, M. I.; Tilley, T. D., Carbon-Carbon Cross-Coupling Reactions Catalyzed by a Two-Coordinate Nickel(II)-Bis(amido) Complex via Observable Ni-I, Ni-II, and Ni-III Intermediates. *Angew. Chem., Int. Ed.* **2014**, *53* (28), 7290.
27. Zheng, B.; Tang, F.; Luo, J.; Schultz, J. W.; Rath, N. P.; Mirica, L. M., Organometallic Nickel(III) Complexes Relevant to Cross-Coupling and Carbon-Heteroatom Bond Formation Reactions. *J. Am. Chem. Soc.* **2014**, *136* (17), 6499.
28. Tang, F. Z.; Rath, N. P.; Mirica, L. M., Stable bis(trifluoromethyl)nickel(III) complexes. *Chem. Comm.* **2015**, *51* (15), 3113.
29. Zhou, W.; Schultz, J. W.; Rath, N. P.; Mirica, L. M., Aromatic Methoxylation and Hydroxylation by Organometallic High-Valent Nickel Complexes. *J. Am. Chem. Soc.* **2015**, *137* (24), 7604.
30. Yu, S.; Dudkina, Y.; Wang, H.; Kholin, K. V.; Kadirov, M. K.; Budnikova, Y. H.; Vivic, D. A., Accessing perfluoroalkyl nickel(II), (III), and (IV) complexes bearing a readily attached [C₄F₈] ligand. *Dalton Trans.* **2015**, *44* (45), 19443.

31. Xu, H. W.; Diccianni, J. B.; Katigbak, J.; Hu, C. H.; Zhang, Y. K.; Diao, T. N., Bimetallic C-C Bond-Forming Reductive Elimination from Nickel. *J. Am. Chem. Soc.* **2016**, *138* (14), 4779.
32. Diccianni, J. B.; Hu, C. H.; Diao, T. N., N-N Bond Forming Reductive Elimination via a Mixed-Valent Nickel(II)-Nickel(III) Intermediate. *Angew. Chem., Int. Ed.* **2016**, *55* (26), 7534.
33. Zhou, W.; Zheng, S. A.; Schultz, J. W.; Rath, N. P.; Mirica, L. M., Aromatic Cyanoalkylation through Double C-H Activation Mediated by Ni(III). *J. Am. Chem. Soc.* **2016**, *138* (18), 5777.
34. Schultz, J. W.; Fuchigami, K.; Zheng, B.; Rath, N. P.; Mirica, L. M., Isolated Organometallic Nickel(III) and Nickel(IV) Complexes Relevant to Carbon-Carbon Bond Formation Reactions. *J. Am. Chem. Soc.* **2016**, *138* (39), 12928.
35. Corona, T.; Draksharapu, A.; Padamati, S. K.; Gamba, I.; Martin-Diaconescu, V.; Acuna-Pares, F.; Browne, W. R.; Company, A., Rapid Hydrogen and Oxygen Atom Transfer by a High-Valent Nickel-Oxygen Species. *J. Am. Chem. Soc.* **2016**, *138* (39), 12987.
36. Bour, J. R.; Camasso, N. M.; Meucci, E. A.; Kampf, J. W.; Canty, A. J.; Sanford, M. S., Carbon-Carbon Bond-Forming Reductive Elimination from Isolated Nickel(III) Complexes. *J. Am. Chem. Soc.* **2016**, *138* (49), 16105.
37. Diccianni, J. B.; Hu, C. H.; Diao, T. N., Binuclear, High-Valent Nickel Complexes: Ni-Ni Bonds in Aryl-Halogen Bond Formation. *Angew. Chem., Int. Ed.* **2017**, *56* (13), 3635.
38. Lee, H.; Borgel, J.; Ritter, T., Carbon-Fluorine Reductive Elimination from Nickel(III) Complexes. *Angew. Chem., Int. Ed.* **2017**, *56* (24), 6966.
39. Dimitrov, V.; Linden, A., A pseudotetrahedral, high-oxidation-state organonickel compound: synthesis and structure of bromotris(1-norbornyl)nickel(IV). *Angew. Chem., Int. Ed.* **2003**, *42* (23), 2631.

40. Carnes, M.; Buccella, D.; Chen, J. Y. C.; Ramirez, A. P.; Turro, N. J.; Nuckolls, C.; Steigerwald, M., A Stable Tetraalkyl Complex of Nickel(IV). *Angew. Chem., Int. Ed.* **2009**, *48* (2), 290.
41. Aihara, Y.; Chatani, N., Nickel-Catalyzed Direct Alkylation of C-H Bonds in Benzamides and Acrylamides with Functionalized Alkyl Halides via Bidentate-Chelation Assistance. *J. Am. Chem. Soc.* **2013**, *135* (14), 5308.
42. Rouquet, G.; Chatani, N., Catalytic Functionalization of C(sp²)-H and C(sp³)-H Bonds by Using Bidentate Directing Groups. *Angew. Chem., Int. Ed.* **2013**, *52* (45), 11726.
43. Bour, J. R.; Camasso, N. M.; Sanford, M. S., Oxidation of Ni(II) to Ni(IV) with Aryl Electrophiles Enables Ni-Mediated Aryl-CF₃ Coupling. *J. Am. Chem. Soc.* **2015**, *137* (25), 8034.
44. Camasso, N. M.; Canty, A. J.; Ariafard, A.; Sanford, M. S., Experimental and Computational Studies of High-Valent Nickel and Palladium Complexes. *Organometallics* **2017**, *36* (22), 4382.
45. Martinez, G. E.; Ocampo, C.; Park, Y. J.; Fout, A. R., Accessing Pincer Bis(carbene) Ni(IV) Complexes from Ni(II) via Halogen and Halogen Surrogates. *J. Am. Chem. Soc.* **2016**, *138* (13), 4290.
46. Chong, E.; Kampf, J. W.; Ariafard, A.; Canty, A. J.; Sanford, M. S., Oxidatively Induced C-H Activation at High Valent Nickel. *J. Am. Chem. Soc.* **2017**, *139* (17), 6058.
47. Watson, M. B.; Rath, N. P.; Mirica, L. M., Oxidative C-C Bond Formation Reactivity of Organometallic Ni(II), Ni(III), and Ni(IV) Complexes. *J. Am. Chem. Soc.* **2017**, *139* (1), 35.
48. D'Accriscio, F.; Borja, P.; Saffon-Merceron, N.; Fustier-Boutignon, M.; Mezailles, N.; Nebra, N., C-H Bond Trifluoromethylation of Arenes Enabled by a Robust, High-Valent Nickel(IV) Complex. *Angew. Chem., Int. Ed.* **2017**, *56* (42), 12898.

49. Robbins, J. L.; Edelstein, N.; Spencer, B.; Smart, J. C., Syntheses and Electronic-Structures of Decamethylmetallocenes. *J. Am. Chem. Soc.* **1982**, *104* (7), 1882.
50. Kolle, U.; Khouzami, F.; Lueken, H., Permethylmetallocenes .3. Decamethylnickelocene - the Neutral Sandwich Complex, the Monocation, the Dication, and Their Addition-Reactions. *Chem. Ber-Recl.* **1982**, *115* (3), 1178.
51. Lee, C. M.; Chuang, Y. L.; Chiang, C. Y.; Lee, G. H.; Liaw, W. F., Mononuclear Ni(III) complexes [Ni-III(L)(P(C₆H₃-3-SiMe₃-2-S)(3))](0/1-) (L = thiolate, selenolate, CH₂CN, Cl, PPh₃): Relevance to the nickel site of [NiFe] hydrogenases. *Inorg. Chem.* **2006**, *45* (26), 10895.
52. Chiou, T. W.; Liaw, W. F., Mononuclear nickel(III) complexes [Ni(III)(OR)(P(C(6)H(3)-3-SiMe(3)-2-S(3)))](-) (R = Me, Ph) containing the terminal alkoxide ligand: Relevance to the nickel site of oxidized-form [NiFe] hydrogenases. *Inorg. Chem.* **2008**, *47* (17), 7908.
53. Lee, C. M.; Chen, C. H.; Liao, F. X.; Hu, C. H.; Lee, G. H., Mononuclear Ni-III-Alkyl Complexes (Alkyl = Me and Et): Relevance to the Acetyl-CoA Synthase and Methyl-CoM Reductase. *J. Am. Chem. Soc.* **2010**, *132* (27), 9256.
54. Kuwamura, N.; Kitano, K.; Hirotsu, M.; Nishioka, T.; Teki, Y.; Santo, R.; Ichimura, A.; Hashimoto, H.; Wright, L. J.; Kinoshita, I., Redox-Controlled, Reversible Rearrangement of a Tris(2-pyridylthio)methyl Ligand on Nickel to an Isomer with an "N,S-Confused" 2-Pyridylthiolate Arm. *Chem. Eur. J.* **2011**, *17* (38), 10708.
55. Pfaff, F. F.; Heims, F.; Kundu, S.; Mebs, S.; Ray, K., Spectroscopic capture and reactivity of S=1/2 nickel(III)-oxygen intermediates in the reaction of a Ni-II-salt with mCPBA. *Chem. Comm.* **2012**, *48* (31), 3730.

56. Chatterjee, S. K.; Roy, S.; Barman, S. K.; Maji, R. C.; Olmstead, M. M.; Patra, A. K., Shuttling of Nickel Oxidation States in N₄S₂ Coordination Geometry versus Donor Strength of Tridentate N₂S Donor Ligands. *Inorg. Chem.* **2012**, *51* (14), 7625.
57. Klein, H. F.; Bickelhaupt, A.; Hammerschmitt, B., Ligand-Induced Fragmentation of Methylnickel Phenolates Containing a 2-Aldehyde Function - Structure of (3-Tert-Butyl-5-Methyl-2-Oxobenzoyl)-Tris(Trimethylphosphine) Nickel. *Organometallics* **1994**, *13* (8), 2944.
58. Klein, H. F.; Bickelhaupt, A.; Jung, T.; Cordier, G., Syntheses and Properties of the 1st Octahedral Diorganonickel(IV) Compounds. *Organometallics* **1994**, *13* (7), 2557.
59. Klein, H. F.; Bickelhaupt, A.; Lemke, M.; Sun, H. J.; Brand, A.; Jung, T.; Rohr, C.; Florke, U.; Haupt, H. J., Trimethylphosphine complexes of diorganonickel(IV) moieties. *Organometallics* **1997**, *16* (4), 668.
60. Mandal, S.; Gould, E. S., Electron-Transfer .126. Reductions of Oxime-Bound Nickel(IV). *Inorg. Chem.* **1995**, *34* (15), 3993.
61. Baucom, E. I.; Drago, R. S., Nickel(II) and Nickel(IV) Complexes of 2,6-Diacetylpyridine Dioxime. *J. Am. Chem. Soc.* **1971**, *93* (24), 6469.
62. Shimada, S.; Rao, M. L. N.; Tanaka, N., Reaction of 1,2-disilylbenzene with bis-[1,2-bis(dimethylphosphino)ethane]nickel(0). Isolation and characterization of the first silylnickel(IV) complex. *Organometallics* **1999**, *18* (3), 291.
63. Chen, W. Z.; Shimada, S.; Tanaka, M.; Kobayashi, Y.; Saigo, K., Reaction of [2-(SiH₃)C₆H₄](2)SiH₂ with Ni(Et₂PCH₂CH₂PEt₂)(PEt₃)(2): Characterization of eta(2)(Si-H)Ni and Ni-IV-H complexes. *J. Am. Chem. Soc.* **2004**, *126* (26), 8072.

64. Padamati, S. K.; Anielone, D.; Draksharapu, A.; Primi, G.; Martin, D. J.; Tromp, M.; Swart, M.; Browne, W. R., Transient Formation and Reactivity of a High-Valent Nickel(IV) Oxido Complex. *J. Am. Chem. Soc.* **2017**, *139* (25), 8718.

Chapter 2

High-Valent Organometallic Nickel Species Relevant to Carbon-Carbon Bond Formation Reactions

2.1 Introduction

Palladium and nickel catalysts are commonly used in cross-coupling reactions, such as Negishi, Kumada and Suzuki couplings.¹⁻⁹ Palladium is the more common catalyst of the two, and typically the palladium-mediated catalytic cycles involves Pd^{0/II} or Pd^{II/IV} oxidation state changes. By comparison, the mechanisms of nickel-catalyzed cross-coupling reactions is less understood. There has been a need to investigate nickel catalysts due to their possible advantages over other metals, as it has a tendency to undergo one-electron redox reactions.¹⁰⁻¹⁸ Many studies also show that Ni^{III} species are key intermediates in C–C and C–heteroatom bond formation reactions.^{2-3, 6-8, 11, 19-23}

In the past several years we have employed tetradentate pyridinophane ligands to stabilize uncommon organometallic Pd^{III/IV} and Ni^{III/IV} complexes.²⁴⁻³³ These high-valent complexes are capable of C–C and C–heteroatom bond formation reactions. In addition, we have recently reported the use of N,N'-dimethyl-2,11-diaza[3.3](2,6)pyridinophane (^{Me}N4) ligand to stabilize high-valent Ni^{III} complexes that undergo C–C bond formation reactions.³⁰ Herein, we report the use of a modified pyridinophane ligand that destabilizes the Ni center to observe changes in reactivity. We tested the effect of the amine substituents on the axial nitrogen by replacing one or both of the methyl groups with a more electron-withdrawing toluenesulfonate (tosyl, Ts) group. Observations of the (^RN4)Ni^{II}Me₂ complexes show the less coordinating the axial ligand is, the more reactive and the less stable the high-valent Ni species are, leading to faster reactivity. Thus, the (^{Ts}N4)Ni^{II}Me₂ complex gives rapid C–C bond formation at low temperatures and is therefore the most reactive of the three complexes.

2.2 Experimental Section

Reagents and Materials. All manipulations were carried out under a nitrogen atmosphere using standard Schlenk and glove box techniques if not indicated otherwise. All reagents for which the synthesis was not given are commercially available from Aldrich, Acros or STREM, and were used as received without further purification. Solvents were purified prior to use by passing through a column of activated alumina using an MBRAUN SPS. $\text{Mg}(\text{CD}_3)_2$,³³ $\text{N,N}'\text{-R-2,11-diaza[3.3](2,6)pyridinophane}$ ($\text{R} = \text{Me, TsMe and Ts}$) ($^{\text{R}}\text{N}_4$),³⁴ $(^{\text{Me}}\text{N}_4)\text{Ni}^{\text{II}}\text{Me}_2$,³⁰ $(^{\text{Me}}\text{N}_4)\text{Ni}^{\text{III}}\text{Me}_2$,³⁰ ferrocenium hexafluorophosphate (FcPF_6),³⁵ acetylferrocene tetrafluoroborate ($^{\text{Ac}}\text{FcBF}_4$)³⁵ were prepared according to the literature procedures. Other abbreviations used throughout the chapter: dimethoxyethane (DME), silver hexafluoroantimony (AgSbF_6), 1-Fluoro-2,4,6-trimethylpyridinium triflate (NFTPT), 5-(trifluoromethyl)dibenzothiophenium trifluoromethanesulfonate (TDTT) and (diacetoxyiodo)benzene ($\text{PhI}(\text{OAc})_2$).

2.2.1 Synthesis of the Nickel Complexes

Preparation of $(^{\text{TsMe}}\text{N}_4)\text{Ni}^{\text{II}}\text{Br}_2$. A modified procedure was used.³⁶ $(\text{DME})\text{NiBr}_2$ (408.0 mg, 1.32 mmol) and $^{\text{TsMe}}\text{N}_4$ (540.1 mg, 1.32 mmol) were dissolved in dichloromethane (DCM) (50 mL) at 20 °C under N_2 , which made the solution turn from orange to green. After the reaction was stirred for 16 hours, the solution was concentrated down to 10 mL. The solution was then filtered and washed with diethyl ether to give a green solid (688.3 mg, 1.10 mmol, 83%). X-ray quality crystals were obtained by a slow diethyl ether diffusion into an acetonitrile solution at 25 °C.

Elemental analysis: found C 37.67, H 3.72, N 7.46%; calculated $\text{C}_{22}\text{H}_{24}\text{Br}_2\text{N}_4\text{NiO}_2\text{S}\cdot\text{DCM}+\text{H}_2\text{O}$
C, 37.84, H 3.87 N, 7.68%

Preparation of (^{TsMe}N₄)Ni^{II}Me₂ (2). A modified procedure was used.³⁶ A solution of MeMgCl in THF (3.0 M, 0.38 mL) was added to a stirred suspension of (^{TsMe}N₄)NiBr₂ (367.5 mg, 0.59 mmol) in THF (5 mL), cooled at -50 °C in a N₂ filled glovebox. The mixture was stirred at this temperature for 30 minutes, and then slowly warmed up to -10 °C over the course of 12 hours. 1,4-dioxane (15 mL) was then added to the deep red solution. The resulting suspension was allowed to sit for one hour in a -35 °C freezer. The suspension was filtered, and the solvent was removed under vacuum at -50 °C and the residue was extracted with pre-cooled diethyl ether (200 mL). The resulting deep red solution was filtered and dried under vacuum giving rise to an orange solid (252.0 mg, 0.51 mmol, 86%). X-ray quality crystals were obtained by a slow pentane diffusion into a THF solution at -35 °C.

¹H NMR (300 MHz, THF-d₈), δ (ppm): 7.95 (d, *J* = 6.3 Hz, 2H, K), 7.48 (m, 4H, J), 7.38 (t, *J* = 6.7 Hz, 2H, I), 7.10 (d, *J* = 6.2 Hz, 2H, H), 6.95 (d, *J* = 14.1 Hz, 2H, G), 6.82 (d, *J* = 13.7 Hz, 2H, F), 5.22 (d, *J* = 13.9 Hz, 2H, E), 4.24 (d, *J* = 13.8 Hz, 2H, D), 2.49 (s, 3H, C), 2.25 (s, 3H, B), -0.92 (s, 6H, A) (Figure 2.1).

APT (500 MHz, THF-d₈), δ (ppm): 159.40 (n), 159.25 (m), 144.62 (l), 138.96 (k), 136.43 (j), 130.92 (i), 128.10 (h), 125.59 (g), 125.08 (f), 64.08 (e), 58.14 (d), 38.30 (c), 21.72 (b), -8.68 (a) (Figure 2.1).

Elemental analysis: found C 51.32, H 5.29, N 9.77%; calculated C₂₄H₃₀N₄NiO₂S•DCM C, 51.57, H 5.54, N 9.66%

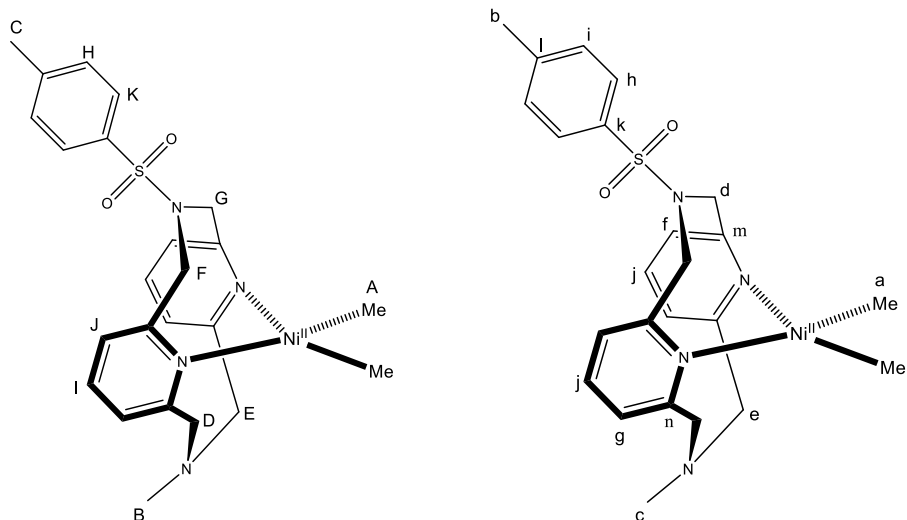


Figure 2.1 Proton (left) and carbon (right) structural assignments from NMR experiments for $(^{\text{TsMe}}\text{N4})\text{Ni}^{\text{II}}\text{Me}_2$

Preparation of $(^{\text{TsMe}}\text{N4})\text{Ni}^{\text{II}}(\text{CD}_3)_2$. A solution of CD_3MgI (2.0 M, 0.59 mL) was added to a stirred suspension of $(^{\text{TsMe}}\text{N4})\text{NiBr}_2$ (256.1 mg, 0.41 mmol) in THF (5 mL), cooled at $-50\text{ }^\circ\text{C}$ in a N_2 filled glovebox, and the mixture stirred for 30 minutes followed by a slow and gradual increase in temperature to $-10\text{ }^\circ\text{C}$ over the course of 12 hours. After stirring for 12 hours, 1,4-dioxane (10 mL) was added to the deep red solution. The resulting suspension was allowed to sit for one hour in a $-35\text{ }^\circ\text{C}$ freezer before the suspension was filtered and the filtrate removed under vacuum. The resulting solid was extracted with pre-cooled diethyl ether (100 mL). The deep red solution was filtered and the filtrate was dried under vacuum giving rise to an orange solid (146.2 mg, 0.29 mmol, 72%). The ^1H NMR spectrum of the product is identical to that of $(^{\text{TsMe}}\text{N4})\text{Ni}^{\text{II}}\text{Me}_2$ except for the missing singlet for the Ni-Me group at -0.92 ppm. The ^2H NMR of $(^{\text{TsMe}}\text{N4})\text{Ni}^{\text{II}}(\text{CD}_3)_2$ shows only a singlet for the Ni-Me group at -1.12 ppm in MeCN.

Preparation of $(^{\text{Ts}}\text{N4})\text{Ni}^{\text{II}}\text{Br}_2$. A modified procedure was used.³⁶ $(\text{DME})\text{NiBr}_2$ (352.0 mg, 1.14 mmol) and $^{\text{Ts}}\text{N4}$ (625.1 mg, 1.14 mmol) were dissolved in 50 ml of DCM at $20\text{ }^\circ\text{C}$ under N_2 , which

made the solution turn from orange to green. After the reaction was stirred for 14 hours, the solution was concentrated, then filtered and washed with diethyl ether to give a green powder (682.0 mg, 0.89 mmol, 78%).

Elemental analysis: found C 39.41, H 4.32, N 6.42%; calculated $C_{28}H_{28}Br_2N_4NiO_4S_2 \cdot DCM + 2H_2O$
C, 39.22, H 3.86 N, 6.31%

Preparation of $(^{15}N_4)Ni^{II}Me_2$ (3). A modified procedure was used.³⁶ A solution of MeMgCl in THF (3.0 M, 0.44 mL) was added to a stirred suspension of $(^{15}N_4)NiBr_2$ (339.8 mg, 0.44 mmol) in THF (5 mL), cooled at $-50\text{ }^\circ\text{C}$ in a N_2 filled glovebox. The mixture was stirred at this temperature for 30 minutes, and then slowly warmed up to $-10\text{ }^\circ\text{C}$ over the course of 12 hours. 1,4-dioxane (15 mL) was then added to the deep red solution. The resulting suspension was allowed to sit for one hour in a $-35\text{ }^\circ\text{C}$ freezer. The suspension was filtered, and the solvent was removed under vacuum at $-50\text{ }^\circ\text{C}$ and the residue extracted with pre-cooled diethyl ether (200 mL). The resulting deep red solution was filtered and dried under vacuum giving rise to an orange solid (107.4 mg, 0.168 mmol, 38%). X-ray quality crystals were obtained by a slow diethyl ether evaporation at $-35\text{ }^\circ\text{C}$.

1H NMR (500 MHz, THF- d_8), δ (ppm): 7.73 (d, $J = 7.9$ Hz, 4H, G), 7.55 (t, $J = 7.7$ Hz, 2H, F), 7.38 (m, 8H, E), 6.81 (d, $J = 14.6$ Hz, 4H, D), 5.18 (d, $J = 14.6$ Hz, 4H, C), 2.25 (s, 6H, B), -1.05 (s, 6H, A) (Figure 2.2).

^{13}C NMR (500 MHz, THF- d_8), δ (ppm): 159.24 (j), 144.50 (i), 138.97 (h), 137.57 (g), 130.86 (f), 128.08 (e), 125.86 (d), 58.54 (c), 21.57 (b), -7.68 (a) (Figure 2.2).

Elemental analysis: found C 51.98, H 4.87, N 7.49%; calculated $C_{30}H_{34}N_4NiO_4S_2 \cdot DCM$ C, 51.54, H 5.02, N 7.76%

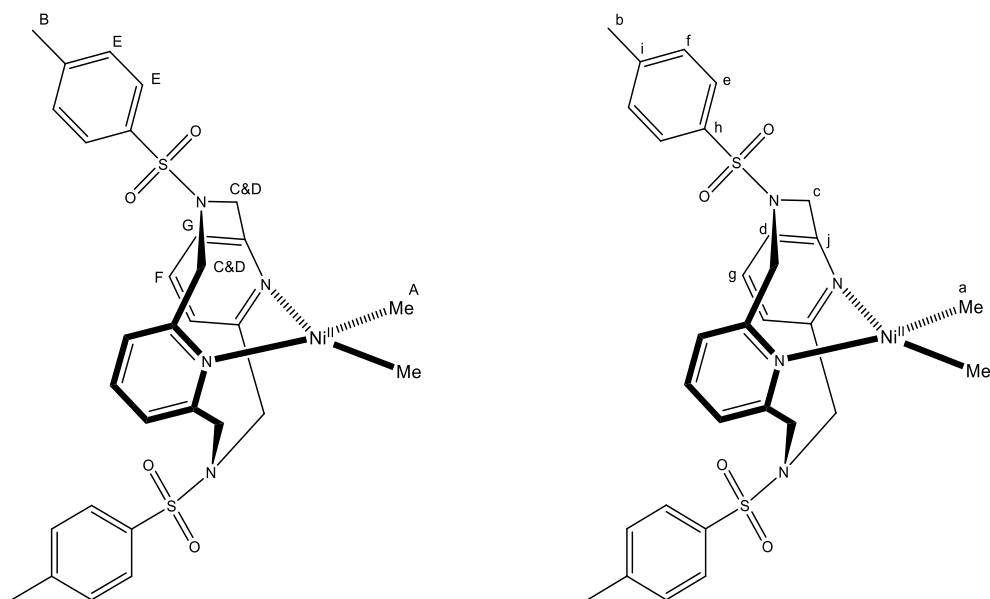


Figure 2.2 Proton (left) and carbon (right) structural assignments from NMR experiments for $(^{Ts}N4)Ni^{II}Me_2$.

Preparation of $(^{Ts}N4)Ni^{II}(CD_3)_2$. A solution of CD_3MgI (2.0 M, 0.67 mL) was added to a stirred suspension of $(^{Ts}N4)NiBr_2$ (206.3 mg, 0.269 mmol) in THF (5 mL), cooled at $-50\text{ }^\circ\text{C}$, and the mixture was stirred for 30 minutes followed by a gradual increase in temperature to $-10\text{ }^\circ\text{C}$ over the course of 12 hours. After stirring for 12 hours, 1,4-dioxane (10 mL) was added to the deep red solution. The resulting suspension was allowed to sit for one hour in a $-35\text{ }^\circ\text{C}$ freezer before the suspension was filtered and the filtrate removed under vacuum. The resulting solid was extracted with pre-cooled diethyl ether (100 mL). The deep red solution was filtered, and the filtrate was dried under vacuum giving rise to an orange solid (40.0 mg, 0.063 mmol, 23%). The 1H -NMR spectrum of the product is identical to that of $(^{Ts}N4)Ni^{II}Me_2$ except for the missing singlet for the Ni-Me group at -1.05 ppm. The 2H NMR of $(^{Ts}N4)Ni^{II}(CD_3)_2$ shows only a singlet for the Ni-Me group at -1.17 ppm.

2.2.2 Reactivity Studies

General procedure for the isolation of the Ni^{III} complexes by EPR. An EPR tube was charged with a solution of (^{TsMe}N₄)Ni^{II}Me₂ or (^{Ts}N₄)Ni^{II}Me₂ in acetonitrile (MeCN) or THF. A butyronitrile (PrCN) or 2-methyl-tetrahydrofuran (MeTHF) solution containing one equivalent of ferrocenium hexafluorophosphate (FcPF₆), silver hexafluoroantimonate (AgSbF₆) or acetylferrocenium tetrafluoroborate (^{Ac}FcBF₄) was then added. The resulting solution of 1:3 MeCN:PrCN or 1:3 THF:MeTHF was shaken for five seconds and then frozen in liquid nitrogen.

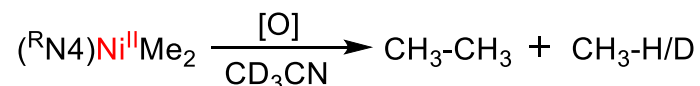
¹H NMR reactivity studies of (^RN₄)NiMe₂ Complexes. General procedure for the reactivity studies of (^RN₄)NiMe₂ complexes (R = Me, TsMe and Ts) (Scheme 2.1). In N₂-filled glove box, a solution of 8-10 mg of (^{Me}N₄)Ni^{II}Me₂, (^{TsMe}N₄)Ni^{II}Me₂ or (^{Ts}N₄)Ni^{II}Me₂ in 2.0 mL of MeCN-d₃ was added into a NMR tube containing one equiv. of 1,3,5-trimethoxybenzene as an internal standard. To this solution an oxidant [^{Ac}FcBF₄, H₂O₂, O₂, CD₃I, 1-Fluoro-2,4,6-trimethylpyridinium triflate (NFTPT), PhI(OAc)₂ or 5-(trifluoromethyl)dibenzothiophenium trifluoromethanesulfonate (TDTT)] was added in MeCN-d₃. For all experiments the NMR tube was filled to the top with additional MeCN-d₃ so that no headspace was left, to avoid the escape of volatiles and sealed with a septum. The reaction mixtures were mixed to form homogeneous solutions. The reaction mixtures were then kept in the dark and periodically monitored by ¹H NMR until no additional changes were observed. The average product yields from at least two independent experiments were determined by NMR integration using 1,3,5-trimethoxybenzene as an internal standard. All data is included in Appendix D.

(^{Me}N₄)Ni^{II}Me₂ and (^{TsMe}N₄)Ni^{II}Me₂ reactivity reactions were performed at 20 °C and the reactivity of (^{Ts}N₄)Ni^{II}Me₂ was performed at -20 °C to minimize Ni black formation.

Ethane ^1H NMR (MeCN-d_3), δ : 0.85 (s). Ethane- d_3 ^1H NMR (MeCN-d_3), δ : 0.81 (sept).

Methane ^1H NMR (MeCN-d_3), δ : 0.20 (s). Methane- d_1 ^1H NMR (MeCN-d_3), δ : 0.18 (t).

Scheme 2.1 General reactivities studies.



Crossover Experiments. General procedure for the crossover experiments of $(\text{R}^{\text{N4}}\text{Ni})\text{Me}_2$ complexes ($\text{R} = \text{Me}$, TsMe and Ts) (Scheme 2.2). In an N_2 -filled glove box, a half equivalent of $(\text{R}^{\text{N4}}\text{Ni})\text{Me}_2$ and a half equivalent of $(\text{R}^{\text{N4}}\text{Ni})(\text{CD}_3)_2$ ($\text{R} = \text{Me}$, TsMe or Ts) in MeCN-d_3 were added to the NMR tube as separate solutions. The NMR tube contained one equivalent of 1,3,5-trimethoxybenzene as an internal standard. To this solution one or two equivalents of $^{\text{Ac}}\text{FcBF}_4$ were added in MeCN-d_3 . For all experiments, the NMR tube was filled to the top with additional MeCN-d_3 so that no headspace was left to avoid the escape of volatiles and sealed with a septum. The reaction mixtures were mixed carefully to form homogeneous solutions. The reaction mixtures were then kept in the dark and periodically monitored by ^1H NMR until no additional changes were observed. The average product yields from at least two independent experiments were determined by NMR integration using 1,3,5-trimethoxybenzene as an internal standard. All the data is included in Appendix D.

When ^2H NMR was used to monitor the crossover experiments, one equivalent of benzene- d_6 was added instead of 1,3,5-trimethoxybenzene as an internal standard, and MeCN was used instead of MeCN-d_3 as the solvent. A blank sample with MeCN-d_3 was used for shimming.

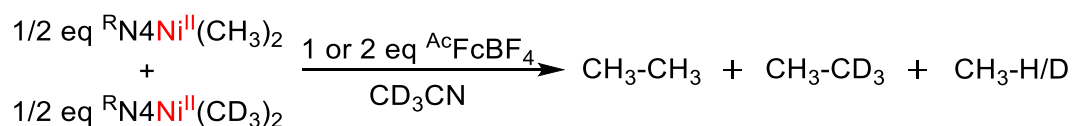
The crossover experiments for (^{Me}N4)Ni^{II}Me₂ and (^{TsMe}N4)Ni^{II}Me₂ were performed at 20 °C and the crossover experiments for (^{Ts}N4)Ni^{II}Me₂ was performed at -20 °C.

Ethane ¹H NMR (MeCN-d₃), δ: 0.85 (s). Ethane-d₃ ¹H NMR (MeCN-d₃), δ: 0.81 (sept).

Ethane-d₆ ²H NMR (MeCN), δ: 0.81 (s). Ethane-d₃ ²H NMR (MeCN), δ: 0.83 (s).³⁷

Methane ¹H NMR (MeCN-d₃), δ: 0.20 (s). Methane-d₁ ¹H NMR (MeCN-d₃), δ: 0.18 (t).

Scheme 2.2 Crossover reactivity.



Catalytic Kumada Cross-Coupling Reactions. General procedure for the Kumada cross-coupling with (^RN4)NiBr₂ (R = Me, TsMe and Ts). A small vial equipped with a magnetic stir bar inside a nitrogen filled glove box was charged with the corresponding alkyl halide or aryl halide substrate (0.1 mmol), decane as internal standard and the Ni complex (3 mg, 0.05 eq) in THF (5.0 mL). The Grignard reagent (1.2 eq) was added slowly to the stirring solution over one hour via syringe, and the resulting solution was stirred at room temperature for 24 hours. A 1-hour, a 2-hour, and a 24-hour aliquot (500 μL) was taken. Then, each reaction mixture was worked up by quenching with 5 mL of saturated NH₄Cl solution and extracting the mixture with diethyl ether (15 mL). The organic layer was separated and dried over MgSO₄. The yield of product(s) was obtained by GC/FID using decane as internal standard and is an average of at least three independent runs, while the identity of the products was confirmed by GC/MSD. All data is included in Appendix E. No cross-coupled products were observed in the absence of (^RN4)NiBr₂.

2.2.3 Physical Measurements

Nuclear Magnetic Resonance. ^1H NMR, ^2H NMR, ^{13}C NMR, APT, gCOSY, NOESY, TOXY, HSQC and HMBC spectra were recorded on a Varian Mercury-300 spectrometer (300.121 MHz), Agilent DD2-500 spectrometer (499.885 MHz) or Agilent DD2-600 spectrometer (599.736 MHz). Chemical shifts are reported in ppm and referenced to residual solvent resonance peaks.³⁸⁻³⁹ Abbreviations for the multiplicity of NMR signals are s (singlet), d (doublet), dd (doublet of doublets), t (triplet), m (multiplet). All the NMR spectra are included in Appendix A.

UV-Vis, EPR and EA. UV-visible spectra were recorded on a Varian Cary 50 Bio spectrophotometer and are reported as λ_{max} , nm (ϵ , $\text{M}^{-1}\cdot\text{cm}^{-1}$). The UV-vis spectra are included in Appendix C. EPR spectra were recorded on a Bruker EMX-PLUS EPR or a JEOL JES-FA EPR spectrometer at X-band (~ 9.2 GHz) frequency in frozen solution at 77 K. The purchase of the Bruker EMX-PLUS EPR spectrometer was supported by the National Science Foundation (MRI, CHE-1429711). Elemental analyses were carried out by the Intertek Pharmaceutical Services.

Electrochemical Measurements. Cyclic voltammetry experiments were performed with a BASi EC Epsilon electrochemical workstation or a CHI 660D Electrochemical Analyzer. The electrochemical measurements were taken in a glove box under nitrogen. A glassy carbon disk electrode ($d = 1.6$ mm) was used as the working electrode for cyclic voltammetry. The auxiliary electrode was a Pt wire for cyclic voltammetry measurements. The non-aqueous references electrode used was a silver wire dipped in a bleach (Ag/AgCl). The reference electrodes were calibrated against Cp_2Fe (Fc). Electrochemical-grade electrolytes from Fluka were used as the supporting electrolyte for electrochemical measurements. All the CV spectra are included in Appendix B.

X-ray Crystallography. All X-ray crystallography experiments were performed by Dr. Nigam Rath. Suitable crystals were mounted on MiTeGen cryoloops in random orientations in a Bruker Kappa Apex-II CCD X-ray diffractometer equipped with an Oxford Cryostream LT device and a fine focus Mo K α radiation X-ray source ($\lambda = 0.71073 \text{ \AA}$). Preliminary unit cell constants were determined with a set of 36 narrow frame scans. Typical data sets consist of combinations of ω and ϕ scan frames with a typical scan width of 0.5° and a counting time of 15–30 s/frame at a crystal-to-detector distance of 4.0 cm. The collected frames were integrated using an orientation matrix determined from the narrow frame scans. Apex II and SAINT software packages (Bruker Analytical X-Ray, Madison, WI, 2008) were used for data collection and data integration. Analysis of the integrated data did not show any decay. Final cell constants were determined by global refinement of xyz centroids of reflections from the complete data sets. Collected data were corrected for systematic errors using SADABS (Bruker Analytical X-Ray, Madison, WI, 2008) based on the Laue symmetry using equivalent reflections. Structure solutions and refinement were carried out using the SHELXTL-PLUS software package. The structures were solved by direct methods and refined successfully in specified crystal systems and space groups. Full matrix least-squares refinements were carried out by minimizing $\sum w(F_o^2 - F_c^2)^2$. The non-hydrogen atoms were refined anisotropically to convergence. Typically, the hydrogen atoms were treated using the appropriate riding model. The complete listings of X-ray diffraction parameters are included in Appendix G.

2.3 Results and Discussion

2.3.1 Synthesis and Characterization of Ni^{II/III} Complexes

The azomacrocyclic ligands N,N'-dimethyl-2,11-diaza[3.3](2,6)pyridinophane (^{Me}N₄), N-(p-toluenesulfonyl),N'-(methyl)-2,11-diaza[3.3](2,6)pyridinophane (^{TsMe}N₄) and N,N'-ditoluenesulfonyl-2,11-diaza[3.3](2,6)pyridinophane (^{Ts}N₄) were synthesized according to a literature procedure (Figure 2.3).³⁴ Complexes (^{Me}N₄)Ni^{II}Me₂, **1**, (^{Me}N₄)Ni^{III}Me₂, **1**⁺, were synthesized as reported previously.³⁰

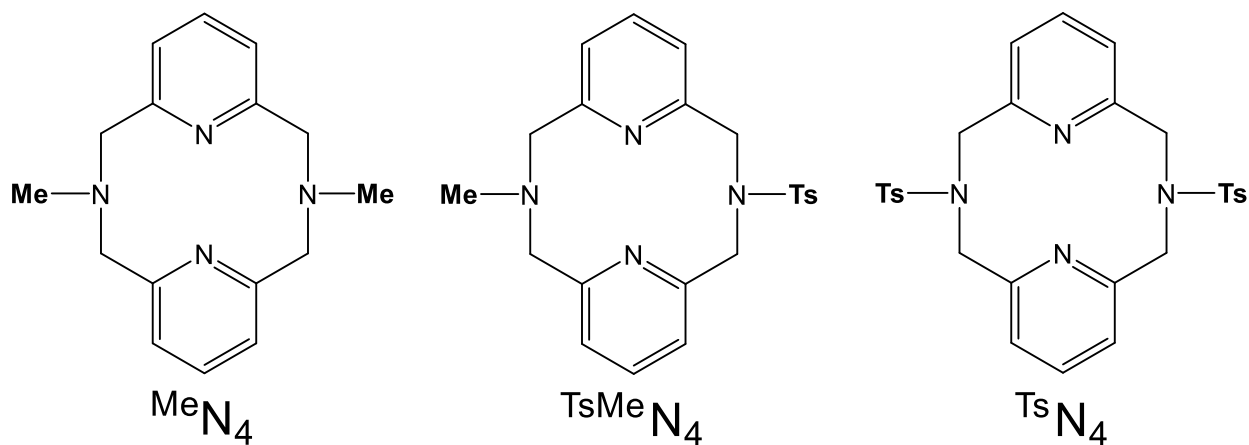


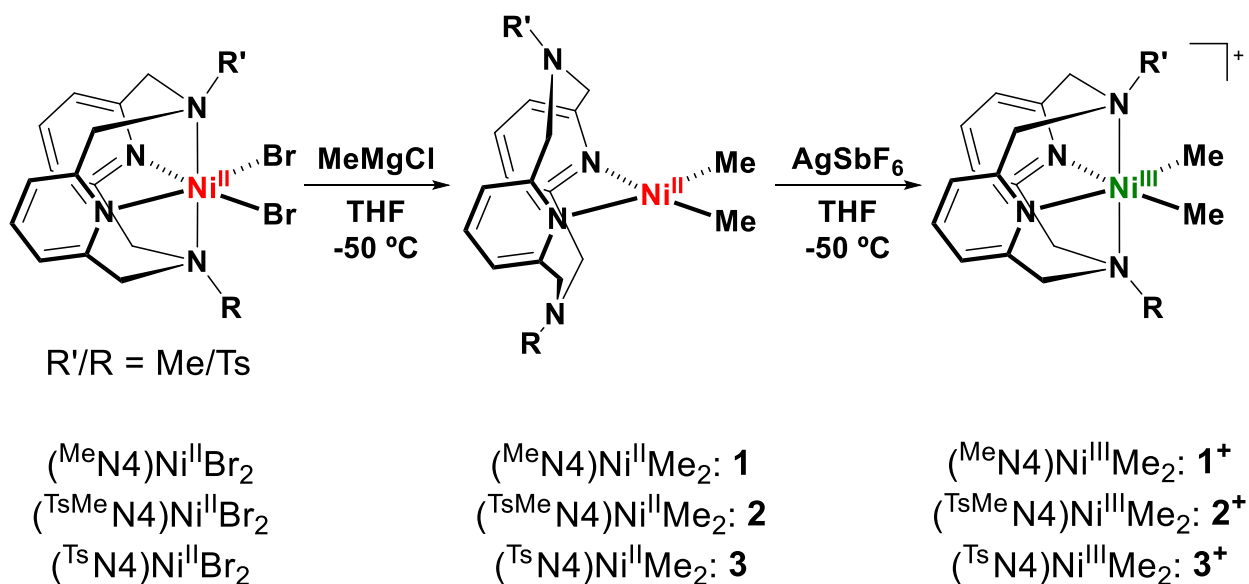
Figure 2.3 Ligands used for stabilizing high-valent nickel complexes.

The dark orange complex (^{TsMe}N₄)Ni^{II}Me₂, **2**, was prepared in 86% yield from the precursor (^{TsMe}N₄)Ni^{II}Br₂ via transmetalation with methylmagnesium chloride (Scheme 2.3). The single crystal X-ray structure of **2** reveals a square planar geometry for the Ni center that is bound to two pyridyl nitrogen atoms from the ^{TsMe}N₄ ligand and two methyl groups, with an average equatorial Ni-N_{pyridyl} bond length of 1.947 Å and an average Ni-C bond length of 1.929 Å (Figure 2.4). As expected, **2** is diamagnetic, likely due to the strong σ-donor methyl groups that favor the

low-spin square planar geometry. The cyclic voltammetry (CV) of **2** exhibits an oxidation process at -890 mV vs Fc^+/Fc (Figure 2.5) which is tentatively assigned to the $\text{Ni}^{\text{III/II}}$ peak.

Using the same process as the complex above, we were able to prepare the orange complex $(^{\text{Ts}}\text{N4})\text{Ni}^{\text{II}}\text{Me}_2$, **3**, in 38% yield from the precursor $(^{\text{Ts}}\text{N4})\text{Ni}^{\text{II}}\text{Br}_2$. Similarly to **2**, the single crystal X-ray structure of **3** reveals a square planar geometry for the Ni center, with an average equatorial Ni- $\text{N}_{\text{pyridyl}}$ bond length of 1.974 Å and an average Ni-C bond length of 1.943 Å (Figure 2.4). Complexes **2** and **3** were both characterized by ^1H and ^{13}C NMR. The CV of **3** exhibits an oxidation process at -430 mV vs Fc^+/Fc (Figure 2.5) which is tentatively assigned to the $\text{Ni}^{\text{III/II}}$ peak. The oxidative potential of the $\text{Ni}^{\text{III/II}}$ peak increases by approximately 500 mV each time a tosyl group is added to axial nitrogen on the ligand.

Scheme 2.3 Synthesis of $(^{\text{R}}\text{N4})\text{NiMe}_2$ complexes.



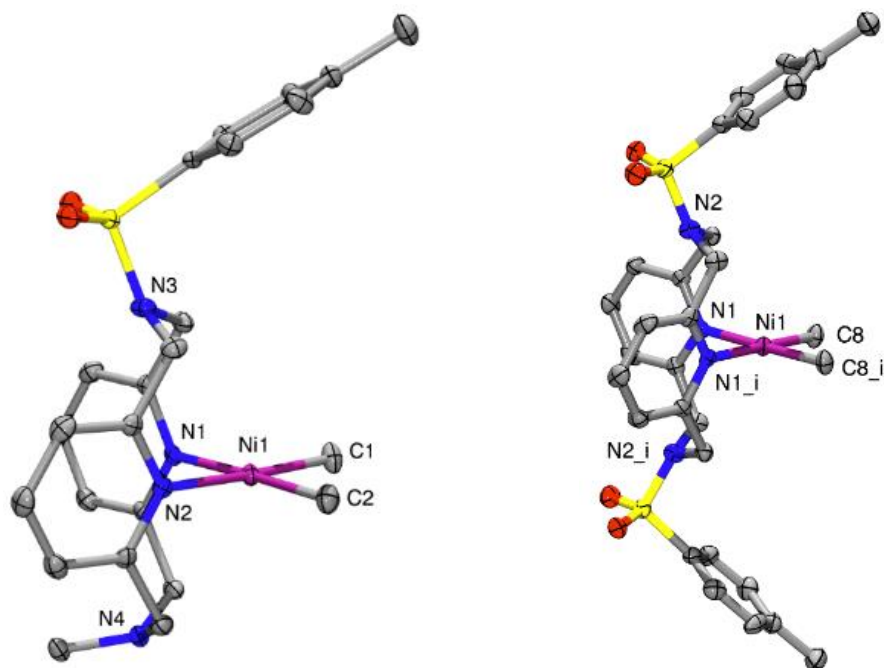


Figure 2.4 ORTEP representation of **2** (left) and **3** (right), with 50% probability thermal ellipsoids. Selected bond distances (Å), **2**: Ni1-C1, 1.934; Ni1-C2, 1.923; Ni1-N1, 1.976; Ni1-N2, 1.971 **3**: Ni1-C8, 1.929; Ni1-C8_i, 1.929; Ni1-N1, 1.974; Ni1-N1_i, 1.974.

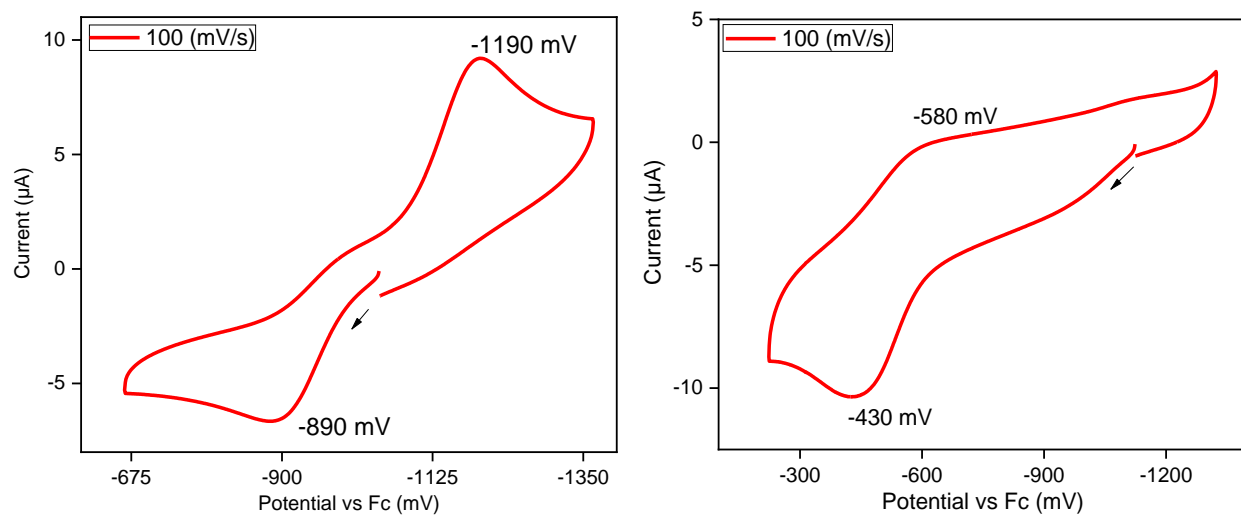


Figure 2.5 CV of **2** (left) in 0.1 M $n\text{Bu}_4\text{NPF}_6/\text{MeCN}$ at RT (100 mV/s scan rate). Redox potential: $E_{(\text{Ni}^{\text{III}})}$ = -890 mV and CV of **3** (right) in 0.1 M $n\text{Bu}_4\text{NPF}_6/\text{MeCN}$ at RT (100 mV/s scan rate). Redox potential: $E_{(\text{Ni}^{\text{III}})}$ = -430 mV.

Both complexes **2** and **3** can be oxidized using one equivalent of silver hexafluoroantimonate (AgSbF_6) in THF at -50 °C to obtain $[(^{\text{TsMe}}\text{N}_4)\text{Ni}^{\text{III}}\text{Me}_2]\text{SbF}_6$, **2**⁺, and

$[(^{\text{TsMe}}\text{N4})\text{Ni}^{\text{III}}\text{Me}_2]\text{SbF}_6$, $\mathbf{3}^+$. The X-Ray structure of $\mathbf{2}^+$ shows a six-coordinate Ni^{III} center in a distorted octahedral geometry. The average equatorial $\text{Ni-N}_{\text{pyridyl}}$ bond lengths are similar with our previously reported organometallic $(^{\text{R}}\text{N4})\text{Ni}^{\text{III}}$ complexes,³⁰⁻³¹ but due to the asymmetry of the $^{\text{TsMe}}\text{N4}$ ligand, the axial $\text{Ni-N}_{\text{amine}}$ bond lengths are not the same. The Ni-N_{Ts} (2.456 Å) bond is longer than the Ni-N_{Me} (2.145 Å) bond (Figure 2.6), likely due to a more electron deficient nature of the tosyl-group resulting in a longer distance away from the Ni center. Although we were not able to obtain X-ray quality crystals for complex $\mathbf{3}^+$ due to its instability, we did observe a decomposition product, which has one hydroxide and one water attached (Figure 2.6).

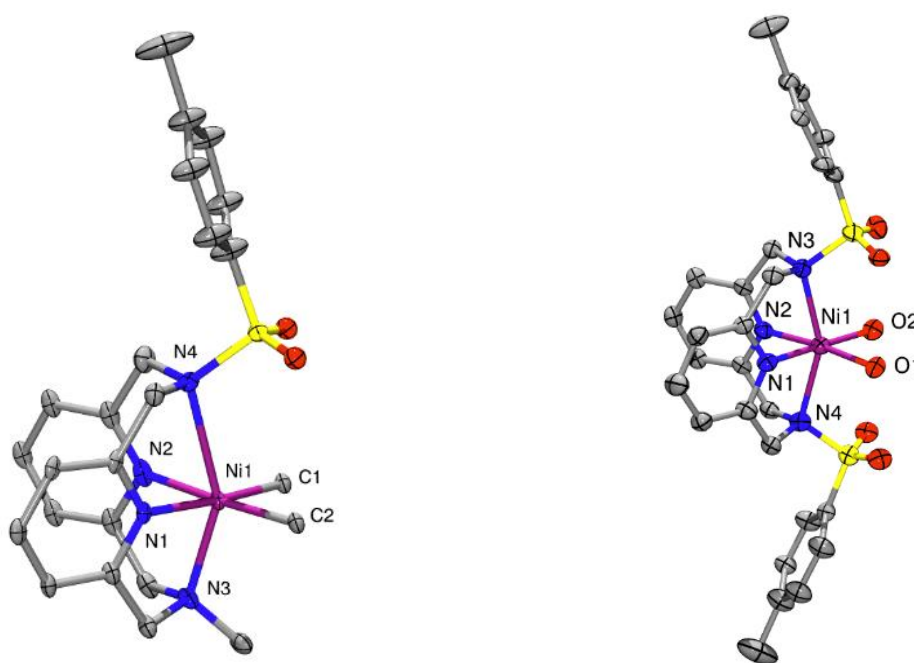


Figure 2.6 ORTEP representation of $\mathbf{2}^+$ (left) and $\mathbf{3}^+_{\text{decomposition}}$ (right) with 50% probability thermal ellipsoids. Selected bond distances (Å), $\mathbf{2}^+$: Ni1-C1, 1.932; Ni1-C2, 1.925; Ni1-N1, 1.968; Ni1-N2, 1.965; Ni1-N3, 2.145; Ni1-N4, 2.456 $\mathbf{3}^+_{\text{decomposition}}$: Ni1-O1, 2.081; Ni1-O2, 1.977; Ni1-N1, 1.908; Ni1-N2, 2.03; Ni1-N3, 2.25; Ni1-N4, 2.29.

The EPR spectrum of complex $\mathbf{2}^+$ exhibits a pseudo-axial signal in a solvent mixture of THF and methyl-THF (MeTHF). A superhyperfine coupling was observed in the g_z direction due to the two axial N donors ($I=1$) coupling to the Ni^{III} center (Figure 2.7). It is noteworthy that the

N_{Me} nitrogen (17.5 G) binds stronger to the metal center than the N_{Ts} nitrogen (5.8 G). This is consistent with the previously shown crystal structure, due to the tosyl group being more electron-withdrawing than a methyl group. When complex 2^+ was further subjected to a solvent mixture of PrCN and MeCN, a different signal was observed in the g_z direction. The observed superhyperfine coupling for this g_z region resulted in a quintet, which was from two axial nitrogens with equally binding strengths to the metal center (Figure 2.7). In this case, we suspect that the N_{Me} and MeCN or PrCN bind in the axial direction because the tosyl ligand does not bind as strongly to the Ni center.

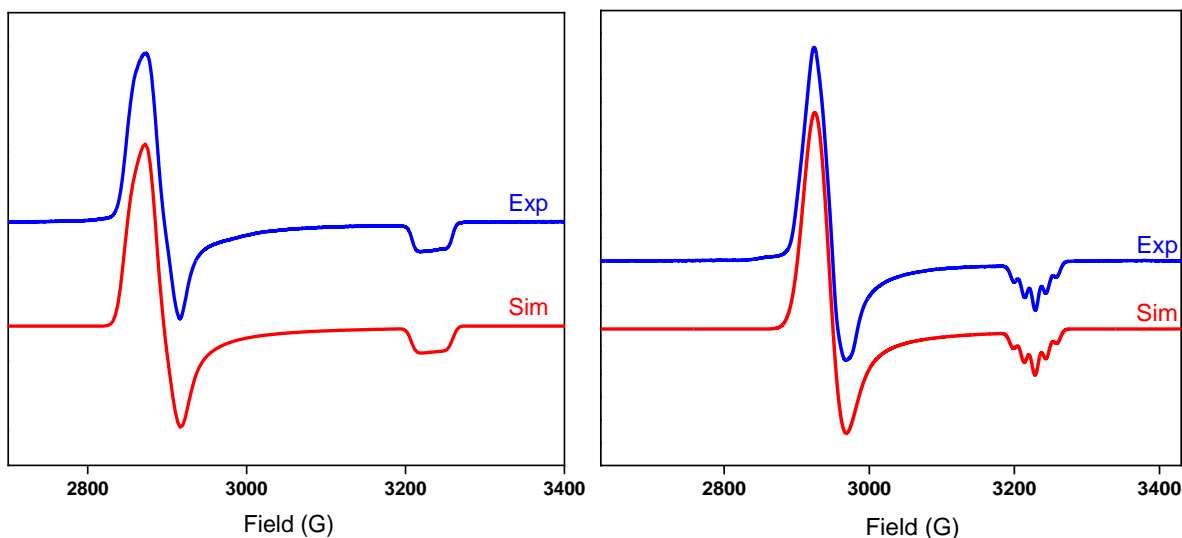


Figure 2.7 Experimental (1:3 THF:MeTHF, 77K) and simulated EPR spectra of 2^+ (left) using the following parameters: $g_x=2.270$ ($A_x=12.0$ G), $g_y=2.243$ ($A_y=12.0$ G), $g_z=2.011$ ($A_z(N)=17.5$ G and $A_z(N)=5.8$ G). Experimental (1:3 MeCN:PrCN, 77K) and simulated EPR spectra of 2^+ (right) using the following parameters: $g_x=2.222$, $g_y=2.202$, $g_z=2.012$ ($A_z(2N)=15.0$ G).

The EPR spectrum of complex 3^+ in MeCN and PrCN shows a rhombic signal with superhyperfine coupling in the g_z region caused by the interaction between the nickel center and two nitrogen atoms (Figure 2.8). This shows that both axial N_{Ts} or two nitrile solvent molecules (MeCN or PrCN) bind in the axial direction to the nickel center. We compared the two N_{Ts} (9.0

G), two N_{Me} (15 G), and two nitrile solvents (15 G) binding in the axial direction, showing that N_{Ts} binds in the weakest manner. The difference in binding allows us to verify that N_{Ts} , instead of the nitrile solvent, is binding in the axial direction. EPR spectrum of 3^+ in THF/MeTHF gives a similar spectrum to the spectrum taken in the solvent mixture MeCN:PrCN, although 3^+ is less stable in the THF/MeTHF solvent system. With these complexes in hand we were able to directly probe the reactivity and characterize the roles each different axial substituent played.

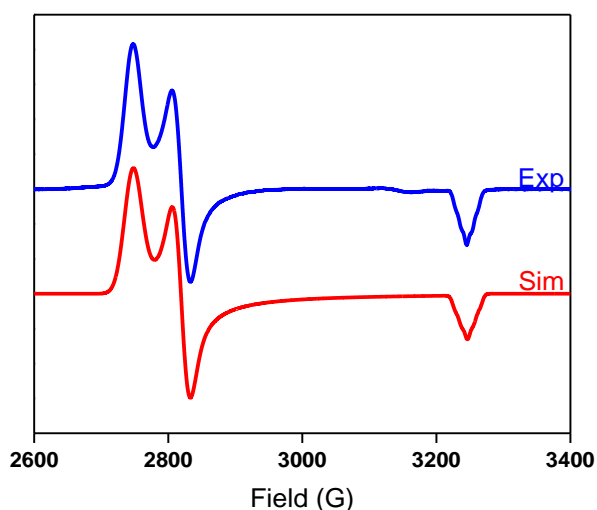


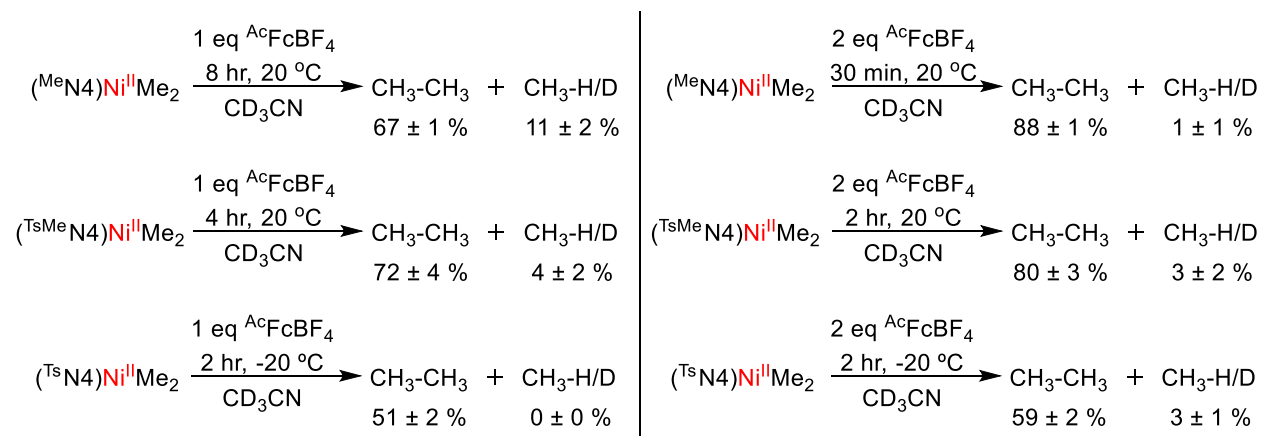
Figure 2.8 Experimental (1:3 MeCN:PrCN, 77K) and simulated EPR spectra of 3^+ using the following parameters: $g_x=2.365$, $g_y=2.304$, $g_z=2.002$ ($A_z(2N) = 9.0$ G).

2.3.2 C–C Bond Formation Reactivity of $(R^N)_4Ni^{II}Me_2$ Complexes

The organometallic reactivities of **1**, **2** and **3** were investigated under different reaction conditions and then compared with each other. Reductive elimination of **1**, **2** or **3** was observed upon oxidation with $^{Ac}F_cBF_4$ in CD_3CN , and the yields of methane and ethane were monitored via 1H NMR over time to track the reaction. As the reactions plateaued, the yield percentages of the products were calculated. Data shows a faster reaction when having more electron withdrawing substituents on the axial amines (Scheme 2.4). Formation of undesired methane is minimized with

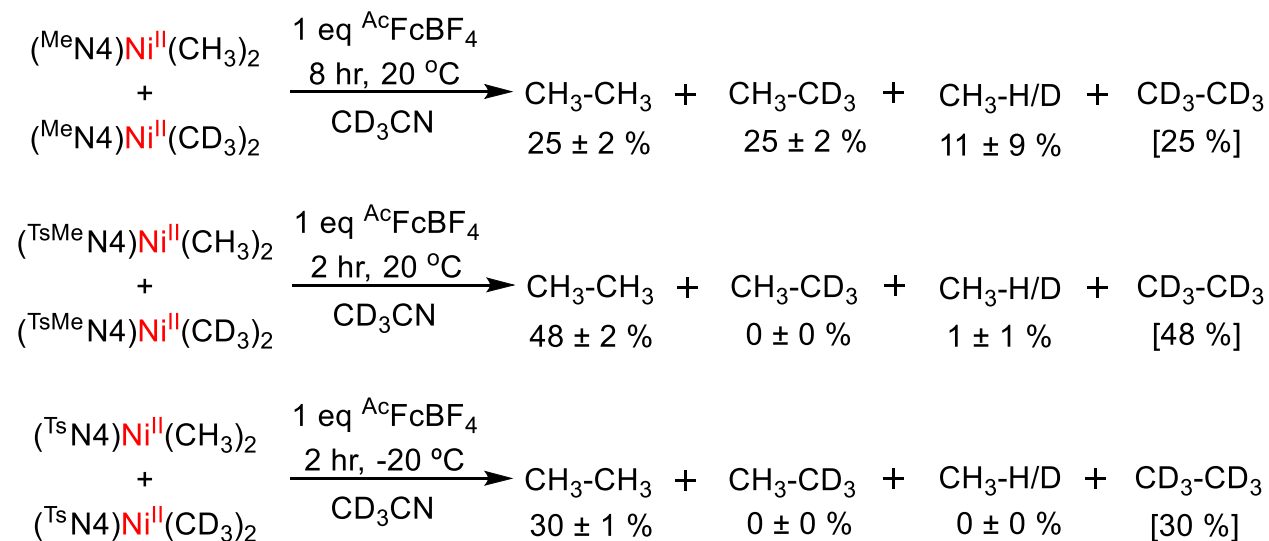
ligands bearing tosyl groups. When performing this reaction on compounds with electron withdrawing groups on the axial amines, the temperature was lowered to prevent Ni black formation. When looking at the data, we noticed that complex **2** gave the highest ethane formation. The reductive elimination of ethane from the Ni^{II} center proceeds through a classical Ni^{II/0} mechanism, as suggested by the formation of an observable amount of Ni black for all reactions. Interestingly, addition of two equivalents of ^{Ac}FcBF₄ to a solution of any of the three complexes **1**, **2** or **3** in CD₃CN resulted in less methane formation for complex **1** relative to the other two complexes, leading to an increased yield of ethane of 88%. The yields increased for the other two complexes to 80% (**2**) and 59% (**3**) respectively. The reaction time for all three complexes was faster when adding two equivalents of ^{Ac}FcBF₄ than with one equivalent. However, the fastest reaction time with two equivalents of ^{Ac}FcBF₄ is when complex **1** is used. Complex **1** was previously reported to proceed through a Ni^{IV} intermediate.³⁰ Complexes **2** and **3** were shown to have a slower reactivity than with complex **1**, when adding two equivalents of ^{Ac}FcBF₄. We suspect that two different mechanisms take place due to the tosyl group weakly binding in a Ni^{III} stage. This allows for the formation of a 5-coordinate system versus a 6-coordinate system, which has been shown previously to give faster reactivity.

Scheme 2.4 C–C bond formation reactivity of the (R₂N₄)Ni^{II}Me₂ complexes with ^{Ac}FcBF₄.



Additional mechanistic studies were employed to probe the observed reactivity for complexes **2** and **3**. Crossover experiments using a 1:1 mixture of $(^R\text{N}4)\text{Ni}^{\text{II}}\text{Me}_2$ and $(^R\text{N}4)\text{Ni}^{\text{II}}(\text{CD}_3)_2$ in CD_3CN revealed two types of results upon addition of one equivalent $^{\text{Ac}}\text{FcBF}_4$. For the previously published complex **1**, a 1:1 mixture of CH_3CH_3 and CH_3CD_3 was generated in ~25% yield for each product after eight hours (Scheme 2.5).³⁰ We observe 48% CH_3CH_3 for complex **2** and 30% CH_3CH_3 for complex **3**, but do not observe CH_3CD_3 for either of these crossover reactions. This gives evidence to support the idea that the last two complexes go through different mechanisms. Confirming by ^2H NMR, we observe 45% CD_3CD_3 and no CH_3CD_3 for complex **2**. When performing these sets of experiments with two equivalents $^{\text{Ac}}\text{FcBF}_4$, we observed no change in complexes **2** and **3** (Appendix D).

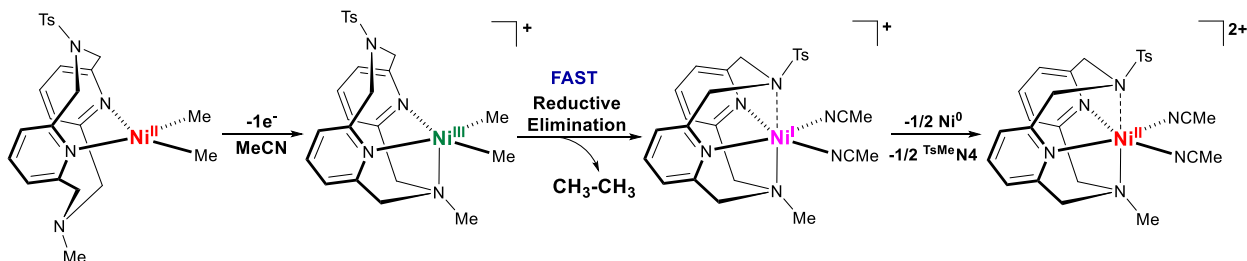
Scheme 2.5 Crossover reactivity studies of the $(^R\text{N}4)\text{Ni}^{\text{II}}\text{Me}_2$ complexes.



Based on the reactivity studies mentioned above, we propose that complexes **2** and **3** proceed through a different C–C bond formation mechanism than complex **1**, which goes through a six-coordinate system.³⁰ The faster ethane formation observed upon one-electron oxidation of the Ni^{II} complex **2** and **3** is proposed to proceed through a five-coordinate Ni^{III} system, which is

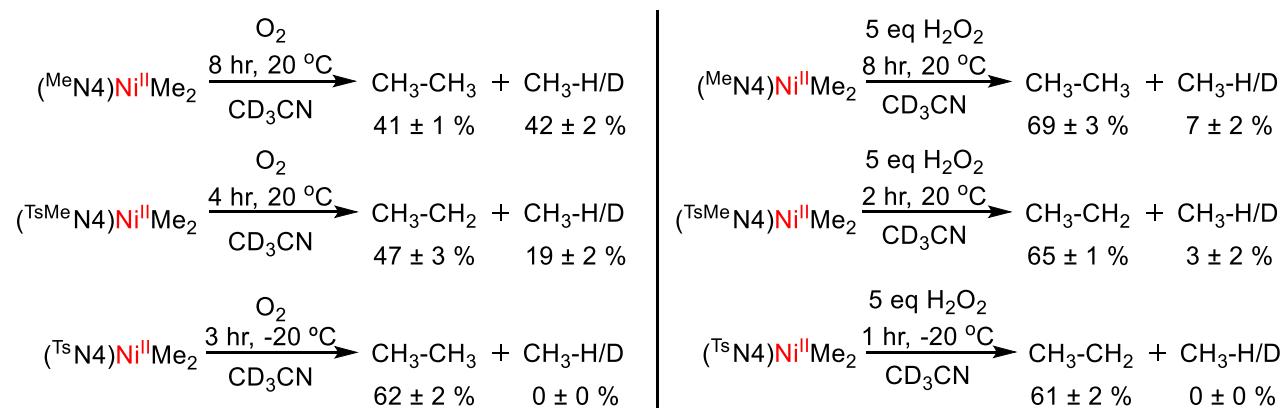
highly reactive (Scheme 2.6). The Ni complex then proceeds through a fast-direct reductive elimination that generates a Ni^I species. Lastly, a disproportionation generates a Ni^{II}-solvent complex (Appendix G) and nickel black.

Scheme 2.6 Proposed mechanism for one-electron oxidation of (^{TsMe}N4)Ni^{II}Me₂, **2**.



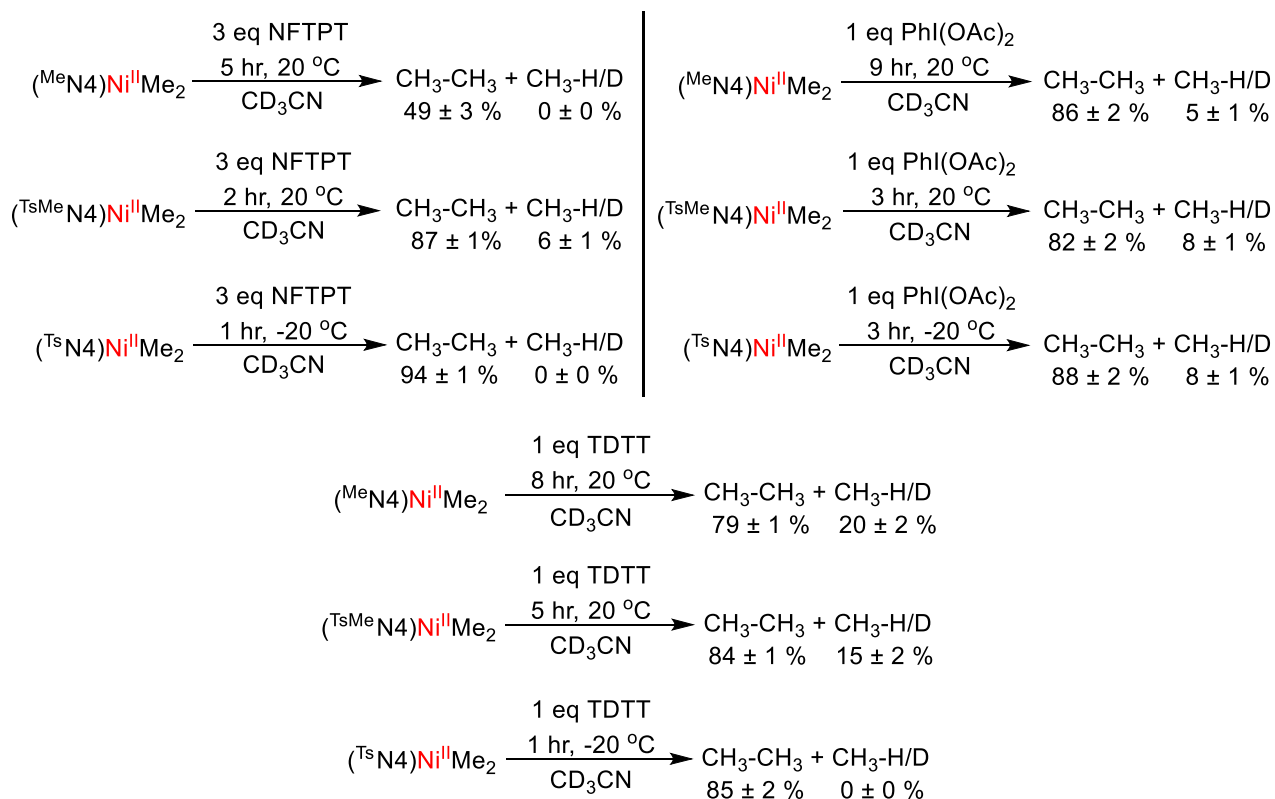
We attempted to use several other oxidants, including O₂ and H₂O₂ as oxidants, to probe for C–X bond formation. Upon reaction of **1**, **2** and **3** with O₂ or H₂O₂, we observed, in all cases, an appreciable amount of ethane formation, with varying amounts of methane (Scheme 2.7). No C–O products were observed due to the complexes' tendencies to undergo reductive elimination with a sp³ carbon. The last two complexes are also too reactive due to fast decomposition of the high-valent Ni^{III} intermediates even at low temperatures.

Scheme 2.7 C–C bond formation reactivity of the (^RN4)Ni^{II}Me₂ complexes with O₂ and H₂O₂.



Other oxidants, including 1-fluoro-2,4,6-trimethylpyridinium triflate (NFTPT), (diacetoxyiodo)benzene (PhI(OAc)₂) and 5-(trifluoromethyl)dibenzothiophenium trifluoromethanesulfonate (TDTT), were also unable to generate new C–X bonds, although high yields of ethane formation were observed in all cases (Scheme 2.8). The trend is consistent with a faster reductive elimination from complexes bearing more electron withdrawing substituents on the axial ligand amines. This is most likely due to the tosyl amine arms binding less tightly to the nickel center, creating five- or four-coordinate conformations, which undergo reductive elimination more rapidly than a six-coordinate geometry.

Scheme 2.8 C–C bond formation reactivity of the (^RN₄)Ni^{II}Me₂ complexes with NFTPT, PhI(OAc)₂ and TDTT.



2.3.3 Catalytic Reactivity of (^RN₄)Ni^{II}Br₂ Complexes

In addition to stoichiometric C–C and C–X bond formation studies, we also investigated the ability of the (^RN₄)NiBr₂ complexes to catalyze cross-coupling reactions (Scheme 2.9). These complexes are capable catalysts for Kumada cross-coupling between aryl iodides and aryl Grignard reagents. (^{TsMe}N₄)NiBr₂ is the most optimal catalyst out of the three complexes that were analyzed, with a 94% yield for aryl-aryl coupling product (Table 2.1). Using ^{TsMe}N₄ as a ligand, we showed that it is the most optimal option in terms of reactivity and stability when utilized in cross-coupling reactions.

Scheme 2.9 Kumada cross-coupling reactions catalyzed by (^RN₄)Ni^{II}Br₂.

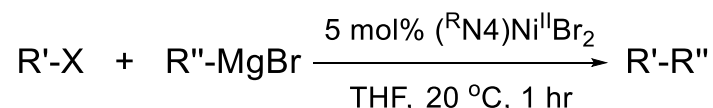


Table 2.1 Kumada cross-Coupling reactions catalyzed by (^RN₄)Ni^{II}Br₂.

R'-X	R''MgX	Yield ^a (%)		
		(^{Me} N ₄)Ni ^{II} Br ₂	(^{TsMe} N ₄)Ni ^{II} Br ₂	(^{Ts} N ₄)Ni ^{II} Br ₂
p-Tolyl-I	PhenylMgBr	73 ± 3	94 ± 4	58 ± 1
p-Tolyl-I	HexylMgBr	35 ± 2	37 ± 3	18 ± 1
Octyl-I	PhenylMgBr	13 ± 2	14 ± 2	4 ± 1

^a Yields (%) were determined by GC-FID vs. decane as internal standard; no coupled products were observed in these reactions in the absence of (^RN₄)NiBr₂.

2.4 Conclusion

In conclusion, we described the use of three different ligands that provide both stabilizing and destabilizing effects on high-valent nickel species. All isolated complexes were fully characterized, and their C–C and C–heteroatom bond formation reactivity tested. ^{TsMe}N₄ and ^{Ts}N₄ complexes make a less stable and more reactive Ni^{III} complex than the ^{Me}N₄ complex.

$(^{\text{Tsm}}\text{N4})\text{Ni}^{\text{II}}\text{Me}_2$ and $(^{\text{Tsn}}\text{N4})\text{Ni}^{\text{II}}\text{Me}_2$ show no crossover reactivity, and therefore have much faster C–C bond formation than the $(^{\text{Me}}\text{N4})\text{Ni}^{\text{II}}\text{Me}_2$ complex. O_2 or H_2O_2 could also be used to oxidize $(^{\text{R}}\text{N4})\text{Ni}^{\text{II}}\text{Me}_2$, leading to C–C bond formation, however, no C–O bond formation was detected. The $(^{\text{R}}\text{N4})\text{Ni}^{\text{II}}\text{Br}_2$ complexes were also shown to be competent catalysts in Kumada coupling reactions. Future work will focus on stabilizing the complexes by adding a cycloneophyl group instead of the dimethyl substrates and probing the C-heteroatom bond formation reactivity.

2.5 Acknowledgements

We thank the National Science Foundation (CHE-1255424) for support. The purchase of the Bruker EMX-PLUS EPR spectrometer was supported by the National Science Foundation (MRI, CHE-1429711). We also thank Dr. Jason W. Schultz for the EPR measurements.

2.6 References

1. Diederich, F.; Stang, P. J., *Metal-Catalyzed Cross-Coupling Reactions*. Wiley-VCH: Weinheim; New York, 1998.
2. Netherton, M. R.; Fu, G. C., Nickel-catalyzed cross-couplings of unactivated alkyl halides and pseudohalides with organometallic compounds. *Adv. Synth. Catal.* **2004**, *346* (13-15), 1525.
3. Frisch, A. C.; Beller, M., Catalysts for cross-coupling reactions with non-activated alkyl halides. *Angew. Chem., Int. Ed.* **2005**, *44* (5), 674.
4. Terao, J.; Kambe, N., Cross-Coupling Reaction of Alkyl Halides with Grignard Reagents Catalyzed by Ni, Pd, or Cu Complexes with pi-Carbon Ligand(s). *Acc. Chem. Res.* **2008**, *41* (11), 1545.
5. Glorius, F., Asymmetric Cross-Coupling of Non-Activated Secondary Alkyl Halides. *Angew. Chem., Int. Ed.* **2008**, *47* (44), 8347.

6. Phapale, V. B.; Cardenas, D. J., Nickel-catalysed Negishi cross-coupling reactions: scope and mechanisms. *Chem. Soc. Rev.* **2009**, *38* (6), 1598.
7. Rudolph, A.; Lautens, M., Secondary Alkyl Halides in Transition-Metal-Catalyzed Cross-Coupling Reactions. *Angew. Chem., Int. Ed.* **2009**, *48* (15), 2656.
8. Knochel, P.; Thaler, T.; Diene, C., Pd-, Ni-, Fe-, and Co-Catalyzed Cross-Couplings Using Functionalized Zn-, Mg-, Fe-, and In-Organometallics. *Isr. J. Chem.* **2012**, *50* (5-6), 547.
9. Hartwig, J. F., *Organotransition Metal Chemistry: From Bonding to Catalysis*. University Science Books: Sausalito, 2010; p 1127 pp.
10. Amatore, C.; Jutand, A., Rates and mechanism of biphenyl synthesis catalyzed by electrogenerated coordinatively unsaturated nickel complexes. *Organometallics* **1988**, *7* (10), 2203.
11. Tsou, T. T.; Kochi, J. K., Mechanism of biaryl synthesis with nickel complexes. *J. Am. Chem. Soc.* **1979**, *101* (25), 7547.
12. Tsou, T. T.; Kochi, J. K., Reductive Coupling of Organometals Induced by Oxidation - Detection of Metastable Paramagnetic Intermediates. *J. Am. Chem. Soc.* **1978**, *100* (5), 1634.
13. Koo, K.; Hillhouse, G. L., Carbon-Nitrogen Bond Formation by Reductive Elimination from Nickel(II) Amido Alkyl Complexes. *Organometallics* **1995**, *14* (9), 4421.
14. Matsunaga, P. T.; Mavropoulos, J. C.; Hillhouse, G. L., Oxygen-Atom Transfer from Nitrous-Oxide (N=O=O) to Nickel Alkyls - Syntheses and Reactions to Nickel(II) Alkoxides. *Polyhedron* **1995**, *14* (1), 175.
15. Lin, B. L.; Clough, C. R.; Hillhouse, G. L., Interactions of aziridines with nickel complexes: Oxidative-addition and reductive-elimination reactions that break and make C-N bonds. *J. Am. Chem. Soc.* **2002**, *124* (12), 2890.

16. Yu, S.; Dudkina, Y.; Wang, H.; Kholin, K. V.; Kadirov, M. K.; Budnikova, Y. H.; Vicic, D. A., Accessing perfluoroalkyl nickel(II), (III), and (IV) complexes bearing a readily attached [C4F8] ligand. *Dalton Trans.* **2015**, 44 (45), 19443.
17. Iluc, V. M.; Miller, A. J. M.; Anderson, J. S.; Monreal, M. J.; Mehn, M. P.; Hillhouse, G. L., Synthesis and Characterization of Three-Coordinate Ni(III)-Imide Complexes. *J. Am. Chem. Soc.* **2011**, 133 (33), 13055.
18. Klein, A.; Budnikova, Y. H.; Sinyashin, O. G., Electron transfer in organonickel complexes of α -diimines: Versatile redox catalysts for C–C or C–P coupling reactions – A review. *J. Organomet. Chem.* **2007**, 692 (15), 3156.
19. Jones, G. D.; Martin, J. L.; McFarland, C.; Allen, O. R.; Hall, R. E.; Haley, A. D.; Brandon, R. J.; Konovalova, T.; Desrochers, P. J.; Pulay, P.; Vicic, D. A., Ligand redox effects in the synthesis, electronic structure, and reactivity of an alkyl-alkyl cross-coupling catalyst. *J. Am. Chem. Soc.* **2006**, 128 (40), 13175.
20. Hu, X., Nickel-catalyzed cross coupling of non-activated alkyl halides: a mechanistic perspective. *Chem. Sci.* **2011**, 2 (10), 1867.
21. Biswas, S.; Weix, D. J., Mechanism and Selectivity in Nickel-Catalyzed Cross-Electrophile Coupling of Aryl Halides with Alkyl Halides. *J. Am. Chem. Soc.* **2013**, 135, 16192.
22. Tasker, S. Z.; Standley, E. A.; Jamison, T. F., Recent advances in homogeneous nickel catalysis. *Nature* **2014**, 509 (7500), 299.
23. Cornella, J.; Edwards, J. T.; Qin, T.; Kawamura, S.; Wang, J.; Pan, C. M.; Gianatassio, R.; Schmidt, M.; Eastgate, M. D.; Baran, P. S., Practical Ni-Catalyzed Aryl-Alkyl Cross-Coupling of Secondary Redox-Active Esters. *J. Am. Chem. Soc.* **2016**, 138 (7), 2174.

24. Khusnutdinova, J. R.; Rath, N. P.; Mirica, L. M., Stable Mononuclear Organometallic Pd(III) Complexes and Their C-C Bond Formation Reactivity. *J. Am. Chem. Soc.* **2010**, *132* (21), 7303.
25. Khusnutdinova, J. R.; Rath, N. P.; Mirica, L. M., Dinuclear Palladium(III) Complexes with a Single Unsupported Bridging Halide Ligand: Reversible Formation from Mononuclear Palladium(II) or Palladium(IV) Precursors. *Angew. Chem., Int. Ed.* **2011**, *50* (24), 5532.
26. Tang, F.; Zhang, Y.; Rath, N. P.; Mirica, L. M., Pd(III) and Pd(IV) Intermediates in the Aerobic C-C bond formation from a Pd(II) Dimethyl Precursor. *Organometallics* **2012**, *31* (18), 6690.
27. Zheng, B.; Tang, F.; Luo, J.; Schultz, J. W.; Rath, N. P.; Mirica, L. M., Organometallic Nickel(III) Complexes Relevant to Cross-Coupling and Carbon-Heteroatom Bond Formation Reactions. *J. Am. Chem. Soc.* **2014**, *136* (17), 6499.
28. Khusnutdinova, J. R.; Rath, N. P.; Mirica, L. M., The Conformational Flexibility of the Tetradentate Ligand tBuN4 is Essential for the Stabilization of (tBuN4)PdIII Complexes. *Inorg. Chem.* **2014**, *53* (24), 13112.
29. Qu, F.; Khusnutdinova, J. R.; Rath, N. P.; Mirica, L. M., Dioxygen activation by an organometallic Pd(II) precursor: formation of a Pd(IV)-OH complex and its C-O bond formation reactivity. *Chem. Comm.* **2014**, *50* (23), 3036.
30. Schultz, J. W.; Fuchigami, K.; Zheng, B.; Rath, N. P.; Mirica, L. M., Isolated Organometallic Nickel(III) and Nickel(IV) Complexes Relevant to Carbon-Carbon Bond Formation Reactions. *J. Am. Chem. Soc.* **2016**, *138* (39), 12928.
31. Tang, F. Z.; Rath, N. P.; Mirica, L. M., Stable bis(trifluoromethyl)nickel(III) complexes. *Chem. Comm.* **2015**, *51* (15), 3113.

32. Tang, F.; Qu, F.; Khusnutdinova, J. R.; Rath, N. P.; Mirica, L. M., Structural and Reactivity Comparison of Organometallic Pd(III) and Pd(IV) Complexes in an Identical Ligand Environment. *Dalton Trans.* **2012**, *41*, 14046.
33. Khusnutdinova, J. R.; Rath, N. P.; Mirica, L. M., The Aerobic Oxidation of a Pd(II) Dimethyl Complex Leads to Selective Ethane Elimination from a Pd(III) Intermediate. *J. Am. Chem. Soc.* **2012**, *134* (4), 2414.
34. Wessel, A. J.; Schultz, J. W.; Tang, F.; Duan, H.; Mirica, L. M., Improved synthesis of symmetrically & asymmetrically N-substituted pyridinophane derivatives. *Org. Biomol. Chem.* **2017**, *15* (46), 9923.
35. Connelly, N. G.; Geiger, W. E., Chemical redox agents for organometallic Chemistry. *Chem. Rev.* **1996**, *96*, 877.
36. Schultz, J. W.; Fuchigami, K.; Zheng, B.; Rath, N. P.; Mirica, L. M., Isolated Organometallic Nickel(III) and Nickel(IV) Complexes Relevant to Carbon-Carbon Bond Formation Reactions. *J. Am. Chem. Soc.* **2016**, *138* (39), 12928.
37. Loaiza, A.; Borchardt, D.; Zaera, F., A NMR method for the analysis of mixtures of alkanes with different deuterium substitutions. *Spectrochimica Acta Part A: Molecular and Biomolecular Spectroscopy* **1997**, *53* (14), 2481.
38. Gottlieb, H. E.; Kotlyar, V.; Nudelman, A., NMR Chemical Shifts of Common Laboratory Solvents as Trace Impurities. *J. Org. Chem.* **1997**, *62* (21), 7512.
39. Fulmer, G. R.; Miller, A. J. M.; Sherden, N. H.; Gottlieb, H. E.; Nudelman, A.; Stoltz, B. M.; Bercaw, J. E.; Goldberg, K. I., NMR Chemical Shifts of Trace Impurities: Common Laboratory Solvents, Organics, and Gases in Deuterated Solvents Relevant to the Organometallic Chemist. *Organometallics* **2010**, *29* (9), 2176.

Chapter 3

Aerobic C–C and C–O Bond Formation Reactions Mediated by High-Valent Organometallic Nickel Species

3.1 Introduction

Nickel catalysts are commonly used for cross-coupling reactions such as Negishi, Kumada and Suzuki couplings.¹⁻¹¹ The most common oxidation states for these catalytic transformation are Ni⁰, Ni^I, and Ni^{II}, although more recent studies show that Ni^{III} and Ni^{IV} oxidation states can also play a key role in catalysis.¹²⁻¹⁹ The formation of C–C and C–heteroatom atom bond formation play a fundamental facet in organic transformations. Today, C–C cross coupling is one of the most powerful tools for the construction of new C-C bonds.¹¹ However, limited examples exist of Ni-mediated C–heteroatom bond formation reactions,¹⁸⁻²⁹ likely due to the difficulty of accessing high-valent organometallic Ni species that can undergo reductive elimination.

In the past several years we have employed tetradentate pyridinophane ligands to stabilize uncommon organometallic Pd^{III/IV} and Ni^{III/IV} complexes.³⁰⁻³⁷ These high-valent complexes are capable of C–C and C–heteroatom bond formations reactions. In addition, we have recently reported the use of the ligand 1,4,7-trimethyl-1,4,7-triazacyclonane to stabilize high-valent Ni^{III/IV} complexes that undergo C–C and C–heteroatom bond formation reactions.²⁹ With this ligand, small amounts of C–O bond formation were observed upon oxidation of (Me₃tacn)Ni^{II}(CH₂CMe₂-*o*-C₆H₄) with oxygen.²⁹ Herein, we report the use of a modified pyridinophane ligand that directly affects that stability and reactivity of the corresponding Ni complexes. We tested the effect of the N substituents on the axial nitrogen by replacing the methyl groups with a more electron-withdrawing toluenesulfonate (tosyl, Ts) group or a bulkier *tert*-butyl group (*t*Bu). By employing a Ni metallacycle structure motif we have been able to isolate Ni^{III} species and also perform uncommon oxidatively-induced C–C and C–O bond formation reactions using O₂ or H₂O₂ as the oxidants. The ability to control the relative reactivity of C–C vs. C–heteroatom bond formation should have important implications in organic transformations.

3.2 Experimental Section

Reagents and Materials. All manipulations were carried out under a nitrogen atmosphere using standard Schlenk and glove box techniques if not indicated otherwise. All reagents for which the synthesis was not given are commercially available from Aldrich, Acros or STREM and were used as received without further purification. Solvents were purified prior to use by passing through a column of activated alumina using an MBRAUN SPS. N,N'-R-2,11-diaza[3.3](2,6)pyridinophane (R= Me, TsMe, Ts and tBu) (^RN₄),³⁸⁻³⁹ (Py)₂Ni^{II}(cycloneophyl),⁴⁰ (^{Me}N₄)Ni^{III}(cycloneophyl),⁴¹ ferrocenium hexafluorophosphate (FcPF₆),⁴² acetylferrocene tetrafluoroborate (^{Ac}FcBF₄)⁴² were prepared according to the literature procedures. Other abbreviations used throughout this chapter: silver hexafluoroantimony (AgSbF₆), 1-Fluoro-2,4,6-trimethylpyridinium triflate (NFTPT), 5-(trifluoromethyl)dibenzothiophenium trifluoromethanesulfonate (TDTT), meta-chloroperoxybenzoic acid (*m*CPBA), xenon difluoride (XeF₂) and (diacetoxyiodo)benzene (PhI(OAc)₂).

3.2.1 Synthesis of the Nickel Complexes

Preparation of (^{Me}N₄)Ni^{II}(cycloneophyl) (1). A slightly modified procedure was used to make the (^{Me}N₄)Ni(cycloneophyl) complex then reported by Mirica and co-worker in 2016.⁴¹ A solution of ^{Me}N₄ (61.6 mg, 0.23 mmol) and (Py)₂Ni^{II}(cycloneophyl) (87.8 mg, 0.25 mmol) in tetrahydrofuran (THF) (5 mL) was stirred at 20 °C for 14 hours. The solution was evaporated and re-dissolved in a minimum amount of THF. After filtration the solution was evaporated to dryness and triturated with pentane five times. The solid was dried under vacuum to obtain an orange-yellow powder (76.1 mg, 0.17 mmol, 72%).

^1H NMR (300 MHz, MeCN- d_3), δ (ppm): 7.51 (m, 2H, I), 7.10 (m, 4H, H), 6.67 (m, 6H, G), 6.38 (t, $J = 6.4$ Hz, 1H, F), 5.88 (d, $J = 5.9$ Hz, 1H, E), 4.22 (m, 4H, D), 2.24 (s, 6H, C), 1.31 (s, 6H, B), 1.15 (s, 2H, A) (Figure 3.1).

Note: further characterization was reported by Mirica and co-workers in 2016.⁴¹

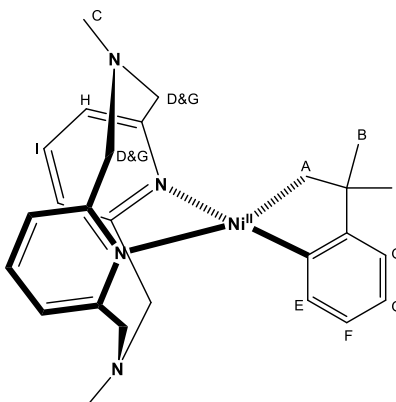


Figure 3.1 Proton structural assignments from NMR experiments for ($^{\text{Me}}\text{N}_4$)Ni $^{\text{II}}$ (cycloneophyl).

Preparation of ($^{\text{Tsm}}\text{MeN}_4$)Ni $^{\text{II}}$ (cycloneophyl) (2). A solution of $^{\text{Tsm}}\text{MeN}_4$ (134.0 mg, 0.33 mmol) and (Py) $_2$ Ni $^{\text{II}}$ (cycloneophyl) (125.0 mg, 0.36 mmol) in THF (5 mL) was stirred at 20 °C for 14 hours. The solution was evaporated and re-dissolved in a minimum amount of THF. After filtration the solution was evaporated to dryness and triturated with pentane five times. The solid was dried under vacuum to obtain a yellow powder (159.5 mg, 0.27 mmol, 81%).

^1H NMR (600 MHz, THF- d_8), δ (ppm): 7.95 (d, $J = 7.8$ Hz, 2H, W), 7.90 (t, $J = 7.0$ Hz, 1H, V), 7.83 (t, $J = 7.1$ Hz, 1H, U), 7.78 (d, $J = 7.5$ Hz, 1H, T), 7.68 (d, $J = 7.5$ Hz, 1H, S), 7.65 (d, $J = 7.8$ Hz, 2H, R), 7.44 (d, $J = 7.4$ Hz, 1H, Q), 7.40 (d, $J = 7.4$ Hz, 1H, P), 7.05 (m, 4H, O), 6.85 (t, $J = 7.2$ Hz, 1H, N), 6.78 (d, $J = 7.0$ Hz, 1H, M), 6.52 (t, $J = 7.0$ Hz, 1H, L), 5.68 (d, $J = 14.4$ Hz, 1H, K), 5.21 (d, $J = 14.4$ Hz, 1H, J), 5.15 (d, $J = 14.5$ Hz, 1H, I), 4.27 (d, $J = 14.2$ Hz, 1H, H), 4.22 (d,

$J = 14.2$ Hz, 1H, G), 2.41 (s, 3H, F), 2.26 (s, 3H, E), 1.40 (s, 3H, D), 1.21 (d, $J = 9.7$ Hz, 1H, C), 1.15 (s, 3H, B), 1.10 (d, $J = 9.7$ Hz, 1H, A) (Figure 3.2).

^{13}C NMR (600 MHz, THF- d_8), δ (ppm): 170.02 (u), 159.17 159.24 159.34 159.45 159.57(t), 144.28 (s), 138.58 (r), 136.81 (q), 136.98 (q'), 135.45 (p), 130.57 (o), 127.75 (n), 125.68 (m), 125.79 (m'), 125.12 (l), 125.28 (l'), 123.44 (k), 122.59 (j), 121.40(i), 63.85 (h), 63.90 (h'), 57.90 (g), 58.08 (g'), 48.51 (f), 41.17 (e), 38.05 (d), 24.95 (c), 33.35 (b), 21.26 (a) (Figure 3.2).

Elemental analysis: found C 61.63, H 6.04, N 8.58%; calculated $\text{C}_{32}\text{H}_{36}\text{N}_4\text{NiO}_2\text{S}\cdot 1.5\cdot\text{H}_2\text{O}$ C, 61.35, H 6.28, N 8.94%

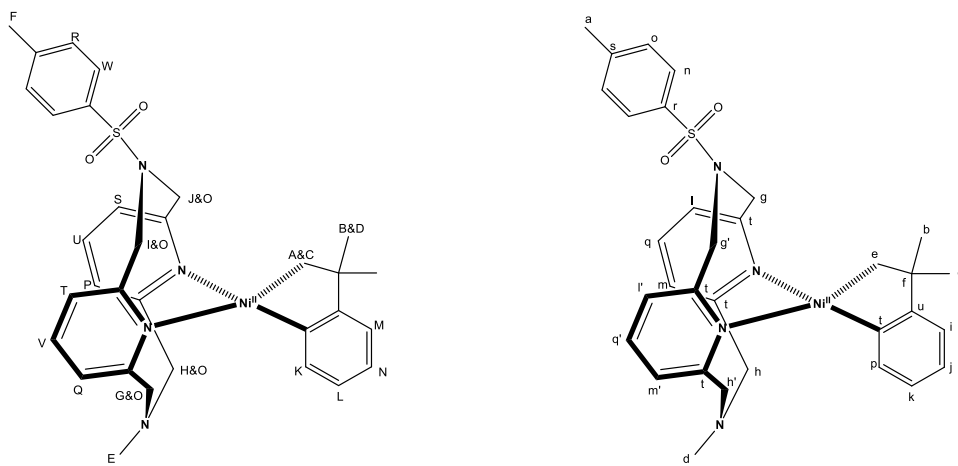


Figure 3.2 Proton (left) and carbon (right) structural assignments from NMR experiments for $(\text{TsMeN}_4)\text{Ni}^{\text{II}}(\text{cycloneophyl})$.

Preparation of $(\text{TsMeN}_4)\text{Ni}^{\text{II}}(\text{cycloneophyl})$ (3). A solution of TsMeN_4 (111.1 mg, 0.203 mmol) and $(\text{Py})_2\text{Ni}^{\text{II}}(\text{cycloneophyl})$ (77.6 mg, 0.224 mmol) in THF (5 mL) was stirred at 20 °C for 14 hours. The solution was evaporated and re-dissolved in a minimum amount of THF. After filtration the solution was evaporated to dryness and triturated with pentane five times. The solid was dried under vacuum to obtain a yellow powder (100.5 mg, 0.136 mmol, 67%).

^1H NMR (500 MHz, THF- d_8), δ (ppm): 7.74 (d, $J = 8.2$ Hz, 4H, M), 7.64 (m, 2H, L), 7.47 (dd, $J = 17.7, 7.6$ Hz, 4H, K), 7.37 (d, $J = 8.2$ Hz, 4H, J), 6.80 (dd, $J = 14.8, 4.7$ Hz, 4H, I), 6.55 (t, $J = 7.3$ Hz, 1H, H), 6.48 (d, $J = 7.4$ Hz, 1H, G), 6.23 (t, $J = 7.3$ Hz, 1H, F), 5.43 (d, $J = 7.3$ Hz, 1H, E), 5.23 (dd, $J = 22.7, 14.7$ Hz, 4H, D), 2.40 (s, 6H, C), 1.15 (s, 6H, B), 0.90 (s, 2H, A) (Figure 3.3).

APT (500 MHz, THF- d_8), δ (ppm): 170.24 (v), 159.47 (u), 159.28 (t), 158.54 (s), 144.42 (r), 138.65 (q), 138.35 (p), 138.12 (o), 135.24 (n), 130.73 (m), 127.92 (l), 126.21 (k), 126.12 (j), 123.81 (i), 123.03 (h), 121.68 (g), 58.62 (f), 58.48 (e), 48.58 (d), 42.38 (c), 34.21 (b), 21.43 (a) (Figure 3.3).

Elemental analysis: found C 59.93, H 5.52, N 6.95%; calculated $\text{C}_{38}\text{H}_{40}\text{N}_4\text{NiO}_4\text{S}_2 \cdot \text{H}_2\text{O}$ C, 60.25, H 5.59, N 7.40%

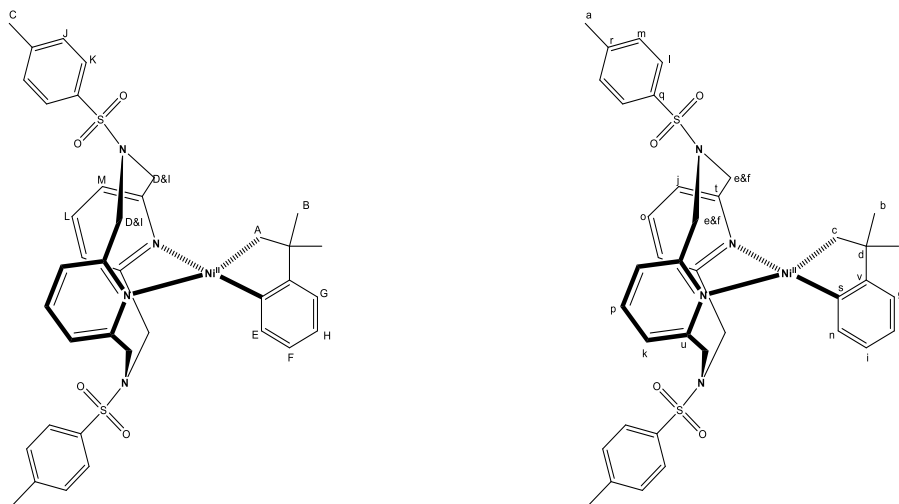


Figure 3.3 Proton (left) and carbon (right) structural assignments from NMR experiments for $(^t\text{BuN}_4)\text{Ni}^{\text{II}}(\text{cycloneophyl})$.

Preparation of $(^t\text{BuN}_4)\text{Ni}^{\text{II}}(\text{cycloneophyl})$ (4). A solution of $(^t\text{BuN}_4)$ (100.7 mg, 0.200 mmol) and $(\text{Py})_2\text{Ni}^{\text{II}}(\text{cycloneophyl})$ (69.8 mg, 0.200 mmol) in THF (5 mL) was stirred at 20 °C for 14 hours.

The solution was evaporated and re-dissolved in a minimum amount of THF. After filtration the

solution was evaporated to dryness and triturated with pentane five times. The solid was dried under vacuum to obtain a yellow powder (78.7 mg, 0.145 mmol, 73%).

^1H NMR (500 MHz, THF- d_8), δ (ppm): 7.44 (t, $J = 7.7$ Hz, 1H, L), 7.39 (t, $J = 7.7$ Hz, 1H, K), 7.05 (d, $J = 7.6$ Hz, 2H, J), 7.00 (d, $J = 7.6$ Hz, 2H, I), 6.65 – 6.56 (m, 5H, H), 6.53 (d, $J = 7.3$ Hz, 1H, G), 6.29 (t, $J = 7.2$ Hz, 1H, F), 5.94 (d, $J = 7.4$ Hz, 1H, E), 4.59 (dd, $J = 19.2, 13.8$ Hz, 2H, D), 1.38 (s, 16H, C), 1.34 (s, 6H, B), 1.27 (s, 2H, A) (Figure 3.4).

APT (500 MHz, THF- d_8), δ (ppm): 169.81 (s), 162.54 (r), 162.48 (q), 161.10 (p), 136.97 (o), 136.88 (n), 136.45 (m), 123.92 (l), 123.79 (k), 123.14 (j), 122.08 (i), 121.32 (h), 60.26 (g), 60.13 (f), 57.70 (e), 48.95 (d), 40.60 (c), 34.43 (b), 28.51 (a) (Figure 3.4).

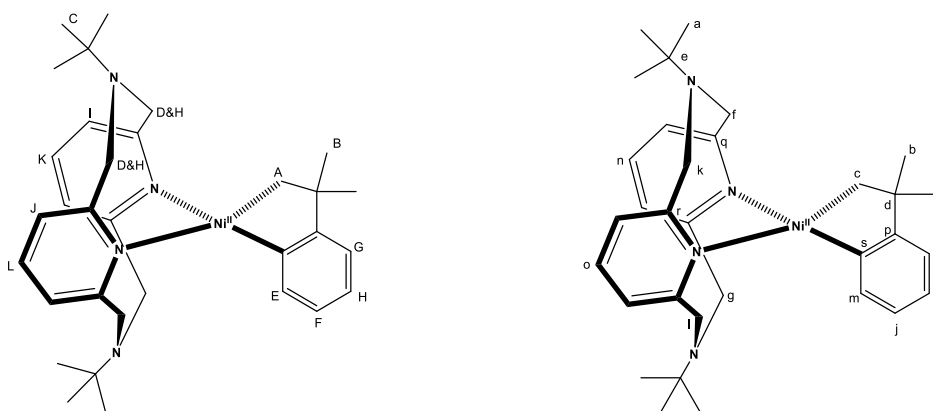


Figure 3.4 Proton (left) and carbon (right) structural assignments from NMR experiments for $(^t\text{Bu}_4\text{N})\text{Ni}^{\text{II}}(\text{cycloneophyl})$.

3.2.2 Reactivity Studies

General procedure for the isolation of the Ni^{III} complexes by EPR. An EPR tube was charged with a solution of $(^{\text{TsMe}}\text{N}_4)\text{Ni}^{\text{II}}(\text{cycloneophyl})$, $(^{\text{Ts}}\text{N}_4)\text{Ni}^{\text{II}}(\text{cycloneophyl})$ or $(^t\text{Bu}_4\text{N})\text{Ni}^{\text{II}}(\text{cycloneophyl})$ in acetonitrile (MeCN) or THF. A butyronitrile (PrCN) or 2-methyl-tetrahydrofuran (MeTHF) solution containing one equivalent of ferrocenium hexafluorophosphate

(FcPF₆), silver hexafluoroantimonate (AgSbF₆) or acetylferrocenium tetrafluoroborate (^{Ac}FcBF₄) was then added. The resulting solution of 1:3 MeCN:PrCN or 1:3 THF:MeTHF was shaken for five seconds and then frozen in liquid nitrogen.

General procedure for the reactivity studies of (^RN₄)Ni(cycloneophyl) complexes. In N₂-filled glove box, a solution of 5-7 mg of (^{Me}N₄)Ni^{II}(cycloneophyl), (^{TsMe}N₄)Ni^{II}(cycloneophyl), (^{Ts}N₄)Ni^{II}(cycloneophyl) or (^{tBu}N₄)Ni^{II}(cycloneophyl) complex in MeCN (2 mL) was added into a 5 mL vial containing 1,3,5-trimethoxybenzene as an internal standard. To this solution different oxidants were added (bubbled O₂ + 10% water, H₂O₂, ^mCPBA, PhI(OAc)₂, NFTPT, TDTT and XeF₂) and stirred for 14 hours at 70 °C. The next day 1 mL of 14% perchloric acid was added and stirred for an additional four hours at 70 °C. To this solution 3 mL of a saturated potassium carbonate solution was added. The solution was then extracted three times with 1 mL of diethyl ether and dried over potassium carbonate for 30 minutes. The solution was filtered and the yield of product(s) were obtained by GC/FID using 1,3,5-trimethoxybenzene as the internal standard and the identity of the products was confirmed by GC/MS.

General procedure for the oxidation studies of (^RN₄)Ni(cycloneophyl) intermediates by cryo-ESI-MS. A solution of 1mM (^RN₄)Ni^{II}(cycloneophyl) complex in 10% H₂O/acetone was saturated with O₂. To a second solution of 1mM (^RN₄)Ni^{II}(cycloneophyl) complex in acetone, 1mM of H₂O₂ was added. To both solutions perchloric acid was added and then the intermediates were analyzed at -80 °C by cryo-ESI-MS. All data is reported in Appendix F.

3.2.3 Physical Measurements

Nuclear Magnetic Resonance. ¹H NMR, ¹³C NMR, APT, gCOSY, NOESY, TOXY, HSQC and HMBC spectra were recorded on a Varian Mercury-300 spectrometer (300.121 MHz), Agilent

DD2-500 spectrometer (499.885 MHz) or Agilent DD2-600 spectrometer (599.736 MHz). Chemical shifts are reported in ppm and referenced to residual solvent resonance peaks.⁴³⁻⁴⁴ Abbreviations for the multiplicity of NMR signals are s (singlet), d (doublet), dd (doublet of doublets), t (triplet), m (multiplet). All the NMR spectra are included in Appendix A.

UV-Vis, EPR and EA. UV-visible spectra were recorded on a Varian Cary 50 Bio spectrophotometer and are reported as λ_{\max} , nm (ϵ , $M^{-1}\cdot\text{cm}^{-1}$). Select UV-vis spectra are shown in Appendix C. EPR spectra were recorded on a Bruker EMX-PLUS EPR or a JEOL JES-FA EPR spectrometer at X-band (~9.2 GHz) frequency in frozen solution at 77 K. The purchase of the Bruker EMX-PLUS EPR spectrometer was supported by the National Science Foundation (MRI, CHE-1429711). Elemental analyses were carried out by the Intertek Pharmaceutical Services.

Electrochemical Measurements. Cyclic voltammetry experiments were performed with a BASi EC Epsilon electrochemical workstation or a CHI 660D Electrochemical Analyzer. The electrochemical measurements were taken in a glove box under nitrogen. A glassy carbon disk electrode ($d = 1.6$ mm) was used as the working electrode for cyclic voltammetry. The auxiliary electrode was a Pt wire for cyclic voltammetry measurements. The non-aqueous references electrode used was a silver wire dipped in a bleach solution (Ag/AgCl). The reference electrodes were calibrated against Cp₂Fe (Fc). Electrochemical-grade electrolytes from Fluka were used as the supporting electrolyte for electrochemical measurements. All CV spectra are included in Appendix B.

X-ray Crystallography. All X-ray crystallography experiments were performed by Dr. Nigam Rath. Suitable crystals were mounted on MiTeGen cryoloops in random orientations in a Bruker Kappa Apex-II CCD X-ray diffractometer equipped with an Oxford Cryostream LT device and a

fine focus Mo K α radiation X-ray source ($\lambda = 0.71073 \text{ \AA}$). Preliminary unit cell constants were determined with a set of 36 narrow frame scans. Typical data sets consist of combinations of ω and ϕ scan frames with a typical scan width of 0.5° and a counting time of 15–30 s/frame at a crystal-to-detector distance of 4.0 cm. The collected frames were integrated using an orientation matrix determined from the narrow frame scans. Apex II and SAINT software packages (Bruker Analytical X-Ray, Madison, WI, 2008) were used for data collection and data integration. Analysis of the integrated data did not show any decay. Final cell constants were determined by global refinement of xyz centroids of reflections from the complete data sets. Collected data were corrected for systematic errors using SADABS (Bruker Analytical X-Ray, Madison, WI, 2008) based on the Laue symmetry using equivalent reflections. Structure solutions and refinement were carried out using the SHELXTL-PLUS software package. The structures were solved by direct methods and refined successfully in specified crystal systems and space groups. Full matrix least-squares refinements were carried out by minimizing $\sum w(\text{Fo}^2 - \text{Fc}^2)^2$. The non-hydrogen atoms were refined anisotropically to convergence. Typically, the hydrogen atoms were treated using the appropriate riding model. The complete listings of X-ray diffraction parameters are included in Appendix G.

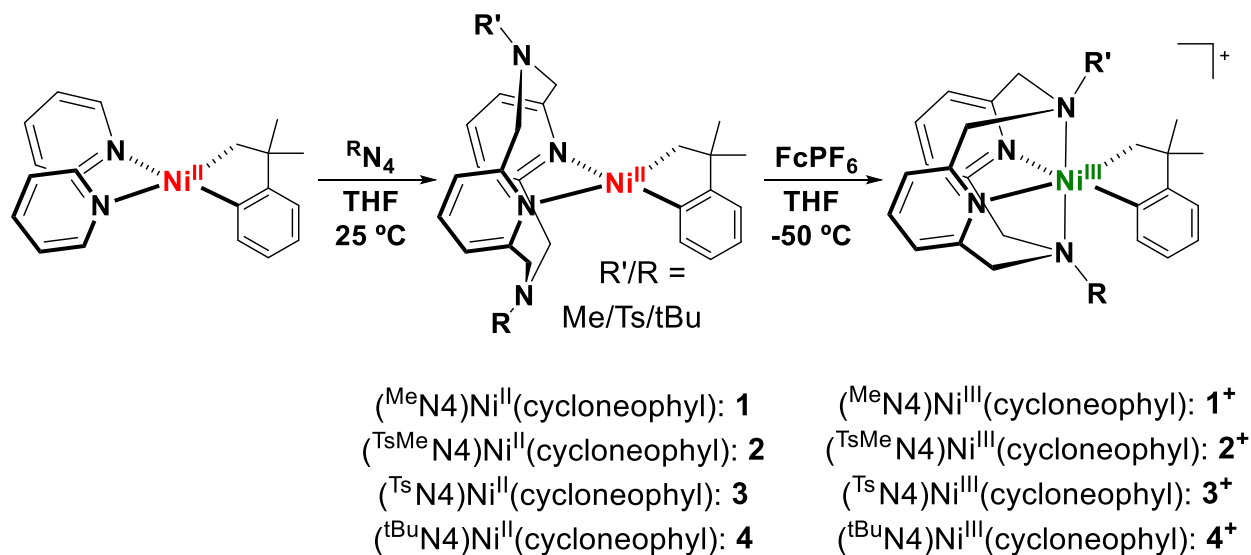
3.3 Results and Discussion

3.3.1 Synthesis and Characterization of Ni^{II/III} Complexes

The azomacrocyclic ligands N,N'-dimethyl-2,11-diaza[3.3](2,6)pyridinophane (^{Me}N₄), N-(p-toluenesulfonyl),N'-(methyl)-2,11-diaza[3.3](2,6)pyridinophane (^{TsMe}N₄) and N,N'-ditoluenesulfonyl-2,11-diaza[3.3](2,6)pyridinophane (^{Ts}N₄) and N,N'-di-*tert*-butyl-2,11-diaza[3.3](2,6)pyridinophane (^{tBu}N₄) were synthesized according to a literature procedure.³⁸⁻³⁹

With these ligands a series of cycloneophyl complexes were synthesized through a ligand exchange of $(\text{py})_2\text{Ni}^{\text{II}}(\text{cycloneophyl})$.^{40, 45} The orange Ni^{II} complex $(^{\text{Me}}\text{N4})\text{Ni}^{\text{II}}(\text{cycloneophyl})$, **1** was prepared in a 72% yield (Scheme 3.1) giving a higher yield than what has previously been reported.⁴⁶

Scheme 3.1 Synthesis of $(^{\text{R}}\text{N4})\text{Ni}(\text{cycloneophyl})$ complexes.



The second complex, a yellow Ni^{II} complex $(^{\text{TsMe}}\text{N4})\text{Ni}^{\text{II}}(\text{cycloneophyl})$, **2** was prepared in a 81% yield and was fully characterized. The CV shows an oxidation potential at -990 mV vs Fc^+/Fc , as well as a smaller oxidation wave at 70 mV and a second oxidation at 750 mV (Table 3.1). The two oxidations are tentatively assigned to the $\text{Ni}^{\text{III/II}}$ and $\text{Ni}^{\text{IV/III}}$ oxidation and the oxidation wave at 70 mV is proposed to correspond to a complex with a κ^3 ligand binding mode. The $\text{Ni}^{\text{III/II}}$ oxidation observed at -990 mV likely corresponds to the conformation of **2** with a κ^4 binding mode.^{29, 47} The third complex, $(^{\text{Ts}}\text{N4})\text{Ni}^{\text{II}}(\text{cycloneophyl})$, **3** was prepared in a 67% yield and was fully characterized by ^1H NMR and ^{13}C NMR. The CV shows an oxidation potential at -400 mV, which is tentatively assigned to the $\text{Ni}^{\text{III/II}}$ couple. Finally, the yellow Ni^{II} complex

(^tBuN4)Ni^{II}(cycloneophyl), **4** was prepared in a 73% yield and was also characterized by ¹H NMR and ¹³C NMR. The CV of complex **4** shows a higher first oxidation potential than the previously mentioned complexes at 200 mV vs Fc⁺/Fc, this might be due to the steric effect that the *tert*-butyl group has, slowing down the reaction due to steric bulk.

Table 3.1 Cyclic voltammetry (CV) data for (^RN4)Ni(cycloneophyl) complexes.

Complex	1	2	3	4
E _(Ni^{III}) (mV) ^{a,b}	-1700	-990	-400	200

^a E_(Ni^{III}) values reported vs Fc⁺/Fc at RT. ^b 100 mV/s scan rate.

The oxidation potentials of complexes **1-4** observed via cyclic voltammetry, can easily be oxidized with one equivalent of acetylferrocenium tetrafluoroborate (^{Ac}FcBF₄) or AgSbF₆ in THF at -50 °C to yield [(^{TsMe}N4)Ni^{III}(cycloneophyl)]BF₄, **2**⁺ and [(^{Ts}N4)Ni^{III}(cycloneophyl)]SbF₆, **3**⁺ and [(^tBuN4)Ni^{III}(cycloneophyl)]BF₄, **4**⁺. The X-ray structures of **2**⁺ and **3**⁺ show six-coordinate Ni^{III} centers in distorted octahedral geometries (Figure 3.5). In complex **2**⁺ the Ni-N_{Ts} (2.527 Å) bond is longer than Ni-N_{Me} (2.199 Å) bond, due to the tosyl group being electron withdrawing and the methyl-group being electron donating. The Ni-N₁ (2.182 Å) bond is longer than expected due to a trans effect of the sp³ carbon vs a sp² carbon. When comparing this to structure **3**⁺, both Ni-N_{Ts} bonds are further away from the Ni^{III} center (2.360 Å and 2.436 Å).

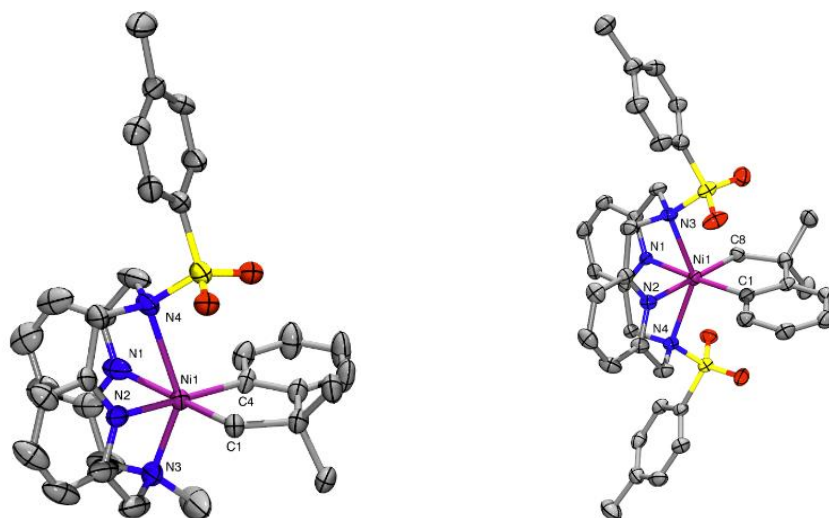


Figure 3.5 ORTEP representation of 2^+ (left) and 3^+ (right) with 50% probability thermal ellipsoids. Selected bond distances (\AA), 2^+ : Ni1-C1, 1.938; Ni1-C4, 1.938; Ni1-N1, 2.182; Ni1-N2, 1.867; Ni1-N3, 2.199; Ni1-N4, 2.527; 3^+ : Ni1-C1, 1.933; Ni1-C8, 1.982; Ni1-N1, 1.993; Ni1-N2, 2.010; Ni1-N3, 2.360; Ni1-N4, 2.436.

The EPR spectrum of complex 2^+ exhibits a rhombic signal with a superhyperfine coupling observed in the g_z direction due to one axial N donors ($I=1$) coupling to the Ni^{III} center (Figure 3.6). This suggests that the N_{TS} does not coordinate in the axial direction at a Ni^{III} stage. Although it is not a well-defined triplet there might be some very weak N_{TS} coupling. Complex 3^+ has a rhombic signal with a superhyperfine coupling to two nitrogen atoms in the g_z direction, suggesting that both N_{TS} 's bind to the nickel center (Figure 3.6). Also, a small amount of unknown Ni^{III} impurity is present in complex 3^+ . Simulation 1 and 2 were added in a 19:1 ratio respectively to simulate the experimental spectra properly. The last complex 4^+ also has a rhombic signal with a superhyperfine coupling observed in the g_z direction due to two axial N donors ($I=1$) coupling to the Ni^{III} center. Suggesting that both nitrogens bind in the axial direction with a strength of 11 G (Figure 3.6). With all the previously mentioned compounds in hand, we turned to probing their reactivity.

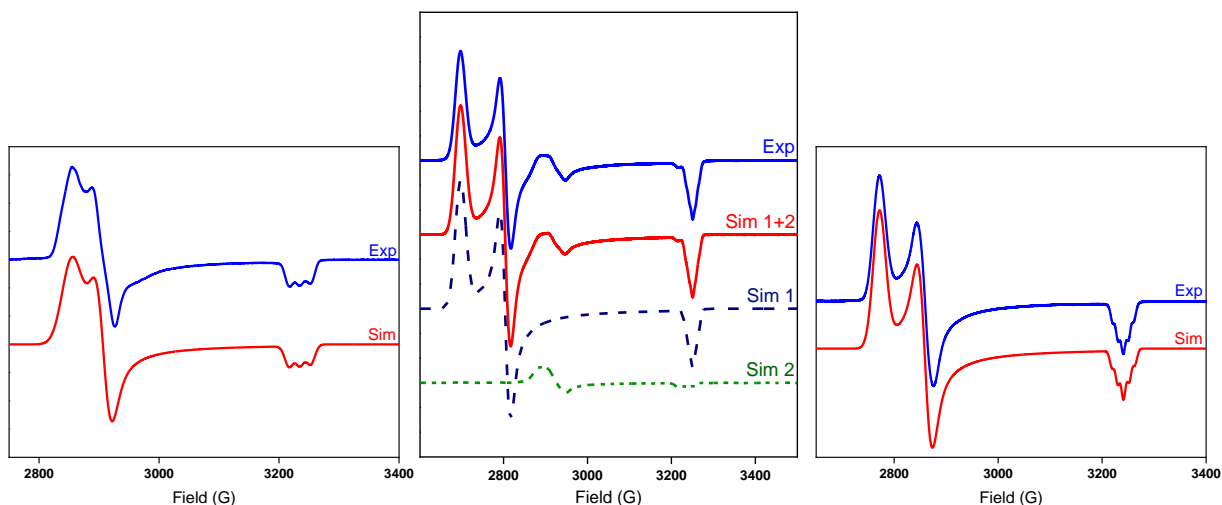


Figure 3.6 Experimental (1:3 MeCN:PrCN, 77K) and simulated EPR spectra of 2^+ (left) using the following parameters: $g_x=2.277$, $g_y=2.235$, $g_z=2.009$ (A_z (N) = 18.0 G). Experimental (1:3 MeCN:PrCN, 77K) and simulated EPR spectra of 3^+ (middle) using the following parameters for sim 1: $g_x=2.409$, $g_y=2.318$, $g_z=2.000$ (A_z (2N) = 8.0 G) and sim 2: $g_x=2.253$, $g_y=2.220$, $g_z=2.010$ (A_z (N) = 18.0 G). Simulation 1 and 2 were added in a 19:1 ratio respectively to simulate the experimental spectra properly. Experimental (1:3 MeCN:PrCN, 77K) and simulated EPR spectra of 4^+ (right) using the following parameters: $g_x=2.345$, $g_y=2.273$, $g_z=2.006$ (A_z (2N) = 11.0 G)

3.3.2 C–C Bond Formation Reactivity of $(^R\text{N}4)\text{Ni}^{\text{II}}(\text{cycloneophyl})$ Complexes

With the new $(^R\text{N}4)\text{Ni}^{\text{II}}(\text{cycloneophyl})$ complexes in hand, we set out to probe the reactivity for C–C and C–heteroatom bond formation reactions. First, we studied the oxidation $(^R\text{N}4)\text{Ni}^{\text{II}}(\text{cycloneophyl})$ with 1-Fluoro-2,4,6-trimethylpyridinium triflate (NFTPT), 5-(trifluoromethyl)dibenzothiophenium trifluoromethanesulfonate (TDTT), xenon difluoride (XeF_2) and (diacetoxyiodo)benzene ($\text{PhI}(\text{OAc})_2$) to observe any C–C and C–X bond formation. Previously these oxidants have been used for other high-valent transition metal chemistry including high-valent nickel chemistry.^{12, 19, 48-51} While no C–heteroatom bond formation was detected with complexes **1-4** we did observe high C–C bond formation. When comparing complex **1-4** with any of the oxidants stated above there is a noticeable trend. More electron withdrawing groups on the amine arm show higher C–C bond formation, with up to 99% conversion with XeF_2 as the oxidant using complex **3**. Although, when adding a *tert*-butyl group on the amine arm, a

drop in C–C bond formation was observed, and we see an increase in unreacted cycloneophyl (Scheme 3.2 and Table 3.2). Most likely this is due to the coordination of the amine arms that creates a six-coordinate high-valent intermediate that is less reactive towards reductive elimination than the five- or four-coordinate intermediates.

Additionally, we studied the oxidation of complexes **1-4** with O₂ and H₂O₂. The use of O₂ and H₂O₂ as an oxidant obviates the requirement for strong/toxic oxidants which generate undesired stoichiometric byproducts, making O₂ and H₂O₂ “greener” reagents for carbon–carbon and carbon–oxygen bond formation. The addition of O₂ to complexes **1-4** gave different shades of orange/red solutions. Solutions were heated for 14 hours at 70 °C, followed by an acidic workup and analyzed by GC-MS FID. To our delight, complexes **1** and **3** showed up to 15% combined yield of C–O bond formation and complex **2** showed up to 41% combined yield of C–O products (Scheme 3.2 and Table 3.2). No C–O bond formation was formed for complex **4** likely due to the steric bulk of the *tert*-butyl group. The GC-MS analysis also confirmed the presence of C–C coupled product for all four complexes with up to ~70% for complex **3**. *meta*-chloroperoxybenzoic acid (*m*CPBA) and H₂O₂ are also capable oxidants for performing C–C and C–O bond formation, but to a lesser extent giving lower yields. For all four complexes, we observe some *tert*-butylbenzene, indicating that some of the cycloneophyl groups immediately eliminates before undergoing oxidation. Complex **2** seems to be the sweet spot of stability vs reactivity to provide the best C–O bond formation results.

Scheme 3.2 General reaction for the formation of the different oxidation products.

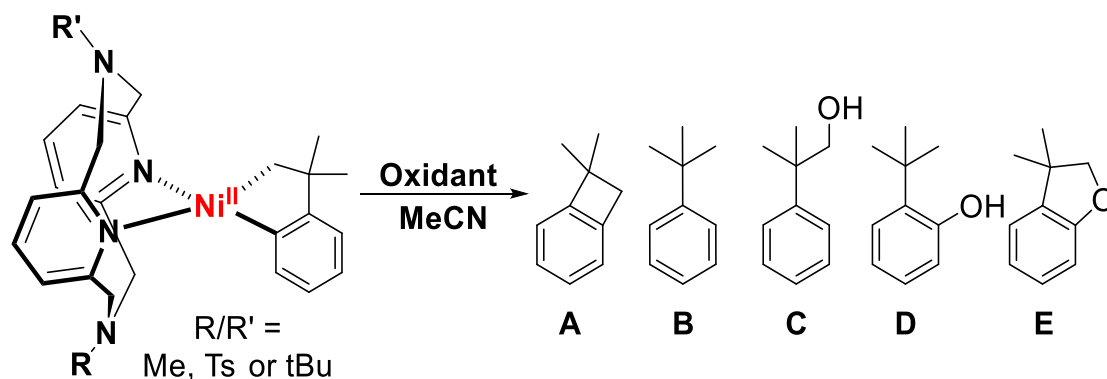


Table 3.2 Yields of the products from the reaction of (^RN₄)Ni^{II}(cycloneophyl) with a variety of oxidants.

Starting Complex	Oxidants	Yields (%) ^a					Sum (%)
		A	B	C	D	E	
(^{Ts} N ₄)Ni ^{II} (cycloneophyl)	O ₂	69	12	2	5	5	93
(^{TsMe} N ₄)Ni ^{II} (cycloneophyl)	O ₂	41	12	2	17	22	94
(^{Me} N ₄)Ni ^{II} (cycloneophyl)	O ₂	35	12	8	3	6	64
(^{tBu} N ₄)Ni ^{II} (cycloneophyl)	O ₂	27	6	0	0	0	33
(^{Ts} N ₄)Ni ^{II} (cycloneophyl)	2 eq. H ₂ O ₂	65	12	0	6	3	64
(^{TsMe} N ₄)Ni ^{II} (cycloneophyl)	2 eq. H ₂ O ₂	48	1	1	3	7	60
(^{Me} N ₄)Ni ^{II} (cycloneophyl)	2 eq. H ₂ O ₂	45	2	0	2	6	55
(^{tBu} N ₄)Ni ^{II} (cycloneophyl)	2 eq. H ₂ O ₂	17	0	0	0	0	17
(^{TsMe} N ₄)Ni ^{II} (cycloneophyl)	2 eq. <i>m</i> CPBA	37	11	4	7	11	70
(^{Ts} N ₄)Ni ^{II} (cycloneophyl)	2 eq. PhI(OAc) ₂	42	10	n/a	n/a	n/a	52
(^{TsMe} N ₄)Ni ^{II} (cycloneophyl)	2 eq. PhI(OAc) ₂	24	13	n/a	n/a	n/a	37
(^{Me} N ₄)Ni ^{II} (cycloneophyl)	2 eq. PhI(OAc) ₂	4	22	n/a	n/a	n/a	26
(^{Ts} N ₄)Ni ^{II} (cycloneophyl)	1 eq. NFTPT	96	4	n/a	n/a	n/a	100
(^{TsMe} N ₄)Ni ^{II} (cycloneophyl)	1 eq. NFTPT	32	27	n/a	n/a	n/a	59
(^{Me} N ₄)Ni ^{II} (cycloneophyl)	1 eq. NFTPT	17	39	n/a	n/a	n/a	56
(^{tBu} N ₄)Ni ^{II} (cycloneophyl)	1 eq. NFTPT	14	44	n/a	n/a	n/a	48
(^{Ts} N ₄)Ni ^{II} (cycloneophyl)	1 eq. TDDT	42	9	n/a	n/a	n/a	51
(^{TsMe} N ₄)Ni ^{II} (cycloneophyl)	1 eq. TDDT	33	15	n/a	n/a	n/a	48
(^{Me} N ₄)Ni ^{II} (cycloneophyl)	1 eq. TDDT	7	19	n/a	n/a	n/a	26
(^{tBu} N ₄)Ni ^{II} (cycloneophyl)	1 eq. TDDT	6	20	n/a	n/a	n/a	26
(^{Ts} N ₄)Ni ^{II} (cycloneophyl)	1 eq. XeF ₂	99	1	n/a	n/a	n/a	100
(^{TsMe} N ₄)Ni ^{II} (cycloneophyl)	1 eq. XeF ₂	50	16	n/a	n/a	n/a	66
(^{Me} N ₄)Ni ^{II} (cycloneophyl)	1 eq. XeF ₂	20	40	n/a	n/a	n/a	60

^a Yields (%) were determined by GC-FID vs. 1,3,5-trimethoxybenzene as internal standard. n/a indicates that no other C-X products were observed.

To better understand the mechanism of the oxidation of O_2 and H_2O_2 , $(^R N_4)Ni^{II}(\text{cycloneophyl})$ was oxidized with O_2 at $-50\text{ }^\circ\text{C}$ in 9:1 acetone- d_6 : D_2O . While no Ni^{IV} intermediates were observed by 1H NMR, the formation of Ni^{III} species was confirmed by EPR spectroscopy. In addition, cryo-electrospray mass spectrometry (cryo-ESI-MS) was employed in an attempt to detect any high-valent Ni intermediates arising from oxidation of $(^R N_4)Ni^{II}(\text{cycloneophyl})$ complexes with O_2 .^{25, 52} Interestingly, oxidation of **2** at $-80\text{ }^\circ\text{C}$ gives rise to two transient species that are tentatively assigned to a Ni^{IV} -hydroperoxo and a Ni^{IV} -hydroxo complex (**A** and **B**, Figure 3.7). The decay of the transient species leads to the formation of a persistent species that likely corresponds to a hydroxylated cycloneophyl (**C**) still bound to the Ni center (Scheme 3.3). The Ni^{III} hydroxylated cycloneophyl then undergoes reductive elimination to form a Ni^I complex and the desired C–O product. For the other two cycloneophyl complexes that form some C–O product (**1** and **3**), only a few high-valent Ni intermediates were observed although the final complexes were detected.

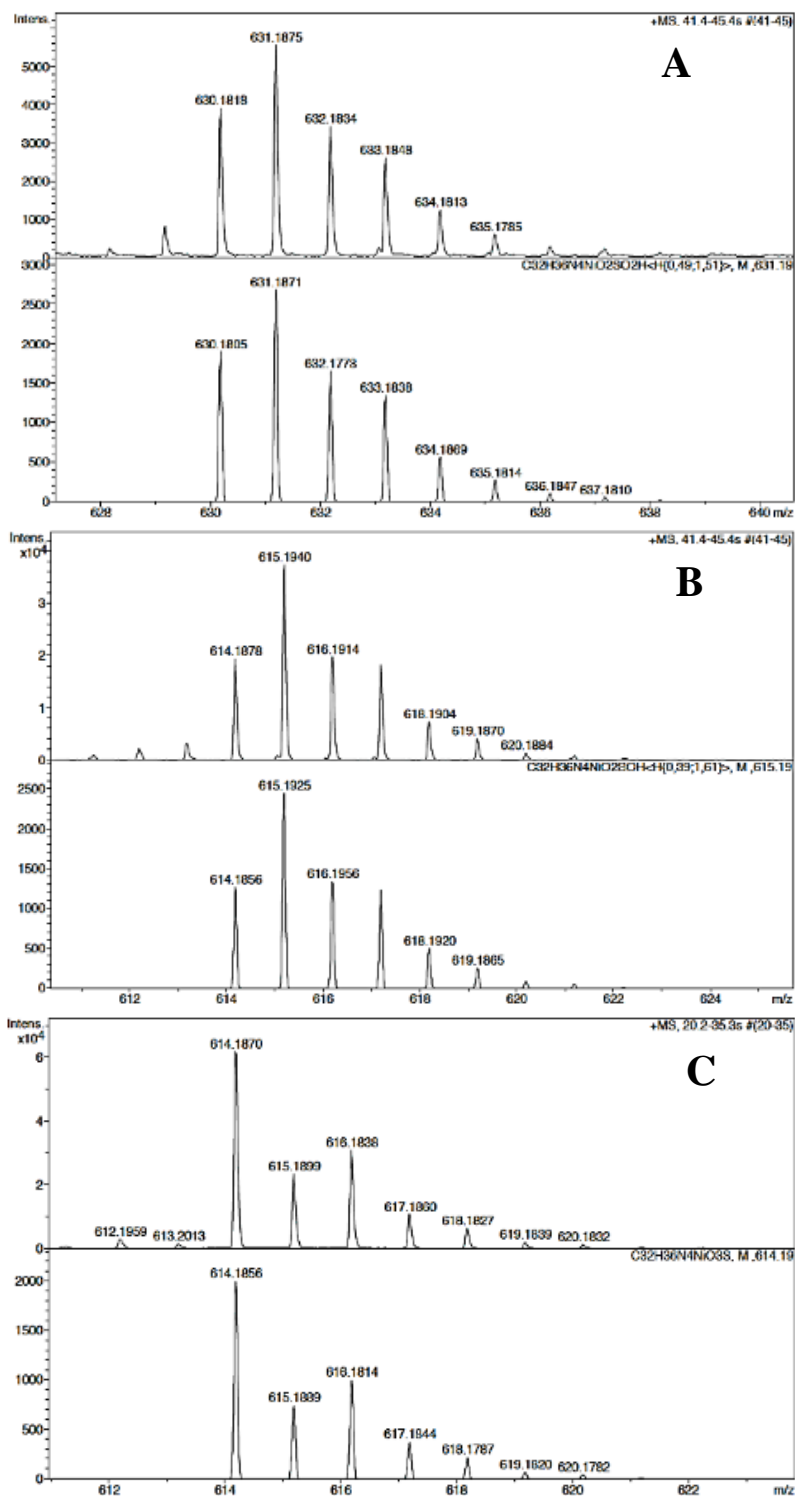
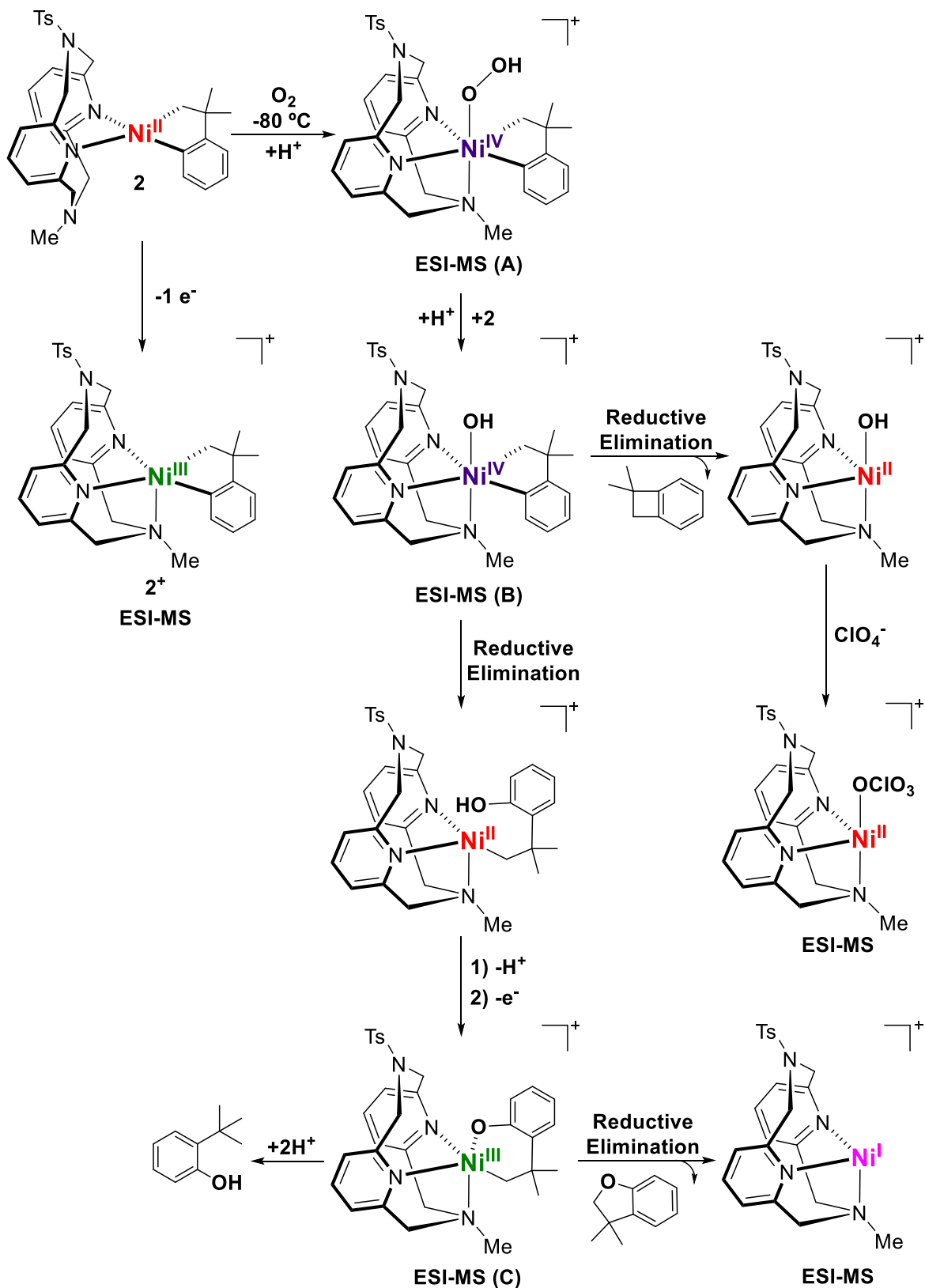


Figure 3.7 Cryo-ESI-MS spectra and simulations showing the isotopic patterns of cationic Ni^{III} and Ni^{IV} intermediates found during the oxidation of **2** with O₂ in 10% H₂O/acetone at -80 °C. From left to right: **A**, [(^{TsMe}N₄)Ni^{IV}(cycloneophyl)(OOH)]⁺ m/z 631.1843 (transient species), **B**, [(^{TsMe}N₄)Ni^{IV}(cycloneophyl)(OH)]⁺ m/z 615.1940 (transient species) and **C**, [(^{TsMe}N₄)Ni^{III}(-CH₂CMe₂-o-C₆H₄-O)]⁺ m/z 614.1862 (persistent species).

Scheme 3.3 Proposed mechanism leading to C–C and C–O bond formation using complex **2** with O₂ as the oxidant.



3.4 Conclusion

In conclusion, we described the use of four different ligands that provide both stabilizing and destabilizing effects on high-valent Ni^{III/IV} species. All isolated complexes were fully characterized, and their C–C and C–heteroatom bond formation reactivity tested. The (^RN₄)Ni^{II}(cycloneophyl) derivatives have low redox potentials that can easily be oxidized with a variety of oxidants. When performing oxidation studies on (^RN₄)Ni^{II}(cycloneophyl) with O₂ and H₂O₂, C–C and C–O bond formation was observed. (^{TsMe}N₄)Ni^{II}(cycloneophyl) yielded up to 41% of C–O bond formation with the overall conversion at 94%. Using cryo-ESI-MS we detected high-valent Ni-oxygen species and propose a mechanism using O₂ and H₂O₂ as the oxidants. Overall, (^{TsMe}N₄)Ni^{II}(cycloneophyl) is the sweet spot of stability vs reactivity for C–O bond formation, but (^{Ts}N₄)Ni^{II}(cycloneophyl) gives the highest C–C formation. All these results are promising, suggesting that the organometallic Ni complexes supported by multidentate ligands can also exhibit bioinspired aerobic oxidation chemistry.

3.5 Acknowledgements

We thank the National Science Foundation (CHE-1255424) for support. The purchase of the Bruker EMX-PLUS EPR spectrometer was supported by the National Science Foundation (MRI, CHE-1429711). We also thank Dr. Michael B. Watson for the EPR measurements and Prof. X. Ribas, Dr. Oriol Planas and Dr. Laura Gómez for the cryo-ESI-MS studies.

3.6 References

1. Diederich, F.; Stang, P. J., *Metal-Catalyzed Cross-Coupling Reactions*. Wiley-VCH: Weinheim; New York, 1998.

2. Netherton, M. R.; Fu, G. C., Nickel-catalyzed cross-couplings of unactivated alkyl halides and pseudohalides with organometallic compounds. *Adv. Synth. Catal.* **2004**, *346* (13-15), 1525.
3. Frisch, A. C.; Beller, M., Catalysts for cross-coupling reactions with non-activated alkyl halides. *Angew. Chem., Int. Ed.* **2005**, *44* (5), 674.
4. Terao, J.; Kambe, N., Cross-Coupling Reaction of Alkyl Halides with Grignard Reagents Catalyzed by Ni, Pd, or Cu Complexes with pi-Carbon Ligand(s). *Acc. Chem. Res.* **2008**, *41* (11), 1545.
5. Glorius, F., Asymmetric Cross-Coupling of Non-Activated Secondary Alkyl Halides. *Angew. Chem., Int. Ed.* **2008**, *47* (44), 8347.
6. Phapale, V. B.; Cardenas, D. J., Nickel-catalysed Negishi cross-coupling reactions: scope and mechanisms. *Chem. Soc. Rev.* **2009**, *38* (6), 1598.
7. Rudolph, A.; Lautens, M., Secondary Alkyl Halides in Transition-Metal-Catalyzed Cross-Coupling Reactions. *Angew. Chem., Int. Ed.* **2009**, *48* (15), 2656.
8. Knochel, P.; Thaler, T.; Diene, C., Pd-, Ni-, Fe-, and Co-Catalyzed Cross-Couplings Using Functionalized Zn-, Mg-, Fe-, and In-Organometallics. *Isr. J. Chem.* **2012**, *50* (5-6), 547.
9. Hartwig, J. F., *Organotransition Metal Chemistry: From Bonding to Catalysis*. University Science Books: Sausalito, 2010; p 1127 pp.
10. Choi, J.; Fu, G. C., Transition metal-catalyzed alkyl-alkyl bond formation: Another dimension in cross-coupling chemistry. *Science* **2017**, *356* (6334).
11. Hu, X., Nickel-catalyzed cross coupling of non-activated alkyl halides: a mechanistic perspective. *Chem. Sci.* **2011**, *2* (10), 1867.

12. Camasso, N. M.; Canty, A. J.; Ariafard, A.; Sanford, M. S., Experimental and Computational Studies of High-Valent Nickel and Palladium Complexes. *Organometallics* **2017**, *36* (22), 4382.
13. Cloutier, J. P.; Zargarian, D., Functionalization of the Aryl Moiety in the Pincer Complex (NCN)(NiBr₂)-Br-III: Insights on Ni-III-Promoted Carbon-Heteroatom Coupling. *Organometallics* **2018**, *37* (9), 1446.
14. Aihara, Y.; Chatani, N., Nickel-Catalyzed Direct Alkylation of C-H Bonds in Benzamides and Acrylamides with Functionalized Alkyl Halides via Bidentate-Chelation Assistance. *J. Am. Chem. Soc.* **2013**, *135* (14), 5308.
15. Cornella, J.; Edwards, J. T.; Qin, T.; Kawamura, S.; Wang, J.; Pan, C. M.; Gianatassio, R.; Schmidt, M.; Eastgate, M. D.; Baran, P. S., Practical Ni-Catalyzed Aryl-Alkyl Cross-Coupling of Secondary Redox-Active Esters. *J. Am. Chem. Soc.* **2016**, *138* (7), 2174.
16. Xu, H. W.; Diccianni, J. B.; Katigbak, J.; Hu, C. H.; Zhang, Y. K.; Diao, T. N., Bimetallic C-C Bond Forming Reductive Elimination from Nickel. *J. Am. Chem. Soc.* **2016**, *138* (14), 4779.
17. Zhang, C.-P.; Wang, H.; Klein, A.; Biewer, C.; Stirnat, K.; Yamaguchi, Y.; Xu, L.; Gomez-Benitez, V.; Vicic, D. A., A Five-Coordinate Nickel(II) Fluoroalkyl Complex as a Precursor to a Spectroscopically Detectable Ni(III) Species. *J. Am. Chem. Soc.* **2013**, *135* (22), 8141.
18. Lee, H.; Borgel, J.; Ritter, T., Carbon-Fluorine Reductive Elimination from Nickel(III) Complexes. *Angew. Chem., Int. Ed.* **2017**, *56* (24), 6966.
19. D'Accriscio, F.; Borja, P.; Saffon-Merceron, N.; Fustier-Boutignon, M.; Mezailles, N.; Nebra, N., C-H Bond Trifluoromethylation of Arenes Enabled by a Robust, High-Valent Nickel(IV) Complex. *Angew. Chem., Int. Ed.* **2017**, *56* (42), 12898.

20. Kogut, E.; Wiencko, H. L.; Zhang, L. B.; Cordeau, D. E.; Warren, T. H., A terminal Ni(III)-imide with diverse reactivity pathways. *J. Am. Chem. Soc.* **2005**, *127* (32), 11248.
21. Pandarus, V.; Zargarian, D., New pincer-type diphosphinito (POCOP) complexes of nickel. *Organometallics* **2007**, *26* (17), 4321.
22. Pandarus, V.; Zargarian, D., New pincer-type diphosphinito (POCOP) complexes of Ni-II and Ni-III. *Chem. Comm.* **2007**, (9), 978.
23. Spasyuk, D. M.; Zargarian, D.; van der Est, A., New POCN-Type Pincer Complexes of Nickel(II) and Nickel(III). *Organometallics* **2009**, *28* (22), 6531.
24. Zheng, B.; Tang, F.; Luo, J.; Schultz, J. W.; Rath, N. P.; Mirica, L. M., Organometallic Nickel(III) Complexes Relevant to Cross-Coupling and Carbon–Heteroatom Bond Formation Reactions. *J. Am. Chem. Soc.* **2014**, *136* (17), 6499.
25. Corona, T.; Draksharapu, A.; Padamati, S. K.; Gamba, I.; Martin-Diaconescu, V.; Acuna-Pares, F.; Browne, W. R.; Company, A., Rapid Hydrogen and Oxygen Atom Transfer by a High-Valent Nickel-Oxygen Species. *J. Am. Chem. Soc.* **2016**, *138* (39), 12987.
26. Bour, J. R.; Camasso, N. M.; Meucci, E. A.; Kampf, J. W.; Canty, A. J.; Sanford, M. S., Carbon–Carbon Bond-Forming Reductive Elimination from Isolated Nickel(III) Complexes. *J. Am. Chem. Soc.* **2016**, *138* (49), 16105.
27. Diccianni, J. B.; Hu, C. H.; Diao, T. N., Binuclear, High-Valent Nickel Complexes: Ni-Ni Bonds in Aryl-Halogen Bond Formation. *Angew. Chem., Int. Ed.* **2017**, *56* (13), 3635.
28. Martinez, G. E.; Ocampo, C.; Park, Y. J.; Fout, A. R., Accessing Pincer Bis(carbene) Ni(IV) Complexes from Ni(II) via Halogen and Halogen Surrogates. *J. Am. Chem. Soc.* **2016**, *138* (13), 4290.

29. Watson, M. B.; Rath, N. P.; Mirica, L. M., Oxidative C–C Bond Formation Reactivity of Organometallic Ni(II), Ni(III), and Ni(IV) Complexes. *J. Am. Chem. Soc.* **2017**, *139* (1), 35.
30. Khusnutdinova, J. R.; Rath, N. P.; Mirica, L. M., Stable Mononuclear Organometallic Pd(III) Complexes and Their C-C Bond Formation Reactivity. *J. Am. Chem. Soc.* **2010**, *132* (21), 7303.
31. Khusnutdinova, J. R.; Rath, N. P.; Mirica, L. M., Dinuclear Palladium(III) Complexes with a Single Unsupported Bridging Halide Ligand: Reversible Formation from Mononuclear Palladium(II) or Palladium(IV) Precursors. *Angew. Chem., Int. Ed.* **2011**, *50* (24), 5532.
32. Tang, F. Z.; Zhang, Y.; Rath, N. P.; Mirica, L. M., Detection of Pd(III) and Pd(IV) Intermediates during the Aerobic Oxidative C-C Bond Formation from a Pd(II) Dimethyl Complex. *Organometallics* **2012**, *31* (18), 6690.
33. Zheng, B.; Tang, F.; Luo, J.; Schultz, J. W.; Rath, N. P.; Mirica, L. M., Organometallic Nickel(III) Complexes Relevant to Cross-Coupling and Carbon-Heteroatom Bond Formation Reactions. *J. Am. Chem. Soc.* **2014**, *136* (17), 6499.
34. Khusnutdinova, J. R.; Rath, N. P.; Mirica, L. M., The Conformational Flexibility of the Tetradentate Ligand tBuN4 is Essential for the Stabilization of (tBuN4)Pd(III) Complexes. *Inorg. Chem.* **2014**, *53* (24), 13112.
35. Qu, F.; Khusnutdinova, J. R.; Rath, N. P.; Mirica, L. M., Dioxygen activation by an organometallic Pd(II) precursor: formation of a Pd(IV)-OH complex and its C-O bond formation reactivity. *Chem. Comm.* **2014**, *50* (23), 3036.
36. Tang, F.; Qu, F.; Khusnutdinova, J. R.; Rath, N. P.; Mirica, L. M., Structural and Reactivity Comparison of Analogous Organometallic Pd(III) and Pd(IV) Complexes. *Dalton Trans.* **2012**, *41* (46), 14046.

37. Khusnutdinova, J. R.; Rath, N. P.; Mirica, L. M., The Aerobic Oxidation of a Pd(II) Dimethyl Complex Leads to Selective Ethane Elimination from a Pd(III) Intermediate. *J. Am. Chem. Soc.* **2012**, *134*, 2414.
38. Wessel, A. J.; Schultz, J. W.; Tang, F.; Duan, H.; Mirica, L. M., Improved synthesis of symmetrically & asymmetrically N-substituted pyridinophane derivatives. *Org. Biomol. Chem.* **2017**, *15* (46), 9923.
39. Che, C. M.; Li, Z. Y.; Wong, K. Y.; Poon, C. K.; Mak, T. C. W.; Peng, S. M., A simple synthetic route to N,N'-dialkyl-2,11-diaza[3.3](2,6)pyridinophanes. Crystal structures of N,N'-di-tert-butyl-2,11-diaza[3.3](2,6)pyridinophane and its copper(II) complex. *Polyhedron* **1994**, *13* (5), 771.
40. Campora, J.; Conejo, M. D.; Mereiter, K.; Palma, P.; Perez, C.; Reyes, M. L.; Ruiz, C., Synthesis of dialkyl, diaryl and metallacyclic complexes of Ni and Pd containing pyridine, alpha-diimines and other nitrogen ligands crystal structures of the complexes cis-NiR(2)py(2) (R = benzyl, mesityl). *J. Organomet. Chem.* **2003**, *683* (1), 220.
41. Schultz, J. W.; Fuchigami, K.; Zheng, B.; Rath, N. P.; Mirica, L. M., Isolated Organometallic Nickel(III) and Nickel(IV) Complexes Relevant to Carbon-Carbon Bond Formation Reactions. *J. Am. Chem. Soc.* **2016**, *138* (39), 12928.
42. Connelly, N. G.; Geiger, W. E., Chemical Redox Agents for Organometallic Chemistry. *Chem. Rev.* **1996**, *96* (2), 877.
43. Gottlieb, H. E.; Kotlyar, V.; Nudelman, A., NMR Chemical Shifts of Common Laboratory Solvents as Trace Impurities. *J. Org. Chem.* **1997**, *62* (21), 7512.
44. Fulmer, G. R.; Miller, A. J. M.; Sherden, N. H.; Gottlieb, H. E.; Nudelman, A.; Stoltz, B. M.; Bercaw, J. E.; Goldberg, K. I., NMR Chemical Shifts of Trace Impurities: Common

Laboratory Solvents, Organics, and Gases in Deuterated Solvents Relevant to the Organometallic Chemist. *Organometallics* **2010**, *29* (9), 2176.

45. Campora, J.; Lopez, J. A.; Palma, P.; del Rio, D.; Carmona, E.; Valerga, P.; Graiff, C.; Tiripicchio, A., Synthesis and Insertion Reactions of the Cyclometalated Palladium^{II} Alkyl Complexes Pd(CH₂CMe₂-o-C₆H₄)L₂. Observation of a Pentacoordinated Intermediate in the Insertion of SO₂. *Inorg. Chem.* **2001**, *40* (17), 4116.

46. Schultz, J. W.; Fuchigami, K.; Zheng, B.; Rath, N. P.; Mirica, L. M., Isolated Organometallic Nickel(III) and Nickel(IV) Complexes Relevant to Carbon-Carbon Bond Formation Reactions. *J. Am. Chem. Soc.* **2016**, *138* (39), 12928.

47. Camasso, N. M.; Sanford, M. S., Design, synthesis, and carbon-heteroatom coupling reactions of organometallic nickel(IV) complexes. *Science* **2015**, *347* (6227), 1218.

48. Bour, J. R.; Camasso, N. M.; Sanford, M. S., Oxidation of Ni(II) to Ni(IV) with Aryl Electrophiles Enables Ni-Mediated Aryl-CF₃ Coupling. *J. Am. Chem. Soc.* **2015**, *137* (25), 8034.

49. Chong, E.; Kampf, J. W.; Ariafard, A.; Canty, A. J.; Sanford, M. S., Oxidatively Induced C-H Activation at High Valent Nickel. *J. Am. Chem. Soc.* **2017**, *139* (17), 6058.

50. Aseman, M. D.; Nabavizadeh, S. M.; Hosseini, F. N.; Wu, G.; Abu-Omar, M. M., Carbon Oxygen Bond Forming Reductive Elimination from Cycloplatinated(IV) Complexes. *Organometallics* **2018**, *37* (1), 87.

51. Silva, F. C. S. E.; Tierno, A. F.; Wengryniuk, S. E., Hypervalent Iodine Reagents in High Valent Transition Metal Chemistry. *Molecules* **2017**, *22* (5).

52. Company, A.; Yao, S. L.; Ray, K.; Driess, M., Dioxygenase-Like Reactivity of an Isolable Superoxo-Nickel(II) Complex. *Chem. Eur. J.* **2010**, *16* (31), 9669.

Chapter 4

Synthesis and Characterization of (^RMe₂TACN)Ni(cycloneophyl) Complexes and Their Reactivity

4.1 Introduction

The synthesis and characterization of high-valent nickel complexes is currently an active research area because of their role as proposed intermediates in various cross-coupling reactions.¹⁻⁴⁵ The reactivity observed from the nickel complexes depends on the stabilization or destabilization of the high-valent complexes leading to a faster or slower reactivity. Either of these outcomes may be desirable depending on the goal that is trying to be accomplished.

Our group has used the 1,4,7-trimethyl-1,4,7-triazacyclonane (^{Me3}TACN) ligand to stabilize high-valent Pd and Ni complexes.⁴⁶⁻⁴⁸ The C–C and C–heteroatom bond formation was also tested in these cases with aerobic oxidants, seeing that it is possible to oxidize nickel and palladium complexes with “greener reagents”. We wanted to take a closer look at the inorganic Ni^{III} complex to determine how the stability was either enhanced or diminished by modification of the N-substituents of the TACN ligand. The modifications tested were the effects of increased steric bulk on one of the amines. One of the methyl substituents was substituted for an isopropyl or *p*-toluenesulfonyl group. This modification leads to the TACN ligand acting more as a bidentate ligand than as a tridentate ligand. The three ligands represented in this study are all TACN-derived ligands including: 1,4,7-trimethyl-1,4,7-triazacyclonane, 1-isopropyl-4,7-dimethyl-1,4,7-triazacyclonane (^{iPrMe2}TACN) and 1-(*p*-toluenesulfonyl)-4,7-dimethyl-1,4,7-triazacyclonane (^{TsMe2}TACN).⁴⁸⁻⁵⁰ This series of ligands can help determine what minor modifications ligands may undergo to increase or decrease their stability or reactivity of the corresponding nickel complexes.

4.2 Experimental Section

Reagents and Materials. All manipulations were carried out under a nitrogen atmosphere using standard Schlenk and glove box techniques if not indicated otherwise. All reagents for which the synthesis was not given are commercially available from Aldrich, Acros or STREM and were used as received without further purification. Solvents were purified prior to use by passing through a column of activated alumina using an MBRAUN SPS. $(\text{Py})_2\text{Ni}^{\text{II}}(\text{cycloneophyl})$,⁵¹ ferrocenium hexafluorophosphate (FcPF_6),⁵² 1-(*p*-toluenesulfonyl)-4,7-dimethyl-1,4,7-triazacyclononane⁵⁰ and 1,4-dimethyl-1,4,7-triazacyclononane⁴⁹ were prepared according to the literature procedures. Other abbreviations used throughout this chapter: 1-Fluoro-2,4,6-trimethylpyridinium triflate (NFTPT) and 5-(trifluoromethyl)dibenzothiophenium trifluoromethanesulfonate (TDTT).

4.2.1 Synthesis of the Ligands and Nickel Complexes

Preparation of 1-isopropyl-4,7-dimethyl-1,4,7-triazacyclononane ($i\text{PrMe}_2\text{TACN}$). HMe_2TACN (120 mg, 0.76 mmol) and 2-bromopropane (86 μL , 0.92 mmol) were added together in a 50 mL round bottom flask. A suspension of potassium carbonate (422 mg, 3.1 mmol) in acetonitrile (7.5 mL) was added and the reaction was refluxed for 16 hours. The solution was filtered and the mother liquor was evaporated. The oil was redissolved in 20 mL of diethyl ether and the solution was extract three times with 10 mL of water. The organic layer was dried with potassium carbonate for 30 minutes and then filtered. The organic layer was evaporated and dried for several hours. The product was a clear oil (66.5 mg, 0.33 mmol, 44%).

^1H NMR (500 MHz, THF- d_8), δ (ppm): 2.88-2.83 (q, $J = 6.6$ Hz, 1H, iPr), 2.71 (s, 4H, $\text{NCH}_2\text{CH}_2\text{N}$), 2.64-2.62 (m, 4H, $\text{NCH}_2\text{CH}_2\text{N}$), 2.58-2.56 (m, 4H, $\text{NCH}_2\text{CH}_2\text{N}$), 2.31 (s, 6H, 2CH_3), 0.95 (d, $J = 6.6$ Hz, 6H, iPr).

APT (500 MHz, THF- d_8), δ (ppm): 58.76, 58.10, 55.97, 52.97, 46.76, 18.74.

Preparation of $^{i\text{PrMe}_2}\text{TACNNi}(\text{cycloneophyl})$. A solution of $^{i\text{PrMe}_2}\text{TACN}$ (22.7 mg, 0.11 mmol) and $(\text{Py})_2\text{Ni}^{\text{II}}(\text{cycloneophyl})$ (43.5 mg, 0.13 mmol) in THF (3 mL) was stirred at 20 °C for 14 hours. The solution was evaporated and redissolved in a minimum amount of THF. Pentane was added to crash out any leftover starting cycloneophyl precursor. The solution was filtered and the mother liquor was evaporated to dryness. The solid obtained was a yellow powder (17.3 mg, 0.041 mmol, 37%).

^1H NMR (500 MHz, THF- d_8), δ (ppm): 6.85-6.84 (d, $J = 6.6$ Hz, 2H, Ar-CH), 6.55-6.57 (m, 1H, Ar-CH), 6.47-6.43 (m, 2H, Ar-CH), 5.56 (b, 2H, $\text{NCH}_2\text{CH}_2\text{N}$), 4.36 (b, 2H, $\text{NCH}_2\text{CH}_2\text{N}$), 3.30-3.27 (d, $J = 15.6$ Hz, 4H, $\text{NCH}_2\text{CH}_2\text{N}$), 3.03-2.98 (q, $J = 6.2$ Hz, 1H iPr), 2.71 (s, 3H, CH_3), 2.57 (s, 6H, 2CH_3), 2.42-2.38 (t, $J = 12.1$ Hz, 4H, $\text{NCH}_2\text{CH}_2\text{N}$), 2.31 (s, 3H, CH_3), 1.15-1.14 (d, $J = 6.6$ Hz, 1H, $-\text{CH}_2-$), 1.08-1.07 (d, $J = 6.6$ Hz, 6H, iPr), 0.96-0.95 (d, $J = 6.6$ Hz, 1H, $-\text{CH}_2-$).

APT (500 MHz, THF- d_8), δ (ppm): 169.98, 161.45, 138.16, 122.48, 121.53, 120.42, 58.87, 58.22, 56.27, 53.09, 48.30, 46.89, 37.42, 19.30, 18.86, 14.54.

Note: Due to the fluxionality of the TACN ligand, broadening was observed for both the proton and carbon NMR spectra. This resulted in less accurate integrations for the spectra observed.

Preparation of $^{\text{TsMe}_2}\text{TACNNi}(\text{cycloneophyl})$. A solution of $^{\text{TsMe}_2}\text{TACN}$ (24.5 mg, 0.081 mmol) and $(\text{Py})_2\text{Ni}^{\text{II}}(\text{cycloneophyl})$ (31.2 mg, 0.090 mmol) in THF (3 mL) was stirred at 20 °C for 14

hours. The solution was evaporated and redissolved in a minimum amount of THF. Pentane was added to crash out any leftover starting cycloneophyl precursor. The solution was filtered and the mother liquor was evaporated to dryness. The solid obtained was a yellow powder (18.3 mg, 0.026 mmol, 32%).

^1H NMR (500 MHz, THF- d_8), δ (ppm): 7.77-7.75 (d, $J = 8.3$ Hz, 2H, Ts), 7.37-7.35 (d, $J = 7.9$ Hz, 2H, Ts), 6.77-6.76 (d, $J = 7.3$ Hz, 1H, Ar-H), 6.58-6.55 (t, $J = 7.2$ Hz, 1H, Ar-H), 6.48-6.43 (m, 2H, Ar-H), 6.21-6.15 (m, 2H, $\text{NCH}_2\text{CH}_2\text{N}$), 5.93-5.90 (m, 2H, $\text{NCH}_2\text{CH}_2\text{N}$), 4.04-3.92 (m, 2H, $\text{NCH}_2\text{CH}_2\text{N}$), 3.70-3.64 (m, 2H, $\text{NCH}_2\text{CH}_2\text{N}$), 3.12-3.02 (m, 2H, $\text{NCH}_2\text{CH}_2\text{N}$), 2.92-2.85 (m, 2H, $\text{NCH}_2\text{CH}_2\text{N}$), 2.66 (s, 3H, CH_3), 2.59 (s, 3H, CH_3), 2.39 (s, 3H, CH_3), 1.66 (s, 3H, CH_3), 1.00 (s, 3H, CH_3), 0.93-0.91 (d, $J = 8.5$ Hz, 1H, $-\text{CH}_2-$), 0.31-0.31 (d, $J = 8.4$ Hz, 1H, $-\text{CH}_2-$).

APT (500 MHz, THF- d_8), δ (ppm): 170.12, 160.30, 144.54, 137.76, 137.55, 130.73, 128.08, 122.75, 121.96, 120.69, 64.87, 63.47, 62.04, 60.21, 56.45, 55.01, 53.56, 50.57, 48.21, 38.07, 37.82, 31.12, 21.55.

4.2.2 Reactivity Studies

General procedure for the isolation of the Ni^{III} complexes by EPR. An EPR tube was charged with a solution of $(^{\text{TsMe}2}\text{TACN})\text{Ni}^{\text{II}}(\text{cycloneophyl})$ or $(^{\text{iPrMe}2}\text{TACN})\text{Ni}^{\text{II}}(\text{cycloneophyl})$ in acetonitrile (MeCN) or THF. A butyronitrile (PrCN) or 2-methyl-tetrahydrofuran (MeTHF) solution containing one equivalent of ferrocenium hexafluorophosphate (FcPF_6) was then added. The resulting solution of 1:3 MeCN:PrCN or 1:3 THF:MeTHF was shaken for five seconds and then frozen in liquid nitrogen.

General procedure for the reactivity studies of $(^{\text{R}}\text{TACN})\text{Ni}(\text{cycloneophyl})$ complexes. In N_2 -filled glove box, a solution of 5-7 mg of $(^{\text{TsMe}2}\text{TACN})\text{Ni}^{\text{II}}(\text{cycloneophyl})$ or

(ⁱPrMe₂TACN)Ni^{II}(cycloneophyl) complex in MeCN (2 mL) was added into a 5 mL vial containing 1,3,5-trimethoxybenzene as an internal standard. To this solution different oxidants were added (bubbled O₂ + 10% water, H₂O₂, NFTPT and TDDT) and stirred for 14 hours at 70 °C. The next day 1 mL of 14% perchloric acid was added and stirred for an additional four hours at 70 °C. To this solution 3 mL of a saturated potassium carbonate solution was added. The solution was then extracted three times with 1 mL of diethyl ether and dried over potassium carbonate for 30 minutes. The solution was filtered and the yield of product(s) was obtained by GC/FID using 1,3,5-trimethoxybenzene as the internal standard and the identity of the products was confirmed by GC/MS.

4.2.3 Physical Measurements

Nuclear Magnetic Resonance. ¹H NMR, ¹³C NMR, APT, gCOSY, NOESY, TOXY, HSQC and HMBC spectra were recorded on an Agilent DD2-500 spectrometer (499.885 MHz). Chemical shifts are reported in ppm and referenced to residual solvent resonance peaks.⁵³⁻⁵⁴ Abbreviations for the multiplicity of NMR signals are s (singlet), d (doublet), dd (doublet of doublets), t (triplet), q (quintet), m (multiplet), b (broad). All the NMR spectra are included in Appendix A.

EPR. EPR spectra were recorded on a Bruker EMX-PLUS EPR or a JEOL JES-FA EPR spectrometer at X-band (~9.2 GHz) frequency in frozen solution at 77 K. The purchase of the Bruker EMX-PLUS EPR spectrometer was supported by the National Science Foundation (MRI, CHE-1429711).

Electrochemical Measurements. Cyclic voltammetry experiments were performed with a BASi EC Epsilon electrochemical workstation or a CHI 660D Electrochemical Analyzer. The electrochemical measurements were taken in a glove box under nitrogen. A glassy carbon disk

electrode ($d = 1.6$ mm) was used as the working electrode for cyclic voltammetry. The auxiliary electrode was a Pt wire for cyclic voltammetry measurements. The non-aqueous reference electrode used was a silver wire dipped in a bleach solution (Ag/AgCl). The reference electrodes were calibrated against Cp₂Fe (Fc). Electrochemical-grade electrolytes from Fluka were used as the supporting electrolyte for electrochemical measurements. All CV spectra are included in Appendix B.

X-ray Crystallography. All X-ray crystallography experiments were performed by Dr. Nigam Rath. Suitable crystals were mounted on MiTeGen cryoloops in random orientations in a Bruker Kappa Apex-II CCD X-ray diffractometer equipped with an Oxford Cryostream LT device and a fine focus Mo K α radiation X-ray source ($\lambda = 0.71073$ Å). Preliminary unit cell constants were determined with a set of 36 narrow frame scans. Typical data sets consist of combinations of ω and ϕ scan frames with a typical scan width of 0.5° and a counting time of 15–30 s/frame at a crystal-to-detector distance of 4.0 cm. The collected frames were integrated using an orientation matrix determined from the narrow frame scans. Apex II and SAINT software packages (Bruker Analytical X-Ray, Madison, WI, 2008) were used for data collection and data integration. Analysis of the integrated data did not show any decay. Final cell constants were determined by global refinement of xyz centroids of reflections from the complete data sets. Collected data were corrected for systematic errors using SADABS (Bruker Analytical X-Ray, Madison, WI, 2008) based on the Laue symmetry using equivalent reflections. Structure solutions and refinement were carried out using the SHELXTL-PLUS software package. The structures were solved by direct methods and refined successfully in specified crystal systems and space groups. Full matrix least-squares refinements were carried out by minimizing $\sum w(F_o^2 - F_c^2)^2$. The non-hydrogen atoms were refined anisotropically to convergence. Typically, the hydrogen atoms were treated using the

appropriate riding model. The complete listings of X-ray diffraction parameters are included in Appendix G.

4.3 Results and Discussion

4.3.1 Synthesis and Characterization of Ni^{II/III} Complexes

The three ligands represented in this study are all TACN-derived ligands, ^{Me3}TACN, ^{iPrMe2}TACN and ^{TsMe2}TACN. The slight modification on the ligands was made to test their reactivity and high-valent nickel stability. ^{Me3}TACN and its corresponding nickel complexes were previously synthesized and characterized and used in this chapter as a comparison.⁴⁸ ^{iPrMe2}TACN was synthesized by adding 2-bromopropane and ^{HMe2}TACN together in a round bottom flask. To this solution a suspension of potassium carbonate in acetonitrile was added and refluxed for 16 hours. The reaction was followed by a work-up to give a clear oil. Lastly, ^{TsMe2}TACN was synthesized according to a literature procedure.⁵⁰ With these ligands, a series of cycloneophyl complexes were synthesized through a ligand exchange of (py)₂Ni^{II}(cycloneophyl).^{51, 55} The yellow Ni^{II} complexes (^{iPrMe2}TACN)Ni^{II}(cycloneophyl), **2** and (^{iPrMe2}TACN)Ni^{II}(cycloneophyl), **3** were prepared in a 37% and 32% yield respectively (Scheme 4.1). The complexes were fully characterized by NMR and X-ray crystallography. The single X-ray crystal structure of **2** and **3** reveals a square planar geometry for the Ni center that is bound to two nitrogen atoms from the TACN ligand and two carbon groups from the cycloneophyl. The bond lengths for both nickel complexes **2** and **3** are very similar and compare well to the bond lengths of complex **1** (Figure 4.1).

Scheme 4.1 Synthesis of (^{RMe2}TACN)Ni(cycloneophyl) complexes.

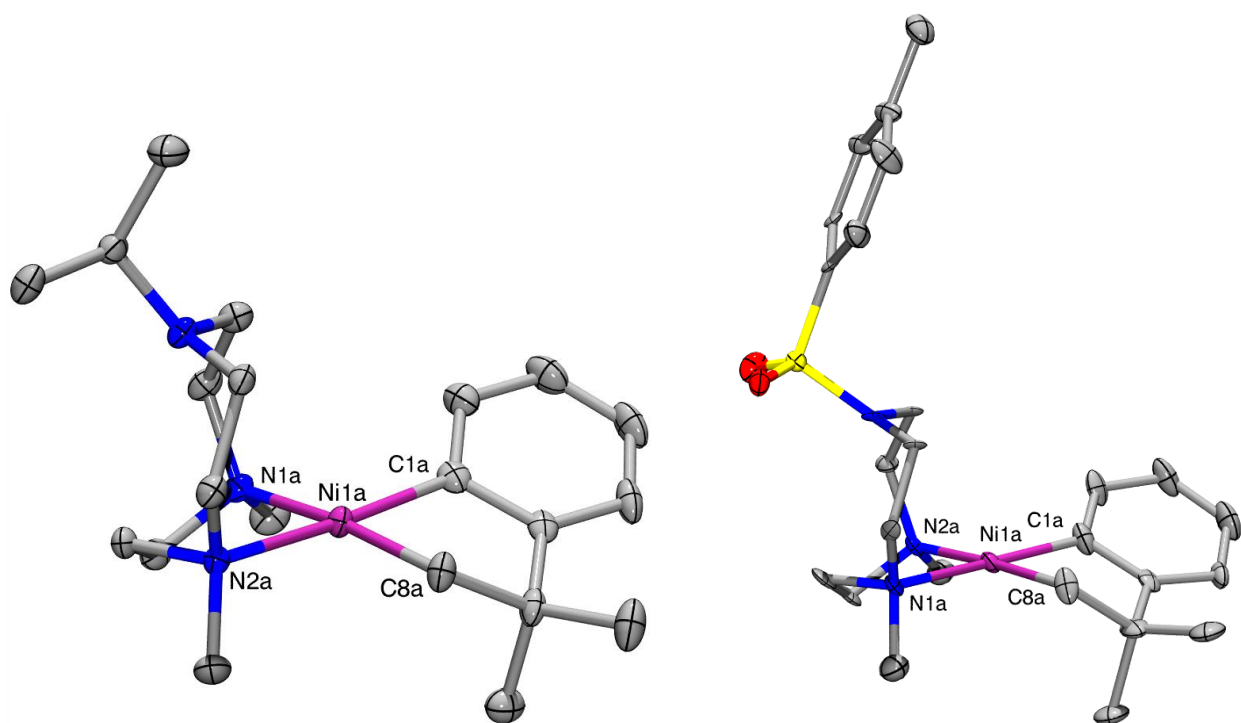
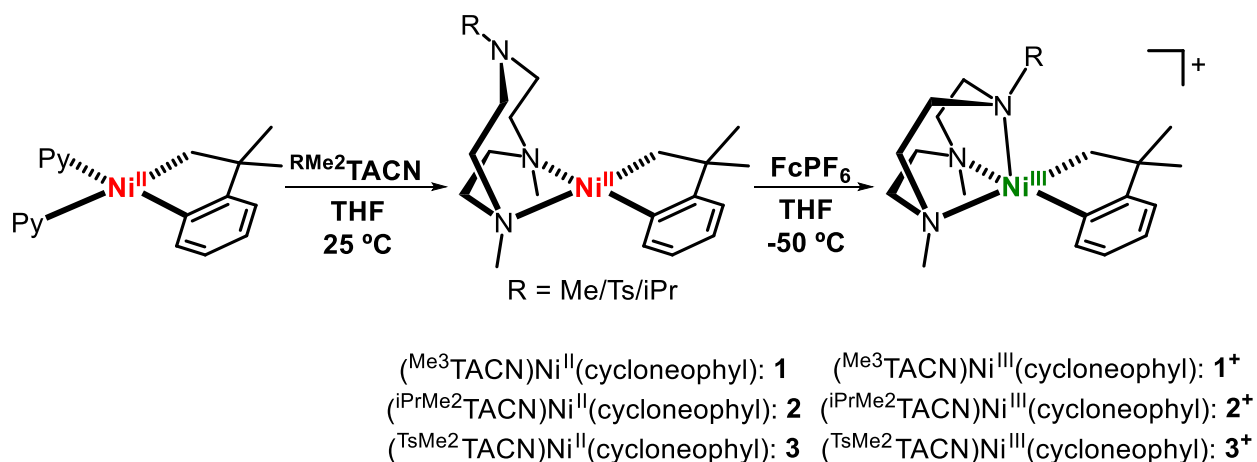


Figure 4.1 ORTEP representation of **2** (left) and **3** (right), with 50% probability thermal ellipsoids. Selected bond distances (Å): **2**: Ni1a-C1a, 1.909; Ni1a-C8a, 1.935; Ni1a-N1a, 2.052; Ni1a-N2a, 2.055 **3**: Ni1a-C1a, 1.920; Ni1a-C8a, 1.944; Ni1a-N1a, 2.077; Ni1a-N2a, 2.075.

The cyclic voltammogram (CV) of **2** in 0.1 M nBu₄NPF₆/MeCN shows an oxidation event at -1025 mV vs ferrocene (Fc), and the CV of complex **3** shows an oxidation event at -490 mV vs Fc (Figure 4.2). These events are tentatively assigned to the oxidation of Ni^{II} to Ni^{III}. When

comparing these oxidation events to complex **1**, complex **1** shows a much lower oxidation potential (-1321 mV vs Fc). The difference in oxidation potential is attributed to the substituent on the nitrogen on the TACN ligand. Varying the substituent from a methyl to an isopropyl or to a tosyl group, we can see the difference in oxidation potential because of the added steric bulk; complex **2** and complex **3** have more electron withdrawing/bulky groups. We are unsure at this point if the steric effects or the electronic effects play the major role in increasing the oxidation potential for complex **3**, it is possible that both play a role in this case.

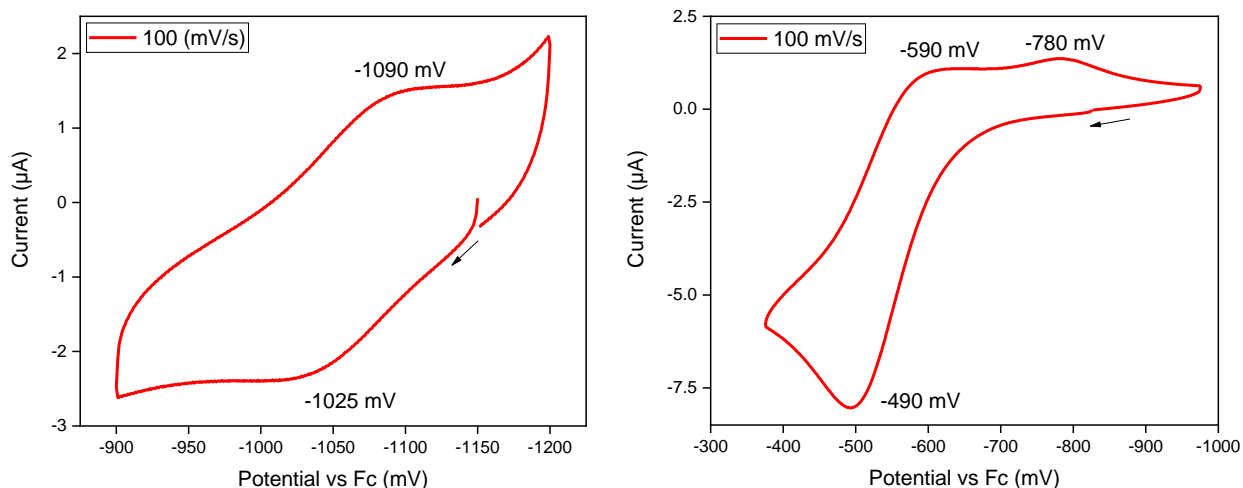


Figure 4.2 CV of **2** (left) in 0.1 M $n\text{Bu}_4\text{NPF}_6/\text{MeCN}$ at RT (100 mV/s scan rate). Redox potential: $E_{(\text{Ni}^{\text{III}})} = -1025$ mV and CV of **3** (right) in 0.1 M $n\text{Bu}_4\text{NPF}_6/\text{MeCN}$ at RT (100 mV/s scan rate). Redox potential: $E_{(\text{Ni}^{\text{III}})} = -490$ mV.

Both complexes **2** and **3** can be oxidized using one equivalent of ferrocenium hexafluorophosphate in THF at -50 °C to obtain $[(^i\text{PrMe}_2\text{TACN})\text{Ni}^{\text{III}}(\text{cycloneophyl})]\text{PF}_6$, **2**⁺, and $[(^{\text{Ts}}\text{Me}_2\text{TACN})\text{Ni}^{\text{III}}(\text{cycloneophyl})]\text{PF}_6$, **3**⁺. The EPR of complex **2**⁺ exhibits a rhombic signal in a solvent mixture of THF and methyl-THF (MeTHF). A superhyperfine coupling was observed in the g_z direction due to one axial amine donors ($I=1$) coupling to the Ni^{III} center (Figure 4.3). The EPR spectrum of complex **2**⁺ looks very similar to the EPR spectrum of complex **1**⁺ and only has one nitrogen binding. When changing solvent mixture to MeCN:PrCN, we still see a triplet

indicating that no acetonitrile is binding in the axial position. This was initially surprising to us because the Ni^{III} complexes we have studied previously prefer an octahedral geometry. Our initial thoughts were that the available MeCN would act as an additional ligand that would bind the complex, however this was not the case as shown in the EPR. There are two reasons why MeCN would not coordinate to the Ni^{III} center, the first of which is the steric interactions from the other two ligands. The ligands distort the complex and end up blocking the site were MeCN would coordinate. The other reason would be that there isn't any electron density required to stabilize 2⁺ and would only serve to cause more steric interactions with ⁱPrMe₂TACN and cycloneophyl ligand. Whatever the cause may be, the result is a five-coordinate semi-stable Ni^{III} complex because the complex could not be isolated.

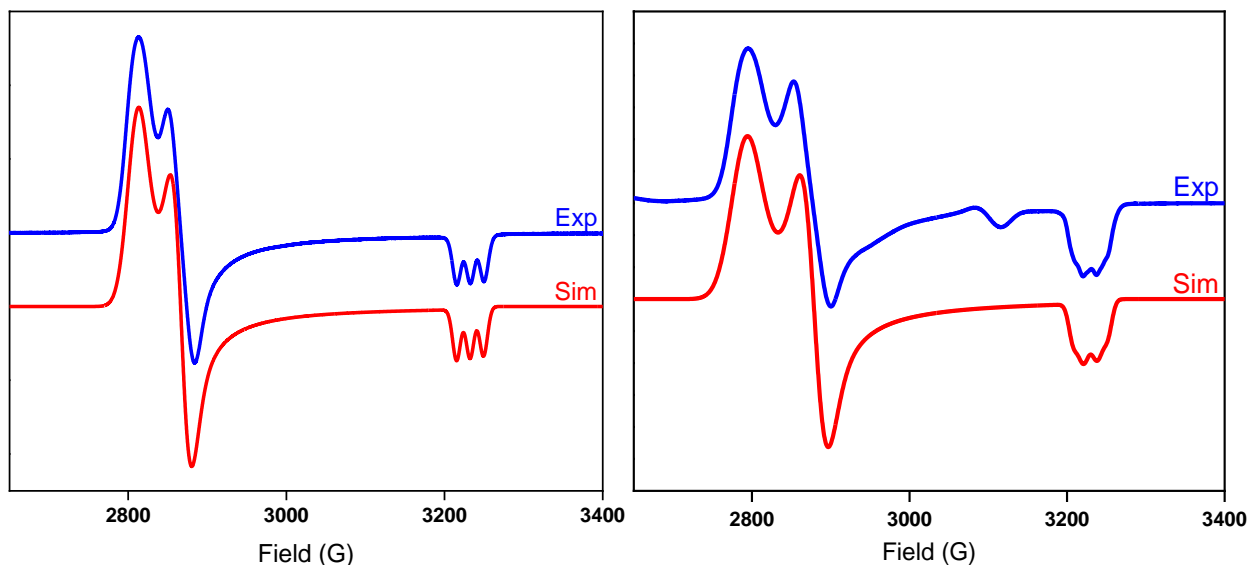


Figure 4.3 Experimental (1:3 THF:MeTHF, 77K) and simulated EPR spectra of 2⁺ (left) using the following parameters: $g_x=2.311$, $g_y=2.267$, $g_z=2.011$ ($A_z(N)=17.0$ G). Experimental (1:3 MeCN:PrCN, 77K) and simulated EPR spectra of 3⁺ (right) using the following parameters: $g_x=2.327$, $g_y=2.257$, $g_z=2.012$ ($A_z(N)=17.0$ G and ($A_z(P)=10$ G).

The EPR spectrum of complex 3⁺ shows a rhombic signal in the g_z direction the observation of a quartet (Figure 4.3). The superhyperfine coupling in the g_z direction indicates that one axial

amine is binding ($A_{1N} = 17 \text{ G}$, $I = 1$) and there is a second coupling of 10 G with $I = \frac{1}{2}$ which might be indicative of the hexafluorophosphate anion binding in the axial position. Also, it is not certain whether the N_{Ts} arm or a MeCN group is binding in the axial direction. Further studies would have to prove this concept because we were not able to obtain a Ni^{III} crystal structure because the complex was very short lived and decays within one minute at room temperature.

4.3.2 C–C Bond Formation Reactivity of $(^{RMe_2}TACN)Ni^{II}(\text{cycloneophyl})$

Complexes

With the new $(^{RMe_2}TACN)Ni^{II}(\text{cycloneophyl})$ complexes in hand, we set out to probe the reactivity for C–C and C–heteroatom bond formation reactions similar to chapter 3. First, we studied the oxidation $(^RN_4)Ni^{II}(\text{cycloneophyl})$ with 1-Fluoro-2,4,6-trimethylpyridinium triflate (NFTPT) and 5-(trifluoromethyl)dibenzothiophenium trifluoromethanesulfonate (TDTT) to observe any C–C and C–X bond formation. While no C–heteroatom bond formation was detected with complexes **2** and **3**, we did observe high C–C bond formation with up to 82% for complex **2** (Scheme 4.2 and Table 4.1). We then tested the oxidation of the cycloneophyl complexes with O_2 and H_2O_2 and we observed up to 9% of C–O bond formation for complex **2** using O_2 as the oxidant and 5% of C–O bond formation for complex **3**. Comparing these results with complex **1**, which gave 5% of hydroxylated product, complex **2** gives a slightly higher C–O bond formation.

Scheme 4.2 General reaction for the formation of the different oxidation products.

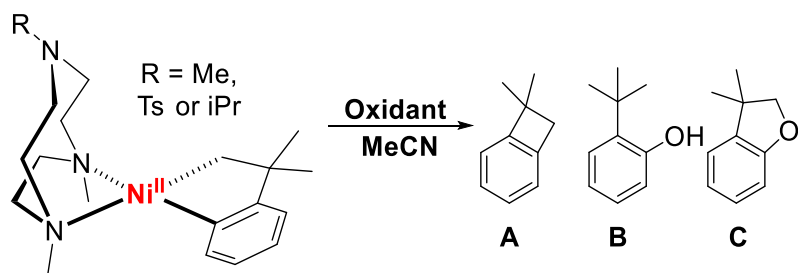


Table 4.1 Yields of the products from the reaction of (^RMe₂TACN)Ni^{II}(cycloneophyl) with a variety of oxidants in MeCN.

Starting Complex	Oxidants	Yields (%) ^a			Sum (%)
		A	B	C	
(ⁱ PrMe ₂ TACN)Ni ^{II} (cycloneophyl)	O ₂	51	4	5	60
(^{Ts} Me ₂ TACN)Ni ^{II} (cycloneophyl)	O ₂	47	0	0	47
(^{Me} Me ₃ TACN)Ni ^{II} (cycloneophyl)	O ₂	40	5	0	45
(ⁱ PrMe ₂ TACN)Ni ^{II} (cycloneophyl)	2 eq. H ₂ O ₂	59	3	2	64
(^{Ts} Me ₂ TACN)Ni ^{II} (cycloneophyl)	2 eq. H ₂ O ₂	26	0	0	26
(ⁱ PrMe ₂ TACN)Ni ^{II} (cycloneophyl)	1 eq. NFTPT	82	n/a	n/a	82
(^{Ts} Me ₂ TACN)Ni ^{II} (cycloneophyl)	1 eq. NFTPT	75	n/a	n/a	75
(ⁱ PrMe ₂ TACN)Ni ^{II} (cycloneophyl)	1 eq. TDDT	65	n/a	n/a	65
(^{Ts} Me ₂ TACN)Ni ^{II} (cycloneophyl)	1 eq. TDDT	58	n/a	n/a	58

^a Yields (%) were determined by GC-FID vs. 1,3,5-trimethoxybenzene as internal standard. n/a indicates that no other C–F products were observed.

4.4 Conclusion

In conclusion, we have presented the synthesis and characterization of new Ni complexes with multidentate ligands. The TACN ligands described are very flexible and can accommodate metal ions in different oxidation states in a variety of conformations. The electrochemical properties of the Ni^{II} complexes were explored which suggest that all the complexes can easily be oxidized to Ni^{III}. In contrast, adding more steric effects on the amine arm increases the oxidation potential. The oxidation of complex **2**⁺ gave an EPR spectrum very similar to complex **1**⁺. The EPR spectrum of complex **3**⁺ shows a quartet in the *g_z* direction. This is not fully understood, and future studies will have to be performed to elucidate what causes this exact coupling. The reactivity studies performed on the new complexes gave high C–C bond formation but no C–heteroatom bond formation. The exception to this was when the complexes were oxidized with O₂, resulting in a 5-9% of C–O bond formation. Current studies are focused on taking advantage of the ability of the TACN ligand to stabilize or destabilize the high-valent Ni species and employ such

organometallic Ni complexes in transformations involving rapid oxidative addition and aerobic oxidation steps for catalytic C–C and C–heteroatom bond formation reactions.

4.5 Acknowledgements

We thank the National Science Foundation (CHE-1255424) for support. The purchase of the Bruker EMX-PLUS EPR spectrometer was supported by the National Science Foundation (MRI, CHE-1429711). We also thank Yung-Ching Wang for the EPR measurements.

4.6 References

1. Tamao, K.; Sumitani, K.; Kumada, M., Selective carbon-carbon bond formation by cross-coupling of Grignard reagents with organic halides. Catalysis by nickel-phosphine complexes. *J. Am. Chem. Soc.* **1972**, *94* (12), 4374.
2. Fu, J.-m.; Sharp, M. J.; Snieckus, V., The directed ortho metalation connection to aryl-aryl cross coupling. A general regiospecific synthesis of phenanthrols. *Tetrahedron Lett.* **1988**, *29* (43), 5459.
3. Giovannini, R.; Studemann, T.; Devasagayaraj, A.; Dussin, G.; Knochel, P., New efficient nickel-catalyzed cross-coupling reaction between two Csp(3) centers. *J. Org. Chem.* **1999**, *64* (10), 3544.
4. Netherton, M. R.; Fu, G. C., Nickel-catalyzed cross-couplings of unactivated alkyl halides and pseudohalides with organometallic compounds. *Adv. Synth. Catal.* **2004**, *346* (13-15), 1525.
5. Powell, D. A.; Fu, G. C., Nickel-catalyzed cross-couplings of organosilicon reagents with unactivated secondary alkyl bromides. *J. Am. Chem. Soc.* **2004**, *126* (25), 7788.

6. Lin, B. L.; Liu, L.; Fu, Y.; Luo, S. W.; Chen, Q.; Guo, Q. X., Comparing nickel- and palladium-catalyzed Heck reactions. *Organometallics* **2004**, *23* (9), 2114.
7. Frisch, A. C.; Beller, M., Catalysts for cross-coupling reactions with non-activated alkyl halides. *Angew. Chem., Int. Ed.* **2005**, *44* (5), 674.
8. Devasagayaraj, A.; Studemann, T.; Knochel, P., A new nickel-catalyzed cross-coupling reaction between sp³ carbon centers. *Angew. Chem., Int. Ed.* **1995**, *34* (23-24), 2723.
9. Phapale, V. B.; Bunuel, E.; Garcia-Iglesias, M.; Cardenas, D. J., Ni-catalyzed cascade formation of C(sp³)-C(sp³) bonds by cyclization and cross-coupling reactions of iodoalkanes with alkyl zinc halides. *Angew. Chem., Int. Ed.* **2007**, *46* (46), 8790.
10. Hull, K. L.; Sanford, M. S., Catalytic and highly regioselective cross-coupling of aromatic C-H substrates. *J. Am. Chem. Soc.* **2007**, *129* (39), 11904.
11. Stuart, D. R.; Fagnou, K., The Catalytic Cross-Coupling of Unactivated Arenes. *Science* **2007**, *316* (5828), 1172.
12. Terao, J.; Kambe, N., Cross-Coupling Reaction of Alkyl Halides with Grignard Reagents Catalyzed by Ni, Pd, or Cu Complexes with pi-Carbon Ligand(s). *Acc. Chem. Res.* **2008**, *41* (11), 1545.
13. Smith, S. W.; Fu, G. C., Nickel-catalyzed asymmetric cross-couplings of racemic propargylic halides with arylzinc reagents. *J. Am. Chem. Soc.* **2008**, *130* (38), 12645.
14. Smith, S. W.; Fu, G. C., Nickel-Catalyzed Negishi Cross-Couplings of Secondary Nucleophiles with Secondary Propargylic Electrophiles at Room Temperature. *Angew. Chem., Int. Ed.* **2008**, *47* (48), 9334.
15. Phapale, V. B.; Cardenas, D. J., Nickel-catalysed Negishi cross-coupling reactions: scope and mechanisms. *Chem. Soc. Rev.* **2009**, *38* (6), 1598.

16. Vechorkin, O.; Hu, X., Nickel-Catalyzed Cross-Coupling of Non-activated and Functionalized Alkyl Halides with Alkyl Grignard Reagents. *Angew. Chem., Int. Ed.* **2009**, *48* (16), 2937.
17. Phapale, V. B.; Guisan-Ceinos, M.; Bunuel, E.; Cardenas, D. J., Nickel-Catalyzed Cross-Coupling of Alkyl Zinc Halides for the Formation of C(sp²)-C(sp³) Bonds: Scope and Mechanism. *Chem. Eur. J.* **2009**, *15* (46), 12681.
18. Everson, D. A.; Shrestha, R.; Weix, D. J., Nickel-Catalyzed Reductive Cross-Coupling of Aryl Halides with Alkyl Halides. *J. Am. Chem. Soc.* **2010**, *132* (3), 920.
19. Lou, S.; Fu, G. C., Nickel/Bis(oxazoline)-Catalyzed Asymmetric Kumada Reactions of Alkyl Electrophiles: Cross-Couplings of Racemic alpha-Bromoketones. *J. Am. Chem. Soc.* **2010**, *132* (4), 1264.
20. Ciszewski, J. T.; Mikhaylov, D. Y.; Holin, K. V.; Kadirov, M. K.; Budnikova, Y. H.; Sinyashin, O.; Vivic, D. A., Redox Trends in Terpyridine Nickel Complexes. *Inorg. Chem.* **2011**, *50* (17), 8630.
21. Yu, X. L.; Yang, T.; Wang, S. L.; Xu, H. L.; Gong, H. G., Nickel-Catalyzed Reductive Cross-Coupling of Unactivated Alkyl Halides. *Org. Lett.* **2011**, *13* (8), 2138.
22. Lin, X. F.; Sun, J.; Xi, Y. Y.; Lin, D. L., How Racemic Secondary Alkyl Electrophiles Proceed to Enantioselective Products in Negishi Cross-Coupling Reactions. *Organometallics* **2011**, *30* (12), 3284.
23. Joshi-Pangu, A.; Wang, C. Y.; Biscoe, M. R., Nickel-Catalyzed Kumada Cross-Coupling Reactions of Tertiary Alkylmagnesium Halides and Aryl Bromides/Triflates. *J. Am. Chem. Soc.* **2011**, *133* (22), 8478.

24. Joshi-Pangu, A.; Ganesh, M.; Biscoe, M. R., Nickel-Catalyzed Negishi Cross-Coupling Reactions of Secondary Alkylzinc Halides and Aryl Iodides. *Org. Lett.* **2011**, *13* (5), 1218.
25. Rosen, B. M.; Quasdorf, K. W.; Wilson, D. A.; Zhang, N.; Resmerita, A.-M.; Garg, N. K.; Percec, V., Nickel-Catalyzed Cross-Couplings Involving Carbon–Oxygen Bonds. *Chem. Rev.* **2011**, *111* (3), 1346.
26. Negishi, E.-i., Magical Power of Transition Metals: Past, Present, and Future (Nobel Lecture). *Angew. Chem., Int. Ed.* **2011**, *50* (30), 6738.
27. Suzuki, A., Cross-Coupling Reactions Of Organoboranes: An Easy Way To Construct C–C Bonds (Nobel Lecture). *Angew. Chem., Int. Ed.* **2011**, *50* (30), 6722.
28. Tobisu, M.; Xu, T.; Shimasaki, T.; Chatani, N., Nickel-Catalyzed Suzuki-Miyaura Reaction of Aryl Fluorides. *J. Am. Chem. Soc.* **2011**, *133* (48), 19505.
29. Tobisu, M.; Yamakawa, K.; Shimasaki, T.; Chatani, N., Nickel-catalyzed reductive cleavage of aryl-oxygen bonds in alkoxy- and pivaloxyarenes using hydrosilanes as a mild reducing agent. *Chem. Comm.* **2011**, *47* (10), 2946.
30. Knochel, P.; Thaler, T.; Diene, C., Pd-, Ni-, Fe-, and Co-Catalyzed Cross-Couplings Using Functionalized Zn-, Mg-, Fe-, and In-Organometallics. *Isr. J. Chem.* **2012**, *50* (5-6), 547.
31. Li, Z.; Jiang, Y. Y.; Fu, Y., Theoretical Study on the Mechanism of Ni-Catalyzed Alkyl-Alkyl Suzuki Cross-Coupling. *Chem. Eur. J.* **2012**, *18* (14), 4345.
32. Binder, J. T.; Cordier, C. J.; Fu, G. C., Catalytic Enantioselective Cross-Couplings of Secondary Alkyl Electrophiles with Secondary Alkylmetal Nucleophiles: Negishi Reactions of Racemic Benzylic Bromides with Achiral Alkylzinc Reagents. *J. Am. Chem. Soc.* **2012**, *134* (41), 17003.

33. Dudnik, A. S.; Fu, G. C., Nickel-Catalyzed Coupling Reactions of Alkyl Electrophiles, Including Unactivated Tertiary Halides, To Generate Carbon-Boron Bonds. *J. Am. Chem. Soc.* **2012**, *134* (25), 10693.
34. Wilsily, A.; Tramutola, F.; Owston, N. A.; Fu, G. C., New Directing Groups for Metal-Catalyzed Asymmetric Carbon-Carbon Bond-Forming Processes: Stereoconvergent Alkyl-Alkyl Suzuki Cross-Couplings of Unactivated Electrophiles. *J. Am. Chem. Soc.* **2012**, *134* (13), 5794.
35. Oelke, A. J.; Sun, J. W.; Fu, G. C., Nickel-Catalyzed Enantioselective Cross-Couplings of Racemic Secondary Electrophiles That Bear an Oxygen Leaving Group. *J. Am. Chem. Soc.* **2012**, *134* (6), 2966.
36. Xu, H.; Zhao, C.; Qian, Q.; Deng, W.; Gong, H., Nickel-catalyzed cross-coupling of unactivated alkyl halides using bis(pinacolato)diboron as reductant. *Chem. Sci.* **2013**, *4* (10), 4022.
37. Zultanski, S. L.; Fu, G. C., Nickel-Catalyzed Carbon-Carbon Bond-Forming Reactions of Unactivated Tertiary Alkyl Halides: Suzuki Arylations. *J. Am. Chem. Soc.* **2013**, *135* (2), 624.
38. Zheng, B.; Tang, F.; Luo, J.; Schultz, J. W.; Rath, N. P.; Mirica, L. M., Organometallic Nickel(III) Complexes Relevant to Cross-Coupling and Carbon-Heteroatom Bond Formation Reactions. *J. Am. Chem. Soc.* **2014**, *136* (17), 6499.
39. Lipschutz, M. I.; Tilley, T. D., Carbon-Carbon Cross-Coupling Reactions Catalyzed by a Two-Coordinate Nickel(II)-Bis(amido) Complex via Observable Ni-I, Ni-II, and Ni-III Intermediates. *Angew. Chem., Int. Ed.* **2014**, *53* (28), 7290.
40. Qin, T.; Cornella, J.; Li, C.; Malins, L. R.; Edwards, J. T.; Kawamura, S.; Maxwell, B. D.; Eastgate, M. D.; Baran, P. S., A general alkyl-alkyl cross-coupling enabled by redox-active esters and alkylzinc reagents. *Science* **2016**, *352* (6287), 801.

41. Cornella, J.; Edwards, J. T.; Qin, T.; Kawamura, S.; Wang, J.; Pan, C. M.; Gianatassio, R.; Schmidt, M.; Eastgate, M. D.; Baran, P. S., Practical Ni-Catalyzed Aryl-Alkyl Cross-Coupling of Secondary Redox-Active Esters. *J. Am. Chem. Soc.* **2016**, *138* (7), 2174.
42. Xu, H. W.; Diccianni, J. B.; Katigbak, J.; Hu, C. H.; Zhang, Y. K.; Diao, T. N., Bimetallic C-C Bond-Forming Reductive Elimination from Nickel. *J. Am. Chem. Soc.* **2016**, *138* (14), 4779.
43. Johnston, C. P.; Smith, R. T.; Allmendinger, S.; MacMillan, D. W. C., Metallaphotoredox-catalysed sp(3)-sp(3) cross-coupling of carboxylic acids with alkyl halides. *Nature* **2016**, *536* (7616), 322.
44. Perez Garcia, P. M.; Di Franco, T.; Epenoy, A.; Scopelliti, R.; Hu, X., From Dimethylamine to Pyrrolidine: The Development of an Improved Nickel Pincer Complex for Cross-Coupling of Nonactivated Secondary Alkyl Halides. *Acs Catal* **2016**, *6* (1), 258.
45. Choi, J.; Fu, G. C., Transition metal-catalyzed alkyl-alkyl bond formation: Another dimension in cross-coupling chemistry. *Science* **2017**, *356* (6334).
46. Khusnutdinova, J. R.; Qu, F.; Zhang, Y.; Rath, N. P.; Mirica, L. M., Formation of the Pd(IV) Complex [(Me₃tacn)PdIVMe₃]⁺ through Aerobic Oxidation of (Me₃tacn)PdIIME₂ (Me₃tacn = N,N',N''-trimethyl-1,4,7-triazacyclononane). *Organometallics* **2012**, *31*, 4627.
47. Qu, F.; Khusnutdinova, J. R.; Rath, N. P.; Mirica, L. M., Dioxygen activation by an organometallic Pd(II) precursor: formation of a Pd(IV)-OH complex and its C-O bond formation reactivity. *Chem. Comm.* **2014**, *50* (23), 3036.
48. Watson, M. B.; Rath, N. P.; Mirica, L. M., Oxidative C-C Bond Formation Reactivity of Organometallic Ni(II), Ni(III), and Ni(IV) Complexes. *J. Am. Chem. Soc.* **2017**, *139* (1), 35.
49. Koek, J. H.; Russell, S. W.; vanderWolf, L.; Hage, R.; Warnaar, J. B.; Spek, A. L.; Kerschner, J.; DelPizzo, L., Improved syntheses, structures, spectral and electrochemical

properties of $[\text{Mn-2(III)}(\mu\text{-O})(\mu\text{-O}(2)\text{CMe})(2)\text{L}(2)](2+)$ and $[\text{Mn-2(IV)}(\mu\text{-O})(3)\text{L}(2)](2+)$ complexes. Two homologous series derived from eight N-substituted 1,4,7-triazacyclononanes. *J Chem Soc Dalton* **1996**, (3), 353.

50. Valyaev, D. A.; Clair, S.; Patrone, L.; Abel, M.; Porte, L.; Chuzel, O.; Parrain, J. L., Grafting a homogeneous transition metal catalyst onto a silicon AFM probe: a promising strategy for chemically constructive nanolithography. *Chem. Sci.* **2013**, 4 (7), 2815.

51. Campora, J.; Conejo, M. D.; Mereiter, K.; Palma, P.; Perez, C.; Reyes, M. L.; Ruiz, C., Synthesis of dialkyl, diaryl and metallacyclic complexes of Ni and Pd containing pyridine, alpha-diimines and other nitrogen ligands crystal structures of the complexes $\text{cis-NiR}(2)\text{py}(2)$ (R = benzyl, mesityl). *J. Organomet. Chem.* **2003**, 683 (1), 220.

52. Connelly, N. G.; Geiger, W. E., Chemical Redox Agents for Organometallic Chemistry. *Chem. Rev.* **1996**, 96 (2), 877.

53. Gottlieb, H. E.; Kotlyar, V.; Nudelman, A., NMR Chemical Shifts of Common Laboratory Solvents as Trace Impurities. *J. Org. Chem.* **1997**, 62 (21), 7512.

54. Fulmer, G. R.; Miller, A. J. M.; Sherden, N. H.; Gottlieb, H. E.; Nudelman, A.; Stoltz, B. M.; Bercaw, J. E.; Goldberg, K. I., NMR Chemical Shifts of Trace Impurities: Common Laboratory Solvents, Organics, and Gases in Deuterated Solvents Relevant to the Organometallic Chemist. *Organometallics* **2010**, 29 (9), 2176.

55. Campora, J.; Lopez, J. A.; Palma, P.; del Rio, D.; Carmona, E.; Valerga, P.; Graiff, C.; Tiripicchio, A., Synthesis and Insertion Reactions of the Cyclometalated Palladium \hat{a} Alkyl Complexes $\text{Pd}(\text{CH}_2\text{CMe}_2\text{-o-C}_6\text{H}_4)\text{L}_2$. Observation of a Pentacoordinated Intermediate in the Insertion of SO_2 . *Inorg. Chem.* **2001**, 40 (17), 4116.

Chapter 5

Catalytic Oxidation Studies for Unactivated Alkanes Using Hypohalites as the Oxidant

5.1 Introduction

Halogenated organic compounds play an important role in organic chemistry, as they exhibit a wide range of biological and pharmacological activities.¹⁻² In organic synthesis, alkyl chlorides also find a use as versatile precursors in many transformations, including cross-coupling reactions.³⁻⁷ The development of new synthetic routes for alkyl halides remains an important challenge, especially for unactivated C–H bonds.^{2,8-11} Recently an effort has been made to develop efficient catalyst for the alkane chlorination in synthetic organic chemistry and industrial chemistry. While several protocols for the conversion of sp^3 C–H centers to C–N and C–O bonds are now available,¹²⁻²¹ fewer methods for the synthesis of C–halogen bonds have been described even though molecules bearing halogen functional groups are prevalent in nature.^{2, 22-25}

Here, we describe a reaction protocol for the oxidation of a C–H bonds to C–Cl bonds using sodium hypochlorite as the chlorine source, in the presence of catalytic amounts of ligand/salt and acetic acid as the additive. The reaction with sodium hypochlorite with different unactivated alkanes afforded alky chlorides as the major products with only trace amounts of dichlorinated products and no oxygenated products. Substrates with strong C–H bonds, such as cyclohexane (BDE = ~100 kcal/mol) or propane (BDE = ~99 kcal/mol) can also undergo chlorination with moderate to high yields.²⁶⁻²⁷ Bromination was also achieved by preparing a solution of NaOCl with a slight excess of NaBr.^{2,22} All the reactions conveniently use hypohalites as a halogen source which are commercially available.

5.2 Experimental Section

Reagents and Materials. All chemicals were available from Aldrich or Fisher and were used as received without further purification. Solvents were purified prior to use by passing through a

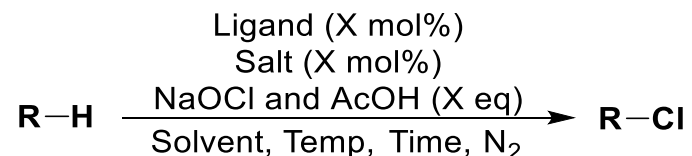
column of activated alumina using an MBraun solvent purification system. Propionitrile, butyronitrile and 1,2-difluorobenzene were distilled and freeze-pump thawed before use. The ligands *N,N'*-dimethyl-2,11-diaza[3.3](2,6)pyridinophane (^{Me}N4), *N*-(*p*-toluenesulfonyl),*N'*-(methyl)-2,11-diaza[3.3](2,6)pyridinophane (^{TsMe}N4), *N,N'*-ditoluensulfonyl-2,11-diaza[3.3](2,6)pyridinophane (^{Ts}N4), *N,N'*-di-*tert*-butyl-2,11-diaza[3.3](2,6)pyridinophane (^{tBu}N4), *N,N'*-dineopentyl-2,11-diaza[3.3](2,6)pyridinophane (^{Np}N4), *N*-(2-methylpyridine),*N'*-(methyl)-2,11-diaza[3.3](2,6)pyridinophane (^{PicMe}N4), *N*-(2-methylpyridine),*N'*-(*p*-toluenesulfonyl)-2,11-diaza[3.3](2,6)pyridinophane (^{PicTs}N4), *N,N'*-di-(2-methylpyridine)-2,11-diaza[3.3](2,6)pyridinophane (^{Pic}N4), *N,N'*-ditoluensulfonyl-2,11-diaza[3.3]-2-pyridinophane-6-bromobenzene (^{Ts}N3CBr) and *N,N'*-di-*tert*-butyl-2,11-diaza[3.3]-2-pyridinophane-6-hydridobenzene (^{tBu}N3CH) were synthesized according to a literature procedure.²⁸⁻³⁰ Other abbreviations used throughout the chapter 1,4,7-trimethyl-1,4,7-triazacyclonane (^{Me3}TACN), 1-toluensulfonyl-4,7-dimethyl-1,4,7-triazacyclonane (^{TsMe2}TACN), 2,2'-bipyridine (bpy), 4,4'-di-*tert*-butyl-2,2'-dipyridyl (dtbbpy) and 1,10-phenanthroline (phen).

5.2.1 General Catalytic Procedure for Unactivated Alkanes

Chlorination. All solids (salt and ligand) were added together and evacuated/flushed with nitrogen three times. Then degassed solvent was added, followed by degassed substrate, acetic acid (AcOH) and sodium hypochlorite (NaOCl) (Scheme 5.1). The reaction was stirred vigorously, and the temperature/length of the reaction time varied and are shown in the reaction schemes. Before GC-MS work up, one equivalent of dodecane was added to the solution. For the work-up 1 mL of 14% perchloric acid was added and stirred for an additional 15 min. To this solution 3 mL of a saturated potassium carbonate solution was added. The solution was then extracted three times with 1 mL of diethyl ether and dried over potassium carbonate for 30 minutes. The solution was filtered and

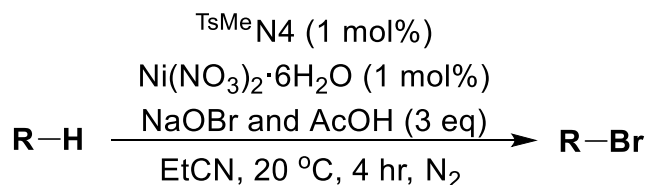
the yield of product(s) was obtained by GC/FID using dodecane as the internal standard. The yield was then converted to turnover numbers (TON) relative to 1 mol% of catalytic loading. The identity of the products was confirmed by GC-MS. All the reactions were performed in duplicate.

Scheme 5.1. General reaction scheme for the chlorination of unactivated C–H bonds.



Bromination. 1 mol % of $\text{Ts}^{\text{Me}}\text{N}_4$ and $\text{Ni}(\text{NO}_3)_2 \cdot 6\text{H}_2\text{O}$ were added together and evacuated/flushed with nitrogen three times. Then degassed propionitrile (EtCN) was added, followed by three equivalents of degassed substrate and acetic acid. Lastly, a mixture of three equivalents of NaOCl and 3.3 equivalents of NaBr was added as the bromination source (Scheme 5.2). The reaction was stirred vigorously for 24 hours at 20 °C. Before GC-MS work up one equivalent of dodecane was added to the solution. For the work-up 1 mL of 14% perchloric acid was added and stirred for an additional 15 min. To this solution 3 mL of a saturated potassium carbonate solution was added. The solution was then extracted 3 times with 1 mL of diethyl ether and dried over potassium carbonate for 30 minutes. The solution was filtered and the yield of product(s) was obtained by GC/FID using dodecane as the internal standard. The yield was then converted to turnover number (TON) relative to 1 mol% of catalyst loading. The identity of the products was confirmed by GC-MS, and all the reactions were performed in duplicate.

Scheme 5.2. General reaction scheme for the bromination of unactivated C–H bonds.



5.2.2 Kinetic Isotope Effect Procedures

KIE Procedure Using a Ni-mediated Chlorination. 1 mol % of TsMe_4N^+ and $\text{Ni(NO}_3)_2 \cdot 6\text{H}_2\text{O}$ were added together and evacuated/flushed with nitrogen three times. Then degassed propionitrile (EtCN) was added, followed by 1.5 equivalents of degassed cyclohexane- d_{12} and 1.5 equivalents of degassed cyclohexane. Lastly, three equivalents of AcOH and NaOCl were added. The reaction was stirred vigorously and monitored over the course of 24 hours at 20 °C. Before GC-MS work up one equivalent of dodecane was added to the solution. For the work-up 1 mL of 14% perchloric acid was added and stirred for an additional 15 min. To this solution 3 mL of a saturated potassium carbonate solution was added. The solution was then extracted 3 times with 1 mL of diethyl ether and dried over potassium carbonate for 30 minutes. The solution was filtered and the yield of product(s) was obtained by GC/FID using dodecane as the internal standard. The identity of the products was confirmed by GC-MS, and all the reactions were performed in duplicate.

KIE Procedure Using Radical Chlorination.

Solutions of thionyl chloride (1 eq) and benzoylperoxide (1 eq) in cyclohexane (0.5 eq) and cyclohexane- d_{12} (0.5 eq) was heated at 90 °C and monitored over the course of several days. Before GC-MS work up one equivalent of dodecane was added to the solution. For the work-up 1 mL of 14% perchloric acid was added and stirred for an additional 15 min. To this solution 3 mL of a saturated potassium carbonate solution was added, make sure to add the base slowly because the

reaction is very acidic. The solution was then extracted 3 times with 1 mL of diethyl ether and dried over potassium carbonate for 30 minutes. The solution was filtered and the yield of product(s) was obtained by GC/FID using dodecane as the internal standard. The identity of the products was confirmed by GC-MS, and all the reactions were performed in duplicate.

5.2.3 Physical Measurements

GC-MS. GC-MS was carried out on an Agilent 7890B using a J&W HP-5ms GC column, (30 m, 0.25 mm, 0.25 μ m, 7 inch cage). Method used: hold at 60 °C for 2 min, ramp (20 °C/min) to 300 °C for 5 min. Note when detecting substrates that have a lower boiling point, the initial temperature was lowered to 40 °C.

5.3 Results and Discussion

5.3.1 Optimization of the Catalytic Chlorination Reaction

Initial optimization for the conditions of alkyl chloride formation was performed with cyclohexane. A variety of parameters were tested and compared. Beginning with the solvents, the catalytic reaction was performed in a variety of solvents (Scheme 5.3). Only trace amounts of halogenated products were obtained when either alcohols, tetrahydrofuran or N,N-dimethylformamide were used as solvents (Table 5.1, entries 1-6). Switching to 1,2-difluorobenzene (DFB) or EtCN as a solvent (Table 5.1, entries 7 and 8) afforded a higher TON. Some other nitrile solvents and acetone were also tested (Table 5.1, entries 9-11) giving moderate yields. Propionitrile was used as the main solvent because it gave the highest TON and was cheaper than 1,2-difluorobenzene. Despite these advantages of propionitrile, it still caused some

chlorination of the solvent to occur. 1,2-difluorobenzene was used when no conversion occurred in propionitrile.

Scheme 5.3 Optimization for a variety of solvents.

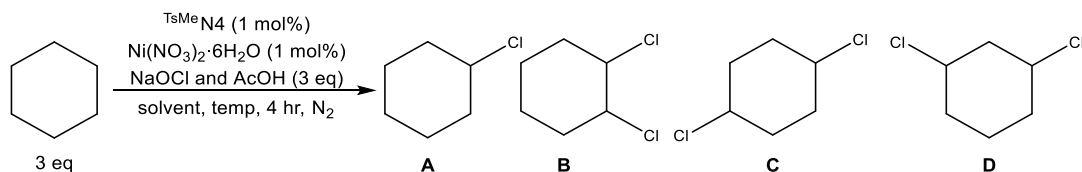


Table 5.1 Optimization for a variety of solvents.

Entry	Solvents	Temperature (°C)	TON ^a			
			A	B	C	D
1	2-butanol	-30	1 ± 0	0 ± 0	0 ± 0	0 ± 0
2	N,N-dimethylformamide	-30	2 ± 1	0 ± 0	0 ± 0	0 ± 0
3	Tetrahydrofuran	-70	5 ± 1	1 ± 1	1 ± 1	1 ± 1
4	Ethanol	-70	1 ± 2	0 ± 0	0 ± 0	0 ± 0
5	2,2,2-trichloroethanol	20	1 ± 1	0 ± 0	0 ± 0	0 ± 0
6	2,2,2-trifluoroethanol	-30	20 ± 3	4 ± 1	8 ± 1	2 ± 1
7	1,2-difluorobenzene	-30	62 ± 3	1 ± 1	5 ± 1	1 ± 1
8	Propionitrile	-70	70 ± 2	3 ± 1	7 ± 1	2 ± 1
9	Acetonitrile	-30	43 ± 2	3 ± 1	8 ± 1	2 ± 1
10	Butyronitrile	-70	42 ± 2	2 ± 1	5 ± 1	1 ± 1
11	Acetone	-70	50 ± 2	2 ± 1	5 ± 1	1 ± 1

^aTON = turnover number of chlorinated products.

After testing the solvents, a variety of parameters were compared, including reaction time, temperature and the amount of solvent used in the general catalytic chlorination reaction (Scheme 5.4). The catalytic reaction was monitored for several hours and after four hours the TON's didn't increase further (Table 5.2, entries 1-4). Different temperatures were used to produce varied results. The TON was lower when the reaction was performed at 20 °C as opposed to -70 °C, indicating that unproductive reaction pathways were occurring at higher temperatures (Table 5.2, entries 3 and 5-7). Another parameter we monitored was the amount of solvent used. When we

used less solvent, we also had to increase the temperature of the reaction, resulting in a lower yield. Using twice the amount of solvent decreased the concentration of the substrate and it became too dilute, resulting in more chlorinated solvent and a lower TON (Table 5.2, entries 3, 8 and 9).

Scheme 5.4 Optimization for different reaction conditions.

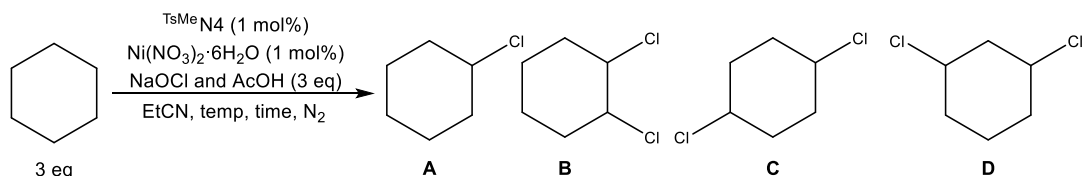
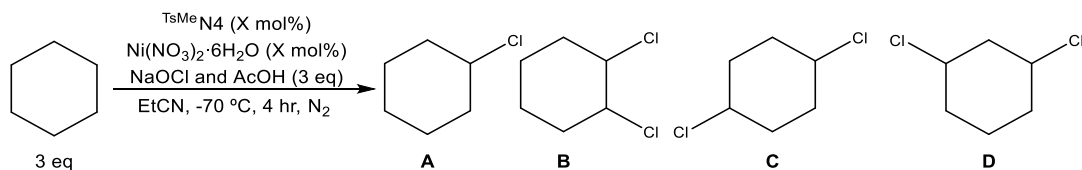


Table 5.2 Optimization for different reaction conditions.

Entry	Solvent amount (mL)	Temperature (°C)	Time (hr)	TON ^a			
				A	B	C	D
1	4	-70	1	60 ± 2	2 ± 1	5 ± 1	2 ± 1
2	4	-70	2	67 ± 2	3 ± 1	6 ± 3	2 ± 1
3	4	-70	4	70 ± 2	3 ± 1	7 ± 1	2 ± 1
4	4	-70	24	71 ± 2	2 ± 1	9 ± 2	2 ± 1
5	4	40	4	32 ± 2	2 ± 1	5 ± 2	2 ± 1
6	4	20	4	50 ± 2	3 ± 1	7 ± 1	2 ± 1
7	4	-30	4	59 ± 3	4 ± 1	10 ± 1	3 ± 1
8	2	-50	4	65 ± 2	4 ± 1	11 ± 1	3 ± 1
9	8	-70	4	51 ± 1	2 ± 1	5 ± 1	1 ± 1

^aTON = turnover number of chlorinated products.

As shown in the general catalytic scheme below (Scheme 5.5), we also varied the catalyst loading, a combination of the ligand and the salt. Using a variety of catalyst loadings, the overall TON changed substantially. Lowering the catalytic loading resulted in the TON increasing up to 4300 when only 0.01 mol% of catalyst was added (Table 5.3). The TON dropped when we increased the catalytic loadings. We also performed a no-catalyst control where the reaction didn't proceed.

Scheme 5.5 Optimization of the catalyst loading.**Table 5.3** Optimization of the catalyst loading.

Entry	Catalyst loading (mol%)	TON ^a			
		A	B	C	D
1	0.0	2 ± 1	0 ± 0	0 ± 0	0 ± 0
2	0.01	4300 ± 2	2 ± 1	6 ± 1	2 ± 1
3	0.05	3100 ± 2	3 ± 1	9 ± 1	2 ± 1
4	0.1	650 ± 1	4 ± 1	10 ± 1	3 ± 1
5	0.5	335 ± 2	4 ± 1	6 ± 2	3 ± 1
6	1.0	70 ± 2	3 ± 1	7 ± 1	2 ± 1
7	2.0	33 ± 1	3 ± 1	9 ± 2	2 ± 1
8	5.0	10 ± 2	2 ± 1	5 ± 1	1 ± 1

^aTON = turnover number of chlorinated products.

Optimization of the amount of substrate, oxidant and additive was tested next (Scheme 5.6). We used one equivalent of cyclohexane and observed that sodium hypochlorite and acetic acid gave a TON of 18 for monochlorocyclohexane plus a TON of 5 for dichlorinated cyclohexane, approximately a 4:1 ratio respectively (Table 5.4, entry 1). Increasing the amount of oxidant and acetic acid gave almost a racemic mixture but increasing the amount of substrate gave a 10:1 product ratio without increasing the amount of chlorinated product generated (Table 5.4, entry 2 and 3). Increasing all three parameters to three equivalents gave a higher yield with a product ratio of 6:1 (Table 5.4, entry 4). Changing oxidant to a crystallin bleach³¹ instead of a solution didn't increase the amount of TON, and the product ratio significantly dropped (Table 5.4, entry 5). Lastly no acetic acid was added as a control to see if this additive was necessary. In this case, the reaction doesn't proceed without acetic acid. We believe the importance of acetic acid is to help

neutralize the reaction mixture, creating a suitable pH for the reaction to proceed (Table 5.4, entry 6).

Scheme 5.6 Substrate, oxidant and additive optimization.

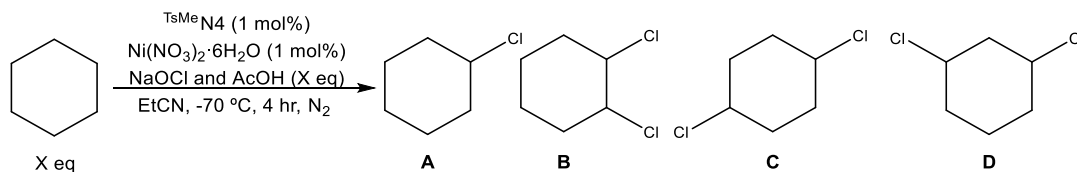


Table 5.4 Amount of substrate, oxidant and additive optimization.

Entry	eq. Cyclohexane	eq. NaOCl	eq. AcOH	TON ^a				Ratio ^c
				A	B	C	D	
1	1	1	1	18 ± 1	1 ± 1	3 ± 1	1 ± 1	4:1
2	1	3	3	24 ± 2	3 ± 1	8 ± 1	3 ± 1	2:1
3	3	1	1	21 ± 2	1 ± 1	1 ± 1	0 ± 0	10:1
4	3	3	3	70 ± 2	3 ± 1	7 ± 1	2 ± 1	6:1
5 ^b	3	3	3	64 ± 3	5 ± 1	12 ± 1	4 ± 1	3:1
6	3	3	0	2 ± 1	0 ± 0	1 ± 1	0 ± 0	2:1

^aTON = turnover number of chlorinated products. ^bNaOCl·5H₂O (3 eq) was used in 0.4 mL ice water. ^cProduct ratio of monochlorination vs dichlorination.

Finally, different ligands and salts were tested with the optimized reaction conditions (Scheme 5.7 and 5.8). Two control reactions were tested, one reaction with no ligand and the second with no salt (Table 5.5, entry 1 and Table 5.6, entry 1). Both reactions gave a negative response, showing that the salt and the ligand are needed for the catalytic reaction to work. A variety of ligands from the Mirica laboratory and commercially available ligands were tested. The ligand that showed the best ratio and the TON gave 70 chlorocyclohexane turnovers and 12 dichlorocyclohexane turnovers, with a respective ratio of 6:1 (Table 5.5, entry 2). Some other ligands gave higher TON but the ratio of monochlorinated product versus dichlorinated product was lower (Table 5.5, entry 8 and 9). The commercially available ligands (Table 5.5, entry 14-19) gave low to moderate TON.

Scheme 5.7 Ligand optimization.

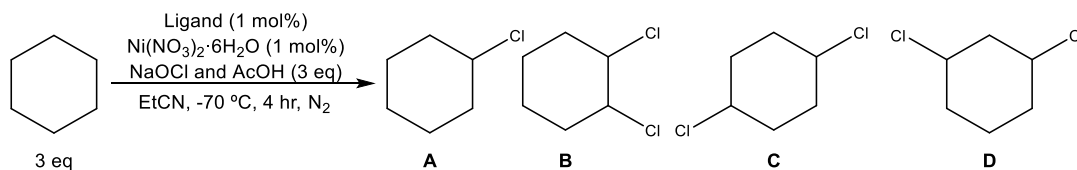


Table 5.5 Ligand optimization.

Entry	Ligand	TON ^a			
		A	B	C	D
1	No ligand	5 ± 1	0 ± 0	0 ± 0	0 ± 0
2	TsMeN4	70 ± 2	3 ± 1	7 ± 1	2 ± 1
3	tBuN4	17 ± 2	0 ± 0	0 ± 0	0 ± 0
4	MeN4	34 ± 2	1 ± 1	2 ± 1	0 ± 0
5	NpN4	62 ± 2	3 ± 1	8 ± 2	2 ± 1
6	TsN4	62 ± 3	3 ± 1	7 ± 1	2 ± 1
7	PicMeN4	66 ± 2	3 ± 1	9 ± 2	2 ± 1
8	PicTsN4	76 ± 2	3 ± 1	9 ± 2	3 ± 1
9	Pic2N4	73 ± 2	4 ± 1	10 ± 2	3 ± 1
10	Me ³ TACN	18 ± 1	0 ± 0	1 ± 1	0 ± 0
11	TsMe ² TACN	42 ± 2	1 ± 1	3 ± 1	1 ± 1
12	TsN3CBr	65 ± 2	3 ± 1	7 ± 1	3 ± 1
13	tBuN3CH	15 ± 1	0 ± 0	1 ± 1	0 ± 0
14	bpy	6 ± 1	0 ± 0	0 ± 0	0 ± 0
15 ^b	bpy	4 ± 1	0 ± 0	0 ± 0	0 ± 0
16	dtbbpy	21 ± 2	1 ± 1	0 ± 0	0 ± 0
17 ^b	dtbbpy	13 ± 2	0 ± 0	0 ± 0	0 ± 0
18	phen	12 ± 1	0 ± 0	0 ± 0	0 ± 0
19 ^b	phen	59 ± 3	5 ± 1	10 ± 1	3 ± 1

^aTON = turnover number of chlorinated products. ^b 2 mol% of ligand was used.

A wide range of first and second row transition metals were tested (Table 5.6). Most salts gave moderate to high TON. Even metals such as zinc, which are less redox active than other metals, gave a high TON, indicating that the redox reactivity doesn't play an important role. The ratio of monochlorinated versus dichlorinated substrate were very similar in most cases, except when the TON drops (Table 5.6, entry 8, 17 and 21). The ratio between the two products increases,

giving a higher selectivity towards the more monochlorinated substrate. The choice of the Ni salt (Table 5.6, entry 10) had a clear influence on the reaction performance giving a high TON and a good ratio between mono vs dichlorination.

Scheme 5.8 Metal salt optimization.

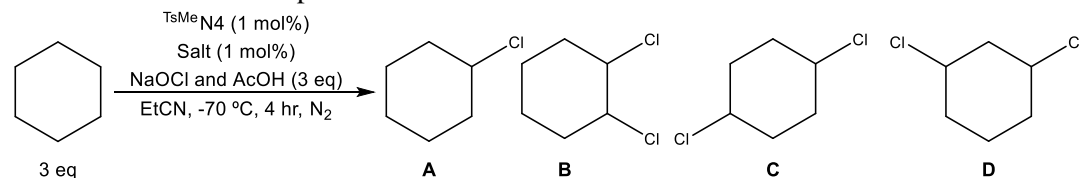


Table 5.6 Metal salt Optimization.

Entry	Salt	TON ^a			
		A	B	C	D
1	No salt	7 ± 1	0 ± 0	0 ± 0	0 ± 0
2	Mn ^{II} (OAc) ₂ ·4H ₂ O	59 ± 3	3 ± 1	9 ± 1	3 ± 1
3	Mn ^{II} (NO ₃) ₂ ·H ₂ O	64 ± 2	6 ± 1	16 ± 3	4 ± 1
4	Fe ^{II} (SO ₄) ₂ ·6H ₂ O	57 ± 2	3 ± 1	9 ± 2	3 ± 1
5	Fe ^{II} (ClO ₄)·H ₂ O	46 ± 2	3 ± 1	7 ± 2	2 ± 1
6	Fe ^{III} (NO ₃) ₂ ·9H ₂ O	39 ± 1	2 ± 1	6 ± 1	2 ± 1
7	Co ^{II} (OAc) ₂ ·4H ₂ O	47 ± 1	2 ± 1	5 ± 1	1 ± 1
8	Co ^{II} (NO ₃) ₂ ·6H ₂ O	30 ± 2	1 ± 1	2 ± 1	1 ± 1
9	Ni ^{II} (OAc) ₂ ·4H ₂ O	64 ± 2	3 ± 1	9 ± 1	2 ± 1
10	Ni ^{II} (NO ₃) ₂ ·6H ₂ O	70 ± 2	3 ± 1	7 ± 1	2 ± 1
11	Ni ^{II} F ₂ ·4H ₂ O	54 ± 1	4 ± 1	8 ± 2	2 ± 1
12	Ni ^{II} Cl ₂ ·6H ₂ O	52 ± 2	3 ± 1	8 ± 1	2 ± 1
13	Ni ^{II} (acac) ₂	59 ± 2	3 ± 1	8 ± 1	2 ± 1
14	Cu ^{II} (OAc) ₂ ·H ₂ O	57 ± 2	3 ± 1	9 ± 1	2 ± 1
15	Cu ^{II} (NO ₃) ₂ ·2.5H ₂ O	30 ± 2	1 ± 1	3 ± 1	1 ± 1
16	Zn ^{II} (NO ₃) ₂ ·6H ₂ O	60 ± 2	4 ± 1	10 ± 2	3 ± 1
17	Rh ^{III} Cl ₃ ·H ₂ O	42 ± 3	1 ± 1	4 ± 1	1 ± 1
18	Pd ^{II} (OAc) ₂	60 ± 1	3 ± 1	8 ± 2	2 ± 1
19	Pd ^{II} (MeCN) ₄ (BF ₄) ₂	58 ± 3	3 ± 1	10 ± 2	2 ± 1
20	Ag ^I NO ₃	64 ± 2	6 ± 1	15 ± 2	1 ± 1
21	Ir ^{III} Cl ₃ ·H ₂ O	36 ± 2	1 ± 1	2 ± 1	1 ± 1

^aTON = turnover number of chlorinated products.

Comparing Company and co-worker's system²⁵ with the one described here, there is an increase in TON from 44 to 70 with the new designed catalytic system and no oxygenated products are observed. The TON can be increased even further by lowering the catalytic loading allowing for high conversion of the cyclohexane substrate. Having the optimized procedure in hand we can now turn to several different types of substrates.

5.3.2 Substrate Scope

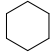
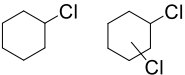

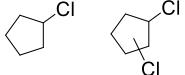
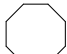
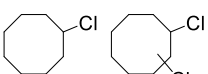
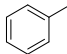
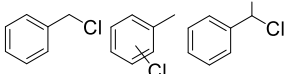
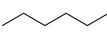
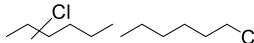
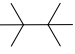
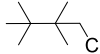
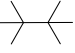
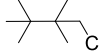
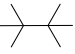
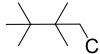
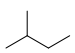
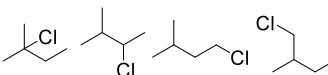
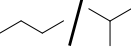
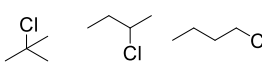
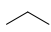
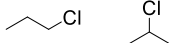
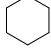
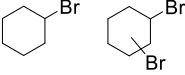

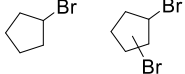
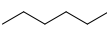
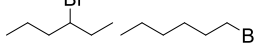
A wide range of unactivated alkanes was subjected to the optimized halogenation protocol. Different functional groups including cycloalkanes, alkanes and toluene were tested with the optimized protocol. When analyzing the cycloalkanes, we noticed that a larger ring size corresponded to a higher TON but a lower ratio of mono vs dichlorination (Table 5.7, entry 1-3). Although cyclohexane has a stronger bond dissociation energy than cyclopentane, a higher chlorination yield was obtained for the cyclohexane substrate (cyclopentane BDE = ~97 kcal/mol, (cyclohexane BDE = ~100 kcal/mol).²⁶ This wasn't the case when comparing cyclohexane vs cyclooctane, since we observed that cyclooctane gave a higher yield than cyclohexane (cyclooctane BDE = ~96 kcal/mol).⁹ When toluene was used as a substrate, the benzylic position was mainly chlorinated with only a small amount of dichlorination (Table 5.7, entry 4).

A variety of alkanes were tested as well. When hexane was used as the substrate, monochlorination mainly occurred to form the products 3-chlorohexane/2-chlorohexane and some 1-chlorohexane, and dichlorination was not observed (Table 5.7, entry 5),³² showing that secondary carbons chlorinate much easier than primary carbons. 2,2,3,3-tetramethylbutane was tested next due to its similarities to methane (Table 5.7, entry 6-8). Chlorination of this substrate occurred with 53 turnovers and no dichlorination is observed when using 1 mol% of catalyst. The

TON increased to 180 and 400 when the catalyst was lowered to 0.1 mol% and 0.01 mol% respectively, indicating that only small amounts of catalyst are needed for the reaction to proceed.

Table 5.7 Substrate scope investigation.

$$\text{R-H} \xrightarrow[\text{EtCN, -70 } ^\circ\text{C, 4 hr, N}_2]{\text{TsMe}_4\text{N}^+\text{ (1 mol\%)} \\ \text{Ni(NO}_3)_2 \cdot 6\text{H}_2\text{O (1 mol\%)} \\ \text{NaOCl and AcOH (3 eq)}} \text{R-Cl}$$

Entry	Substrates	Products	TON ^a
1			70, 12
2			44, 4
3			80, 15
4			56, 7, 2
5			45, 5
6 ^b			53
7 ^{b, c}			180
8 ^{b, d}			400
9 ^b			25, 20, 7, 5
10 ^b	 4:96		44, 23, <1
11 ^b			13, <1
12 ^e			20, 2
13 ^e			13, <1
14 ^e			12, <1

^a TON = turnover number of chlorinated products. ^b DFB was used as solvent at -30 °C. ^c Catalyst loading was decreased to 0.1 mol%. ^d Catalyst loading was decreased to 0.01 mol%. ^e NaOBr, prepared by treatment of NaOCl with a slight excess of NaBr, was used as oxidant at 20 °C.

The following three substrates are gasses at 20 °C but at -70 °C they become liquids, so a known amount was added to the reaction mixture in 1,2-difluorobenzene because no reaction occurs in propionitrile (Table 5.7, entry 9-11). 2-Methylbutane was tested because it has primary, secondary and tertiary carbons to determine if the catalyst plays a significant role or if it is mostly radical chemistry. In the chlorination of 2-methylbutane with the catalyst, the reactivity ratio of the different hydrogen types is tertiary : secondary : primary = 18.8:7.5:1. If we look at radical chlorination of 2-methylbutane the selectivity ratio is 5:4:1, indicating the catalyst plays a significant role in the selectivity of the products.³³⁻³⁴

A mixture of isobutane and butane (96:4) was used for the catalytic chlorination reaction. The tertiary carbon of isobutane was chlorinated predominately which makes sense because tertiary carbons are the most reactive. Butane, which was also present in the reaction mixture, chlorinated predominantly at the secondary carbon. The selectivity of radical chemistry for butane is 3:7 ratio^{32, 35-37} of primary vs secondary carbons and when comparing this to how the catalyst performs primary secondary carbons get chlorinated. In this case the nickel catalyst plays a significant role in the formation of 2-chlorobutane predominately.

We also tested propane. For propane, mainly the primary C–H bonds were chlorinated, and the secondary C–H bond were chlorinated only in a trace amount. The theoretical calculation would be a 3:1 ratio of primary vs secondary carbons, and for radical chemistry at 25 °C an almost equimolar mixture was observed (43:57).^{35-36, 38-41} This means that when the Ni catalyst is used, the product observation drastically changes when compared to a reaction performing pure radical chemistry. Using the Ni catalyst, primary 1-chloropropane with a trace amount of 2-chloropropane was observed. In general, the reactivity ratios for primary, secondary and tertiary carbon-hydrogen

bonds are 1:3.8:5 for radical chlorination, indicating that the nickel catalyst plays a significant role in the selectivity of primary, secondary and tertiary carbon-hydrogen bond formation.³⁵⁻³⁶

Lastly, the bromination reaction was tested for three different substrates (Table 5.7, entry 12-14). Sodium hypobromite was prepared by a treatment of NaOCl with a slight excess of NaBr and the reaction was performed at 20 °C. For all three substrates the TON for bromination decreased but the reaction still occurs, and for all the substrates tested no oxygenated products were observed.

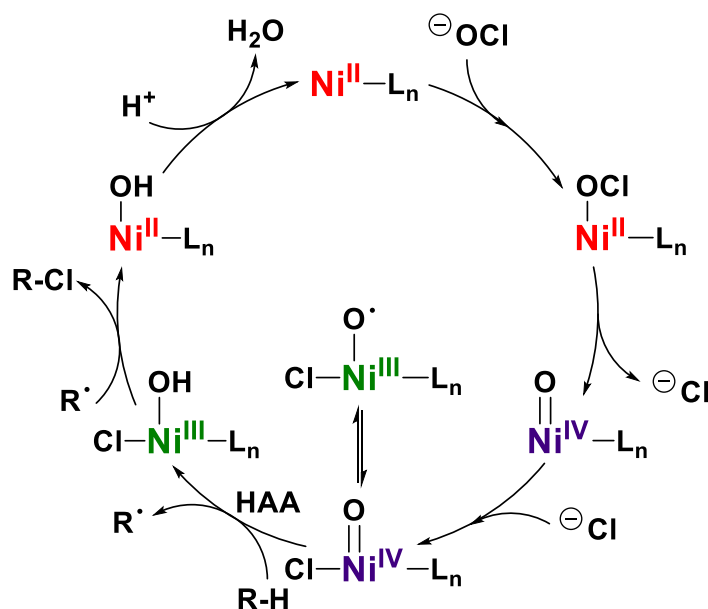
5.3.3 Kinetic Isotope Effect Determination

Preliminary studies were performed to determine the Kinetic Isotope Effect (KIE) for the chlorination reaction to observe if the reaction goes thru a radical mechanism or thru a different mechanism. KIE's were determined using an equimolar mixture of cyclohexane and cyclohexane-d₁₂ as the substrates.⁴²⁻⁴³ The KIE for the chlorination by the catalyst was found to be 1.9 ± 0.1 . By comparison, performing the chlorination using a known radical chlorination, a KIE of 1.0 ± 0.1 was obtained,⁴⁰ indicating that there is a difference between radical chemistry and the Ni-mediated chlorination catalytic process.

There are two possible mechanisms for this new transformation which are outlined in schemes below (Scheme 5.9 and 5.10). While the details are yet to be elucidated, similar catalytic cycles have been described in the literature.^{2, 25, 44} In the first catalytic cycle the hypochlorite anion adds to the Ni^{II} starting material to generate a Ni^{II}(OCl) intermediate (Scheme 5.9). The Ni^{II}(OCl) loses Cl generating a Ni^{IV}(=O) intermediate and rebinding of the chlorine produces a Ni^{IV}(=O)Cl species, which can also be written as a Ni^{III}(O•)Cl species. This intermediate undergoes a hydrogen atom abstraction (HAA) to generate a Ni^{III}(OH)Cl intermediate which then helps produce the

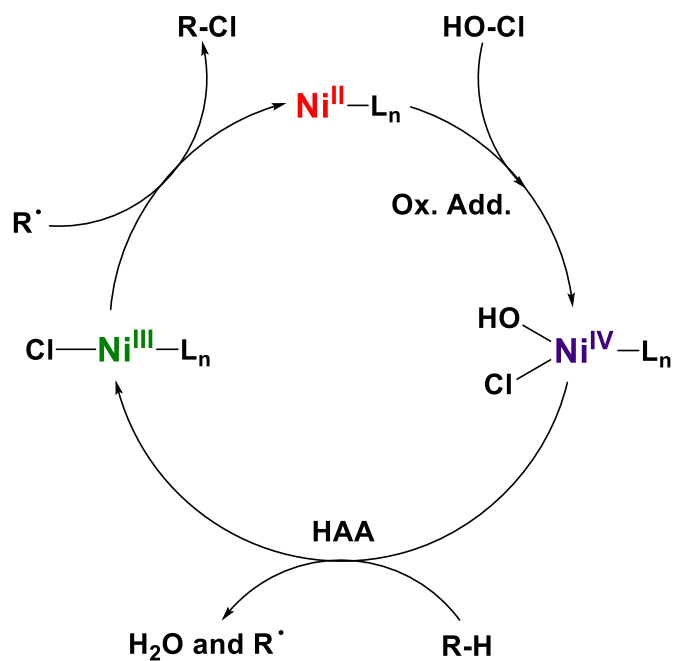
chlorinated product. In the final step the $\text{Ni}^{\text{II}}(\text{OH})$ intermediate gets protonated and loses water to regenerate the starting Ni^{II} complex.

Scheme 5.9 Proposed C–H chlorination mechanism.



For the second proposed catalytic cycle the Ni^{II} undergoes an oxidative addition to form a $\text{Ni}^{\text{IV}}(\text{OH})\text{Cl}$ intermediate (Scheme 5.10). From the Ni^{IV} intermediate, a hydrogen atom abstraction is performed to generate a $\text{Ni}^{\text{III}}\text{Cl}$ intermediate. Lastly, for the product forming step we suggest a chlorine atom transfer from the $\text{Ni}^{\text{III}}\text{Cl}$ complex to the carbon radical center and regeneration of the Ni^{II} starting complex. When looking at the second step in this mechanism the OH group is cis to the Cl group which might explain why we only see chlorination and no hydroxylation.

Scheme 5.9 Alternative C–H chlorination mechanism.



5.4 Conclusion

A catalytic method for unactivated alkane bonds using sodium hypochlorites was presented. The results demonstrate a high TON and a good selectivity of mono vs di-chlorination. The substrates have strong C–H bonds, such as cyclohexane (BDE = ~100 kcal/mol), which might indicate that in the future, methane could be chlorinated (BDE = ~104 kcal/mol). For all substrates tested, no oxygenated products were observed. The halogenation agents are as simple as sodium hypochlorite or hypobromite which are readily available commercially. Substrates similar to methane were also tested such as 2,2,3,3-tetramethylbutane and gasses such as propane and isobutane/butane and 2-methylbutane. Using 2-methylbutane as a substrate provided a direct comparison of primary, secondary and tertiary carbons, by comparing the ratios of products observed. The result indicated that we were not observing radical chemistry and that the catalyst was helping the selectivity of the products. The KIE determinations showed a significant

difference in radical vs non-radical chemistry. Further exploration of this catalytic halogenation reaction will focus on light alkane activation and using a chiral substrate and catalyst one could probe enantioselective transformations.

5.5 Acknowledgements

Thank you to the Mirica laboratory members (present and past) for the small amounts of different types of ligands for the optimization of the chlorination procedure. We would like to thank the Department of Energy (DE-FG02-11ER16256) and the National Science Foundation (CHE-1255424) for their support.

5.6 References

1. Podgorsek, A.; Zupan, M.; Iskra, J., Oxidative Halogenation with "Green" Oxidants: Oxygen and Hydrogen Peroxide. *Angew. Chem., Int. Ed.* **2009**, *48* (45), 8424.
2. Liu, W.; Groves, J. T., Manganese Porphyrins Catalyze Selective C–H Bond Halogenations. *J. Am. Chem. Soc.* **2010**, *132* (37), 12847.
3. Terao, J.; Kambe, N., Cross-Coupling Reaction of Alkyl Halides with Grignard Reagents Catalyzed by Ni, Pd, or Cu Complexes with pi-Carbon Ligand(s). *Acc. Chem. Res.* **2008**, *41* (11), 1545.
4. Glorius, F., Asymmetric Cross-Coupling of Non-Activated Secondary Alkyl Halides. *Angew. Chem., Int. Ed.* **2008**, *47* (44), 8347.
5. Frisch, A. C.; Beller, M., Catalysts for cross-coupling reactions with non-activated alkyl halides. *Angew. Chem., Int. Ed.* **2005**, *44* (5), 674.
6. Netherton, M. R.; Fu, G. C., Nickel-catalyzed cross-couplings of unactivated alkyl halides and pseudohalides with organometallic compounds. *Adv. Synth. Catal.* **2004**, *346* (13-15), 1525.

7. Anderson, T. J.; Jones, G. D.; Vicic, D. A., Evidence for a Ni-I active species in the catalytic cross-coupling of alkyl electrophiles. *J. Am. Chem. Soc.* **2004**, *126* (26), 8100.
8. Nesterov, D. S.; Nesterova, O. V.; Pombeiro, A. J. L., Homo- and heterometallic polynuclear transition metal catalysts for alkane C–H bonds oxidative functionalization: Recent advances. *Coord. Chem. Rev.* **2018**, *355*, 199.
9. Pombeiro, A. J. L.; Costa Guedes da Silva, M. F. C., *Alkane Functionalization*. 1 ed.; Wiley: 2019.
10. Newhouse, T.; Baran, P. S., If C–H Bonds Could Talk: Selective C–H Bond Oxidation. *Angew. Chem., Int. Ed.* **2011**, *50* (15), 3362.
11. Mack, J. B. C.; Gipson, J. D.; Du Bois, J.; Sigman, M. S., Ruthenium-Catalyzed C–H Hydroxylation in Aqueous Acid Enables Selective Functionalization of Amine Derivatives. *J. Am. Chem. Soc.* **2017**, *139* (28), 9503.
12. Hartwig, J. F., Evolution of C–H Bond Functionalization from Methane to Methodology. *J. Am. Chem. Soc.* **2016**, *138* (1), 2.
13. Cernak, T.; Dykstra, K. D.; Tyagarajan, S.; Vachal, P.; Krska, S. W., The medicinal chemist's toolbox for late stage functionalization of drug-like molecules. *Chem. Soc. Rev.* **2016**, *45* (3), 546.
14. Gomez, L.; Garcia-Bosch, I.; Company, A.; Benet-Buchholz, J.; Polo, A.; Sala, X.; Ribas, X.; Costas, M., Stereospecific C–H Oxidation with H₂O₂ Catalyzed by a Chemically Robust Site-Isolated Iron Catalyst. *Angew. Chem., Int. Ed.* **2009**, *48* (31), 5720.
15. Neufeldt, S. R.; Sanford, M. S., Controlling Site Selectivity in Palladium-Catalyzed C–H Bond Functionalization. *Acc. Chem. Res.* **2012**, *45* (6), 936.

16. Wappes, E. A.; Nakafuku, K. M.; Nagib, D. A., Directed beta C–H Amination of Alcohols via Radical Relay Chaperones. *J. Am. Chem. Soc.* **2017**, *139* (30), 10204.
17. Wappes, E. A.; Fosu, S. C.; Chopko, T. C.; Nagib, D. A., Triiodide-Mediated delta-Amination of Secondary C–H Bonds. *Angew. Chem., Int. Ed.* **2016**, *55* (34), 9974.
18. Kim, C.; Chen, K.; Kim, J. H.; Que, L., Stereospecific alkane hydroxylation with H₂O₂ catalyzed by an iron(II)-tris(2-pyridylmethyl)amine complex. *J. Am. Chem. Soc.* **1997**, *119* (25), 5964.
19. Dequirez, G.; Pons, V.; Dauban, P., Nitrene Chemistry in Organic Synthesis: Still in Its Infancy? *Angew. Chem., Int. Ed.* **2012**, *51* (30), 7384.
20. Gigant, N.; Dequirez, G.; Retailleau, P.; Gillaizeau, I.; Dauban, P., Catalytic Selective Oxyamidation of Cyclic Enamides using Nitrenes. *Chem. Eur. J.* **2012**, *18* (1), 90.
21. Solans-Monfort, X.; Fierro, J. L. G.; Hermosilla, L.; Sieiro, C.; Sodupe, M.; Mas-Balleste, R., O–O Bond activation in H₂O₂ and (CH₃)₃C–OOH mediated by [Ni(cyclam)(CH₃CN)₂](ClO₄)₂: Different mechanisms to form the same Ni(III) product? *Dalton Trans.* **2011**, *40* (26), 6868.
22. Sathyamoorthi, S.; Banerjee, S.; Du Bois, J.; Burns, N. Z.; Zare, R. N., Site-selective bromination of sp³ C–H bonds. *Chem. Sci.* **2018**, *9* (1), 100.
23. Liu, W.; Groves, J. T., Manganese Catalyzed C–H Halogenation. *Acc. Chem. Res.* **2015**, *48* (6), 1727.
24. Goldup, S. M.; Leigh, D. A.; McBurney, R. T.; McGonigal, P. R.; Plant, A., Ligand-assisted nickel-catalysed sp³-sp³ homocoupling of unactivated alkyl bromides and its application to the active template synthesis of rotaxanes. *Chem. Sci.* **2010**, *1* (3), 383.

25. Corona, T.; Draksharapu, A.; Padamati, S. K.; Gamba, I.; Martin-Diaconescu, V.; Acuna-Pares, F.; Browne, W. R.; Company, A., Rapid Hydrogen and Oxygen Atom Transfer by a High-Valent Nickel-Oxygen Species. *J. Am. Chem. Soc.* **2016**, *138* (39), 12987.
26. Tian, Z. X.; Fattahi, A.; Lis, L.; Kass, S. R., Cycloalkane and cycloalkene C–H bond dissociation energies. *J. Am. Chem. Soc.* **2006**, *128* (51), 17087.
27. Blanksby, S. J.; Ellison, G. B., Bond dissociation energies of organic molecules. *Acc. Chem. Res.* **2003**, *36* (4), 255.
28. Wessel, A. J.; Schultz, J. W.; Tang, F.; Duan, H.; Mirica, L. M., Improved synthesis of symmetrically & asymmetrically N-substituted pyridinophane derivatives. *Org. Biomol. Chem.* **2017**, *15* (46), 9923.
29. Che, C. M.; Li, Z. Y.; Wong, K. Y.; Poon, C. K.; Mak, T. C. W.; Peng, S. M., A simple synthetic route to N,N'-dialkyl-2,11-diaza[3.3](2,6)pyridinophanes. Crystal structures of N,N'-di-tert-butyl-2,11-diaza[3.3](2,6)pyridinophane and its copper(II) complex. *Polyhedron* **1994**, *13* (5), 771.
30. Zhou, W.; Schultz, J. W.; Rath, N. P.; Mirica, L. M., Aromatic Methoxylation and Hydroxylation by Organometallic High-Valent Nickel Complexes. *J. Am. Chem. Soc.* **2015**, *137* (24), 7604.
31. Kirihaara, M.; Okada, T.; Sugiyama, Y.; Akiyosh, M.; Matsunaga, T.; Kimura, Y., Sodium Hypochlorite Pentahydrate Crystals (NaOCl center dot 5H(2)O): A Convenient and Environmentally Benign Oxidant for Organic Synthesis. *Org. Process Res. Dev.* **2017**, *21* (12), 1925.
32. Colebour.N; Stern, E. S., Chlorination of Some N-Alkanes and Alkyl Chlorides. *J. Chem. Soc.* **1965**, (Jun), 3599.

33. Hass, H. B.; McBee, E. T.; Weber, P., Chlorination of paraffins - Factors affecting yields of isomeric monochlorides and dichlorides. *Ind Eng Chem* **1936**, 28, 333.
34. Hass, H. B.; McBee, E. T.; Weber, P., Syntheses from natural gas hydrocarbons - Identity of monochlorides from chlorination of simpler paraffins. *Ind Eng Chem* **1935**, 27, 1190.
35. Scala, A. A., Gas-Phase Free-Radical Halogenation of Hydrocarbons - Undergraduate Experiment. *J. Chem. Educ.* **1972**, 49 (8), 573.
36. Scala, A. A., Free radical halogenation, selectivity, and thermodynamics: The Polanyi principle and Hammond's postulate. *J. Chem. Educ.* **2004**, 81 (11), 1661.
37. Bell, T. N.; Perkins, K. A.; Perkins, P. G., Chlorination of Paraffin Hydrocarbons .3. Chlorination of Normal-Butane, 1-Chlorobutane, and 2-Chlorobutane. *J. Phys. Chem.* **1981**, 85 (2), 160.
38. Reyerson, L. H.; Yuster, S., The chlorination of propane II The heterogeneous reaction. *J. Phys. Chem.* **1935**, 39 (8), 1111.
39. Yuster, S.; Reyerson, L. H., The chlorination of propane I The homogeneous reaction. *J. Phys. Chem.* **1935**, 39 (6), 859.
40. Krasniewski, J. M.; Mosher, M. W., Free-Radical Chlorination of Alkanes by Thionyl Chloride. *J. Org. Chem.* **1974**, 39 (9), 1303.
41. Aver'yanov, V. A.; Svechnikova, A. A.; Ermakov, A. I., Effect of solvents on the selectivity of free-radical chlorination of functionalized ethanes, propanes, and tetrachloroethene. *Kinet Catal+* **2002**, 43 (2), 175.
42. Ma, L.; Pan, Y.; Man, W. L.; Kwong, H. K.; Lam, W. W. Y.; Chen, G.; Lau, K. C.; Lau, T. C., Highly Efficient Alkane Oxidation Catalyzed by [Mn-V(N)(CN)(4)](2-). Evidence for [Mn-VII(N)(O)(CN)(4)](2-) as an Active Intermediate. *J. Am. Chem. Soc.* **2014**, 136 (21), 7680.

43. Tran, B. L.; Driess, M.; Hartwig, J. F., Copper-Catalyzed Oxidative Dehydrogenative Carboxylation of Unactivated Alkanes to Allylic Esters via Alkenes. *J. Am. Chem. Soc.* **2014**, *136* (49), 17292.
44. van Pee, K. H., Enzymatic Chlorination and Bromination. *Method Enzymol* **2012**, *516*, 237.

Chapter 6

Catalytic Hydroxylation Studies using *m*CPBA as the Oxidant

6.1 Introduction

In nature, a variety of biologically essential transformations are catalyzed by iron containing enzymes such as methane monooxygenases, cytochrome P450 and bleomycin. In particular, the soluble methane monooxygenases are widely investigated metalloenzymes that catalyze the oxidation of methane to methanol using dioxygen.¹⁻¹¹ These enzymes inspired us to put significant efforts into reproducing the functional aspect of the non-heme diiron enzymes by designing model complexes that catalyzed unique selective chemical transformations such as methane oxidation using dioxygen or peroxide. The conventional hydroxylation processes usually require high temperatures and high pressures, and will give only a mixture of alcohol and aldehyde/ketone as the over-oxidized product. In recent years, catalytic oxidation of saturated hydrocarbons under mild conditions has become an exciting and challenging scientific goal and has received greater attention.¹²⁻¹⁶ Although iron complexes are considered to be one of the most promising catalysts for this transformation, a variety of metal-based homogeneous catalysts have been reported by replacing iron with different transition metals such as Mn, Co, Cu, Ru and Os.¹⁷⁻³⁰ The recent development of the nickel dioxygen complexes, which exhibit hydrogen abstraction from aliphatic carbon atoms in a similar manner to the high-valent iron and copper complexes,³¹⁻³⁷ indicates the ability of nickel complexes to act as the oxidizing agents.

Additional challenges are encountered in enantioselective C–H oxidations.³⁸⁻³⁹ Firstly, facile overoxidation of secondary alcohols with respect to the C–H precursor usually eliminates the chirality. Secondly, reagents that are both chiral and are capable of oxygenating aliphatic C–H bonds thru mechanisms that induce enantioselectivity are scarce. Instead, enantioselective C–H oxidation is common in enzymes, where the combination of subtle interaction in the active site helps substrate orientation and the formation of the oxidized product. Not surprisingly, example

of enantioselective sp^3 C–H oxidation with nonenzymatic systems are rare and limited to relatively weak C–H bonds.⁴⁰⁻⁴⁹

Herein we describe the development of a catalytic hydroxylation reaction using *m*CPBA as the oxidant. We aim to construct more efficient and alcohol selective catalysts for alkane hydroxylation. A reaction protocol for the oxidation of cyclohexane and later for *tert*-butylcyclohexane was described using a catalytic amount of ligand and salt to form hydroxylated products and limiting overoxidized products.

6.2 Experimental Section

Reagents and Materials. All chemicals were available from Aldrich or Fisher and were used as received without further purification. Solvents were purified prior to use by passing through a column of activated alumina using an MBraun solvent purification system. 1,2-difluorobenzene were distilled and freeze-pump thawed before use. The ligands *N,N'*-dimethyl-2,11-diaza[3.3](2,6)pyridinophane (^{Me}N4), *N*-(*p*-toluenesulfonyl),*N'*-(methyl)-2,11-diaza[3.3](2,6)pyridinophane (^{TsMe}N4), *N,N'*-ditoluensulfonyl-2,11-diaza[3.3](2,6)pyridinophane (^{Ts}N4), *N,N'*-di-*tert*-butyl-2,11-diaza[3.3](2,6)pyridinophane (^{tBu}N4), *N*-(2-methylpyridine),*N'*-(methyl)-2,11-diaza[3.3](2,6)pyridinophane (^{PicMe}N4), *N*-(2-methylpyridine),*N'*-(*p*-toluenesulfonyl)-2,11-diaza[3.3](2,6)pyridinophane (^{PicTs}N4), *N,N'*-di-(2-methylpyridine)-2,11-diaza[3.3](2,6)pyridinophane (^{Pic}N4), and *N,N'*-di-((*R,S*)-1-phenylethyl)-2,11-diaza[3.3]-2-pyridinophane-6-hydridobenzene (^{racPE}N3CH) were synthesized according to a literature procedure.⁵⁰⁻⁵² Other abbreviations used throughout the chapter meta-chloroperoxybenzoic acid (*m*CPBA) 1,4,7-trimethyl-1,4,7-triazacyclonane (^{Me3}TACN) and 1-toluensulfonyl-4,7-dimethyl-1,4,7-triazacyclonane (^{TsMe2}TACN).

6.2.1 General Catalytic Procedure for Unactivated Alkanes

Hydroxylation. All solids (salt, ligand and oxidant) were added together and evacuated/flushed with nitrogen three times. Then degassed solvent was added (0.5 mol/L), followed by degassed substrate. The reaction was stirred vigorously, and the temperature/length of the reaction time varies as shown in the reaction schemes. Before GC-MS work up, one equivalent of dodecane was added to the solution. For the work-up 1 mL of 14% perchloric acid was added and stirred for an additional 15 min. To this solution 3 mL of a saturated potassium carbonate solution was added. The solution was then extracted three times with 1 mL of diethyl ether and dried over potassium carbonate for 30 minutes. The solution was filtered and the yield of product(s) were obtained by GC/FID using dodecane as the internal standard. The identity of the products was confirmed by GC-MS. All the reactions were performed in duplicate.

Catalyst. A solution of $\text{Ni}(\text{ClO}_4)_2 \cdot 6\text{H}_2\text{O}$ in methanol (1 mL) and a solution of ligand in methanol (1 mL) were added together. The reaction was stirred at 20 °C for 30 minutes and the solution turns pink. Then acetonitrile (1.5 mL) was added and stirred for another 30 minutes at 20 °C. Next a solution of NaBPh_4 was added and pink solid crashed out. The solid was filtered and washed with cold methanol and dried for a day on the schlenk line.³⁵

6.2.2 Physical Measurements

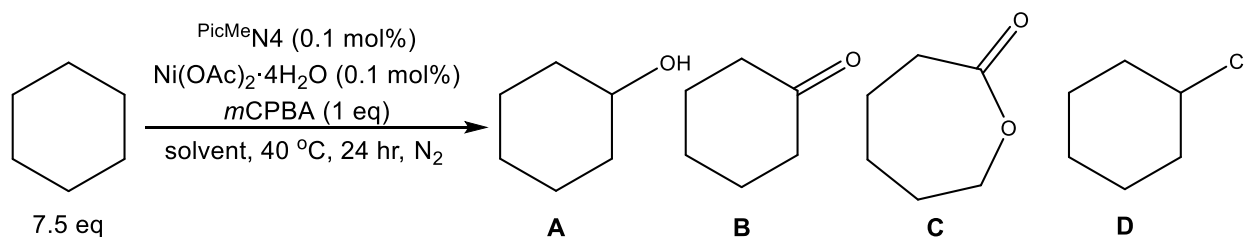
GC-MS. GC-MS was carried out on an Agilent 7890B using a J&W HP-5ms GC column, (30 m, 0.25 mm, 0.25 μm , 7 inch cage). Method used: hold at 60 °C for 2 min, ramp (20 °C/min) to 300 °C for 5 min. Note when detecting substrates that have a lower boiling point, the initial temperature was lowered to 40 °C.

6.3 Results and Discussion

6.3.1 Optimization of the Catalytic Hydroxylation Reaction

Initial hydroxylation studies were performed on cyclohexane, and a variety of parameters were tested and compared with each other. The first parameter was solvent. The catalytic reaction was performed in a variety of solvents (Scheme 6.1).

Scheme 6.1 Optimization for a variety of solvents.



All the solvents tested performed similarly (Table 6.1, entry 1-5). Although small adjustments and a mixture of dichloromethane and acetonitrile (3:1) gave the best conversion for hydroxylated product, it wasn't the highest yield. The reaction was completed in four hours, so there was no need to let the reaction run for 24 hours (Table 6.1, entry 5-6). Next the catalytic loading was increased to observe any changes in hydroxylated product formation. Using a higher catalytic loading decreased the hydroxylated product formation to only 7% (Table 6.1, entry 7). Next the oxidant was changed to hydrogen peroxide instead of mCPBA (Table 6.1, entry 8). Observations show that almost no conversion was detected using hydrogen peroxide as the oxidant, which differs from Costas and co-workers who performed the catalytic reaction with H₂O₂ using a manganese catalyst resulting in up to 85% ketone formation.³⁹ Lastly, the catalyst was pre-made and then used in the oxidation reaction, instead of forming the catalyst *in situ* (Table 6.1, entry 9). The pre-made catalyst has an octahedral geometry with two MeCN molecules and the

multidentate ligand attached to the nickel center (Appendix G). Results show that similar conversions were obtained when using the pre-made catalyst vs. forming the catalyst *in situ*. From these results, we decided to always make the catalyst in-situ instead of pre-making the catalyst.

Table 6.1 Optimization for a variety of solvents.

Entry	Solvents	Time (hr)	Yields ^a (%)			
			A	B	C	D
1	Acetonitrile	24	27 ± 3	4 ± 1	4 ± 1	4 ± 1
2	Dichloroethane	24	20 ± 2	2 ± 1	3 ± 1	3 ± 1
3	Dichloromethane:acetonitrile (3:1)	24	24 ± 3	1 ± 1	3 ± 1	4 ± 1
4	1,2-difluorobenzene	24	19 ± 2	2 ± 1	2 ± 1	5 ± 1
5	Dichloromethane:acetonitrile (3:1)	1	15 ± 2	1 ± 1	1 ± 1	2 ± 1
6	Dichloromethane:acetonitrile (3:1)	4	25 ± 2	1 ± 1	3 ± 1	3 ± 1
7	Dichloromethane:acetonitrile (3:1) ^b	4	7 ± 2	1 ± 1	1 ± 1	1 ± 1
8	Dichloromethane:acetonitrile (3:1) ^c	4	2 ± 2	1 ± 1	1 ± 1	1 ± 1
9	Dichloromethane:acetonitrile (3:1) ^d	4	20 ± 2	2 ± 1	2 ± 1	3 ± 1

^a Yield based on one equivalent of internal standard, yield determined by GC-MS FID. ^b 1 mol% ligand and Ni salt. ^c H₂O₂ was used as the oxidant instead of *m*CPBA. ^d using a pre-made catalyst instead of adding everything in-situ.

After testing a variety of parameters, we tested different ligands with the optimized reaction conditions (Scheme 6.2). The first two control reactions were performed containing one without ligand and one without nickel salt. The results indicate that both the ligand and salt are needed for the reaction to proceed (Table 6.2, entry 1-2). A variety of pyridinophane ligands were tested (Table 6.2, entry 3-9), and most of these ligands gave between 21-31% of hydroxylated product. Some outliers were detected which didn't give any conversion at all (table 6.2, entry 8-9). The next couple of ligands are TACN-type ligands, which were tested using 0.1 mol% and 0.2 mol% of ligand. The results produced gave negative results, giving no hydroxylated product (Table 6.2, entry 10-13). Lastly a chiral N3CH ligand was tested, which gave 5% hydroxylated product (Table 6.2, entry 14). This indicates that N4-type ligands perform the best in these hydroxylation studies,

also when looking at the selectivity of the products we get relatively high selectivity for alcohol vs. ketone formation, in comparison to Palaniandavar and co-workers.³⁴⁻³⁵

Scheme 6.2 Optimization for a variety of ligands.

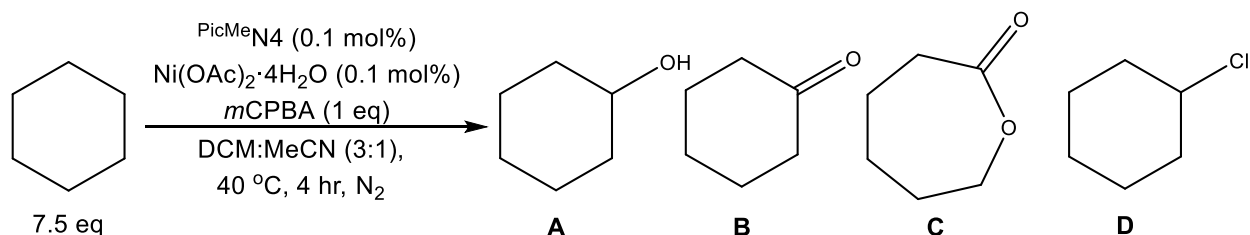


Table 6.2 Optimization for a variety of ligands.

Entry	Ligand	Yields ^a (%)			
		A	B	C	D
1	No ligand	2 ± 1	0 ± 0	0 ± 0	0 ± 0
2	$\text{TsMeN}_4^{\text{b}}$	3 ± 1	0 ± 0	0 ± 0	0 ± 0
3	TsMeN_4	31 ± 2	4 ± 1	5 ± 1	5 ± 1
4	tBuN_4^{c}	30 ± 2	1 ± 1	2 ± 1	3 ± 1
5	MeN_4	21 ± 2	1 ± 1	6 ± 1	3 ± 1
6	TsN_4^{c}	21 ± 1	1 ± 1	4 ± 1	3 ± 1
7	PicMeN_4	25 ± 2	1 ± 1	3 ± 1	3 ± 1
8	PicTsN_4	1 ± 1	0 ± 0	3 ± 0	0 ± 0
9	Pic_2N_4	2 ± 1	1 ± 1	0 ± 0	1 ± 1
10	Me_3TACN	2 ± 1	1 ± 1	3 ± 1	1 ± 1
11	$\text{Me}_3\text{TACN}^{\text{d}}$	1 ± 1	0 ± 0	3 ± 1	1 ± 1
12	TsMe_2TACN	1 ± 1	1 ± 1	1 ± 1	0 ± 0
13	$\text{TsMe}_2\text{TACN}^{\text{d}}$	1 ± 1	1 ± 1	2 ± 1	1 ± 1
14	$\text{racPE}_3\text{N}_3\text{CH}$	5 ± 1	1 ± 1	1 ± 1	2 ± 1

^a Yield based on one equivalent of internal standard, yield determined by GC-MS FID. ^b No nickel salt. ^c solvent was changed to MeCN. ^d 0.2 mol% of ligand was used.

6.3.2 Hydroxylation of *tert*-Butylcyclohexane

The next substrate of focus is *tert*-butylcyclohexane which was used to test potential enantioselective oxidation with $m\text{CPBA}$ (Scheme 6.3). We decided to first use the N_4 -type ligands

because of the promising results shown above. Standard conditions involved a solvent mixture of dichloromethane and acetonitrile (3:1) at 40 °C under nitrogen. The pyridinophane ligands showed promising results (Table 6.3, entry 1-5). The results show that we obtain a mixture of cis and trans 4-*tert*-butylcyclohexanol, 3-*tert*-butylcyclohexanol and 5-(*tert*-butyl)oxepan-2-one. We were not able to determine whether 3-*tert*-butylcyclohexanol was cis or trans. Contrasting to this, we were able to observe both cis and trans 4-*tert*-butylcyclohexanol, with a slight increase of observed trans over cis version. trans-4-*tert*-butylcyclohexanol is more stable due to the substituents existing in the equatorial positions resulting in less steric hindrance. ^{PicMe}N4 ligand showed almost full selectivity towards 3-*tert*-butylcyclohexanol (Table 6.3, entry 5). Lastly, we did test on chiral pyridinophane-type ligand, , in which case 5% of 3-*tert*-butylcyclohexanol was obtained. Ongoing work in the Mirica laboratory is focusing on the synthesis of chiral N4 ligands to be employed in enantioselective transformations.

Scheme 6.3 Oxidation of *tert*-butylcyclohexane with *m*CPBA.

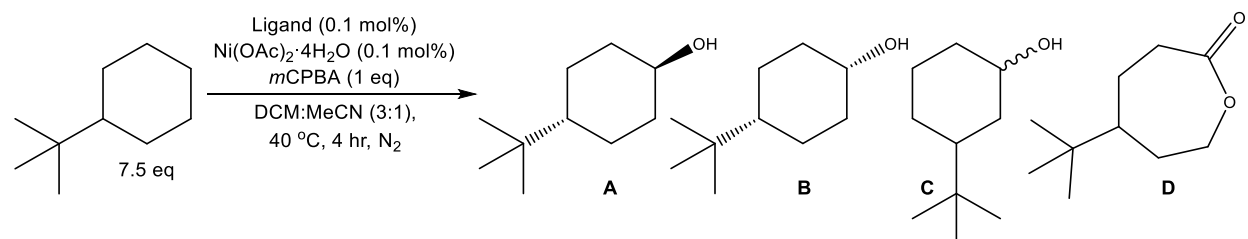


Table 6.3 Oxidation of *tert*-butylcyclohexane with *m*CPBA.

Entry	Ligand	Yields ^a (%)			
		A	B	C	D
1	^{TsMe} N4	36 ± 3	16 ± 2	31 ± 3	6 ± 1
2	^{tBu} N4	24 ± 2	20 ± 1	30 ± 3	5 ± 1
3	^{Me} N4	32 ± 3	26 ± 2	33 ± 2	7 ± 2
4	^{Ts} N4	35 ± 2	16 ± 1	30 ± 1	5 ± 1
5	^{PicMe} N4	1 ± 1	1 ± 1	32 ± 1	2 ± 1
6 ^b	^{racPE} N3CH	2 ± 1	1 ± 1	5 ± 1	0 ± 0

^a Yield based on one equivalent of internal standard, yield determined by GC-MS FID. ^b The ligand is chiral.

6.4 Conclusion

In conclusion we described a catalytic hydroxylation reaction using *m*CPBA as the oxidant. The initial optimization was performed on cyclohexane and then later tested on *tert*-butylcyclohexane. The nickel complexes made in-situ adapts most likely an octahedral coordination geometry around the nickel center to catalyze the hydroxylation of the alkanes. We believe this because an X-ray quality crystal was obtained when pre-making the catalyst, showing two acetonitrile's and the pyridinophane binding to the nickel center. The observed variation in alcohol selectivity for *tert*-butyl-cyclohexane oxidation suggest the involvement of a metal-based oxidant rather than a freely diffusing radical in the reaction. The proposed mechanism of the Ni catalyzed alkane oxidation involves *m*CPBA binding to the Ni^{II} center, by replacing an acetonitrile molecule. Next homolytic or heterolytic O–O bond cleavage of *m*CPBA generated the Ni^{III}–O(H) or Ni^{IV}–O(H) intermediate and lastly oxidation of the alkane occurs by the intermediate. A more detailed mechanistic study would need to be performed to investigate the mechanism of the catalytic oxidation of the alkanes with *m*CPBA.

6.5 Acknowledgements

Thank you to the Mirica laboratory members (present and past) for the small amounts of different types of ligands for the optimization of the hydroxylation procedure. We would also like to thank the Department of Energy (DE-FG02-11ER16256) and the National Science Foundation (CHE-1255424) for their support.

6.6 References

1. Colby, J.; Dalton, H., Characterization of the 2nd Prosthetic Group of the Flavoenzyme NADH-Acceptor Reductase (Component-C) of the Methane Mono-Oxygenase from *Methylococcus-Capsulatus* (Bath). *Biochem. J.* **1979**, *177* (3), 903.
2. Colby, J.; Dalton, H.; Whittenbury, R., Biological and Biochemical Aspects of Microbial-Growth on C1 Compounds. *Annu. Rev. Microbiol.* **1979**, *33*, 481.
3. Vincent, J. B.; Olivierlilley, G. L.; Averill, B. A., Proteins Containing Oxo-Bridged Dinuclear Iron Centers - a Bioinorganic Perspective. *Chem. Rev.* **1990**, *90* (8), 1447.
4. Lipscomb, J. D., Biochemistry of the Soluble Methane Monooxygenase. *Annu. Rev. Microbiol.* **1994**, *48*, 371.
5. Feig, A. L.; Lippard, S. J., Reactions of non-heme iron(II) centers with dioxygen in biology and Chemistry. *Chem. Rev.* **1994**, *94* (3), 759.
6. Wallar, B. J.; Lipscomb, J. D., Dioxygen Activation by Enzymes Containing Binuclear Non-Heme Iron Clusters. *Chem. Rev.* **1996**, *96* (7), 2625.
7. Baik, M. H.; Newcomb, M.; Friesner, R. A.; Lippard, S. J., Mechanistic studies on the hydroxylation of methane by methane monooxygenase. *Chem. Rev.* **2003**, *103* (6), 2385.
8. Carson, E. C.; Lippard, S. J., Oxidation of sulfide, phosphine, and benzyl substrates tethered to N-donor pyridine ligands in carboxylate-bridged diiron(II) complexes. *J. Am. Chem. Soc.* **2004**, *126* (11), 3412.
9. Tshuva, E. Y.; Lippard, S. J., Synthetic models for non-heme carboxylate-bridged diiron metalloproteins: Strategies and tactics. *Chem. Rev.* **2004**, *104* (2), 987.
10. Costas, M.; Mehn, M. P.; Jensen, M. P.; Que, L., Jr., Dioxygen activation at mononuclear nonheme iron active sites: Enzymes, models, and intermediates. *Chem. Rev.* **2004**, *104* (2), 939.

11. Kryatov, S. V.; Rybak-Akimova, E. V.; Schindler, S., Kinetics and mechanisms of formation and reactivity of non-heme iron oxygen intermediates. *Chem. Rev.* **2005**, *105* (6), 2175.
12. Costas, M.; Chen, K.; Que, L., Biomimetic nonheme iron catalysts for alkane hydroxylation. *Coord. Chem. Rev.* **2000**, *200*, 517.
13. Barton, D. H. R.; Doller, D., The Selective Functionalization of Saturated-Hydrocarbons - Gif Chemistry. *Acc. Chem. Res.* **1992**, *25* (11), 504.
14. Shilov, A. E.; Shteinman, A. A., Oxygen atom transfer into C-H bond in biological and model chemical systems. Mechanistic aspects. *Acc. Chem. Res.* **1999**, *32* (9), 763.
15. Stavropoulos, P.; Celenligil-Cetin, R.; Tapper, A. E., The Gif paradox. *Acc. Chem. Res.* **2001**, *34* (9), 745.
16. Punniyamurthy, T.; Velusamy, S.; Iqbal, J., Recent advances in transition metal catalyzed oxidation of organic substrates with molecular oxygen. *Chem. Rev.* **2005**, *105* (6), 2329.
17. Komatsuzaki, H.; Sakamoto, N.; Satoh, M.; Hikichi, S.; Akita, M.; Moro-oka, Y., The first synthesis and structural characterization of alkylperoxo complex of manganese(II). *Inorg. Chem.* **1998**, *37* (26), 6554.
18. Seo, M. S.; Kim, J. Y.; Annaraj, J.; Kim, Y.; Lee, Y. M.; Kim, S. J.; Kim, J.; Nam, W., [Mn(tmc)(O₂)](+) : A side-on peroxido manganese(III) complex bearing a non-heme ligand. *Angew. Chem., Int. Ed.* **2007**, *46* (3), 377.
19. Nehru, K.; Kim, S. J.; Kim, I. Y.; Seo, M. S.; Kim, Y.; Kim, S. J.; Kim, J.; Nam, W., A highly efficient non-heme manganese complex in oxygenation reactions. *Chem. Comm.* **2007**, (44), 4623.

20. Chavez, F. A.; Mascharak, P. K., Co(III)-alkylperoxo complexes: Syntheses, structure-reactivity correlations, and use in the oxidation of hydrocarbons. *Acc. Chem. Res.* **2000**, *33* (8), 539.
21. Jacobson, R. R.; Tyeklár, Z.; Farooq, A.; Karlin, K. D.; Liu, S.; Zubieta, J., A Cu₂-O₂ Complex: Crystal-Structure and Characterization of a Reversible Dioxygen Binding System. *J. Am. Chem. Soc.* **1988**, *110*, 3690.
22. Kitajima, N.; Fujisawa, K.; Morooka, Y.; Toriumi, K., Mu-Eta-2-Eta-2-Peroxo Binuclear Copper Complex, [Cu(Hb(3,5-Ipr2pz)₃)₂(O₂)]. *J. Am. Chem. Soc.* **1989**, *111* (24), 8975.
23. Aboeella, N. W.; Kryatov, S. V.; Gherman, B. F.; Brennessel, W. W.; Young, V. G.; Sarangi, R.; Rybak-Akimova, E. V.; Hodgson, K. O.; Hedman, B.; Solomon, E. I.; Cramer, C. J.; Tolman, W. B., Dioxygen activation at a single copper site: Structure, bonding, and mechanism of formation of 1 : 1 Cu-O₂ adducts. *J. Am. Chem. Soc.* **2004**, *126* (51), 16896.
24. Mirica, L. M.; Ottenwaelder, X.; Stack, T. D. P., Structure and Spectroscopy of Copper-Dioxygen Complexes. *Chem. Rev.* **2004**, *104* (2), 1013.
25. Que, L., Jr.; Tolman, W. B., Bis(m-oxo)dimetal "diamond" cores in copper and iron complexes relevant to biocatalysis. *Angewandte Chemie, International Edition* **2002**, *41* (7), 1114.
26. Cramer, C. J.; Tolman, W. B., Mononuclear CuO₂ complexes: Geometries, spectroscopic properties, electronic structures, and reactivity. *Acc. Chem. Res.* **2007**, *40* (7), 601.
27. Kojima, T.; Matsuo, H.; Matsuda, Y., Catalytic hydrocarbon oxygenation by ruthenium-pyridylamine complexes with alkyl hydroperoxides: a mechanistic insight. *Inorg. Chim. Acta* **2000**, *300*, 661.

28. Okumura, T.; Morishima, Y.; Shiozaki, H.; Yagyu, T.; Funahashi, Y.; Wawa, T.; Jitsukawa, K.; Masuda, H., Characteristics of mononuclear ruthenium-oxo complexes adjusted by axial ligand for the catalysis of oxygen-transfer reactions. *Bull. Chem. Soc. Jpn.* **2007**, *80* (3), 507.
29. Schröder, D.; Schwarz, H., C-H and C-C Bond Activation by Bare Transition-Metal Oxide Cations in the Gas Phase. *Angew. Chem., Int. Ed.* **1995**, *34* (18), 1973.
30. Yu, W.-Y.; Sit, W. N.; Lai, K.-M.; Zhou, Z.; Chan, A. S. C., Palladium-Catalyzed Oxidative Ethoxycarbonylation of Aromatic C-H Bond with Diethyl Azodicarboxylate. *J. Am. Chem. Soc.* **2008**, *130* (11), 3304.
31. Nagataki, T.; Tachi, Y.; Itoh, S., Ni-II(TPA) as an efficient catalyst for alkane hydroxylation with m-CPBA. *Chem. Comm.* **2006**, (38), 4016.
32. Nagataki, T.; Ishii, K.; Tachi, Y.; Itoh, S., Ligand effects on Ni-II-catalysed alkane-hydroxylation with m-CPBA. *Dalton Trans.* **2007**, (11), 1120.
33. Nagataki, T.; Itoh, S., Catalytic alkane hydroxylation reaction with nickel(II) complexes supported by di- and triphenol ligands. *Chem. Lett.* **2007**, *36* (6), 748.
34. Balamurugan, M.; Mayilmurugan, R.; Suresh, E.; Palaniandavar, M., Nickel(ii) complexes of tripodal 4N ligands as catalysts for alkane oxidation using m-CPBA as oxidant: ligand stereoelectronic effects on catalysis. *Dalton Trans.* **2011**, *40* (37), 9413.
35. Sankaralingam, M.; Balamurugan, M.; Palaniandavar, M.; Vadivelu, P.; Suresh, C. H., Nickel(II) Complexes of Pentadentate N5 Ligands as Catalysts for Alkane Hydroxylation by Using m-CPBA as Oxidant: A Combined Experimental and Computational Study. *Chem. Eur. J.* **2014**, *20* (36), 11346.

36. Pfaff, F. F.; Heims, F.; Kundu, S.; Mebs, S.; Ray, K., Spectroscopic capture and reactivity of S=1/2 nickel(III)-oxygen intermediates in the reaction of a Ni-II-salt with mCPBA. *Chem. Comm.* **2012**, 48 (31), 3730.
37. Solans-Monfort, X.; Fierro, J. L. G.; Hermosilla, L.; Sieiro, C.; Sodupe, M.; Mas-Balleste, R., O-O Bond activation in H₂O₂ and (CH₃)₃C-OOH mediated by [Ni(cyclam)(CH₃CN)₂](ClO₄)₂: Different mechanisms to form the same Ni(III) product? *Dalton Trans.* **2011**, 40 (26), 6868.
38. Zheng, C.; You, S. L., Recent development of direct asymmetric functionalization of inert C-H bonds. *RSC Adv.* **2014**, 4 (12), 6173.
39. Milan, M.; Bietti, M.; Costas, M., Highly Enantioselective Oxidation of Nonactivated Aliphatic C-H Bonds with Hydrogen Peroxide Catalyzed by Manganese Complexes. *Acs Central Sci* **2017**, 3 (3), 196.
40. Groves, J. T.; Viski, P., Asymmetric Hydroxylation, Epoxidation, and Sulfoxidation Catalyzed by Vaulted Binaphthyl Metalloporphyrins. *J. Org. Chem.* **1990**, 55 (11), 3628.
41. Groves, J. T.; Viski, P., Asymmetric Hydroxylation by a Chiral Iron Porphyrin. *J. Am. Chem. Soc.* **1989**, 111 (22), 8537.
42. Zhang, R.; Yu, W. Y.; Lai, T. S.; Che, C. M., Enantioselective epoxidation of trans-disubstituted alkenes by D-2-symmetric chiral dioxoruthenium(VI) porphyrins. *Abstr. Pap. Am. Chem. Soc.* **1999**, 218, U730.
43. Zhang, R.; Yu, W. Y.; Che, C. M., Catalytic enantioselective oxidation of aromatic hydrocarbons with D-4-symmetric chiral ruthenium porphyrin catalysts. *Tetrahedron-Asymmetr* **2005**, 16 (21), 3520.

44. Hamada, T.; Irie, R.; Mihara, J.; Hamachi, K.; Katsuki, T., Highly enantioselective benzylic hydroxylation with concave type of (salen)manganese(III) complex. *Tetrahedron* **1998**, *54* (34), 10017.
45. Hamachi, K.; Irie, R.; Katsuki, T., Asymmetric benzylic oxidation using a Mn-salen complex as catalyst. *Tetrahedron Lett.* **1996**, *37* (28), 4979.
46. Murahashi, S. I.; Noji, S.; Komiya, N., Catalytic enantioselective oxidation of alkanes and alkenes using (salen)manganese complexes bearing a chiral binaphthyl strapping unit. *Adv. Synth. Catal.* **2004**, *346* (2-3), 195.
47. Murahashi, S.; Noji, S.; Hirabayashi, T.; Komiya, N., Manganese-catalyzed enantioselective oxidation of C-H bonds of alkanes and silyl ethers to optically active ketones. *Tetrahedron-Asymmetr* **2005**, *16* (21), 3527.
48. Wang, F.; Wang, D. H.; Wan, X. L.; Wu, L. Q.; Chen, P. H.; Liu, G. S., Enantioselective Copper-Catalyzed Intermolecular Cyanotrifluoromethylation of Alkenes via Radical Process. *J. Am. Chem. Soc.* **2016**, *138* (48), 15547.
49. Zhang, W.; Wang, F.; McCann, S. D.; Wang, D. H.; Chen, P. H.; Stahl, S. S.; Liu, G. S., Enantioselective cyanation of benzylic C-H bonds via copper-catalyzed radical relay. *Science* **2016**, *353* (6303), 1014.
50. Wessel, A. J.; Schultz, J. W.; Tang, F.; Duan, H.; Mirica, L. M., Improved synthesis of symmetrically & asymmetrically N-substituted pyridinophane derivatives. *Org. Biomol. Chem.* **2017**, *15* (46), 9923.
51. Che, C. M.; Li, Z. Y.; Wong, K. Y.; Poon, C. K.; Mak, T. C. W.; Peng, S. M., A simple synthetic route to N,N'-dialkyl-2,11-diaza[3.3](2,6)pyridinophanes. Crystal structures of N,N'-di-

tert-butyl-2,11-diaza[3.3](2,6)pyridinophane and its copper(II) complex. *Polyhedron* **1994**, *13* (5), 771.

52. Zhou, W.; Schultz, J. W.; Rath, N. P.; Mirica, L. M., Aromatic Methoxylation and Hydroxylation by Organometallic High-Valent Nickel Complexes. *J. Am. Chem. Soc.* **2015**, *137* (24), 7604.

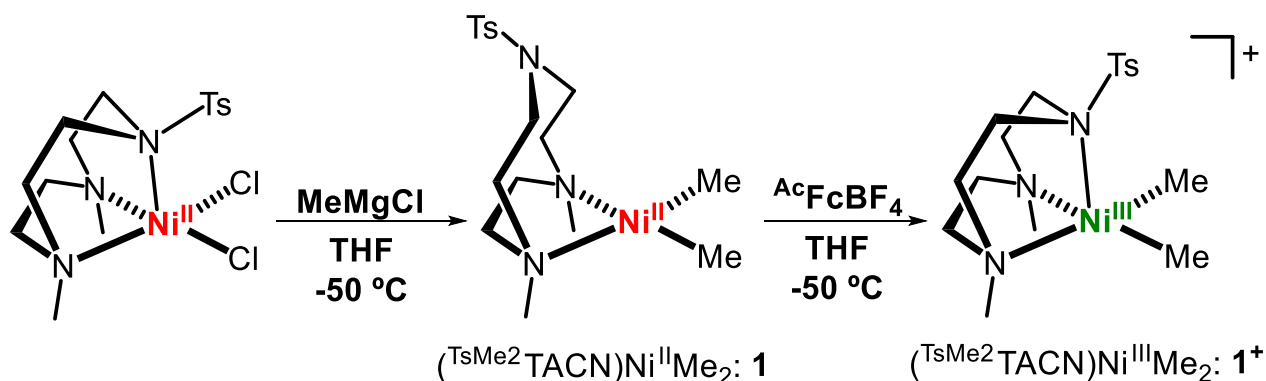
Chapter 7

Future Directions

7.1 A New (^{TsMe₂}TACN)NiMe₂ Complex and its Reactivity

In chapter 2, Ni-dimethyl complexes were introduced, and in chapter 4 a new TACN ligand was introduced. By combining both aspects, a new complex was created to test the C–C and C–heteroatom bond formation (Scheme 7.1). Preliminary studies were performed on complex **1**.

Scheme 7.1 Synthesis of (^{TsMe₂}TACN)NiMe₂ complexes.



The light orange complex (^{TsMe₂}TACN)NiMe₂, **1**, was prepared in a 10% yield from the precursor (^{TsMe₂}TACN)NiCl₂ via transmetalation with methylmagnesium chloride. Complex **1**, was very unstable and decomposed rapidly at room temperature, especially in solution. The cyclic voltammetry (CV) of **1** exhibits an oxidation at -310 mV and 620 mV vs Fc⁺/Fc which are tentatively assigned to the Ni^{III/II} and Ni^{IV/III} oxidation peak (Figure 7.1).

Complex **1** can easily be oxidized with one equivalent of acetylferrocenium tetrafluoroborate (AcFcBF₄) in tetrahydrofuran at -50 °C to obtain [^{TsMe₂}TACN)Ni^{III}Me₂]⁺BF₄⁻, **1**⁺. The EPR spectrum of complex **1**⁺ exhibits an inverse axial spectrum in a solvent mixture containing THF and methyl-THF, indicating that $g_x = g_y < g_z$ (Figure 7.2). The Ni^{III} complex is very short lived and decays within ten seconds at room temperature.

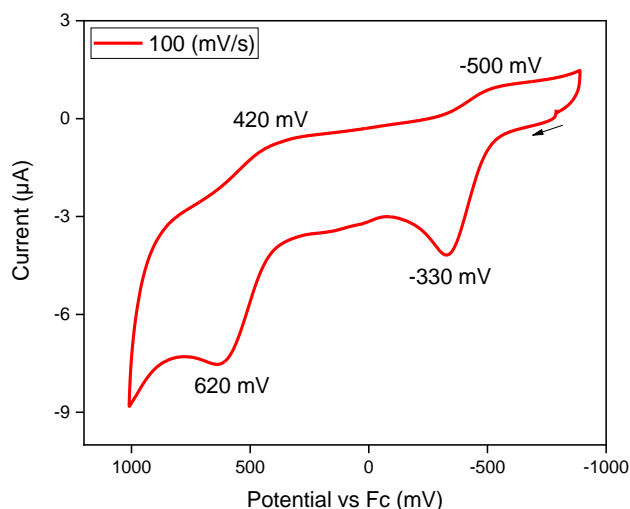


Figure 7.1 CV of **1** in 0.1 M $n\text{Bu}_4\text{NPF}_6/\text{MeCN}$ at RT (100 mV/s scan rate). Redox potentials: $E_{(\text{Ni}^{\text{III}})}$ = -330 mV and $E_{(\text{Ni}^{\text{IV}})}$ = 620 mV.

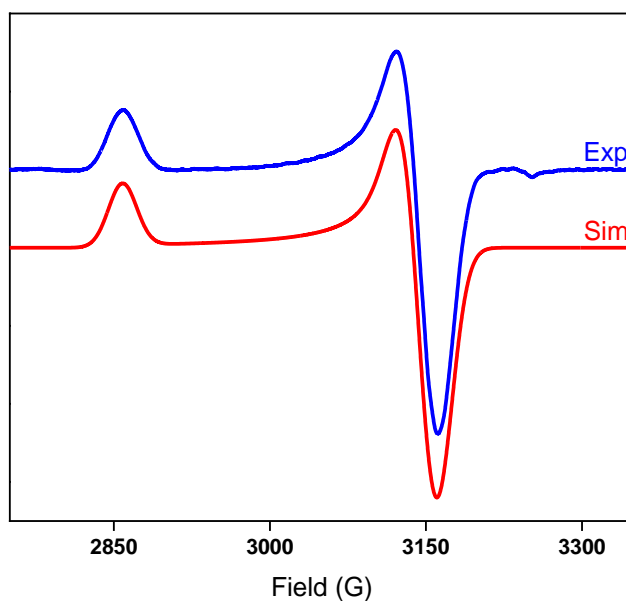
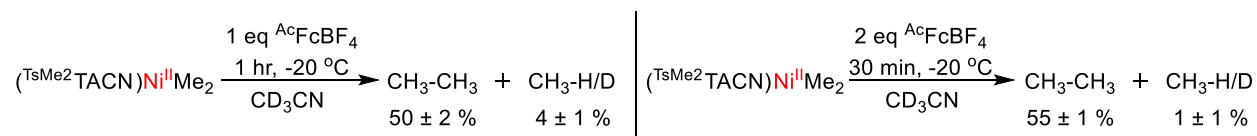


Figure 7.2 Experimental (1:3 THF:MeTHF, 77K) and simulated EPR spectra of **1**⁺ using the following parameters: $g_x = 2.070$, $g_y = 2.055$, $g_z = 2.274$.

The organometallic reactivity of complex **1** was investigated. The reductive elimination of complex **1** was observed upon oxidation with one equivalent of AcFcBF_4 in CD_3CN , and the product formation was monitored via ^1H NMR. The reaction was monitored over the course of 24 hours; after analyzing the data, we determined that the reaction was finished in one hour with an

observed 50% ethane formation and almost no methane formation (Scheme 7.2). Addition of two equivalents of ${}^{\text{Ac}}\text{FcBF}_4$ showed an even faster reductive elimination, reacting completely in 30 minutes with a slight increase in ethane yield and a decrease in methane formation. These reactions were performed at $-20\text{ }^\circ\text{C}$ due to the fast decomposition of the starting material. Future studies will need to be performed on C–heteroatom bond formation, one example of which is dioxygen and hydrogen peroxide for any C–O bond formations or with 1-Fluoro-2,4,6-trimethylpyridinium triflate, 5-(trifluoromethyl)dibenzothiophenium trifluoromethanesulfonate, or xenon difluoride for any C–F or C–CF₃ bond formation reactivity.¹ Also, a detailed mechanistic study will need to be performed for these transformations, especially since (TACN)NiMe₂ complexes have not been synthesized previously.

Scheme 7.2 C–C bond formation reactivity of the $({}^{\text{Tsm}}\text{Me}_2\text{TACN})\text{Ni}^{\text{II}}\text{Me}_2$ complex with ${}^{\text{Ac}}\text{FcBF}_4$.



7.2 A New (${}^{\text{iPr}^3}\text{TACN})\text{Ni}(\text{cycloneophyl})$ Complex

In chapter 4 we saw a variety of triazacyclononane ligands that were able to stabilize high-valent nickel complexes, and we observed C–C and C–O bond formation. We were able to show that adding a slightly larger group on the axial amine can increase the reactivity. Preliminary studies are shown here for the characterization of $({}^{\text{iPr}^3}\text{TACN})\text{Ni}^{\text{II}}(\text{cycloneophyl})$, **2**, and $({}^{\text{iPr}^3}\text{TACN})\text{Ni}^{\text{II}}(\text{cycloneophyl})$, **2**⁺ (Scheme 7.3). Complex **2** was synthesized through a ligand exchange reaction.²⁻³ The X-ray structure shows a square planer geometry for complex **2** (Figure 7.3). The CV of complex **2** exhibits two oxidation potentials one at -310 mV and one at 620 mV vs Fc^+/Fc (Figure 7.3), which are tentatively assigned to the $\text{Ni}^{\text{III/II}}$ and $\text{Ni}^{\text{IV/III}}$ oxidation peak.

Scheme 7.3 Synthesis of $(iPr^3TACN)Ni(cycloneophyl)$ complexes.

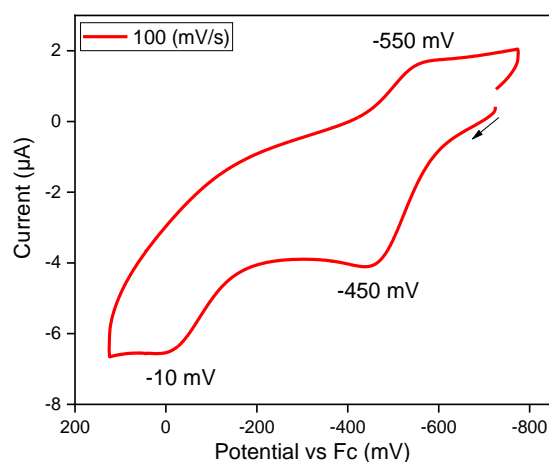
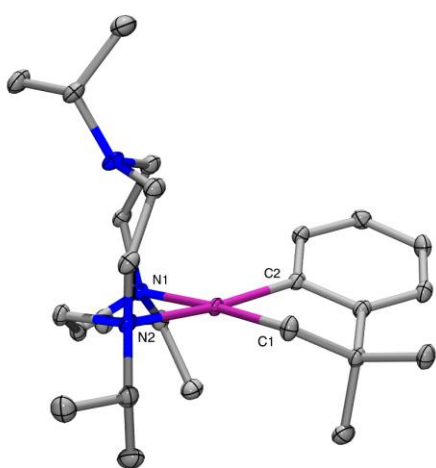
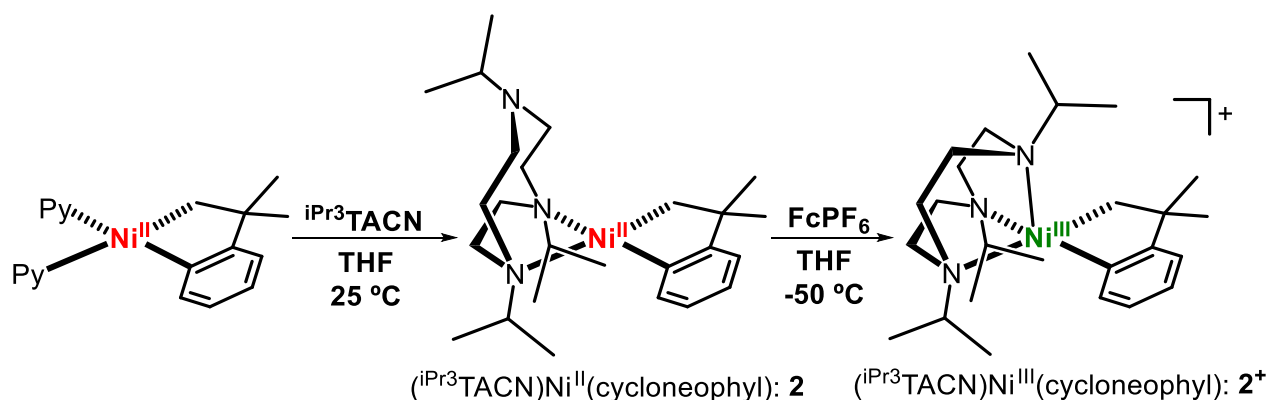


Figure 7.3 ORTEP representation of **2** (left) with 50% probability thermal ellipsoids. Selected bond distances (Å), **2**: Ni1-C1, 1.933; Ni1-C2, 1.919; Ni1-N1, 2.102; Ni1-N2, 2.098, and CV of **2** (right) 0.1 M $nBu_4NPF_6/MeCN$ at RT (100 mV/s scan rate). Redox potentials: $E_{(Ni^{III})} = -450$ mV and $E_{(Ni^{II})} = -10$ mV vs. Fc/Fc^+ .

Complex **2** can easily be oxidized with one equivalent of ferrocenium hexafluorophosphate ($FcPF_6$) in tetrahydrofuran at -50 °C to obtain complex $\mathbf{2}^+$. The EPR spectrum of complex $\mathbf{2}^+$ was taken in two different solvent mixtures with the first being a mixture of THF and methyl-THF (Figure 7.4). The EPR spectrum shows a rhombic signal with triplet in the g_z . The superhyperfine coupling observed in the g_z direction is due to one axial amine arm binding to the Ni^{III} center with 16.5 gauss. The EPR spectrum looks very similar to the $(Me^3TACN)Ni^{II}(cycloneophyl)$ except for some impurities that we suspect is a hydroxylated species. We have derived this conclusion based

on similar observations made by Mirica and co-workers in 2016.⁴ The second spectrum was taken in a mixture of acetonitrile and butyronitrile. The EPR spectrum shows an axial signal with a quintet in the g_z direction due to two nitrogens binding (17 G each). The first nitrogen is from the axial amine arm and the second is from acetonitrile giving a much cleaner spectrum than in the tetrahydrofuran solvent mixture.

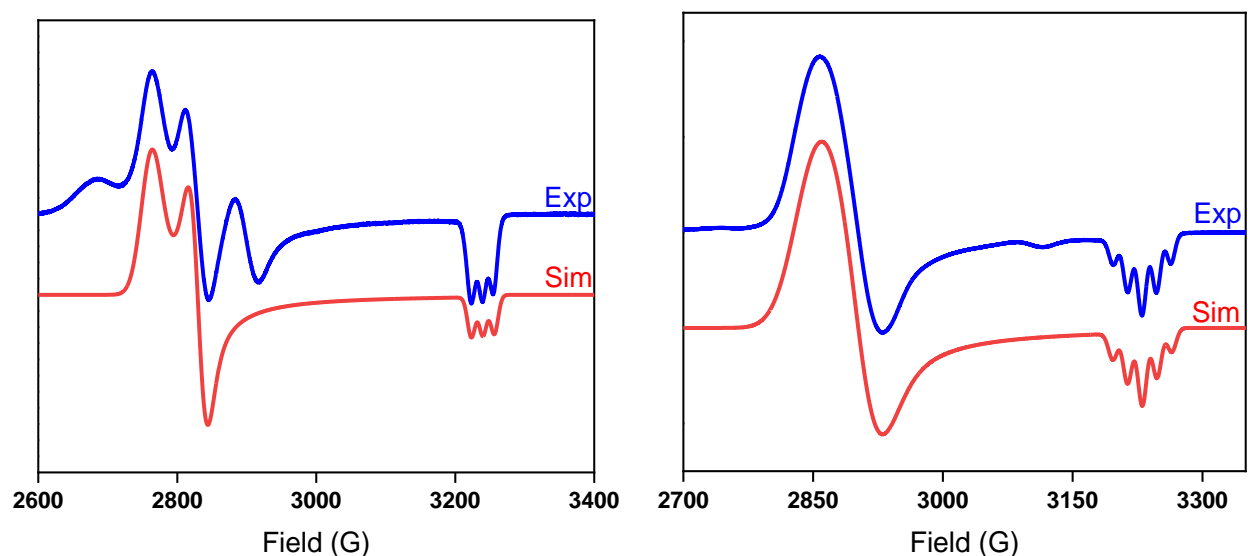


Figure 7.4 Experimental (1:3 THF:MeTHF, 77K) and simulated EPR spectra of 2^+ using the following parameters (left): $g_x = 2.353$, $g_y = 2.297$, $g_z = 2.007$ (A_z (N) = 16.5 G) and experimental (1:3 MeCN:PrCN, 77K) and simulated EPR spectra of 2^+ using the following parameters (right): $g_x = 2.353$, $g_y = 2.297$, $g_z = 2.007$ (A_z (2N) = 17.0 G).

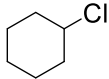
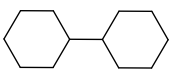
Future studies will focus of the C–C and C–heteroatom bond formation from the Ni^{II} , Ni^{III} and possibly the Ni^{IV} complexes and propose a mechanism. Another option is to synthesize the dimethyl complex and test the C–C and C–heteroatom bond formation.

7.3 Reductive Dimerization of Alkyl Halides

In chapter 5 we were able to make alkyl halides through the chlorination of bleach and a catalytic amount of catalyst. Using the alkyl halide, we now wanted to couple two of these

substrates Methods for the mild, direct dimerization of carbonyls (pinacol coupling), and aryl halides (Ullmann reaction) are available, yet a general, mild method for the direct dimerization of alkyl halides has been limited.⁵⁻¹² Successful sp^3 -carbon-to- sp^3 -carbon coupling are generally limited to halides that are activated towards oxidative addition, and lack β -hydrogen atoms (for example, allylic and benzylic chlorides).¹³⁻¹⁴ There have been recent reports about the coupling of unactivated alkyl halides with alkyl organometallics under mild conditions using highly reactive palladium and nickel catalyst.¹⁵⁻¹⁶ Using a published protocol for the coupling of alkyl halides by Weix and co-workers,¹² we were able to perform a control reaction with 1-chlorooctane resulting in a 95% product yield (Table 7.1). Using a smaller alkyl chain or chlorocyclohexane, we observe a significant drop in yield. Further optimization needs to be performed to increase the yields. Our ideas for optimization include changing from a manganese metal to a zinc metal, using alkyl bromides instead of alkyl chlorides, and using a solvent mixture of tetrahydrofuran and N-methyl-2-pyrrolidone (NMP) instead of N,N-dimethylformamide (DMF). With regards to the change in solvent mixtures, we aren't sure how much more optimized it can get because a large amount of solvents has already been tested by Weix and co-workers.¹¹⁻¹²

Table 7.1 Reductive dimerization of alkyl halides substrate scope.

$\text{R}-\text{Cl} \xrightarrow[\text{DMF, 80 }^\circ\text{C, 36hr}]{\substack{3 \text{ mol } \% \text{ (DME)NiCl}_2 \\ 3 \text{ mol } \% \text{ terpyridine} \\ 0.5 \text{ eq NaI, 1 eq Mn}}} \text{R}-\text{R}$		
Substrate	Product	Yield (%)
1-Chlorooctane	Hexadecane	95
1-Chlorobutane	Octane	10
		12

7.4 References

1. Silva, F. C. S. E.; Tierno, A. F.; Wengryniuk, S. E., Hypervalent Iodine Reagents in High Valent Transition Metal Chemistry. *Molecules* **2017**, *22* (5).
2. Campora, J.; Lopez, J. A.; Palma, P.; del Rio, D.; Carmona, E.; Valerga, P.; Graiff, C.; Tiripicchio, A., Synthesis and Insertion Reactions of the Cyclometalated Palladium^{II} Alkyl Complexes Pd(CH₂CMe₂-o-C₆H₄)L₂. Observation of a Pentacoordinated Intermediate in the Insertion of SO₂. *Inorg. Chem.* **2001**, *40* (17), 4116.
3. Campora, J.; Conejo, M. D.; Mereiter, K.; Palma, P.; Perez, C.; Reyes, M. L.; Ruiz, C., Synthesis of dialkyl, diaryl and metallacyclic complexes of Ni and Pd containing pyridine, alpha-diimines and other nitrogen ligands crystal structures of the complexes cis-NiR(2)py(2) (R = benzyl, mesityl). *J. Organomet. Chem.* **2003**, *683* (1), 220.
4. Watson, M. B.; Rath, N. P.; Mirica, L. M., Oxidative C–C Bond Formation Reactivity of Organometallic Ni(II), Ni(III), and Ni(IV) Complexes. *J. Am. Chem. Soc.* **2016**.
5. Hirao, T., Catalytic reductive coupling of carbonyl compounds - The pinacol coupling reaction and beyond. *Metal Catalyzed Reductive C-C Bond Formation: A Departure from Preformed Organometallic Reagents* **2007**, *279*, 53.
6. Hassan, J.; Sevignon, M.; Gozzi, C.; Schulz, E.; Lemaire, M., Aryl-aryl bond formation one century after the discovery of the Ullmann reaction. *Chem. Rev.* **2002**, *102* (5), 1359.
7. Chatterjee, A.; Joshi, N. N., Evolution of the stereoselective pinacol coupling reaction. *Tetrahedron* **2006**, *62* (52), 12137.
8. Everson, D. A.; Shrestha, R.; Weix, D. J., Nickel-Catalyzed Reductive Cross-Coupling of Aryl Halides with Alkyl Halides. *J. Am. Chem. Soc.* **2010**, *132* (3), 920.

9. Biswas, S.; Weix, D. J., Mechanism and Selectivity in Nickel-Catalyzed Cross-Electrophile Coupling of Aryl Halides with Alkyl Halides. *J. Am. Chem. Soc.* **2013**, *135*, 16192.
10. Everson, D. A.; Jones, B. A.; Weix, D. J., Replacing Conventional Carbon Nucleophiles with Electrophiles: Nickel-Catalyzed Reductive Alkylation of Aryl Bromides and Chlorides. *J. Am. Chem. Soc.* **2012**, *134* (14), 6146.
11. Goldup, S. M.; Leigh, D. A.; McBurney, R. T.; McGonigal, P. R.; Plant, A., Ligand-assisted nickel-catalysed sp(3)-sp(3) homocoupling of unactivated alkyl bromides and its application to the active template synthesis of rotaxanes. *Chem. Sci.* **2010**, *1* (3), 383.
12. Prinsell, M. R.; Everson, D. A.; Weix, D. J., Nickel-catalyzed, sodium iodide-promoted reductive dimerization of alkyl halides, alkyl pseudohalides, and allylic acetates. *Chem. Comm.* **2010**, *46* (31), 5743.
13. Corbet, J. P.; Mignani, G., Selected patented cross-coupling reaction technologies. *Chem. Rev.* **2006**, *106* (7), 2651.
14. Meijere, A. d.; Diederich, F., *Metal-Catalyzed Cross-Coupling Reactions*. Wiley-VCH: Weinheim, New York, 2004.
15. Frisch, A. C.; Beller, M., Catalysts for cross-coupling reactions with non-activated alkyl halides. *Angew. Chem., Int. Ed.* **2005**, *44* (5), 674.
16. Rudolph, A.; Lautens, M., Secondary Alkyl Halides in Transition-Metal-Catalyzed Cross-Coupling Reactions. *Angew. Chem., Int. Ed.* **2009**, *48* (15), 2656.

Appendix A

Select NMR Spectra of Ligands and Metal Complexes

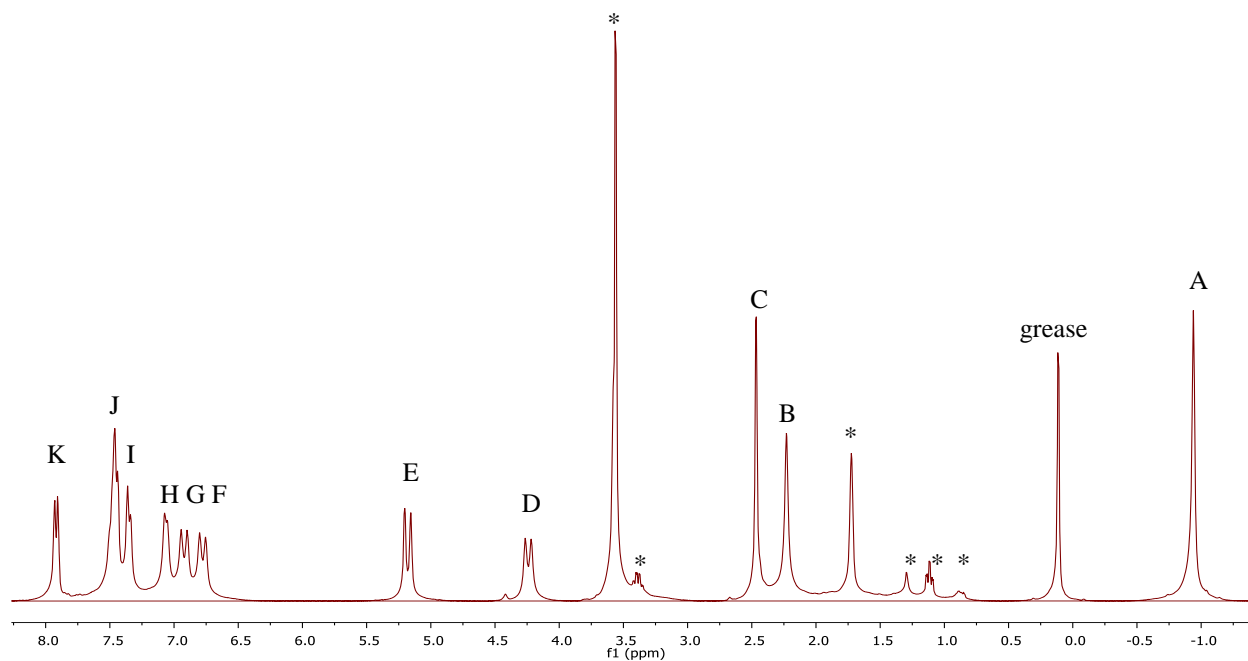


Figure A1. ¹H NMR spectrum of (^{TsMe}N₄)Ni^{II}Me₂ in THF-d₈ (300 MHz). Peaks marked with an asterisk correspond to a trace amount of solvent (THF-d₈, THF and pentane).

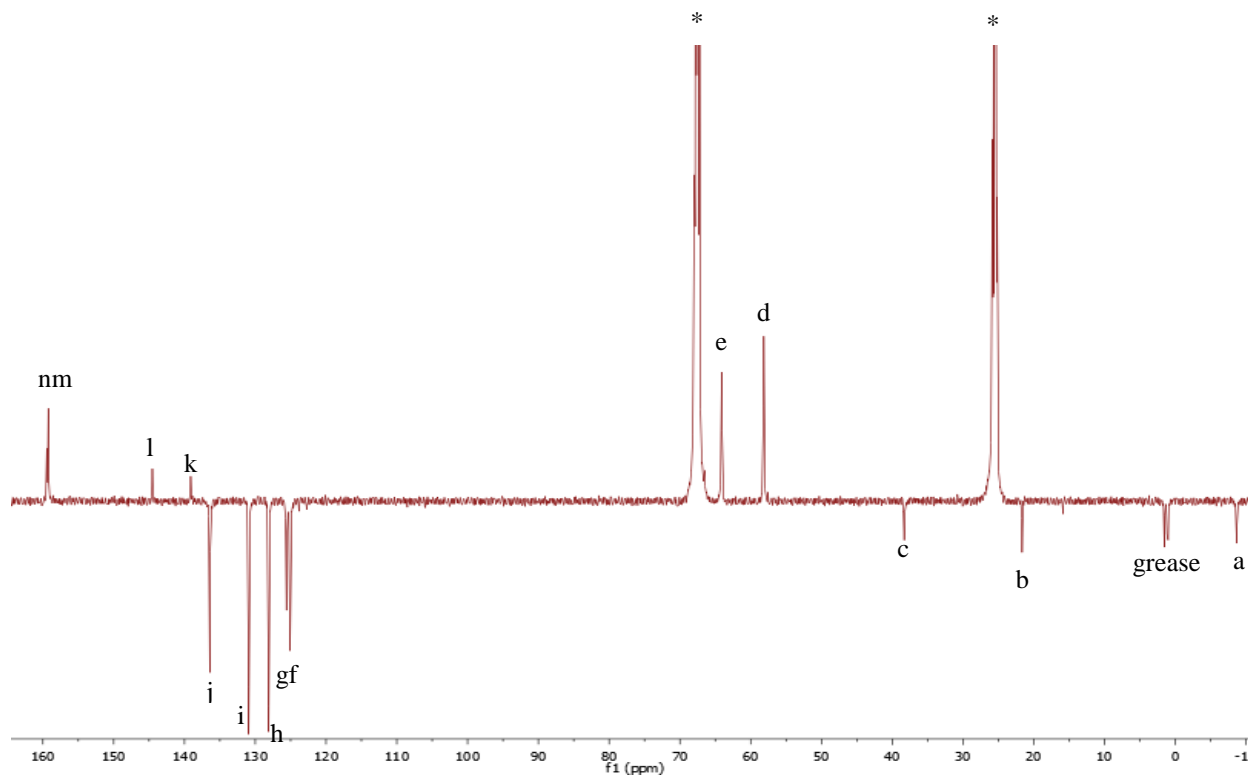


Figure A2. APT spectrum of (^{TsMe}N₄)Ni^{II}Me₂ in THF-d₈ (500 MHz). Peaks marked with an asterisk correspond to a trace amount of solvent (THF-d₈ and THF).

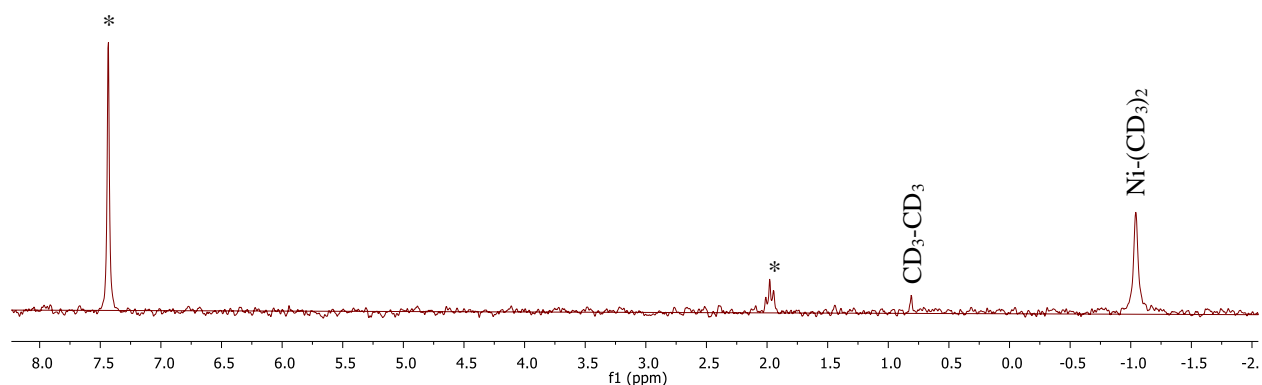


Figure A3. ^2H NMR spectrum of $(^{\text{TsMe}}\text{N}_4)\text{Ni}^{\text{II}}(\text{CD}_3)_2$ in MeCN with benzene- d_6 as standard (500 MHz). Peaks marked with an asterisk correspond to a trace amount of solvent (benzene- d_6 and MeCN).

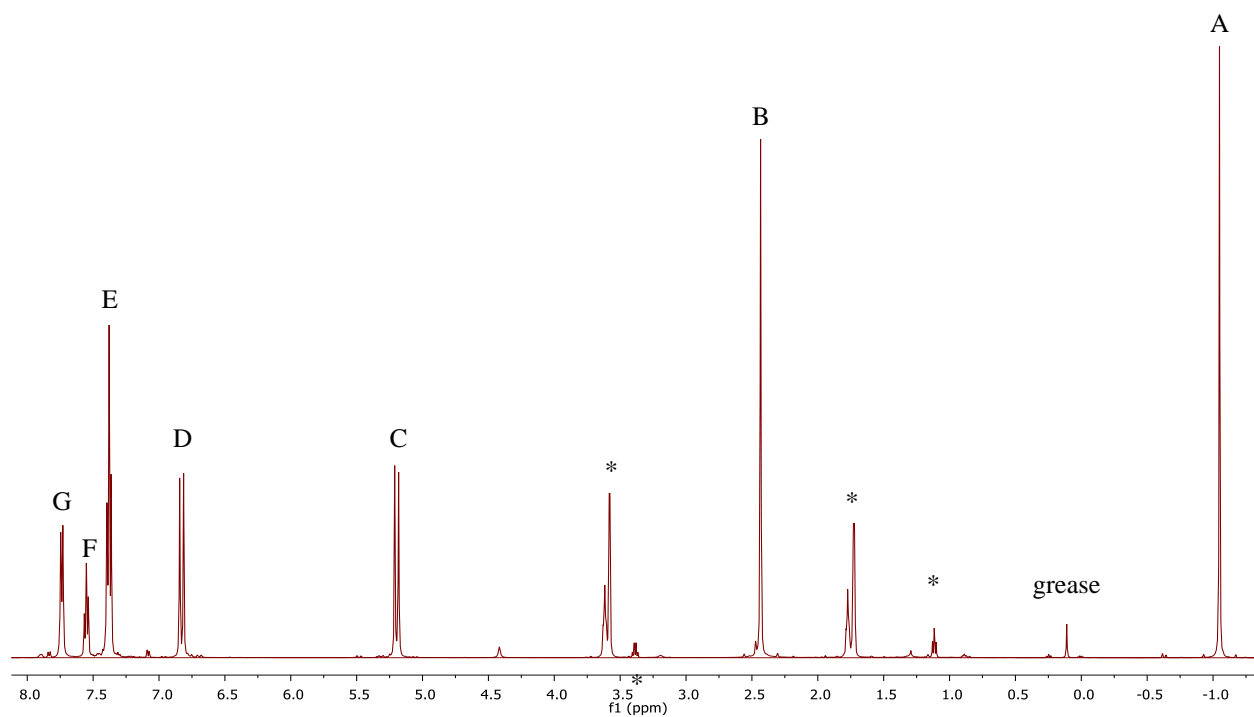


Figure A4. ^1H NMR spectrum of $(^{\text{Ts}}\text{N}_4)\text{Ni}^{\text{II}}\text{Me}_2$ in THF- d_8 (500 MHz). Peaks marked with an asterisk correspond to a trace amount of solvent (THF- d_8 , THF and diethyl ether).

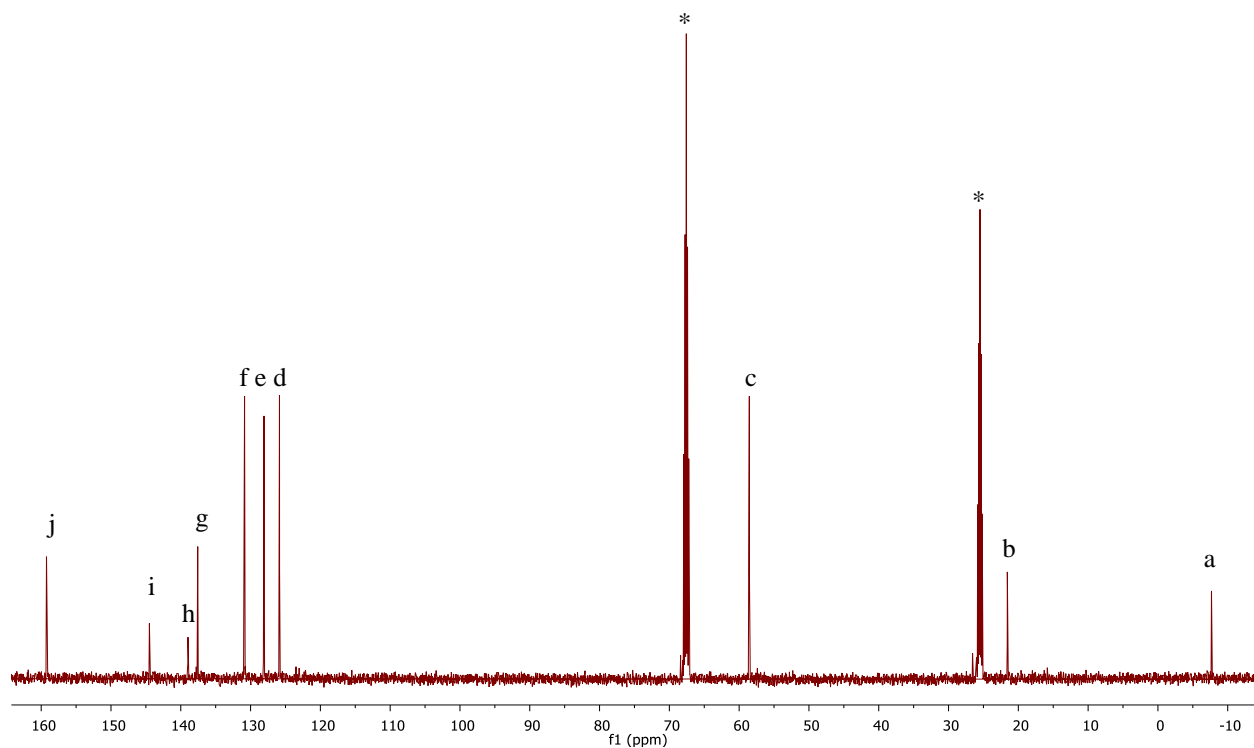


Figure A5. ^{13}C NMR spectrum of $(^{\text{Ts}}\text{N}_4)\text{Ni}^{\text{II}}\text{Me}_2$ in THF-d_8 (500 MHz). Peaks marked with an asterisk correspond to a trace amount of solvent (THF-d_8).

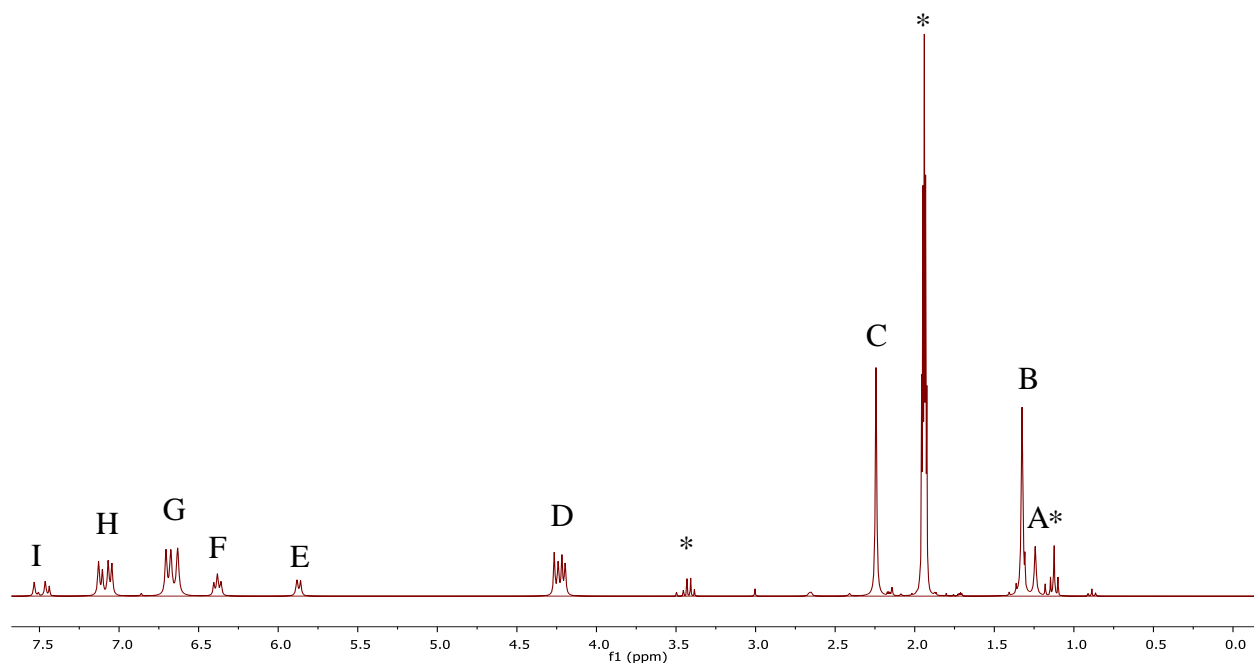


Figure A6. ^1H NMR spectrum of $(^{\text{Me}}\text{N}_4)\text{Ni}^{\text{II}}(\text{cycloneophyl})$ in MeCN-d_3 (300 MHz). Peaks marked with an asterisk correspond to a trace amount of solvent (MeCN-d_3 and diethyl ether).

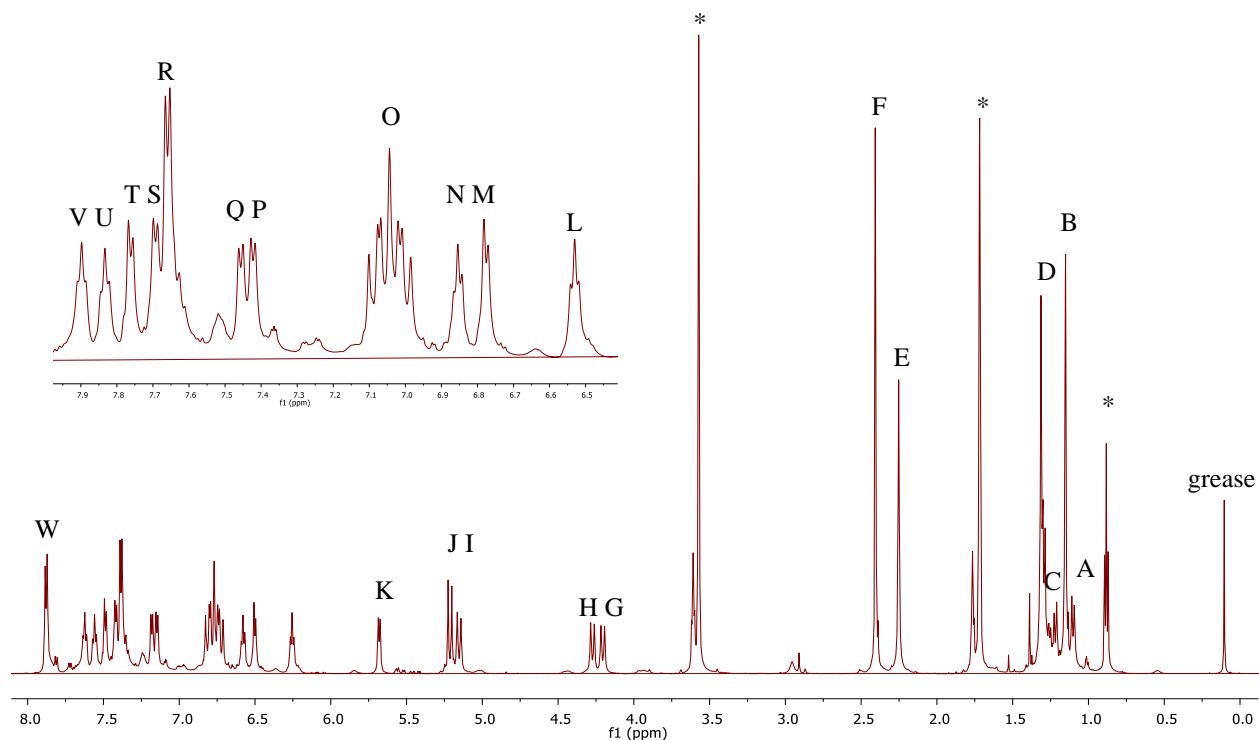


Figure A7. ¹H NMR spectrum of (^{TsMe}N₄)Ni^{II}(cycloneophyl) in THF-d₈ (600 MHz). Peaks marked with an asterisk correspond to a trace amount of solvent (THF-d₈, THF and pentane).

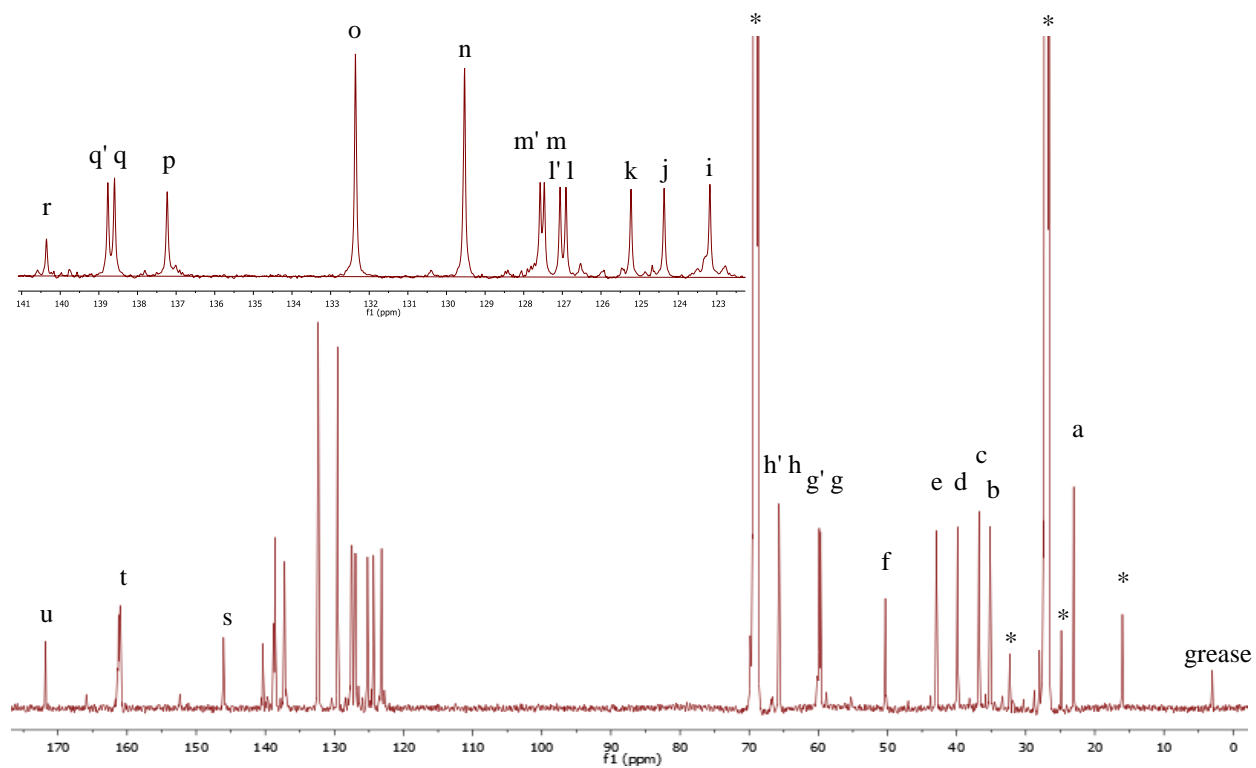


Figure A8. ¹³C NMR spectrum of (^{TsMe}N₄)Ni^{II}(cycloneophyl) in THF-d₈ (600 MHz). Peaks marked with an asterisk correspond to a trace amount of solvent (THF-d₈, THF and pentane).

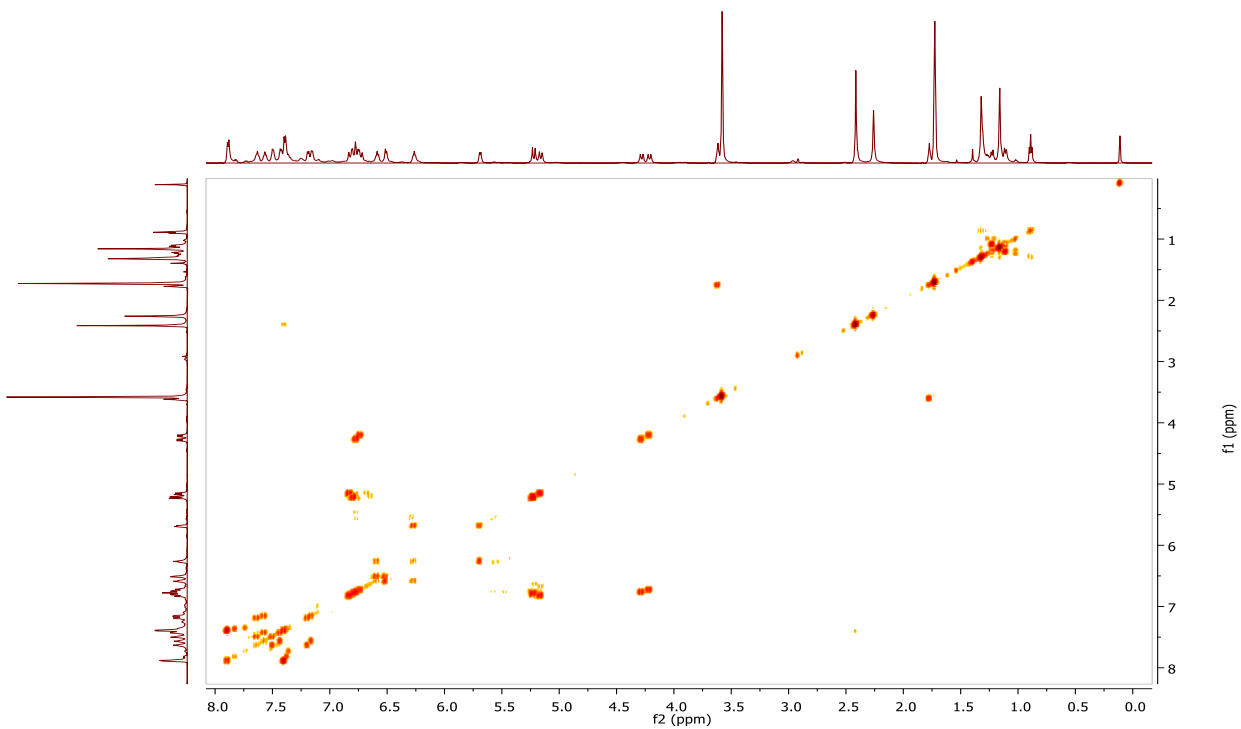


Figure A9. ^1H - ^1H gCOSY spectrum of $(^{\text{TsMe}}\text{N}_4)\text{Ni}^{\text{II}}(\text{cycloneophyl})$ in THF-d_8 (600 MHz).

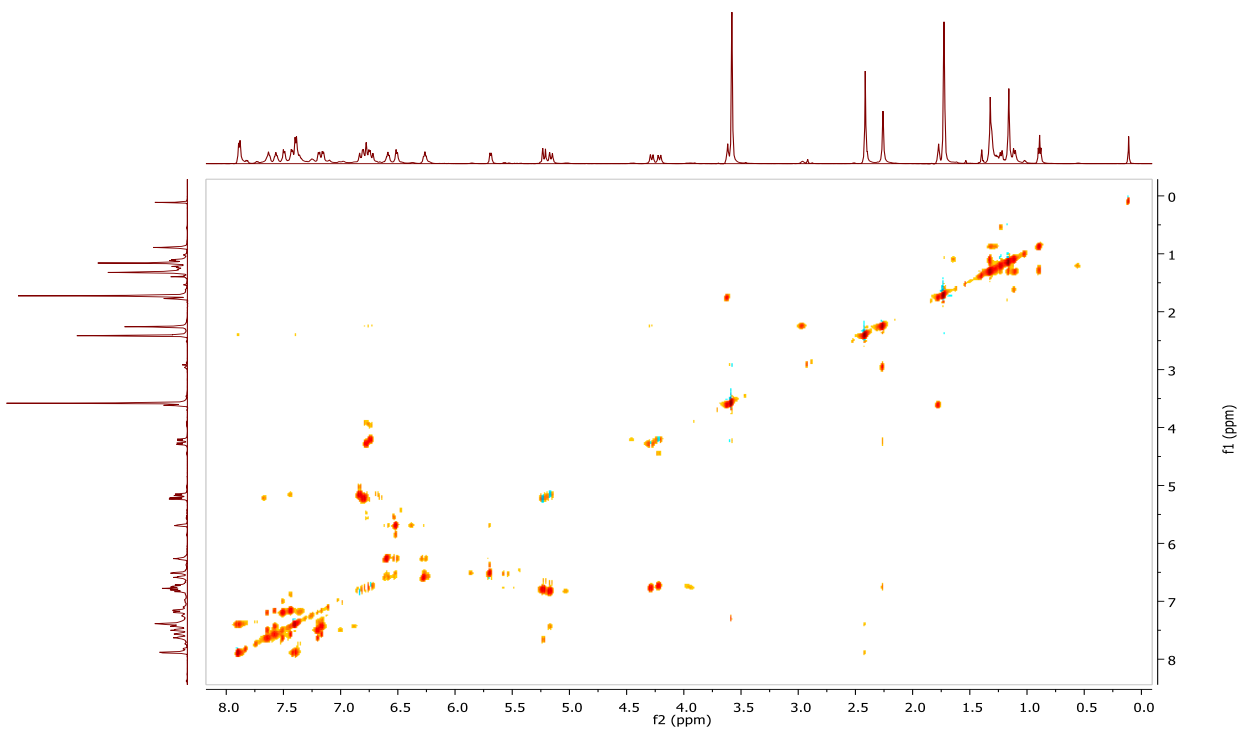


Figure A10. ^1H - ^1H TOXY spectrum of $(^{\text{TsMe}}\text{N}_4)\text{Ni}^{\text{II}}(\text{cycloneophyl})$ in THF-d_8 (600 MHz).

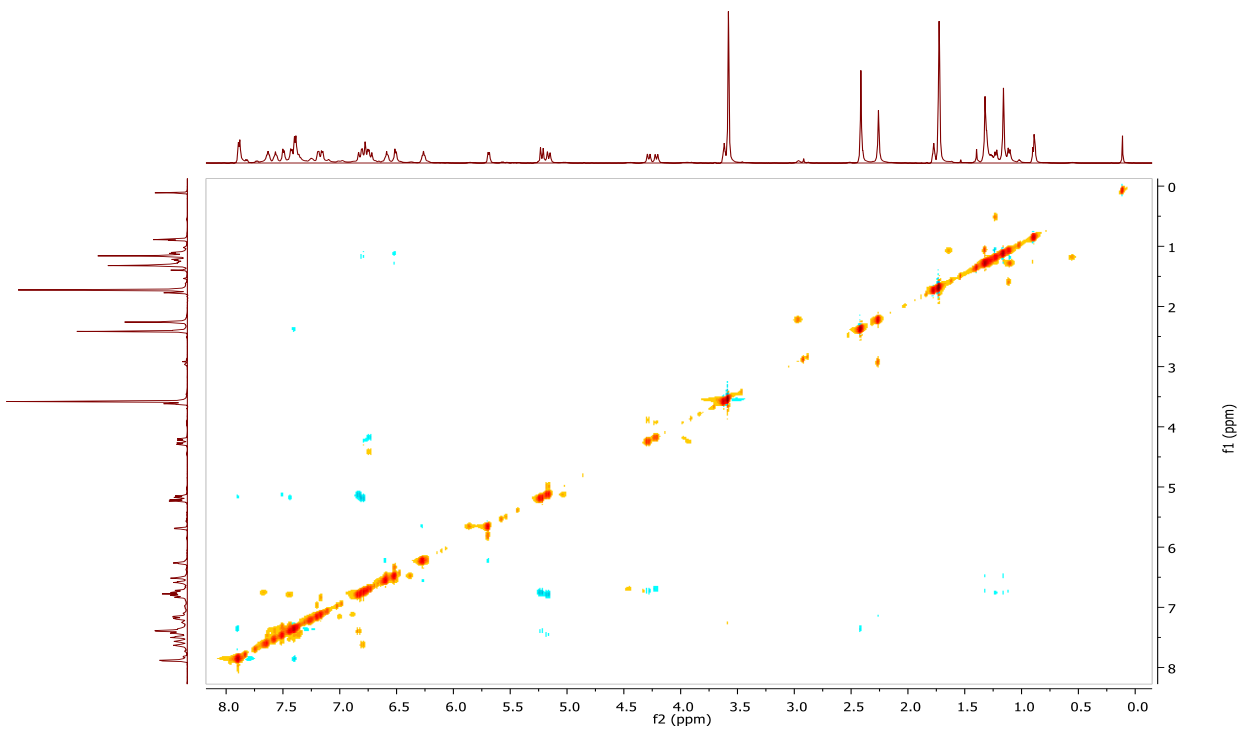


Figure A11. ^1H - ^1H NOESY spectrum of $(^{\text{TsMe}}\text{N}_4)\text{Ni}^{\text{II}}$ (cycloneophyl) in THF-d_8 (600 MHz).

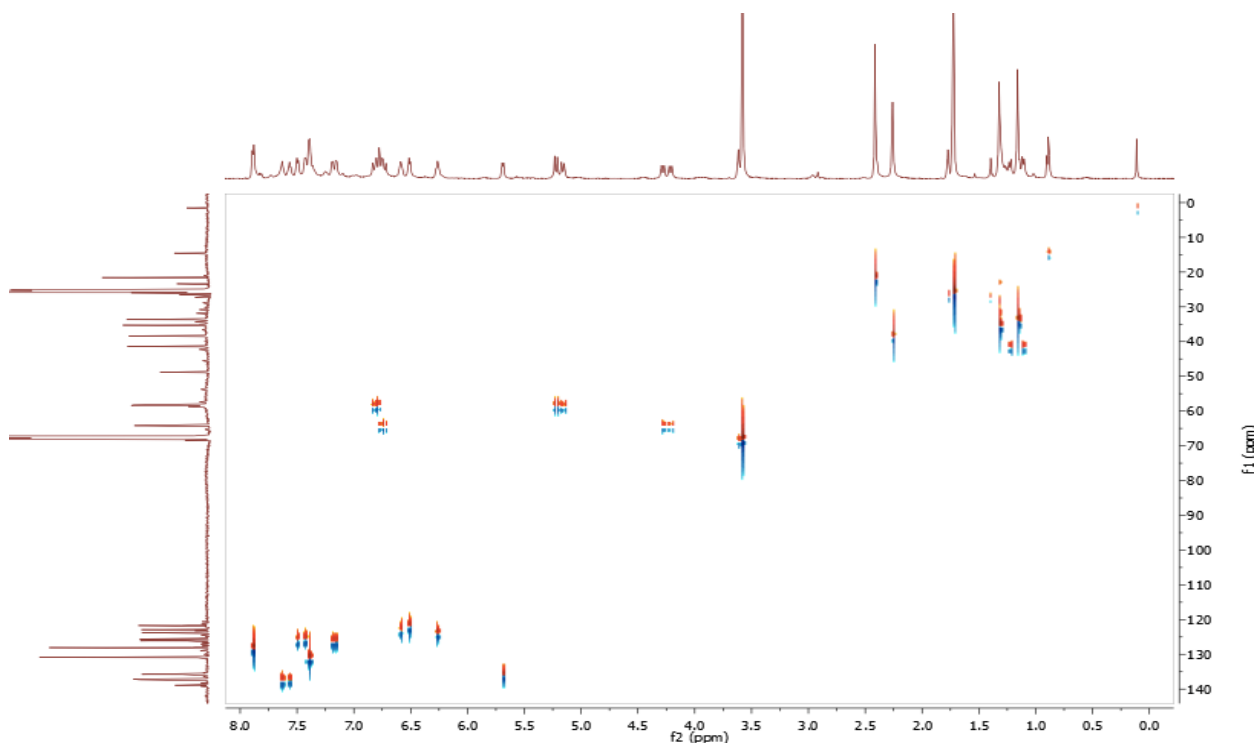


Figure A12. ^1H - ^{13}C HSQC spectrum of $(^{\text{TsMe}}\text{N}_4)\text{Ni}^{\text{II}}$ (cycloneophyl) in THF-d_8 (600 MHz).

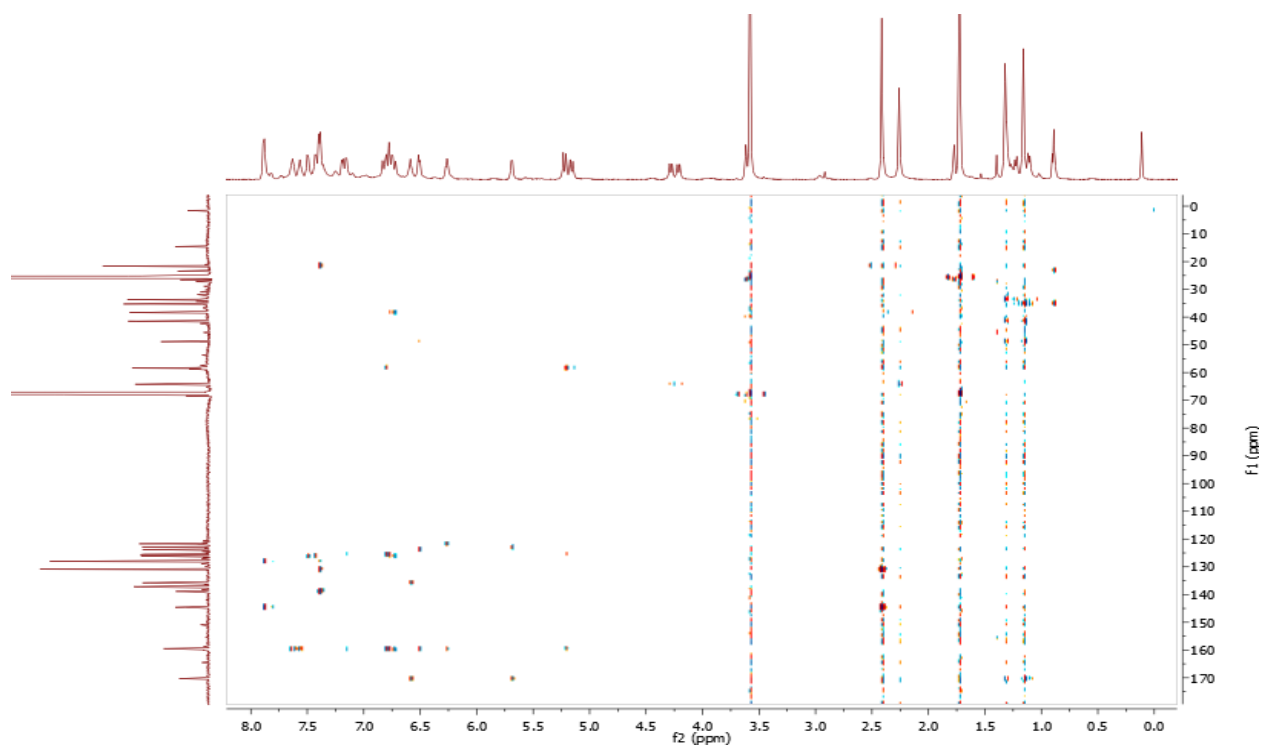


Figure A13. ^1H - ^{13}C HMBC spectrum of $(^{\text{TsMe}}\text{N}_4)\text{Ni}^{\text{II}}(\text{cycloneophyl})$ in THF-d_8 (600 MHz).

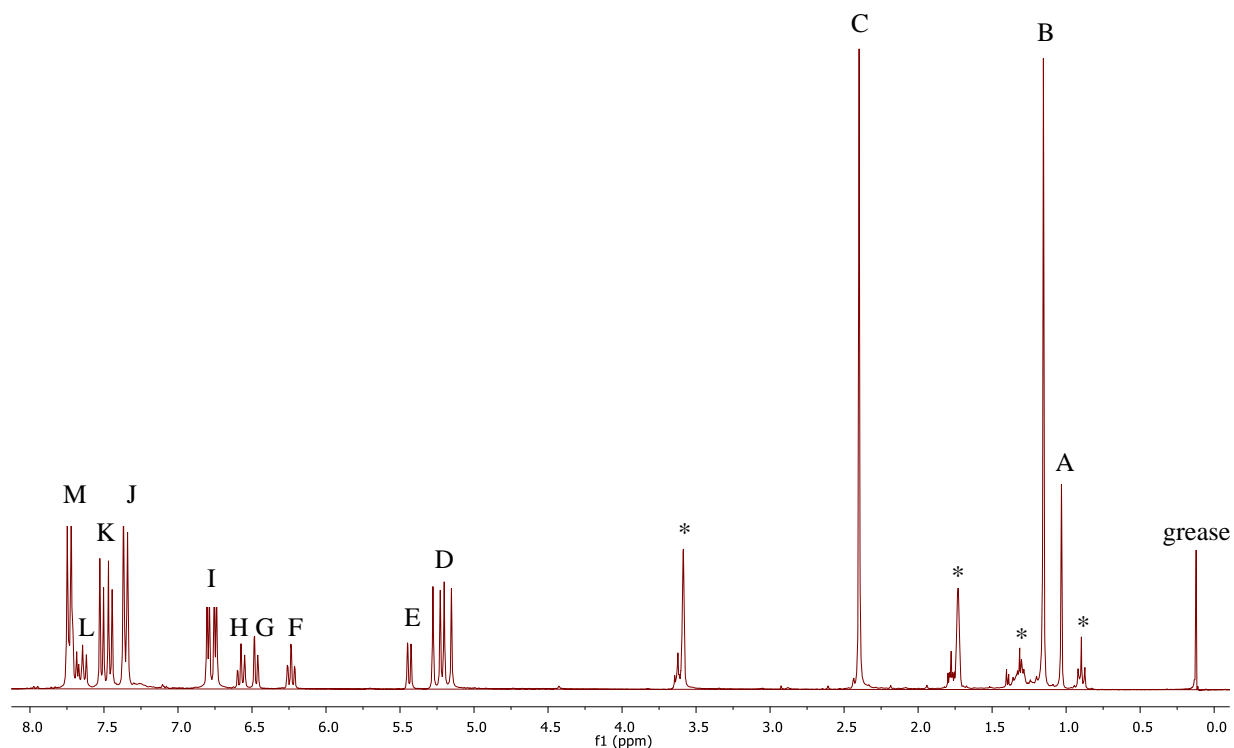


Figure A14. ^1H NMR spectrum of $(^{\text{Ts}}\text{N}_4)\text{Ni}^{\text{II}}(\text{cycloneophyl})$ in THF-d_8 (500 MHz). Peaks marked with an asterisk correspond to a trace amount of solvent (THF-d_8 and pentane).

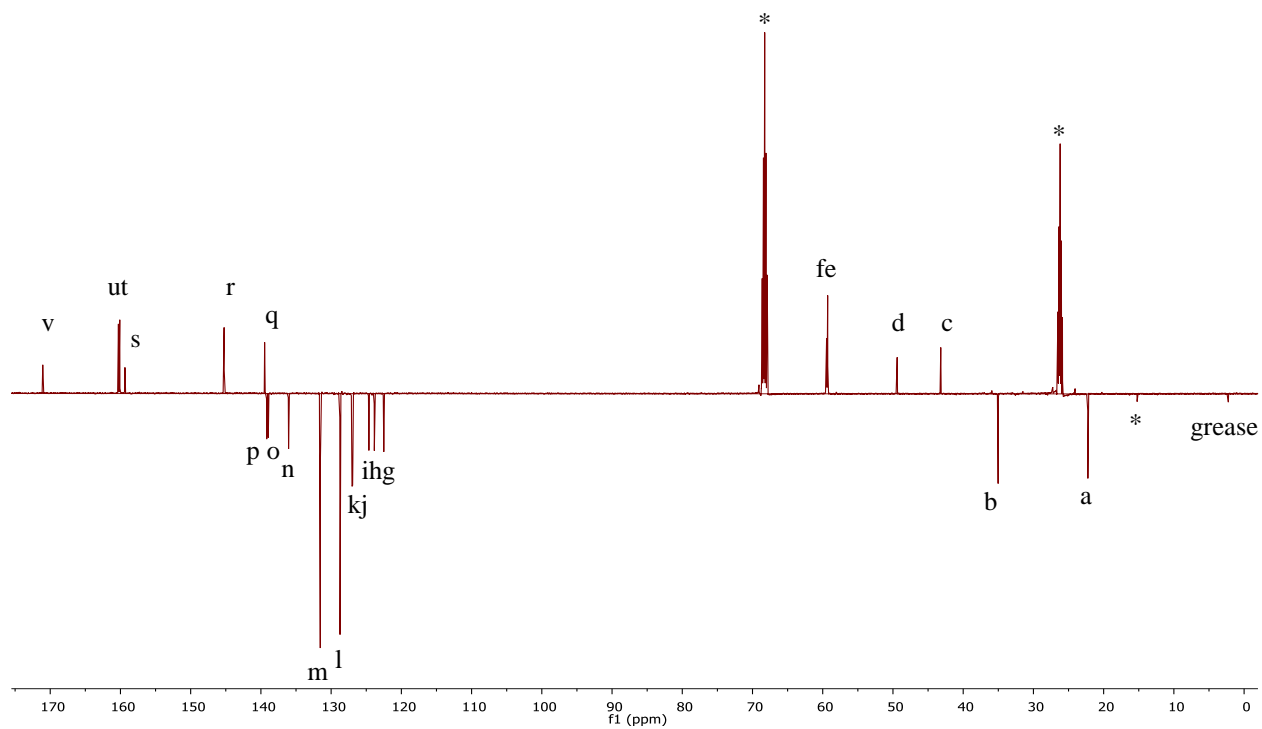


Figure A15. APT spectrum of $(\text{TsN}_4)\text{Ni}^{\text{II}}(\text{cycloneophyl})$ in THF-d_8 (500 MHz). Peaks marked with an asterisk correspond to a trace amount of solvent (THF-d_8 and pentane).

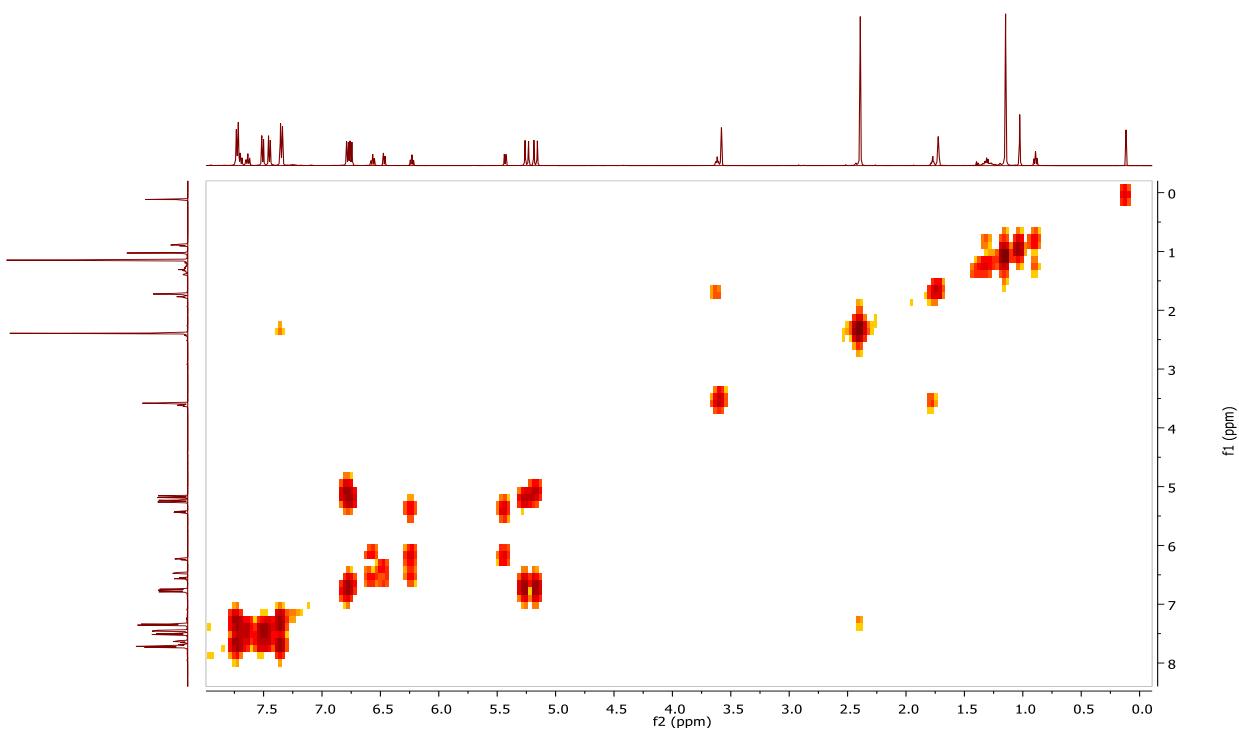


Figure A16. ^1H - ^1H gCOSY spectrum of $(\text{TsN}_4)\text{Ni}^{\text{II}}(\text{cycloneophyl})$ in THF-d_8 (500 MHz).

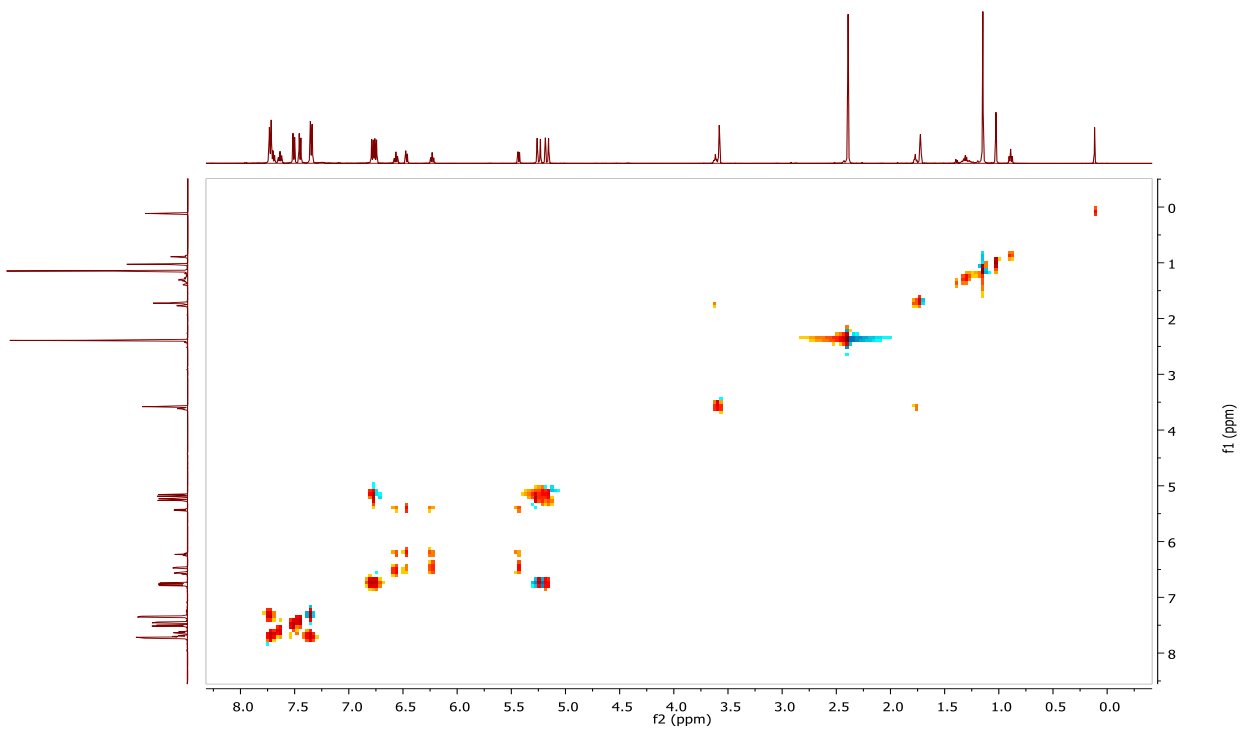


Figure A17. ^1H - ^1H TOXY spectrum of $(^{15}\text{N}_4)\text{Ni}^{\text{II}}(\text{cycloneophyl})$ in THF-d_8 (500 MHz).

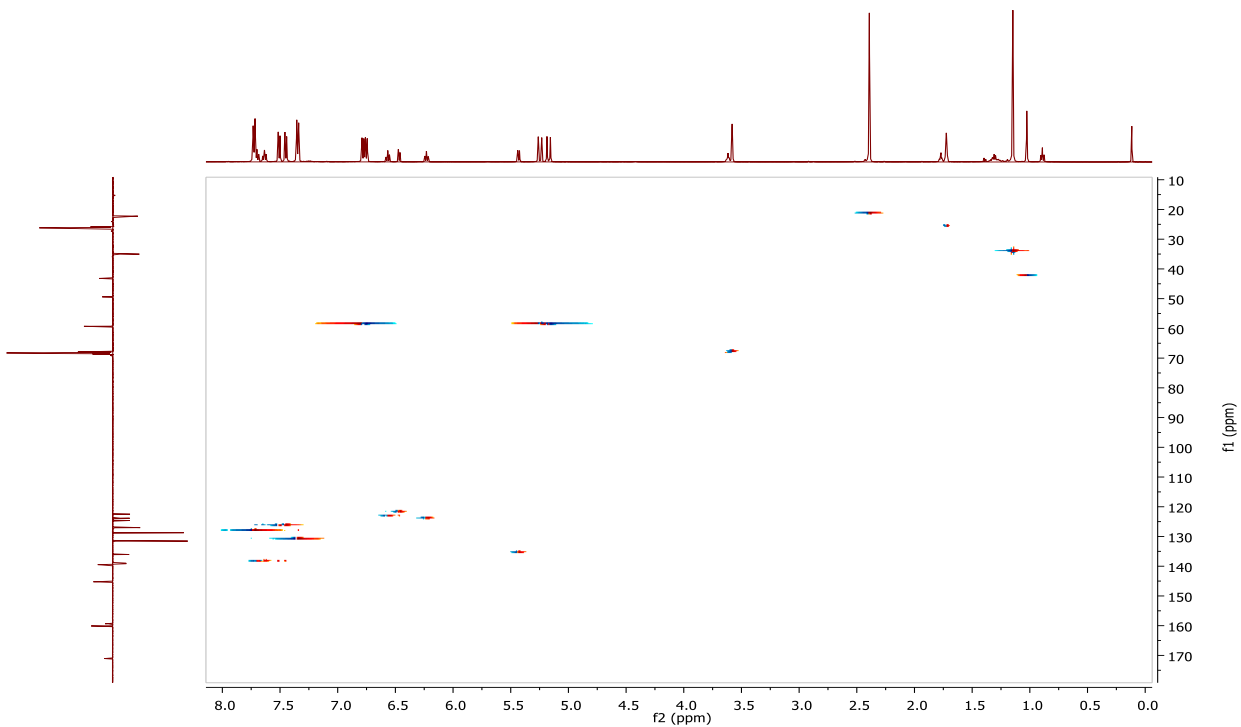


Figure A18. ^1H - ^{13}C HSQC spectrum of $(^{15}\text{N}_4)\text{Ni}^{\text{II}}(\text{cycloneophyl})$ in THF-d_8 (500 MHz).

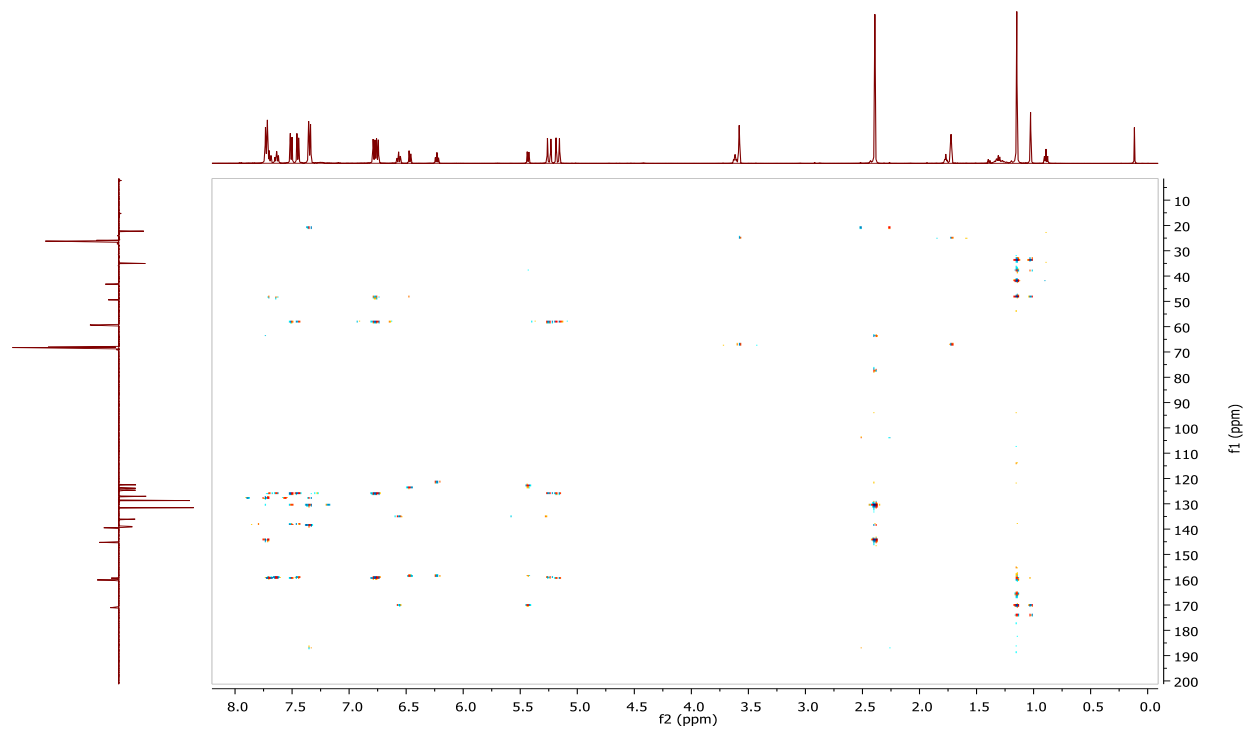


Figure A19. ^1H - ^{13}C HMBC spectrum of $(\text{TsN4})\text{Ni}^{\text{II}}(\text{cycloneophyl})$ in THF-d_8 (500 MHz).

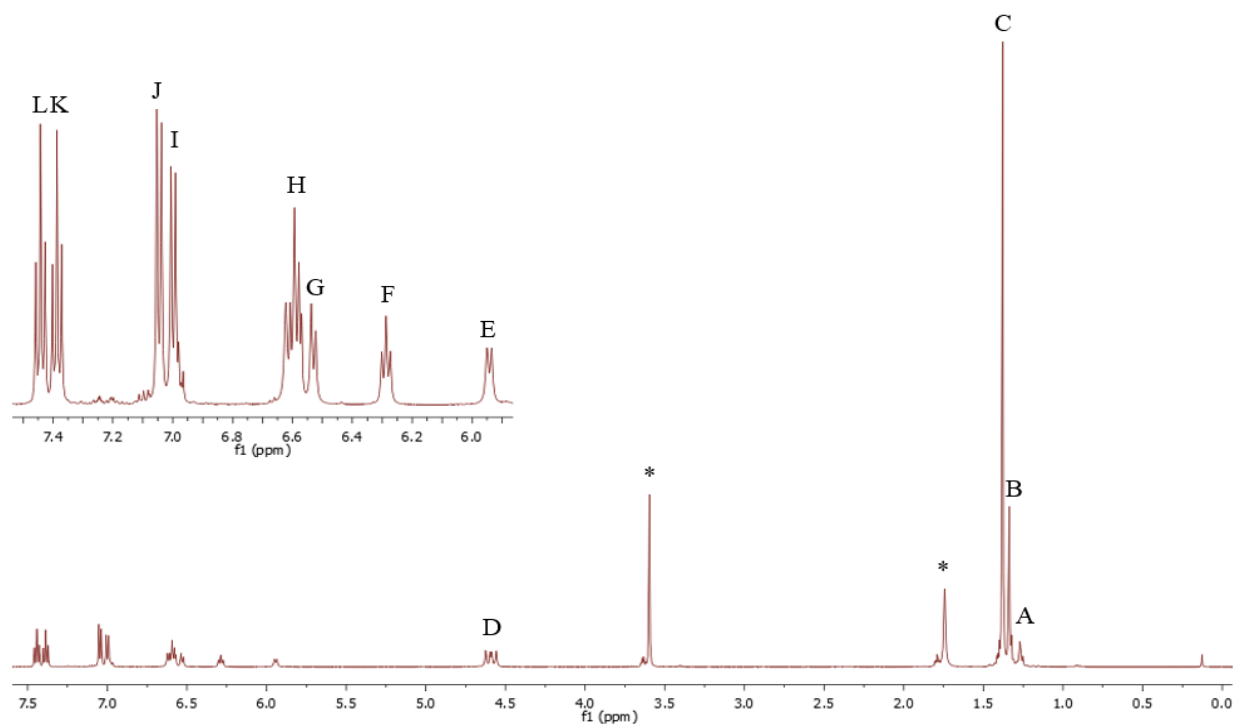


Figure A20. ^1H NMR spectrum of $(\text{tBuN4})\text{Ni}^{\text{II}}(\text{cycloneophyl})$ in THF-d_8 (500 MHz). Peaks marked with an asterisk correspond to a trace amount of solvent (THF-d_8).

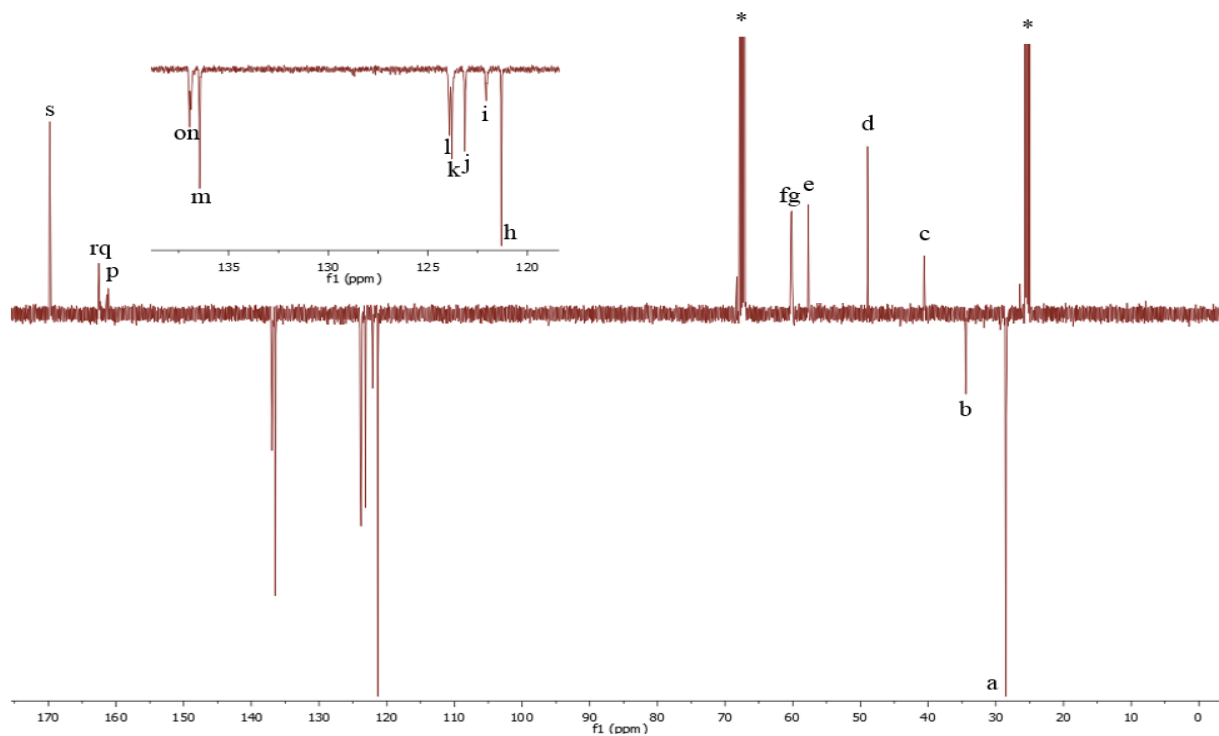


Figure A21. APT spectrum of $(t\text{Bu}_4\text{N})\text{Ni}^{\text{II}}(\text{cycloneophyl})$ in THF-d_8 (500 MHz). Peaks marked with an asterisk correspond to a trace amount of solvent (THF-d_8).

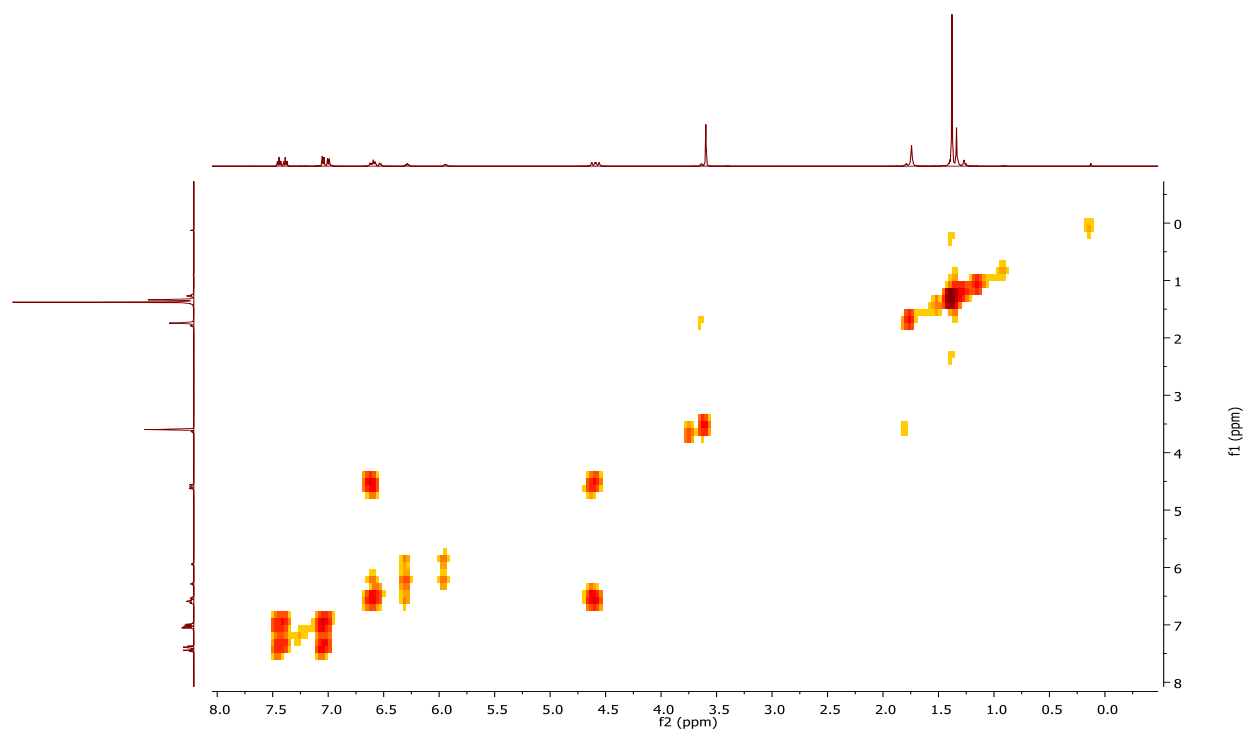


Figure A22. ^1H - ^1H gCOSY spectrum of $(t\text{Bu}_4\text{N})\text{Ni}^{\text{II}}(\text{cycloneophyl})$ in THF-d_8 (500 MHz).

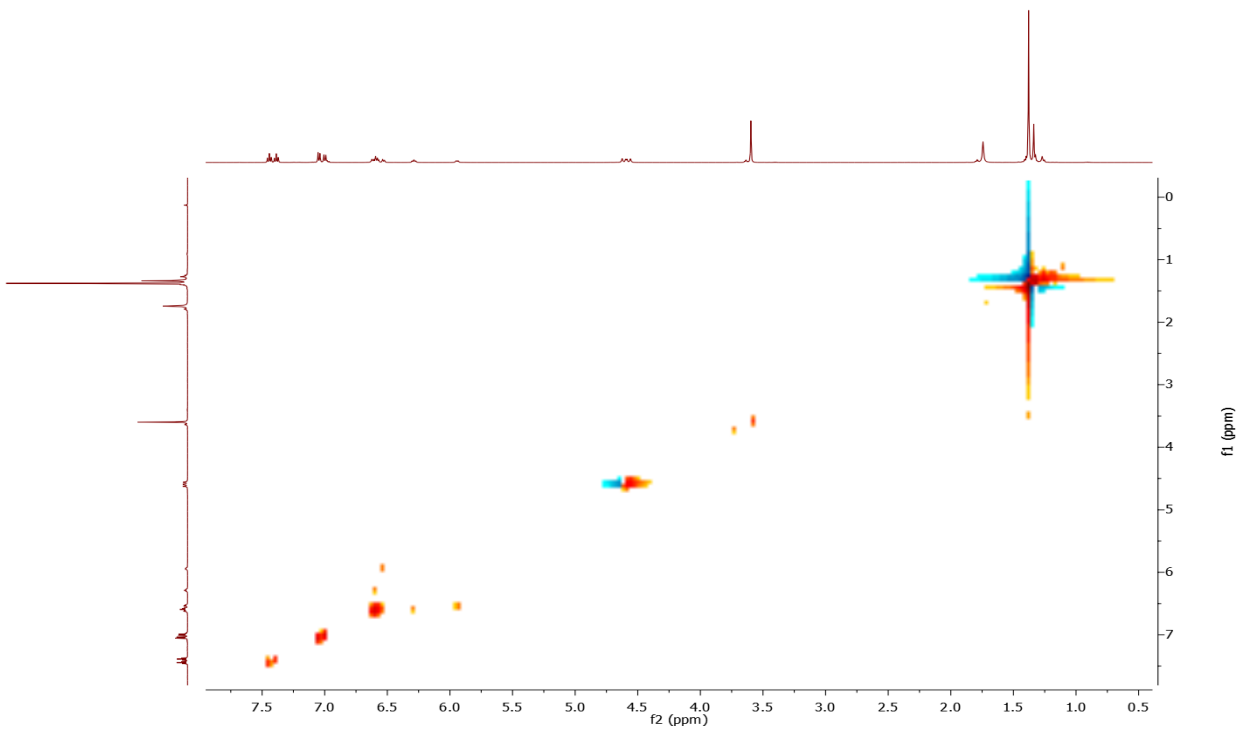


Figure A23. ^1H - ^1H TOXY spectrum of $(^t\text{BuN}_4)\text{Ni}^{\text{II}}(\text{cycloneophyl})$ in THF-d_8 (500 MHz).

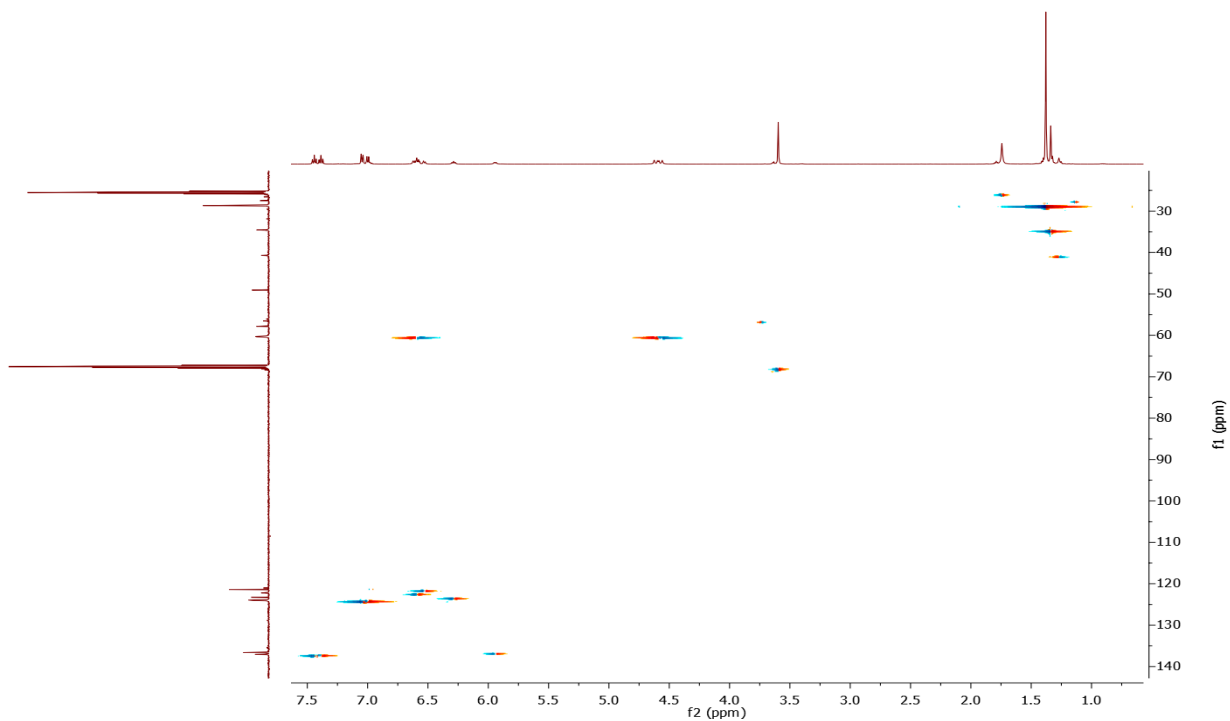


Figure A24. ^1H - ^{13}C HSQC spectrum of $(^t\text{BuN}_4)\text{Ni}^{\text{II}}(\text{cycloneophyl})$ in THF-d_8 (500 MHz).

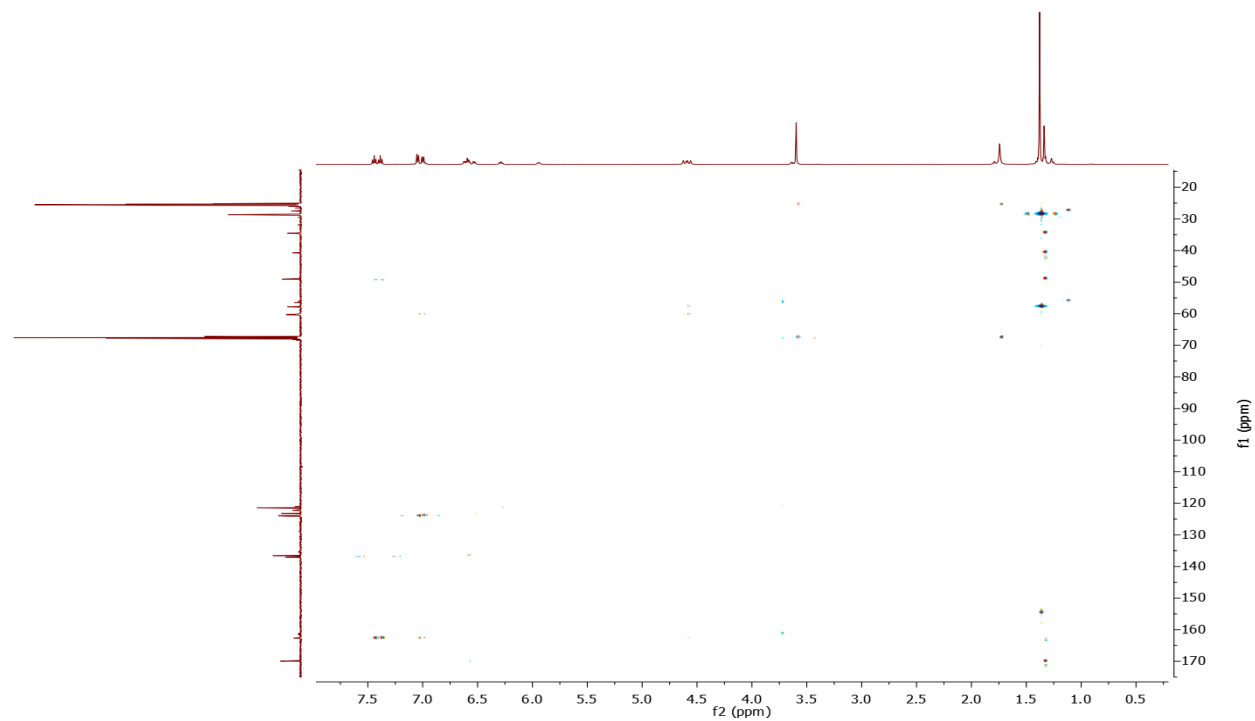


Figure A25. ^1H - ^{13}C HMBC spectrum of $(^t\text{Bu}_4\text{N})\text{Ni}^{\text{II}}(\text{cycloneophyl})$ in THF-d_8 (500 MHz).

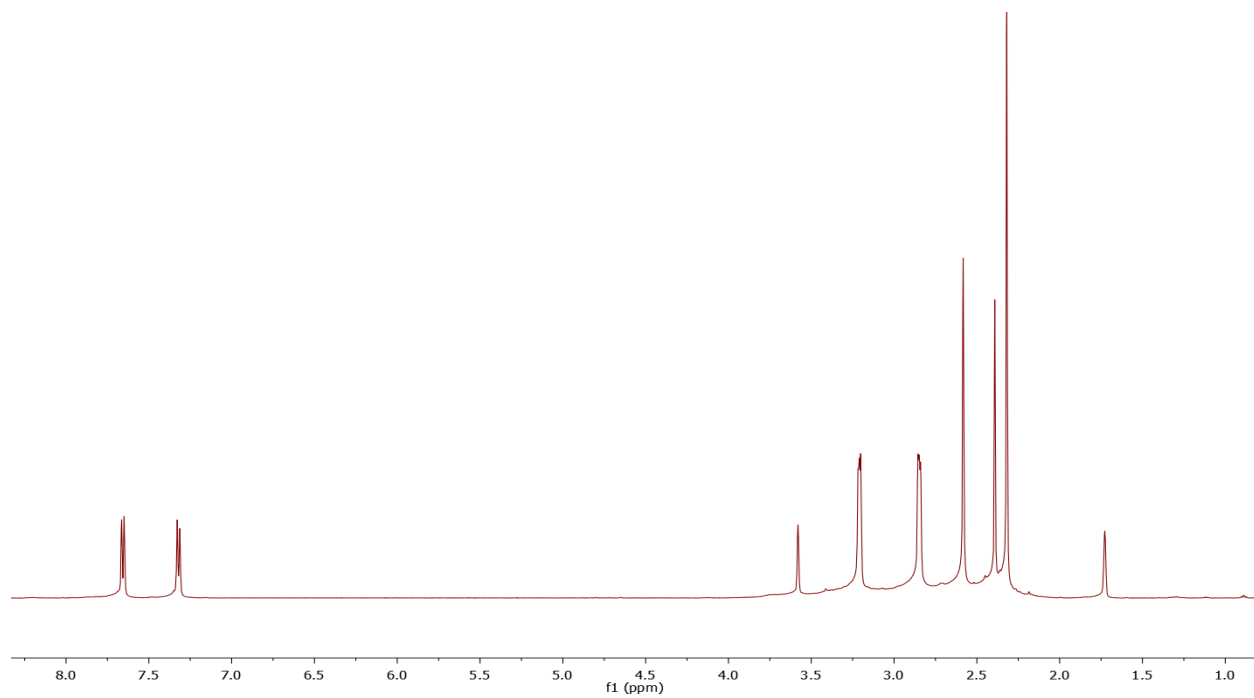


Figure A26. ^1H NMR spectrum of TsMe_2TACN in THF-d_8 (500 MHz).

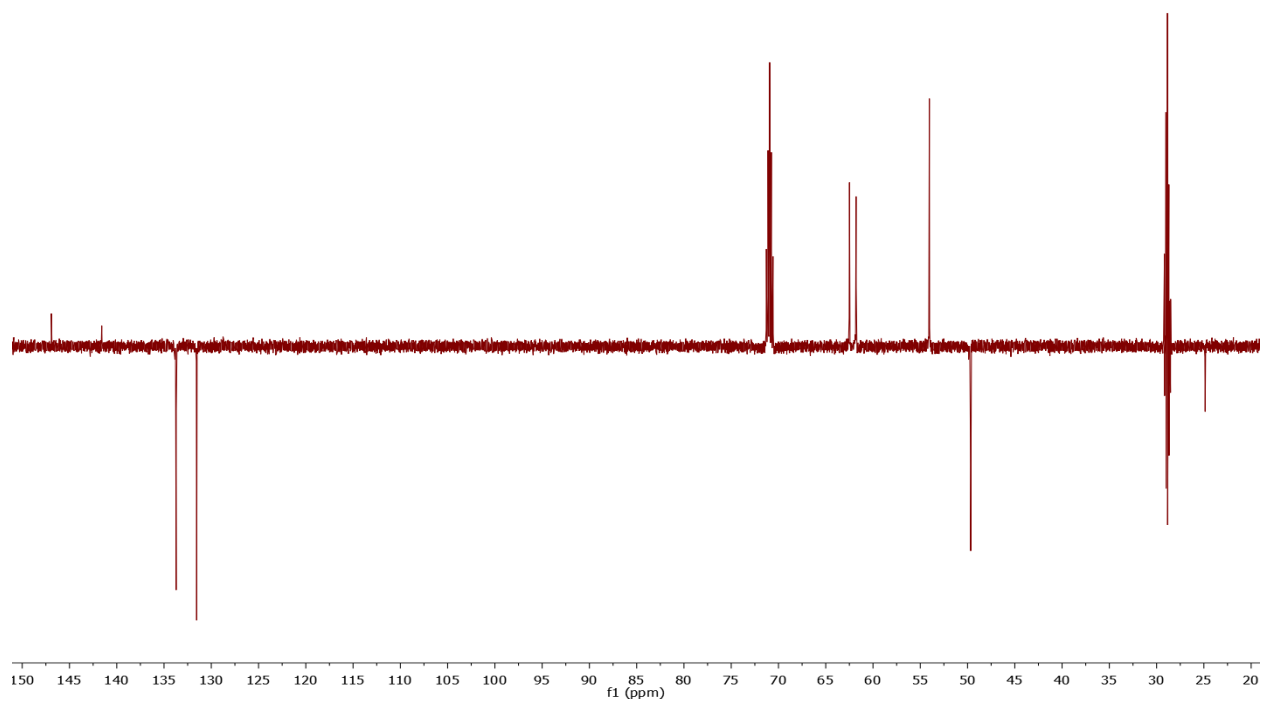


Figure A27. APT spectrum of ${}^{\text{TsMe}_2}\text{TACN}$ in THF- d_8 (500 MHz).

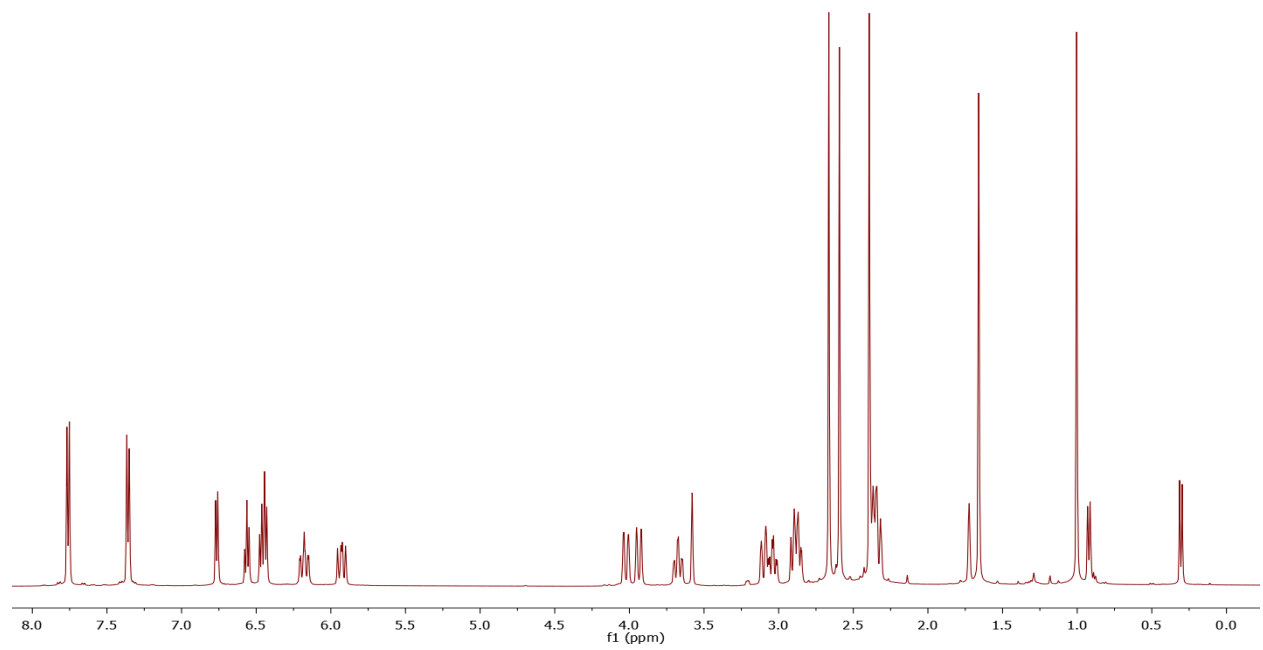


Figure A28. ${}^1\text{H}$ NMR spectrum of $({}^{\text{TsMe}_2}\text{TACN})\text{Ni}^{\text{II}}(\text{cycloneophyl})$ in THF- d_8 (500 MHz).

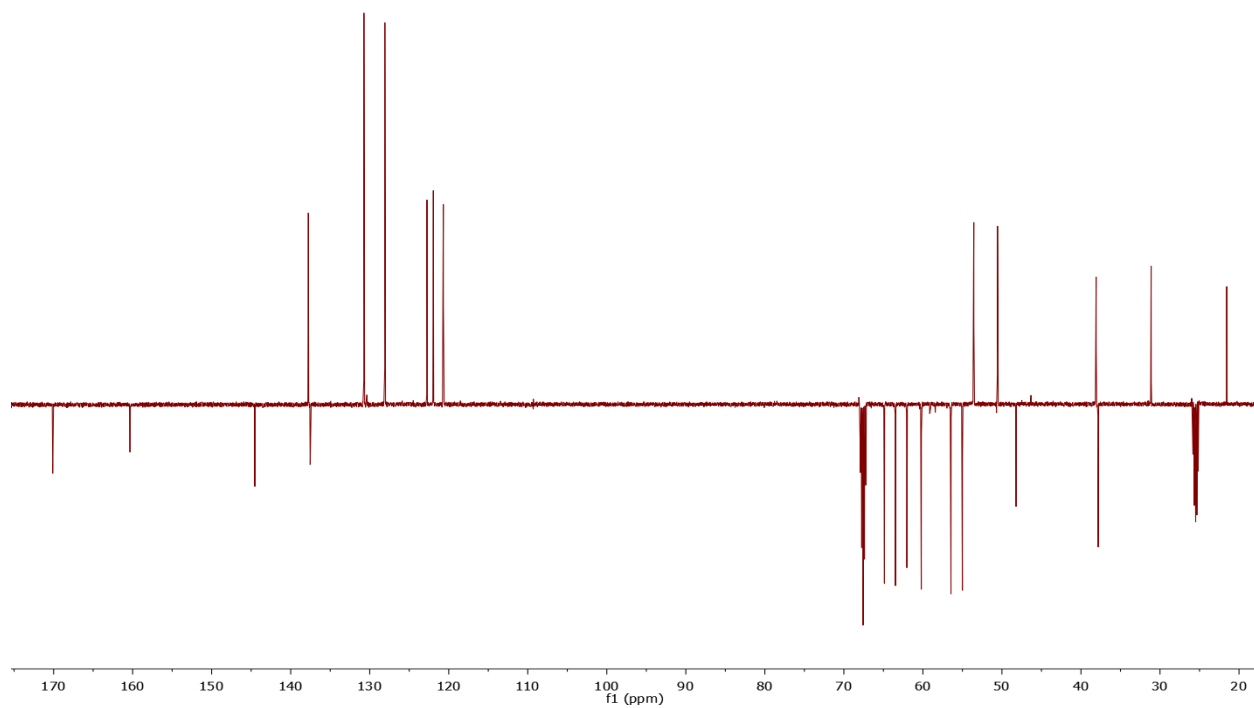


Figure A29. APT spectrum of $(\text{TsMe}_2\text{TACN})\text{Ni}^{\text{II}}(\text{cycloneophyl})$ in THF-d_8 (500 MHz).

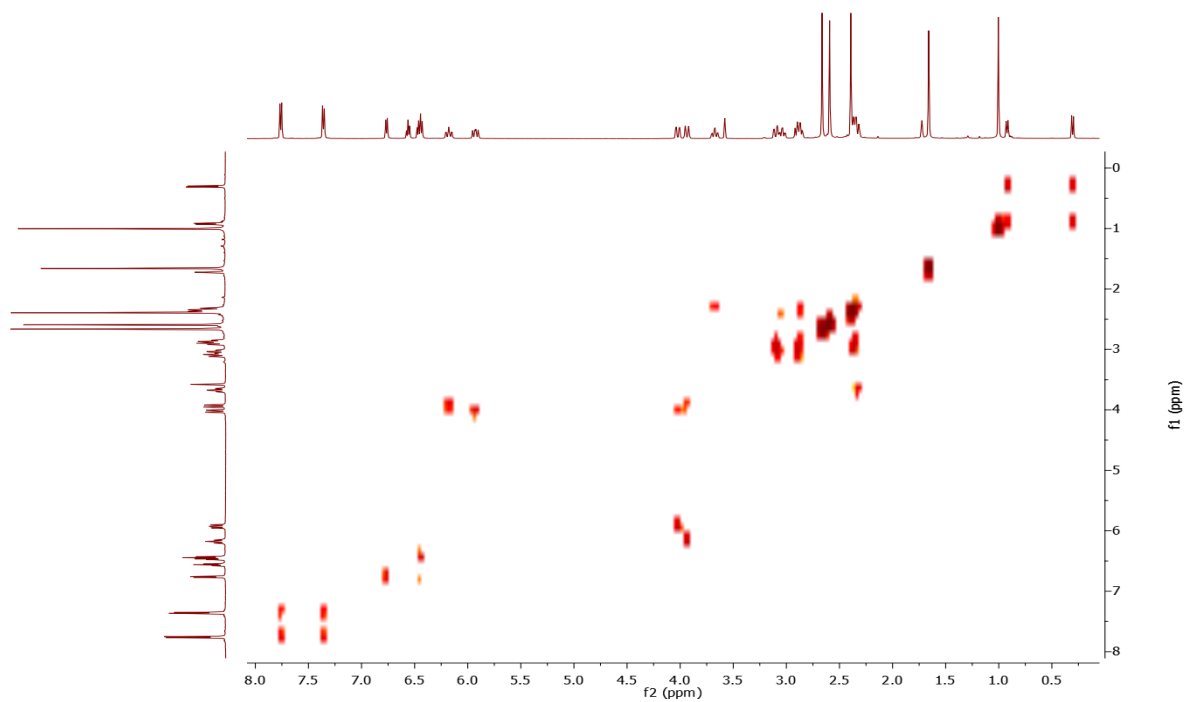


Figure A30. ^1H - ^1H gCOSY spectrum of $(\text{TsMe}_2\text{TACN})\text{Ni}^{\text{II}}(\text{cycloneophyl})$ in THF-d_8 (500 MHz).

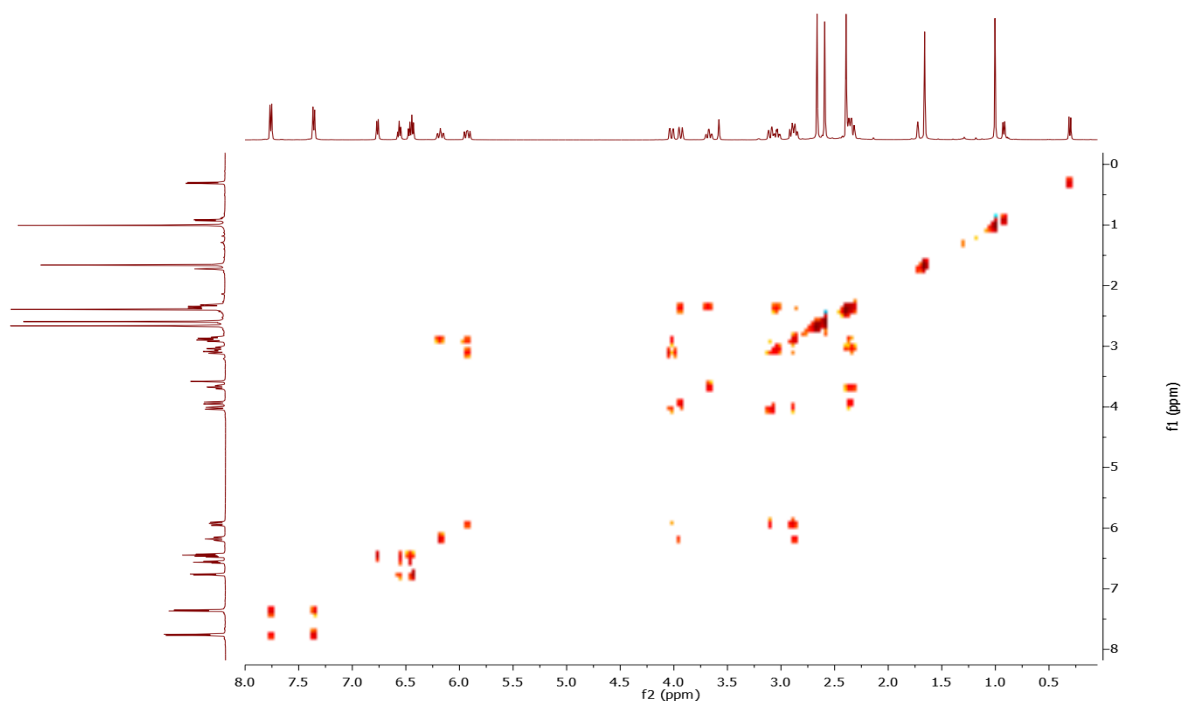


Figure A31. ^1H - ^1H TOXY spectrum of $(^{\text{TsMe}_2}\text{TACN})\text{Ni}^{\text{II}}(\text{cycloneophyl})$ in THF-d_8 (500 MHz).

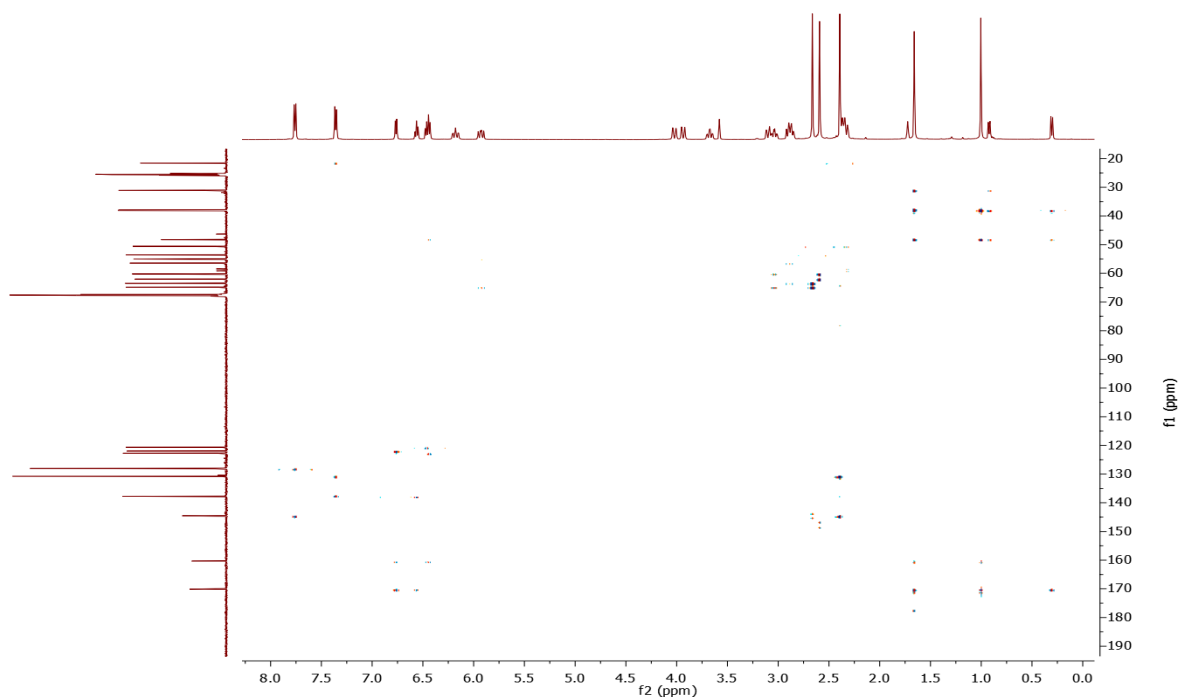


Figure A32. ^1H - ^{13}C HMBC spectrum of $(^{\text{TsMe}_2}\text{TACN})\text{Ni}^{\text{II}}(\text{cycloneophyl})$ in THF-d_8 (500 MHz).

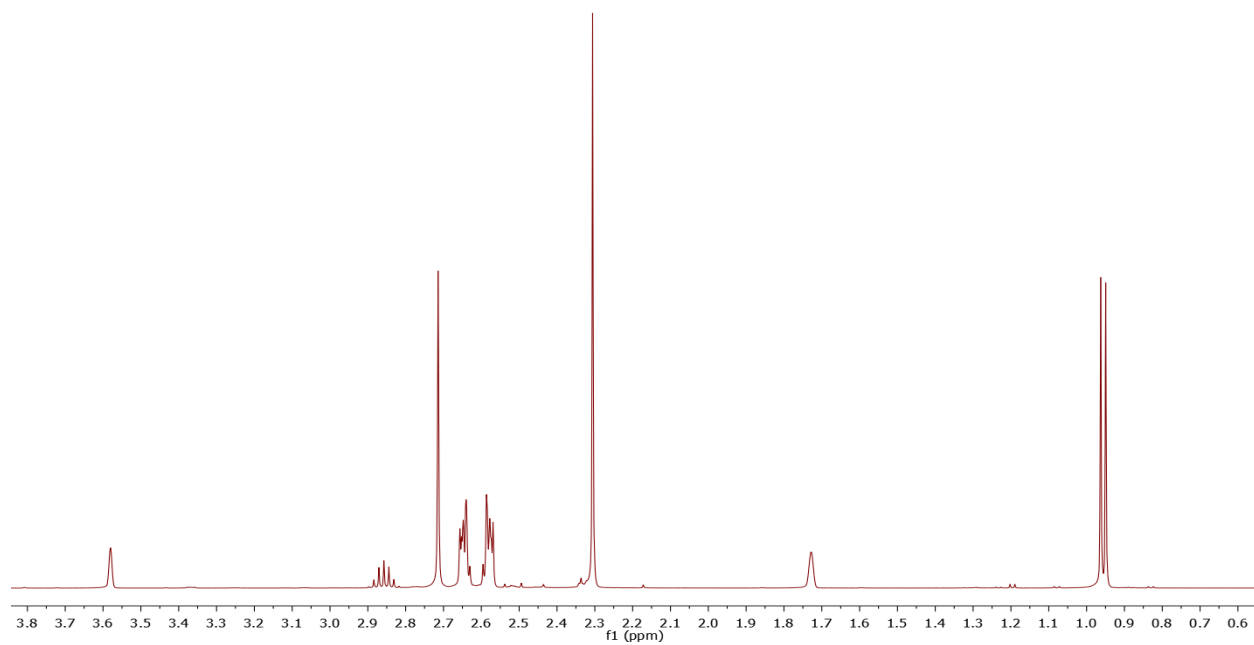


Figure A33. ^1H NMR spectrum of $i\text{PrMe}_2\text{TACN}$ in THF-d_8 (500 MHz).

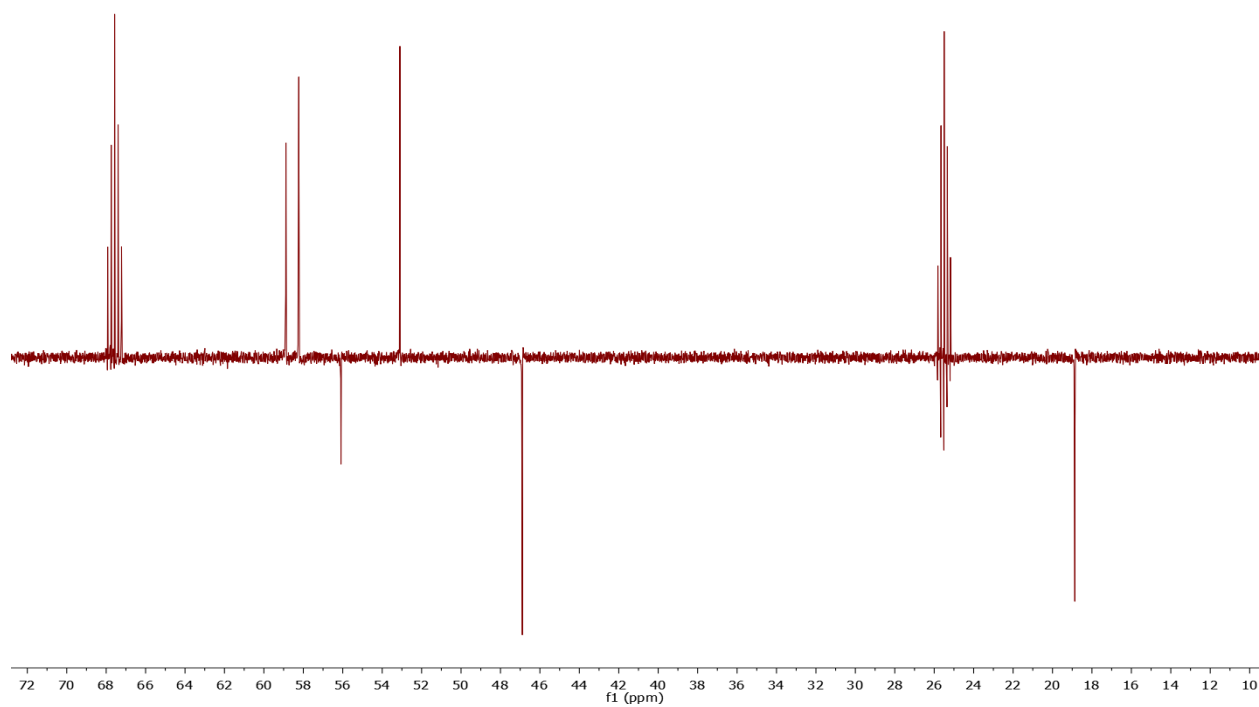


Figure A34. APT spectrum of $i\text{PrMe}_2\text{TACN}$ in THF-d_8 (500 MHz).

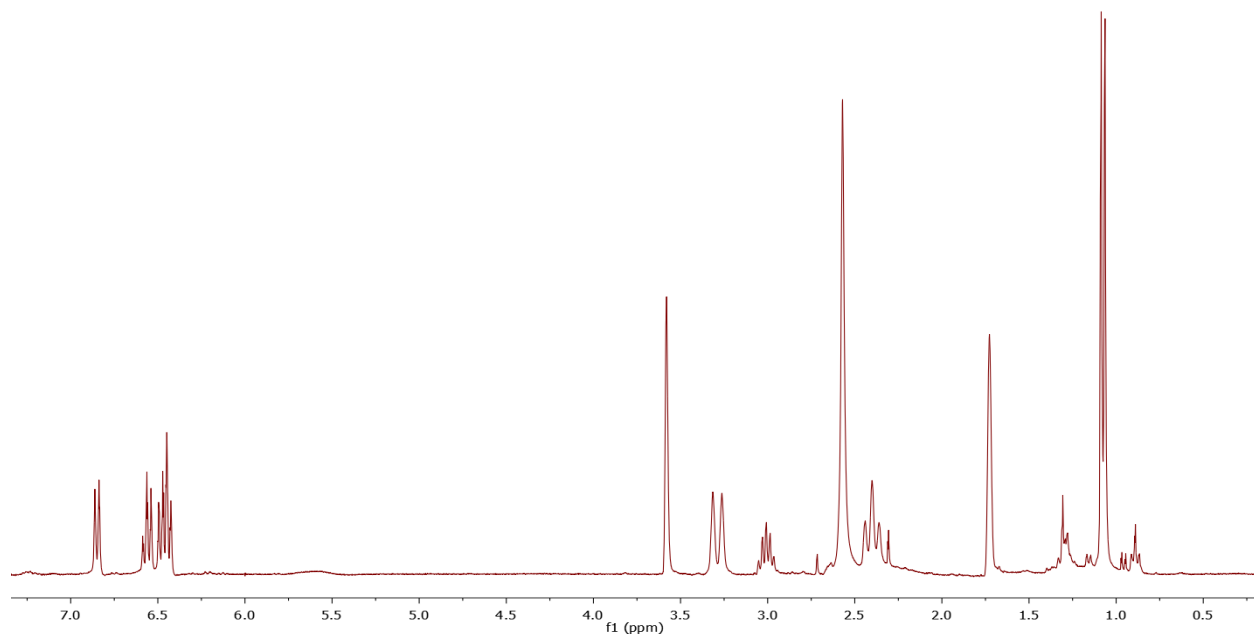


Figure A35. ^1H NMR spectrum of $(i\text{PrMe}_2\text{TACN})\text{Ni}^{\text{II}}(\text{cycloneophyl})$ in THF-d_8 (500 MHz).

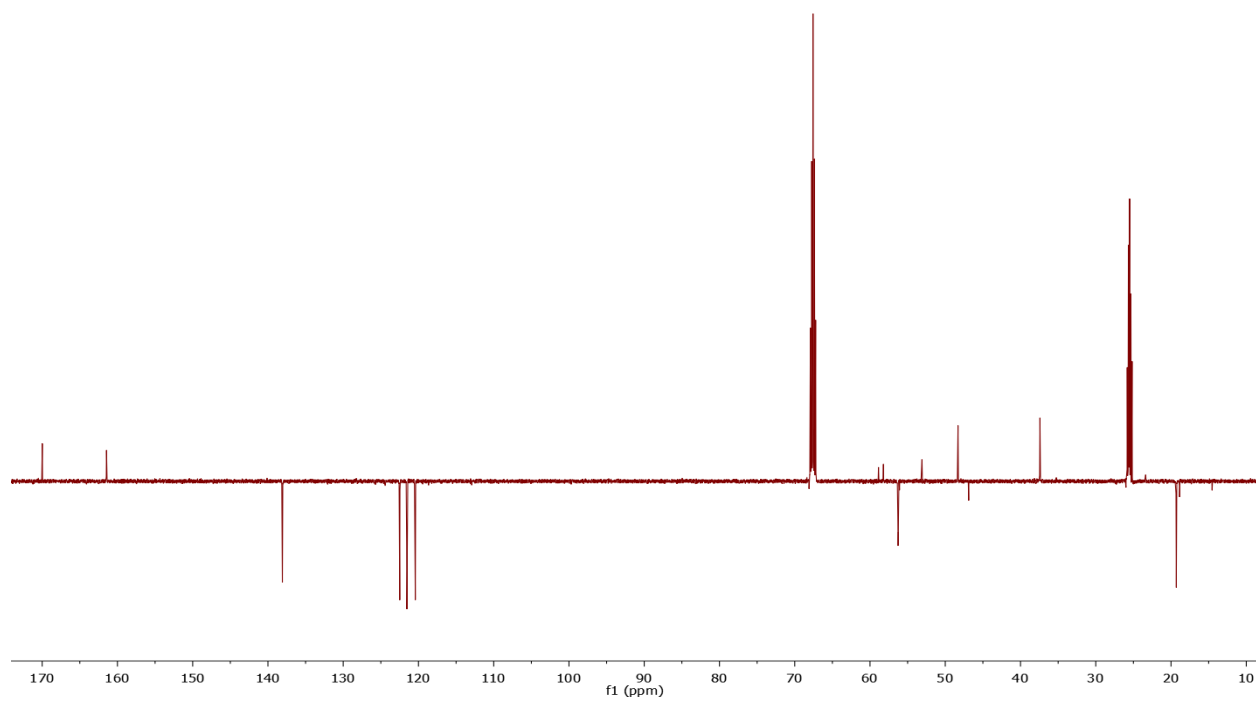


Figure A36. APT spectrum of $(i\text{PrMe}_2\text{TACN})\text{Ni}^{\text{II}}(\text{cycloneophyl})$ in THF-d_8 (500 MHz).

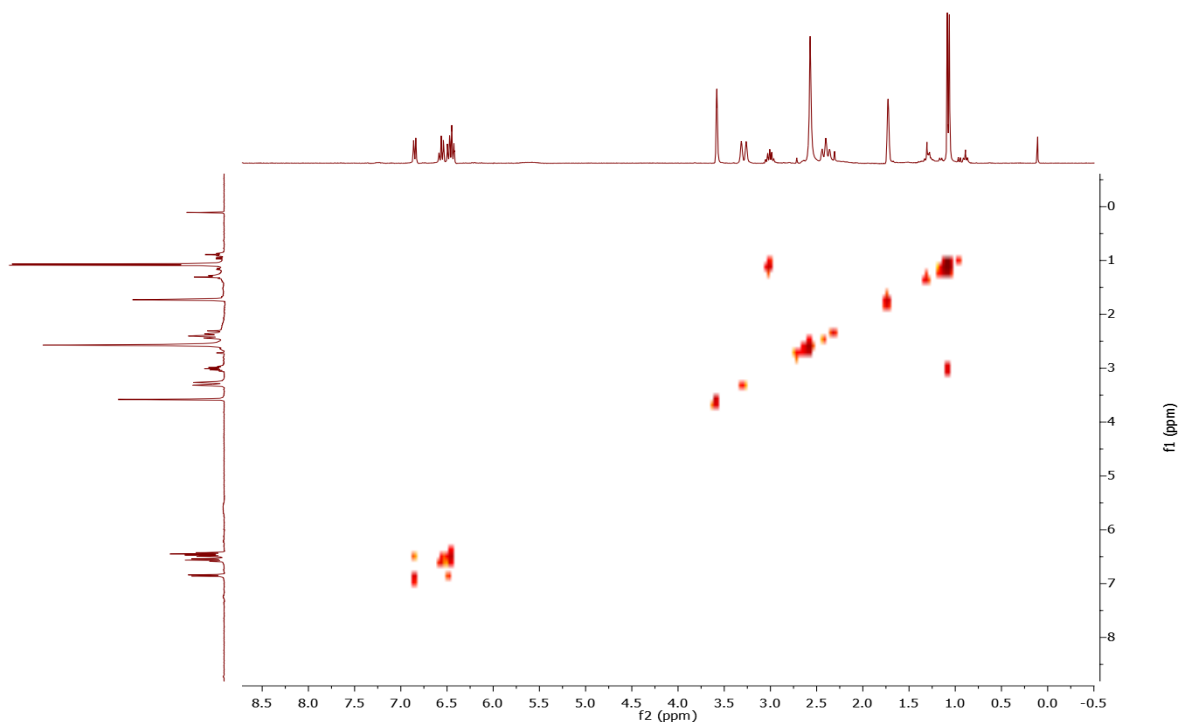


Figure A37. ^1H - ^1H gCOSY spectrum of $(i\text{PrMe}_2\text{TACN})\text{Ni}^{\text{II}}(\text{cycloneophyl})$ in THF-d_8 (500 MHz).

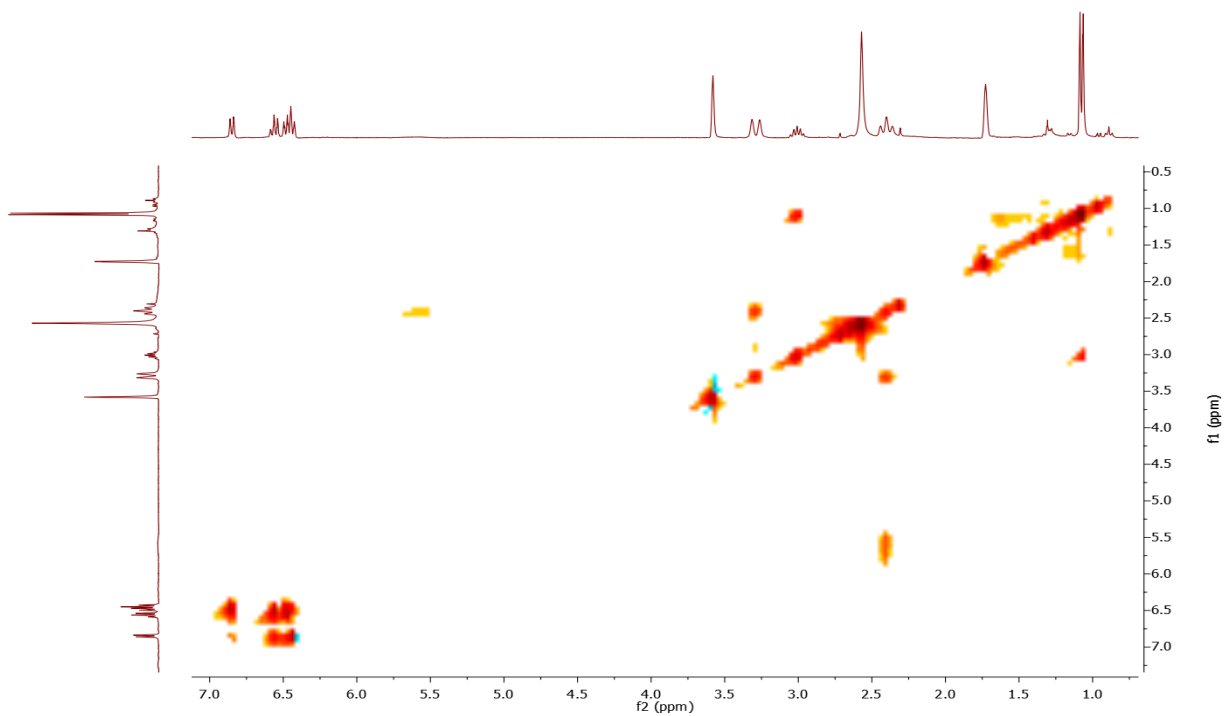


Figure A38. ^1H - ^1H TOXY spectrum of $(i\text{PrMe}_2\text{TACN})\text{Ni}^{\text{II}}(\text{cycloneophyl})$ in THF-d_8 (500 MHz).

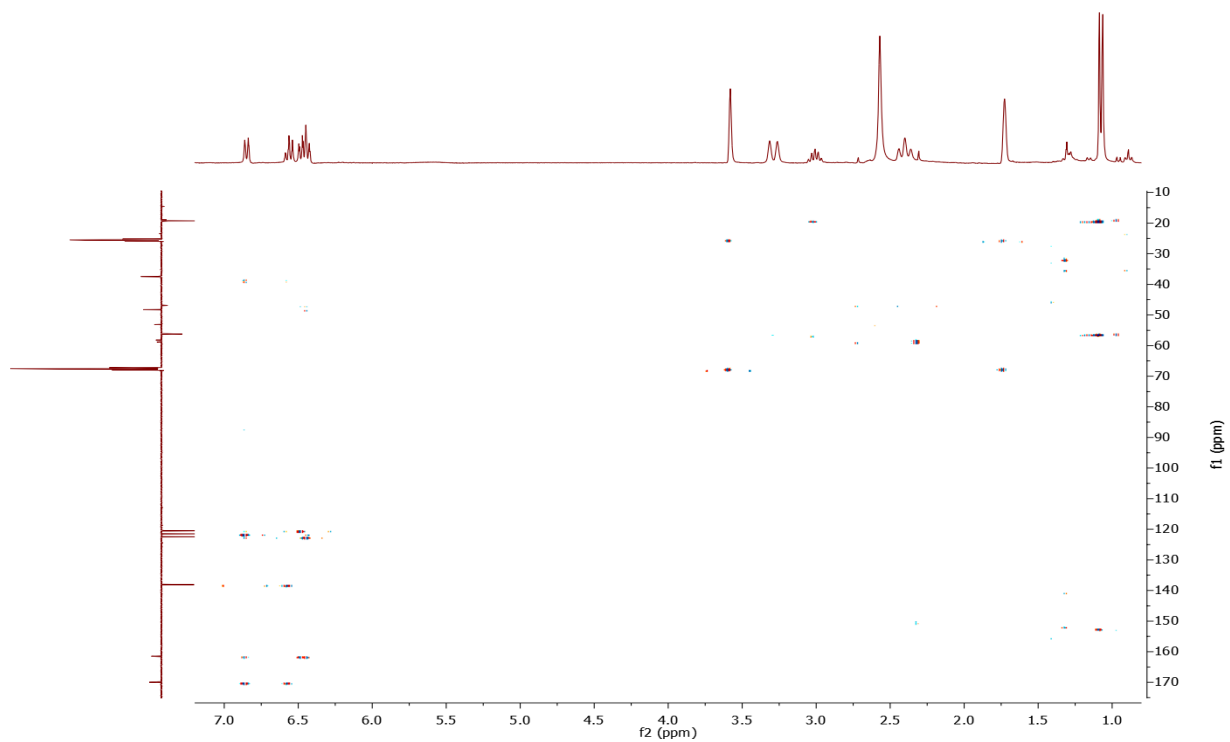


Figure A39. ^1H - ^{13}C HMBC spectrum of $(i\text{PrMe}_2\text{TACN})\text{Ni}^{\text{II}}(\text{cycloneophyl})$ in THF-d_8 (500 MHz).

Appendix B

Select Cyclic Voltammetry (CV) Spectra

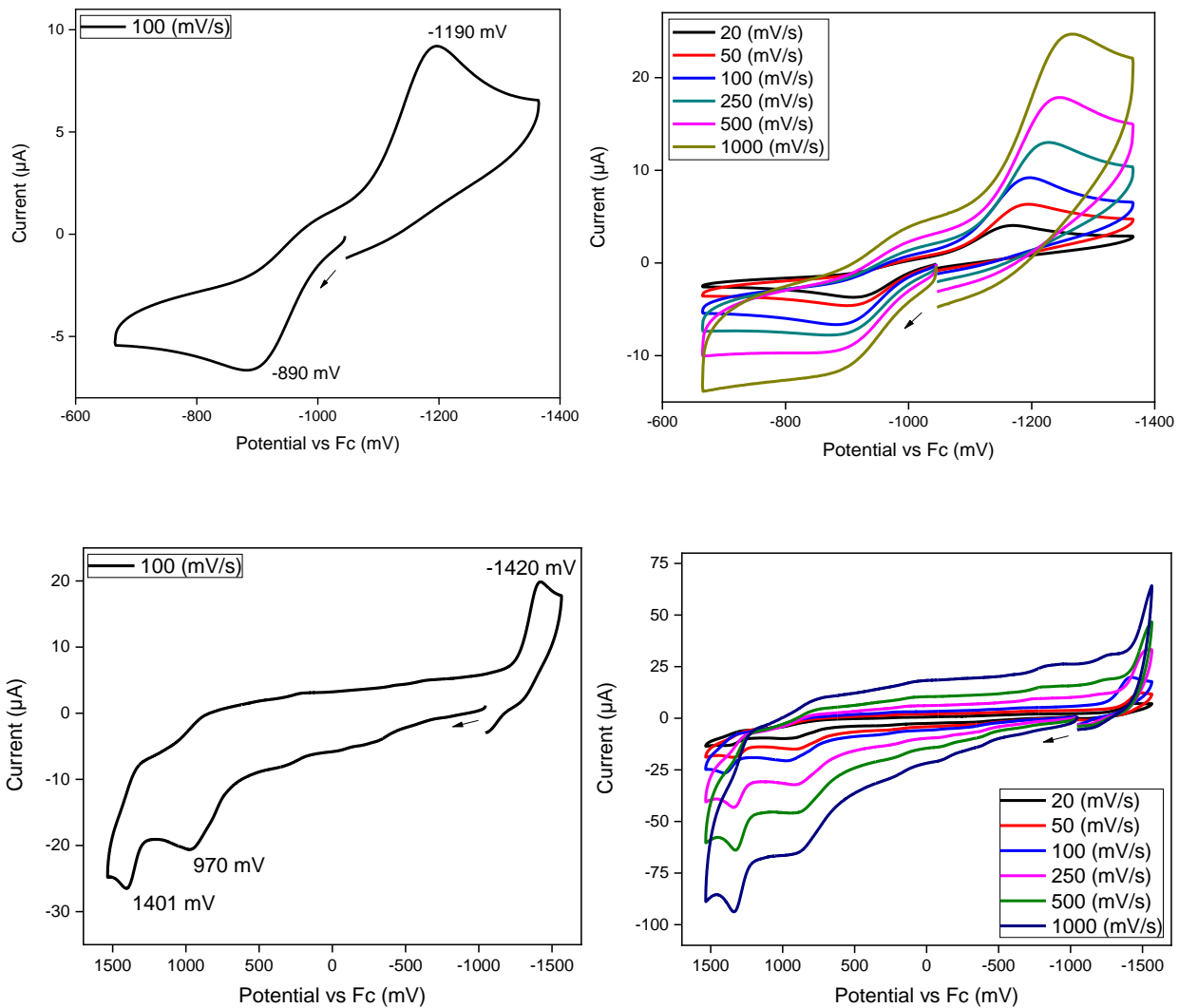


Figure B1. CVs of $(\text{TsMeN}_4)\text{Ni}^{\text{II}}\text{Me}_2$ in 0.1 M $n\text{Bu}_4\text{NPF}_6/\text{MeCN}$ at RT, at 100 mV/s scan rate (left) and variable scan rates (right).

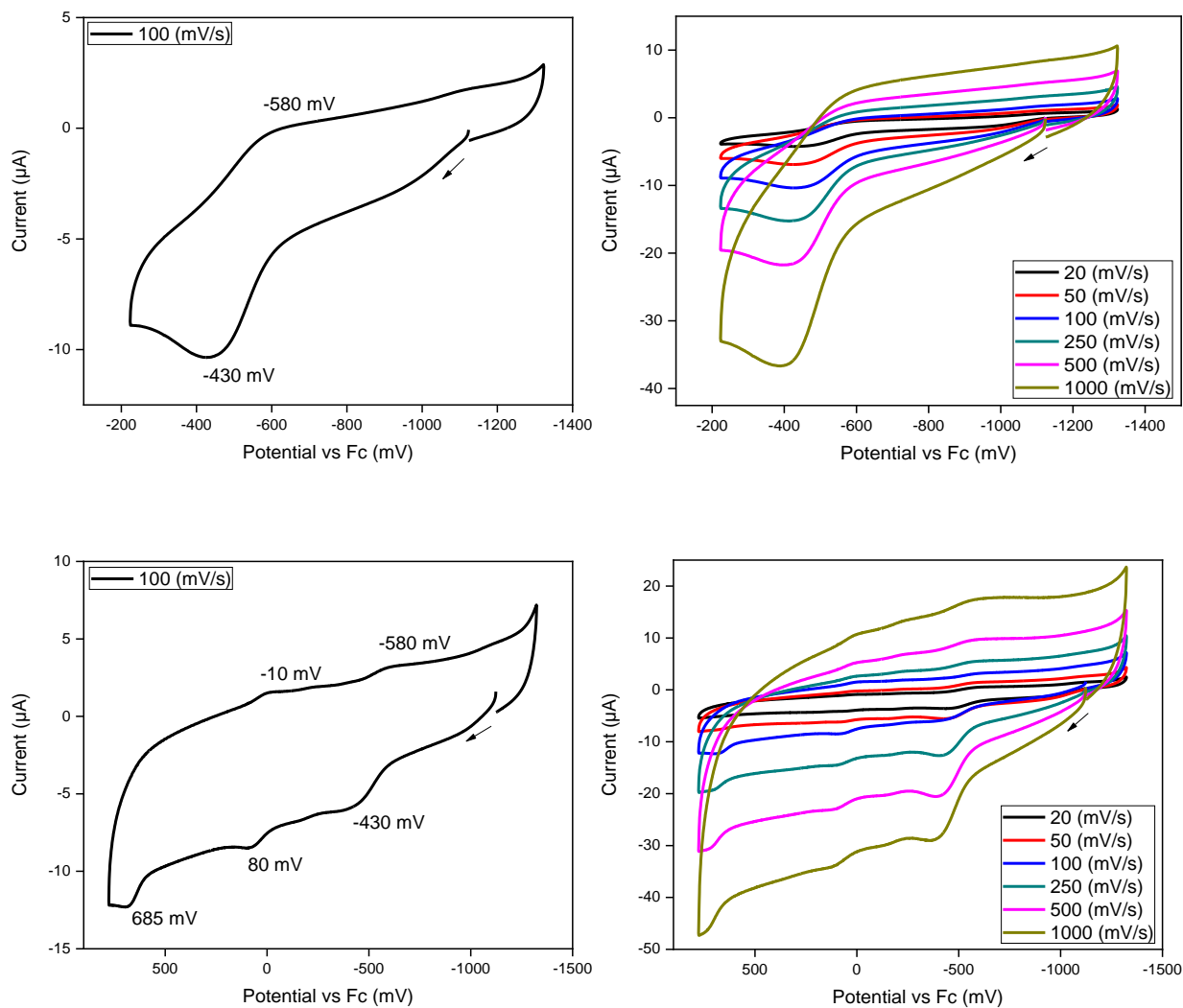


Figure B2. CVs of $(\text{TsN4})\text{Ni}^{\text{II}}\text{Me}_2$ in 0.1 M $n\text{Bu}_4\text{NPF}_6/\text{MeCN}$ at RT, at 100 mV/s scan rate (left) and variable scan rates (right).

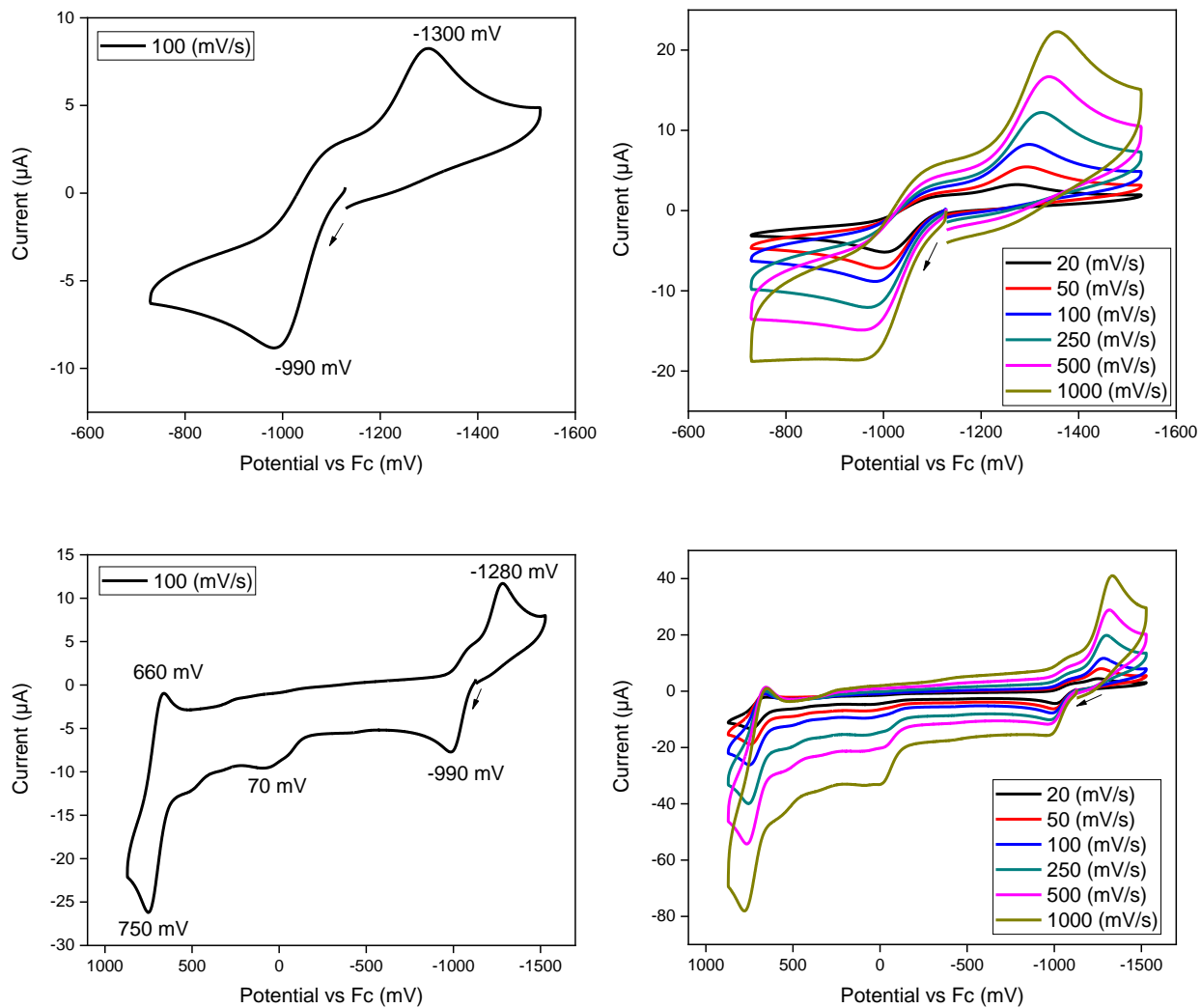


Figure B3. CVs of $(\text{TsMe}_4\text{N})\text{Ni}^{\text{II}}(\text{cycloneophyl})$ in 0.1 M $n\text{Bu}_4\text{NPF}_6/\text{MeCN}$ at RT, at 100 mV/s scan rate (left) and variable scan rates (right).

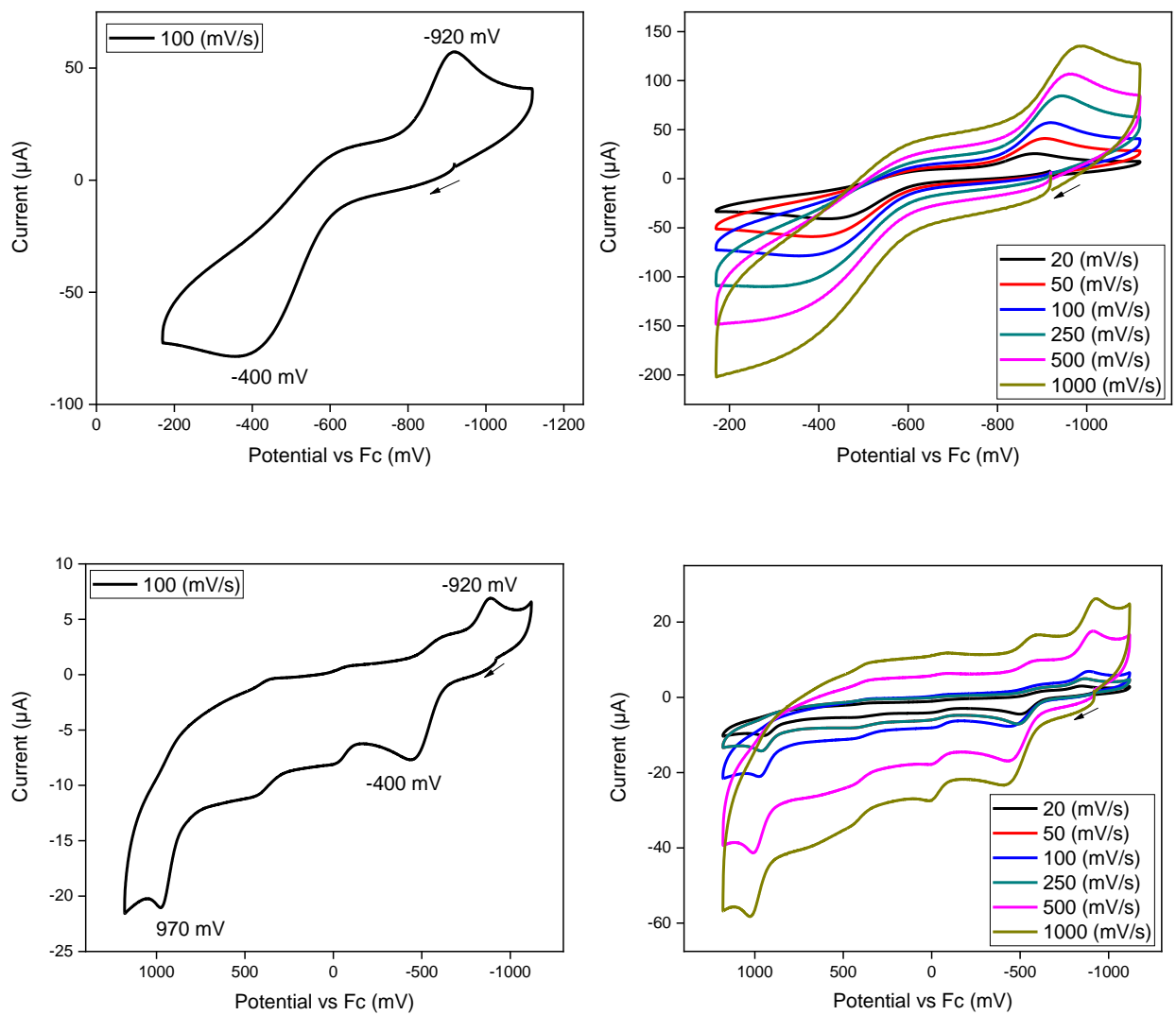


Figure B4. CVs of $(T^5N_4)Ni^{II}(\text{cyclonophyl})$ in 0.1 M $nBu_4NPF_6/MeCN$ at RT, at 100 mV/s scan rate (left) and variable scan rates (right).

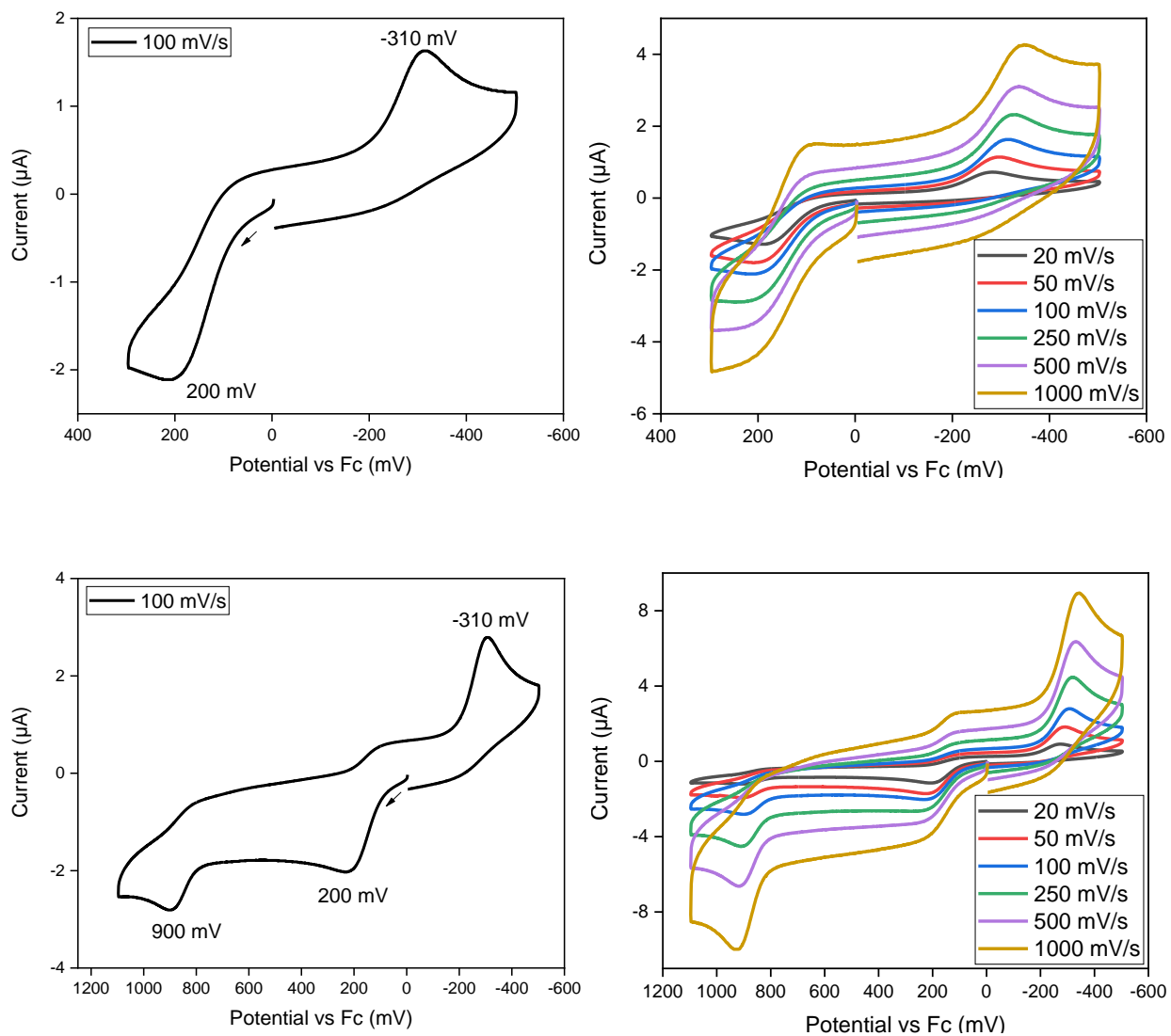


Figure B5. CVs of $(t\text{Bu}_4\text{N})\text{Ni}^{\text{II}}(\text{cycloneophyl})$ in $0.1 \text{ M } n\text{Bu}_4\text{NPF}_6/\text{MeCN}$ at RT, at 100 mV/s scan rate (left) and variable scan rates (right).

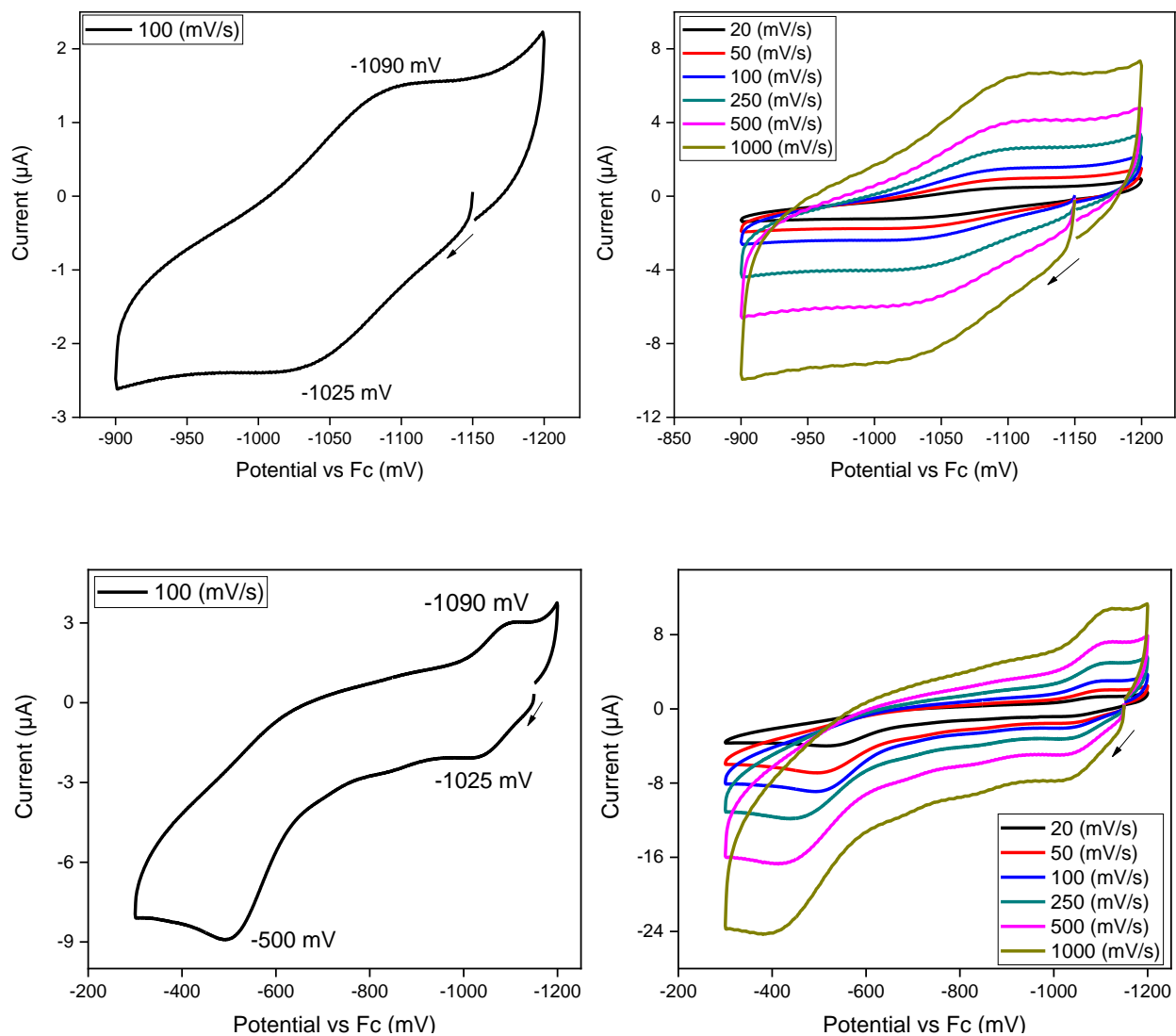


Figure B6. CVs of $(i\text{PrMe}_2\text{TACN})\text{Ni}^{\text{II}}(\text{cycloneophyl})$ in 0.1 M $n\text{Bu}_4\text{NPF}_6/\text{MeCN}$ at RT, at 100 mV/s scan rate (left) and variable scan rates (right).

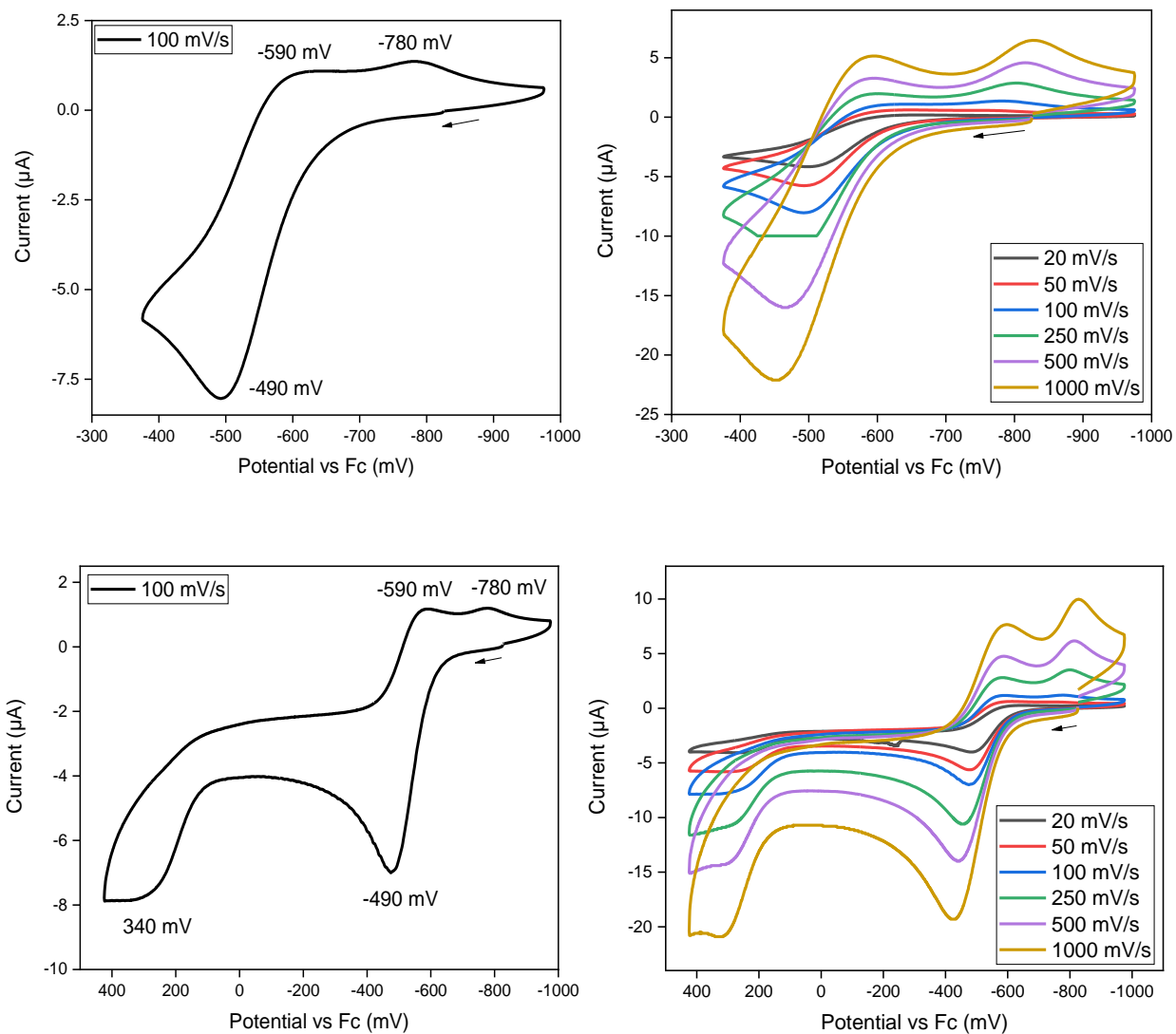


Figure B7. CVs of $(\text{TsMe}_2\text{TACN})\text{Ni}^{\text{II}}(\text{cycloneophyl})$ in 0.1 M $n\text{Bu}_4\text{NPF}_6/\text{MeCN}$ at RT, at 100 mV/s scan rate (left) and variable scan rates (right).

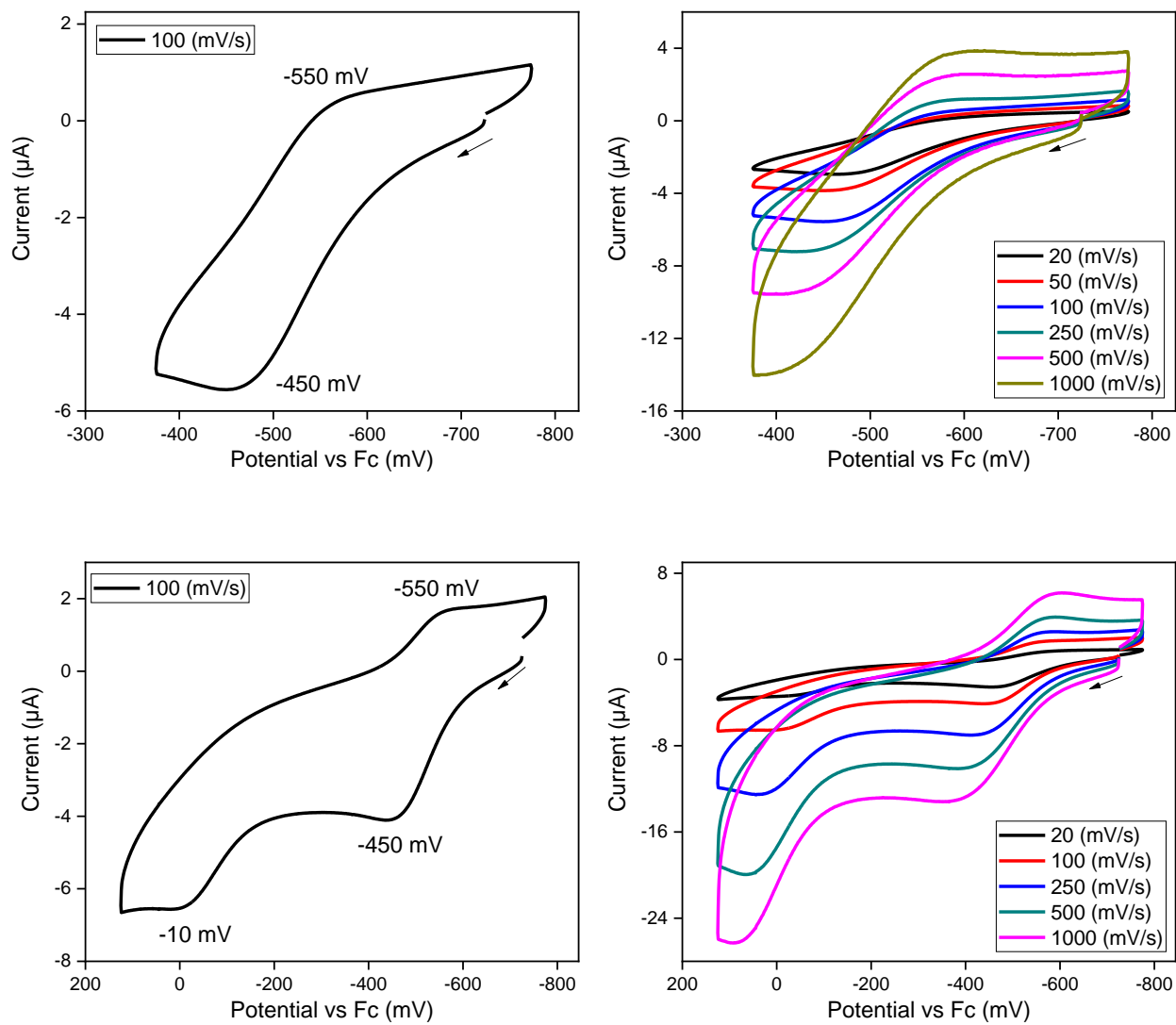


Figure B8. CVs of $(iPr_3TACN)Ni^{II}(cycloneophyl)$ in 0.1 M $nBu_4NPF_6/MeCN$ at RT, at 100 mV/s scan rate (left) and variable scan rates (right).

Appendix C

Select Ultraviolet-Visible Spectroscopy (UV-Vis) Spectra

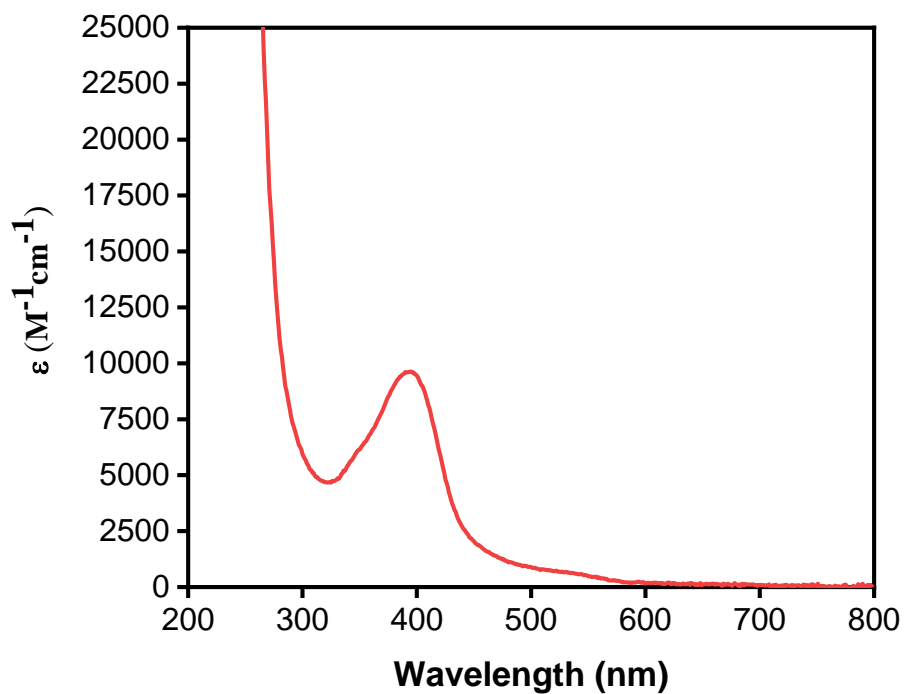


Figure C1. UV-visible spectrum of $(^{\text{TsMe}}\text{N4})\text{Ni}^{\text{II}}\text{Me}_2$ in THF (3.125×10^{-5} M).

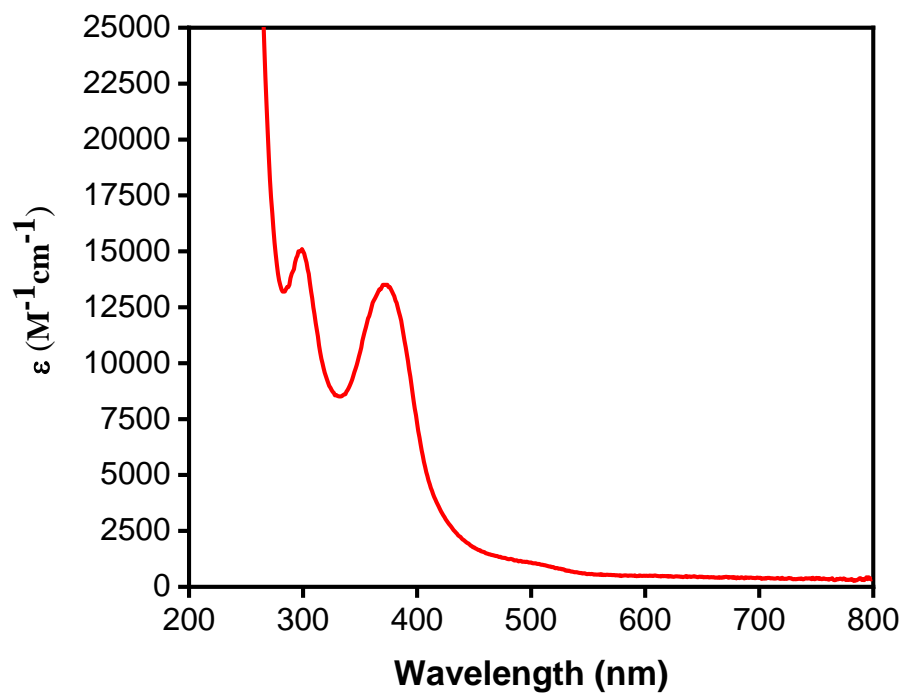


Figure C2. UV-visible spectrum of $(^{\text{TsMe}}\text{N4})\text{Ni}^{\text{II}}(\text{cycloneophyl})$ in THF (1.25×10^{-4} M).

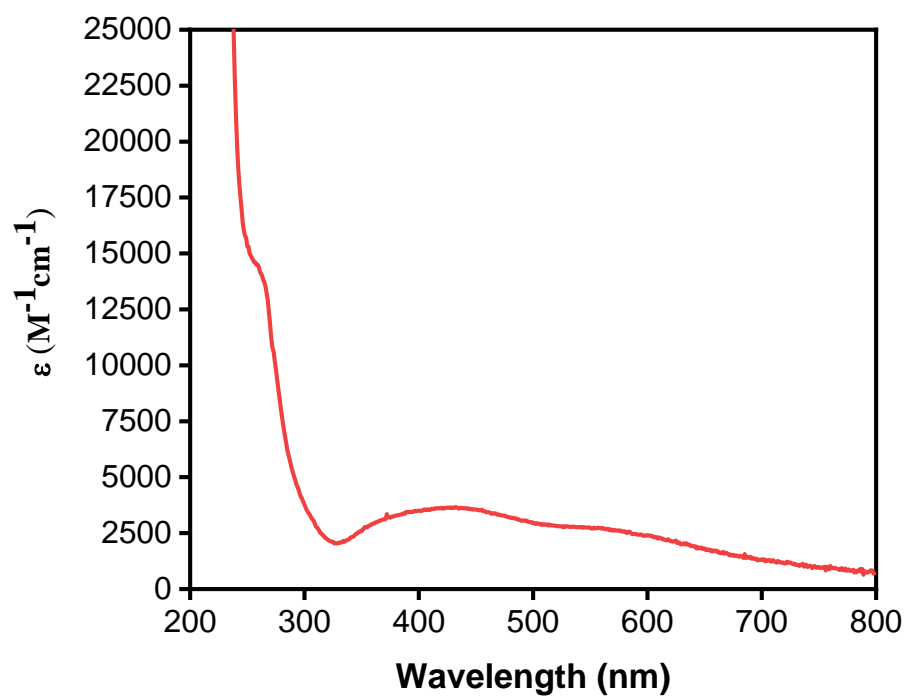


Figure C3. UV-visible spectrum of $(\text{TsMeN}_4)\text{Ni}^{\text{III}}(\text{cycloneophyl})$ in THF (6.25×10^{-5} M).

Appendix D

Supplemental Reactivity Data

Reactivity of (^RN4)Ni^{II}Me₂ with ^{Ac}FcBF₄

Table D1. Yields of the products upon oxidation of (^{Me}N4)Ni^{II}Me₂ with one equivalent of ^{Ac}FcBF₄ in MeCN-d₃ at 20 °C.

Time (hr)	CH ₃ -CH ₃ (%)	CH ₃ -H/D (%)
0.5	25 ± 3	3 ± 1
1	34 ± 2	6 ± 1
2	41 ± 3	7 ± 2
4	60 ± 1	10 ± 2
8	67 ± 1	11 ± 2
24	72 ± 2	9 ± 1

Table D2. Yields of the products upon oxidation of (^{Me}N4)Ni^{II}Me₂ with two equivalents of ^{Ac}FcBF₄ in MeCN-d₃ at 20 °C.

Time (hr)	CH ₃ -CH ₃ (%)	CH ₃ -H/D (%)
0.5	88 ± 1	1 ± 1
1	87 ± 2	1 ± 1
2	89 ± 1	2 ± 1
4	86 ± 3	1 ± 2
8	85 ± 1	3 ± 2
24	85 ± 2	1 ± 1

Table D3. Yields of the products upon oxidation of (^{TsMe}N4)Ni^{II}Me₂ with one equivalent of ^{Ac}FcBF₄ in MeCN-d₃ at 20 °C.

Time (hr)	CH ₃ -CH ₃ (%)	CH ₃ -H/D (%)
0.25	54 ± 2	1 ± 1
0.5	63 ± 1	2 ± 2
1	67 ± 2	2 ± 1
2	70 ± 2	3 ± 2
4	72 ± 1	4 ± 2
8	72 ± 1	4 ± 1
24	71 ± 2	1 ± 1

Table D4. Yields of the products upon oxidation of (¹⁵N₄)Ni^{II}Me₂ with two equivalents of ^{Ac}FcBF₄ in MeCN-d₃ at 20 °C.

Time (hr)	CH₃-CH₃ (%)	CH₃-H/D (%)
0.25	71 ± 1	2 ± 1
0.5	75 ± 1	2 ± 1
1	77 ± 2	3 ± 1
2	80 ± 3	3 ± 2
4	80 ± 4	2 ± 2
8	79 ± 2	3 ± 1
24	81 ± 1	1 ± 1

Table D5. Yields of the products upon oxidation of (¹⁵N₄)Ni^{II}Me₂ with one equivalent of ^{Ac}FcBF₄ in MeCN-d₃ at -20 °C.

Time (hr)	CH₃-CH₃ (%)	CH₃-H/D (%)
0.5	40 ± 1	0 ± 0
1	45 ± 1	0 ± 0
2	51 ± 2	0 ± 0
4	49 ± 1	0 ± 0
8	51 ± 1	0 ± 0
24	49 ± 2	1 ± 1

Table D6. Yields of the products upon oxidation of (¹⁵N₄)Ni^{II}Me₂ with two equivalents of ^{Ac}FcBF₄ in MeCN-d₃ at -20 °C.

Time (hr)	CH₃-CH₃ (%)	CH₃-H/D (%)
0.5	50 ± 1	2 ± 1
1	55 ± 1	2 ± 1
2	59 ± 1	3 ± 1
4	58 ± 2	2 ± 1
8	57 ± 1	3 ± 1
24	58 ± 2	1 ± 1

Table D7. Yields of the products upon oxidation of $(^{TsMe_2}TACN)Ni^{II}Me_2$ with one equivalent of $^{Ac}FcBF_4$ in MeCN- d_3 at -20 °C.

Time (hr)	CH₃-CH₃ (%)	CH₃-H/D (%)
0.5	43 ± 1	2 ± 1
1	50 ± 1	4 ± 1
2	47 ± 2	3 ± 1
4	49 ± 1	4 ± 1
8	50 ± 1	2 ± 1
24	49 ± 2	4 ± 1

Table D8. Yields of the products upon oxidation of $(^{TsMe_2}TACN)Ni^{II}Me_2$ with two equivalents of $^{Ac}FcBF_4$ in MeCN- d_3 at -20 °C.

Time (hr)	CH₃-CH₃ (%)	CH₃-H/D (%)
0.5	55 ± 1	1 ± 1
1	56 ± 1	1 ± 1
2	54 ± 2	1 ± 1
4	56 ± 1	1 ± 1
8	55 ± 1	1 ± 1
24	55 ± 2	1 ± 1

Reactivity of (^RN4)Ni^{II}Me₂ with O₂

Table D9. Yields of the products upon oxidation of (^{Me}N4)Ni^{II}Me₂ with O₂ bubbled through a solution of MeCN-d₃ for 5 min at 20 °C.

Time (hr)	CH ₃ -CH ₃ (%)	CH ₃ -H/D (%)
0.5	27 ± 3	26 ± 3
1	28 ± 1	25 ± 1
2	30 ± 2	29 ± 2
4	35 ± 2	35 ± 3
8	41 ± 1	42 ± 2
24	41 ± 2	41 ± 1

Table D10. Yields of the products upon oxidation of (^{TsMe}N4)Ni^{II}Me₂ with O₂ bubbled through a solution of MeCN-d₃ for 5 min at 20 °C.

Time (hr)	CH ₃ -CH ₃ (%)	CH ₃ -H/D (%)
0.5	34 ± 1	10 ± 2
1	39 ± 2	15 ± 3
2	43 ± 2	17 ± 2
4	47 ± 3	19 ± 2
8	48 ± 1	20 ± 1
24	53 ± 4	19 ± 3

Table D11. Yields of the products upon oxidation of (^{Ts}N4)Ni^{II}Me₂ with O₂ bubbled through a solution of MeCN-d₃ for 5 min at -20 °C.

Time (hr)	CH ₃ -CH ₃ (%)	CH ₃ -H/D (%)
0.5	50 ± 3	0 ± 0
1	52 ± 2	0 ± 0
3	62 ± 2	0 ± 0
5	63 ± 2	0 ± 0
8	65 ± 1	0 ± 0
24	65 ± 1	0 ± 0

Reactivity of (^RN4)Ni^{II}Me₂ with H₂O₂

Table D12. Yields of the products upon oxidation of (^{Me}N4)Ni^{II}Me₂ with five equivalents of H₂O₂ in MeCN-d₃ at 20 °C.

Time (hr)	CH ₃ -CH ₃ (%)	CH ₃ -H/D (%)
0.5	41 ± 2	5 ± 2
1	54 ± 3	6 ± 2
2	59 ± 2	7 ± 1
4	65 ± 1	8 ± 2
8	69 ± 3	7 ± 2
24	70 ± 2	7 ± 1

Table D13. Yields of the products upon oxidation of (^{TsMe}N4)Ni^{II}Me₂ with five equivalents of H₂O₂ in MeCN-d₃ at 20 °C.

Time (hr)	CH ₃ -CH ₃ (%)	CH ₃ -H/D (%)
0.5	54 ± 2	10 ± 2
1	61 ± 2	16 ± 1
2	65 ± 2	13 ± 2
4	68 ± 1	13 ± 2
8	70 ± 1	13 ± 1
24	72 ± 2	11 ± 2

Table D14. Yields of the products upon oxidation of (^{Ts}N4)Ni^{II}Me₂ with five equivalents of H₂O₂ in MeCN-d₃ at -20 °C.

Time (hr)	CH ₃ -CH ₃ (%)	CH ₃ -H/D (%)
0.5	59 ± 2	0 ± 0
1	61 ± 2	0 ± 0
3	61 ± 1	0 ± 0
5	60 ± 1	0 ± 0
8	59 ± 2	0 ± 0
24	56 ± 2	0 ± 0

Reactivity of (^RN4)Ni^{II}Me₂ with 1-Fluoro-2,4,6-trimethylpyridinium triflate (NFTPT)

Table D15. Yields of the products upon oxidation of (^{Me}N4)Ni^{II}Me₂ with three equivalents of NFTPT in MeCN-d₃ at 20 °C.

Time (hr)	CH ₃ -CH ₃ (%)	CH ₃ -H/D (%)
0.5	37 ± 2	5 ± 2
1	40 ± 1	6 ± 2
2	45 ± 2	7 ± 1
5	49 ± 3	9 ± 2
8	48 ± 1	8 ± 2
24	49 ± 2	9 ± 1

Table D16. Yields of the products upon oxidation of (^{TsMe}N4)Ni^{II}Me₂ with three equivalents of NFTPT in MeCN-d₃ at 20 °C.

Time (hr)	CH ₃ -CH ₃ (%)	CH ₃ -H/D (%)
0.5	84 ± 2	5 ± 1
1	84 ± 2	6 ± 1
2	87 ± 1	6 ± 1
4	87 ± 1	6 ± 2
8	85 ± 3	5 ± 3
24	87 ± 1	5 ± 2

Table D17. Yields of the products upon oxidation of (^{Ts}N4)Ni^{II}Me₂ with three equivalents of NFTPT in MeCN-d₃ at -20 °C.

Time (hr)	CH ₃ -CH ₃ (%)	CH ₃ -H/D (%)
0.5	88 ± 2	0 ± 0
1	94 ± 1	0 ± 0
3	96 ± 1	0 ± 0
5	95 ± 1	0 ± 0
8	95 ± 2	0 ± 0
24	90 ± 2	0 ± 0

Reactivity of (^RN4)Ni^{II}Me₂ with PhI(OAc)₂

Table D18. Yields of the products upon oxidation of (^{Me}N4)Ni^{II}Me₂ with one equivalent of PhI(OAc)₂ in MeCN-d₃ at 20 °C.

Time (hr)	CH ₃ -CH ₃ (%)	CH ₃ -H/D (%)
0.5	54 ± 1	9 ± 1
1	58 ± 3	11 ± 2
2	60 ± 1	10 ± 2
4	68 ± 2	12 ± 1
8	74 ± 2	11 ± 1
24	75 ± 1	12 ± 2

Table D19. Yields of the products upon oxidation of (^{TsMe}N4)Ni^{II}Me₂ with one equivalent of PhI(OAc)₂ in MeCN-d₃ at 20 °C.

Time (hr)	CH ₃ -CH ₃ (%)	CH ₃ -H/D (%)
0.25	66 ± 2	10 ± 1
1	81 ± 2	10 ± 1
3	82 ± 2	8 ± 1
7	85 ± 1	6 ± 2
24	85 ± 1	7 ± 2

Table D20. Yields of the products upon oxidation of (^{Ts}N4)Ni^{II}Me₂ with one equivalent of PhI(OAc)₂ in MeCN-d₃ at -20 °C.

Time (hr)	CH ₃ -CH ₃ (%)	CH ₃ -H/D (%)
0.5	65 ± 2	5 ± 1
1	76 ± 3	6 ± 2
3	88 ± 2	8 ± 1
5	88 ± 1	7 ± 2
8	89 ± 1	7 ± 1
24	90 ± 1	8 ± 1

Reactivity of (^RN4)Ni^{II}Me₂ with 5-(trifluoromethyl)dibenzothiophenium trifluoromethanesulfonate (TDTT)

Table D21. Yields of the products upon oxidation of (^{Me}N4)Ni^{II}Me₂ with one equivalent of TDTT in MeCN-d₃ at 20 °C.

Time (hr)	CH₃-CH₃ (%)	CH₃-H/D (%)
0.25	44 ± 2	15 ± 3
1	60 ± 3	18 ± 1
3	69 ± 1	19 ± 2
5	73 ± 2	18 ± 2
8	79 ± 1	20 ± 2
24	77 ± 2	19 ± 2

Table D22. Yields of the products upon oxidation of (^{TsMe}N4)Ni^{II}Me₂ with one equivalent of TDTT in MeCN-d₃ at 20 °C.

Time (hr)	CH₃-CH₃ (%)	CH₃-H/D (%)
0.25	48 ± 2	12 ± 1
1	62 ± 2	12 ± 2
3	77 ± 1	14 ± 1
5	84 ± 1	14 ± 2
7	86 ± 2	13 ± 1
24	88 ± 1	12 ± 1

Table D23. Yields of the products upon oxidation of (^{Ts}N4)Ni^{II}Me₂ with one equivalent of TDTT in MeCN-d₃ at -20 °C.

Time (hr)	CH₃-CH₃ (%)	CH₃-H/D (%)
0.5	72 ± 3	0 ± 0
1	85 ± 1	0 ± 0
3	85 ± 1	0 ± 0
5	88 ± 1	0 ± 0
8	90 ± 1	0 ± 0
24	90 ± 2	0 ± 0

Crossover Experiment between $(^{\text{Me}}\text{N4})\text{Ni}^{\text{II}}\text{Me}_2$ and $(^{\text{Me}}\text{N4})\text{Ni}^{\text{II}}(\text{CD}_3)_2$ with $^{\text{Ac}}\text{FcBF}_4$

Table D24. Yields of the products from the crossover experiments of $(^{\text{Me}}\text{N4})\text{Ni}^{\text{II}}\text{Me}_2$ and $(^{\text{Me}}\text{N4})\text{Ni}^{\text{II}}(\text{CD}_3)_2$ with one equivalent of $^{\text{Ac}}\text{FcBF}_4$ in MeCN-d_3 at 20 °C analyzed by ^1H NMR.

Time (hr)	$\text{CH}_3\text{-CH}_3$ (%)	$\text{CH}_3\text{-CD}_3$ (%)	$\text{CH}_3\text{-H/D}$ (%)	$[\text{CD}_3\text{-CD}_3]$ (%)
0.5	14 ± 2	14 ± 2	7 ± 3	14
1	17 ± 1	16 ± 2	8 ± 2	17
2	21 ± 1	22 ± 2	10 ± 2	21
4	23 ± 2	21 ± 1	11 ± 1	23
8	25 ± 2	25 ± 2	11 ± 1	25
24	24 ± 1	24 ± 2	11 ± 2	24

Table D25. Yields of the products from the crossover experiments of $(^{\text{Me}}\text{N4})\text{Ni}^{\text{II}}\text{Me}_2$ and $(^{\text{Me}}\text{N4})\text{Ni}^{\text{II}}(\text{CD}_3)_2$ with two equivalents of $^{\text{Ac}}\text{FcBF}_4$ in MeCN-d_3 at 20 °C analyzed by ^1H NMR.

Time (hr)	$\text{CH}_3\text{-CH}_3$ (%)	$\text{CH}_3\text{-CD}_3$ (%)	$\text{CH}_3\text{-H/D}$ (%)	$[\text{CD}_3\text{-CD}_3]$ (%)
0.5	34 ± 1	6 ± 1	5 ± 1	34
1	35 ± 2	7 ± 2	6 ± 2	35
2	35 ± 2	9 ± 1	6 ± 2	35
4	34 ± 1	8 ± 2	7 ± 2	34
8	36 ± 1	7 ± 1	6 ± 1	36
24	35 ± 2	7 ± 1	5 ± 2	35

Crossover Experiment between $(^{TsMe}N_4)Ni^{II}Me_2$ and $(^{TsMe}N_4)Ni^{II}(CD_3)_2$ with $^{Ac}FcBF_4$ **Table D26.** Yields of the products from the crossover experiments of $(^{TsMe}N_4)Ni^{II}Me_2$ and $(^{TsMe}N_4)Ni^{II}(CD_3)_2$ with one equivalent of $^{Ac}FcBF_4$ in MeCN- d_3 at 20 °C analyzed by 1H NMR.

Time (hr)	CH ₃ -CH ₃ (%)	CH ₃ -CD ₃ (%)	CH ₃ -H/D (%)	[CD ₃ -CD ₃] (%)
0.5	20 ± 2	0 ± 0	1 ± 1	20
1	32 ± 3	0 ± 0	2 ± 1	32
2	48 ± 2	0 ± 0	1 ± 1	48
4	47 ± 2	0 ± 0	1 ± 1	47
8	45 ± 3	0 ± 0	2 ± 1	45
24	47 ± 1	0 ± 0	1 ± 1	47

Table D27. Yields of the products from the crossover experiments of $(^{TsMe}N_4)Ni^{II}Me_2$ and $(^{TsMe}N_4)Ni^{II}(CD_3)_2$ with two equivalents of $^{Ac}FcBF_4$ in MeCN- d_3 at 20 °C analyzed by 1H NMR.

Time (hr)	CH ₃ -CH ₃ (%)	CH ₃ -CD ₃ (%)	CH ₃ -H/D (%)	[CD ₃ -CD ₃] (%)
0.5	27 ± 3	0 ± 0	1 ± 1	27
1	35 ± 2	0 ± 0	1 ± 1	35
2	47 ± 3	0 ± 0	1 ± 1	47
4	45 ± 2	0 ± 0	2 ± 1	45
8	47 ± 1	0 ± 0	1 ± 1	47
24	46 ± 2	0 ± 0	1 ± 1	46

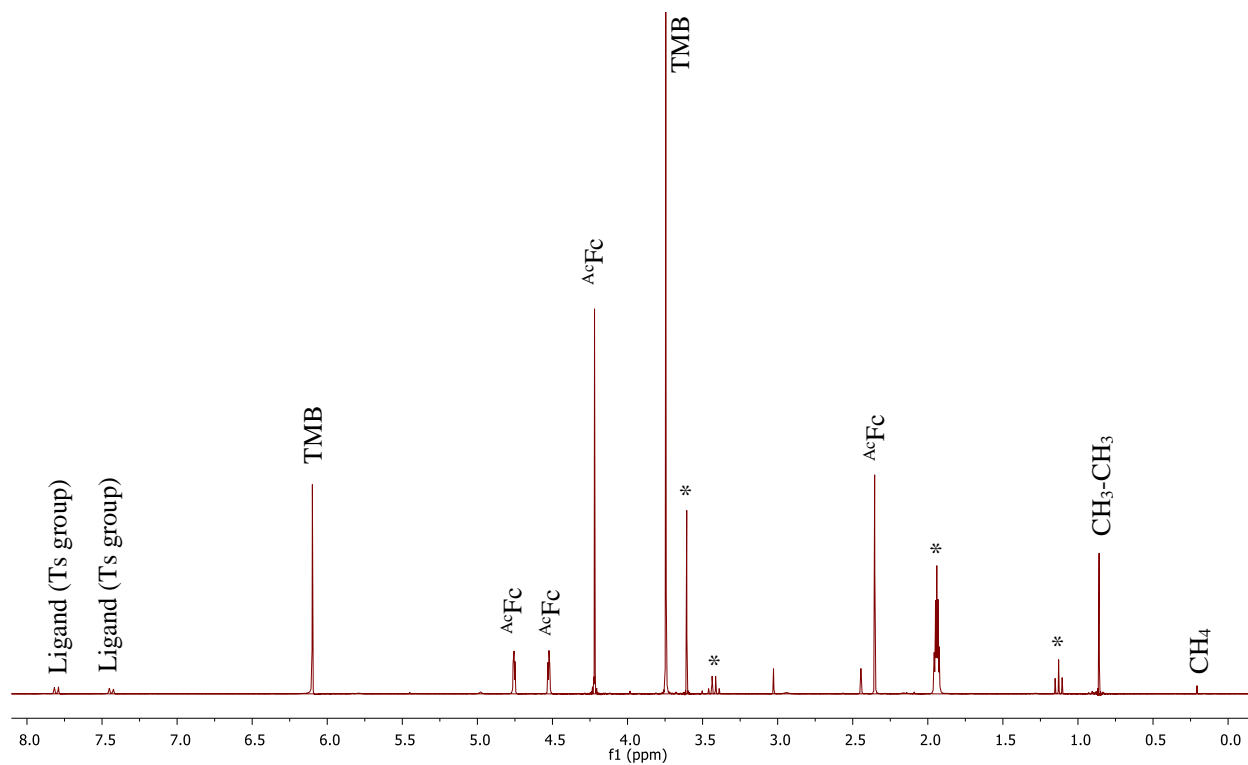


Figure D1. ^1H NMR of $\frac{1}{2}$ equivalent of $(^{\text{TsMe}}\text{N}_4)\text{NiMe}_2$ and $\frac{1}{2}$ equivalent of $(^{\text{TsMe}}\text{N}_4)\text{Ni}(\text{CD}_3)_2$ plus one equivalent of $^{\text{Ac}}\text{FcBF}_4$ in MeCN-d_3 . ^2H NMR spectrum show of the two-hour time point. No cross-over product is visible ($\text{CD}_3\text{-CH}_3$). Peaks marked with an asterisk correspond to a trace amount of solvent (MeCN-d_3 , diethyl ether and 1,4-dioxane (3.60 ppm)).

Table D28. Yields of the products from the crossover experiments of $(^{TsMe}N_4)Ni^{II}Me_2$ and $(^{TsMe}N_4)Ni^{II}(CD_3)_2$ with one equivalent of $^{Ac}FcBF_4$ in acetonitrile at 20 °C analyzed by 2H NMR.

Time (hr)	CD_3-CD_3 (%)	CH_3-CD_3 (%)	CH_3-H/D (%)	$[CH_3-CH_3]$ (%)
0.5	22 ± 3	0 ± 0	1 ± 1	22
1	34 ± 2	0 ± 0	1 ± 1	34
2	45 ± 3	0 ± 0	1 ± 1	45
4	46 ± 2	0 ± 0	1 ± 1	46
8	45 ± 1	0 ± 0	2 ± 1	45
24	44 ± 1	0 ± 0	2 ± 1	44

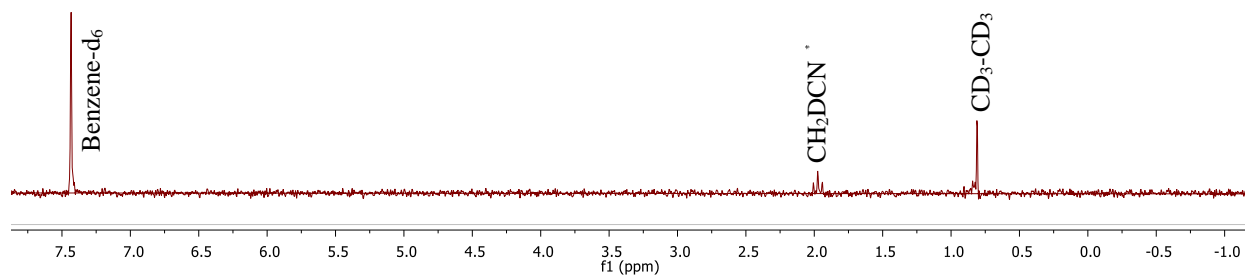


Figure D2. 2H NMR of $\frac{1}{2}$ equivalent of $(^{TsMe}N_4)NiMe_2$ and $\frac{1}{2}$ equivalent of $(^{TsMe}N_4)Ni(CD_3)_2$ plus one equivalent of $^{Ac}FcBF_4$ in acetonitrile. 2H NMR spectrum show of the 2-hour time point. No cross-over product is visible (CD_3-CH_3).

Crossover Experiment between $(^{15}\text{N}_4)\text{Ni}^{\text{II}}\text{Me}_2$ and $(^{15}\text{N}_4)\text{Ni}^{\text{II}}(\text{CD}_3)_2$ with $^{13}\text{C}\text{FcBF}_4$

Table D29. Yields of the products from the crossover experiments of $(^{15}\text{N}_4)\text{Ni}^{\text{II}}\text{Me}_2$ and $(^{15}\text{N}_4)\text{Ni}^{\text{II}}(\text{CD}_3)_2$ with one equivalent of $^{13}\text{C}\text{FcBF}_4$ in MeCN-d_3 at $-20\text{ }^\circ\text{C}$ analyzed by ^1H NMR.

Time (hr)	$\text{CH}_3\text{-CH}_3$ (%)	$\text{CH}_3\text{-CD}_3$ (%)	$\text{CH}_3\text{-H/D}$ (%)	$[\text{CD}_3\text{-CD}_3]$ (%)
0.5	15 ± 2	0 ± 0	0 ± 0	15
1	25 ± 2	0 ± 0	0 ± 0	25
2	30 ± 1	0 ± 0	0 ± 0	30
4	32 ± 3	0 ± 0	0 ± 0	32
8	31 ± 1	0 ± 0	0 ± 0	31
24	32 ± 2	0 ± 0	0 ± 0	32

Table D30. Yields of the products from the crossover experiments of $(^{15}\text{N}_4)\text{Ni}^{\text{II}}\text{Me}_2$ and $(^{15}\text{N}_4)\text{Ni}^{\text{II}}(\text{CD}_3)_2$ with two equivalents of $^{13}\text{C}\text{FcBF}_4$ in MeCN-d_3 at $-20\text{ }^\circ\text{C}$ analyzed by ^1H NMR.

Time (hr)	$\text{CH}_3\text{-CH}_3$ (%)	$\text{CH}_3\text{-CD}_3$ (%)	$\text{CH}_3\text{-H/D}$ (%)	$[\text{CD}_3\text{-CD}_3]$ (%)
0.5	19 ± 2	0 ± 0	0 ± 0	19
1	29 ± 2	0 ± 0	0 ± 0	29
2	36 ± 1	0 ± 0	0 ± 0	36
4	37 ± 2	0 ± 0	0 ± 0	37
8	36 ± 2	0 ± 0	0 ± 0	36
24	37 ± 1	0 ± 0	0 ± 0	37

Appendix E

Supplemental Kumada Cross-Coupling Reactions Data

Kumada Cross-Coupling of *p*-Iodotoluene and PhenylMgBr:

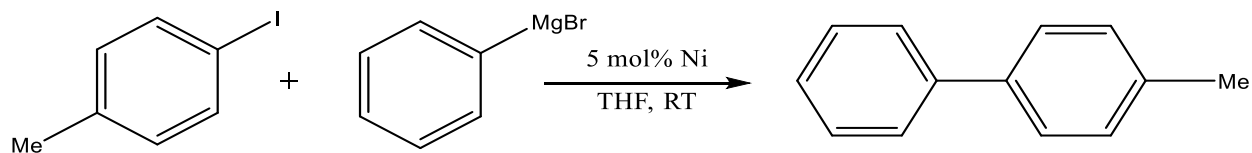


Table E1. Products and yields for the Kumada cross-coupling reaction of *p*-iodotoluene and phenylMgBr catalyzed by 5 mol % $(\text{Me}_4\text{N})\text{Ni}^{\text{II}}\text{Br}_2$.

Product	Structure	Yield (%)		
		1 hour	2 hours	24 hours
Toluene		7 ± 1	8 ± 2	8 ± 1
Biphenyl		9 ± 1	11 ± 2	10 ± 1
Phenyl-THF		2 ± 1	1 ± 1	2 ± 1
4-Methyl-1,1'-biphenyl		78 ± 3	80 ± 2	80 ± 2
4,4'-Dimethyl-1,1'-biphenyl		2 ± 1	2 ± 1	2 ± 1

Table E2. Products and yields for the Kumada cross-coupling reaction of *p*-iodotoluene and phenylMgBr catalyzed by 5 mol % (^{TsMe}N4)Ni^{II}Br₂.

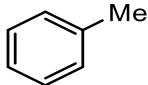
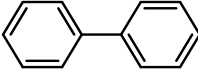
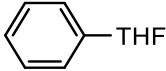
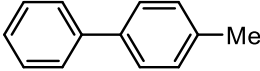
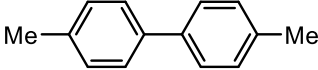
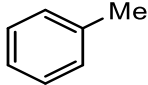
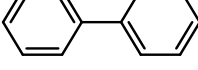
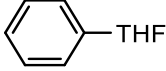
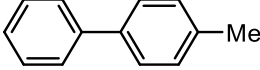
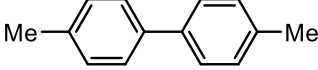
Product	Structure	Yield (%)		
		1 hour	2 hours	24 hours
Toluene		10 ± 1	11 ± 1	11 ± 2
Biphenyl		17 ± 5	16 ± 3	16 ± 2
Phenyl-THF		4 ± 1	3 ± 1	3 ± 1
4-Methyl-1,1'-biphenyl		94 ± 4	95 ± 2	95 ± 2
4,4'-Dimethyl-1,1'-biphenyl		2 ± 1	2 ± 1	2 ± 1

Table E3. Products and yields for the Kumada cross-coupling reaction of *p*-iodotoluene and phenylMgBr catalyzed by 5 mol % (^{Ts}N4)Ni^{II}Br₂.

Product	Structure	Yield (%)		
		1 hour	2 hours	24 hours
Toluene		8 ± 1	8 ± 1	8 ± 1
Biphenyl		28 ± 2	30 ± 2	30 ± 1
Phenyl-THF		17 ± 1	16 ± 2	17 ± 1
4-Methyl-1,1'-biphenyl		58 ± 1	60 ± 2	60 ± 1
4,4'-Dimethyl-1,1'-biphenyl		5 ± 1	6 ± 1	6 ± 1

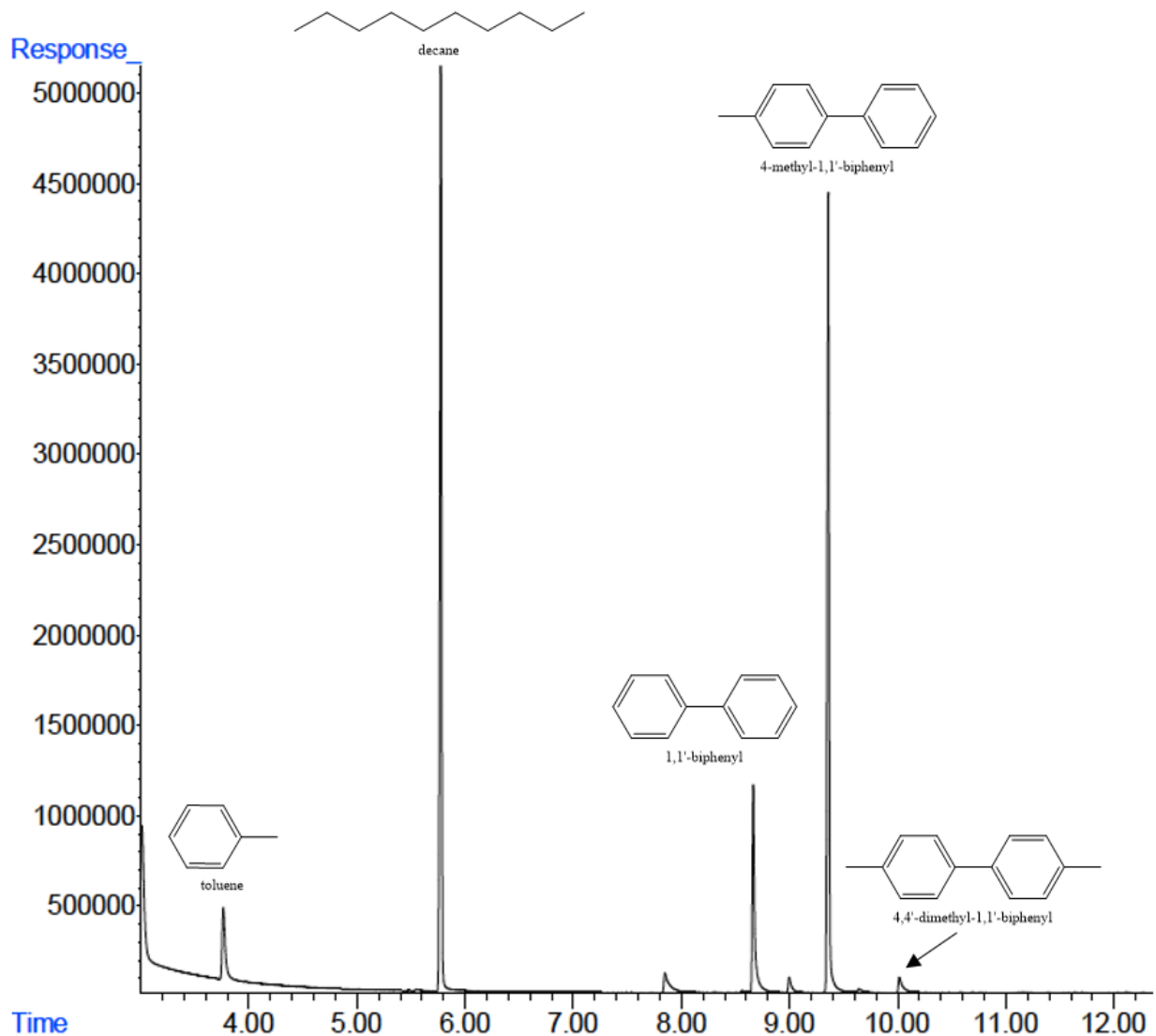


Figure E1. Representative GC chromatogram for the Kumada cross-coupling of *p*-iodotoluene with phenylMgBr catalyzed by 5 mol% (^{TsMe}N4)Ni^{II}Br₂ at one hour.

Kumada Cross-Coupling of *p*-Iodotoluene and HexylMgBr:

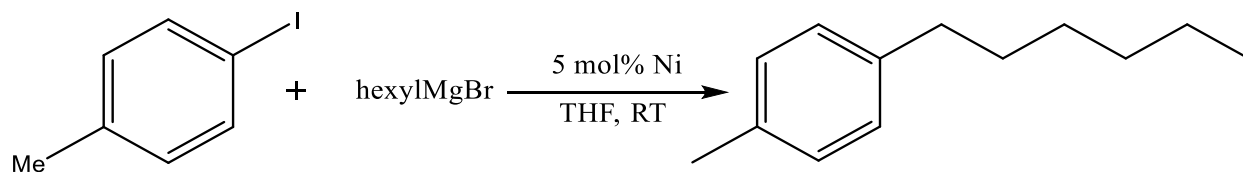


Table E4. Products and yields from the Kumada cross-coupling reactions of *p*-iodotoluene and hexylMgBr catalyzed by 5 mol % (Me₄N)⁺Ni^{II}Br₂⁻.

Product	Structure	Yield (%)		
		1 hour	2 hours	24 hours
Toluene		5 ± 1	6 ± 1	6 ± 1
Dodecane	C ₁₂ H ₂₆	6 ± 2	6 ± 2	8 ± 1
4,4'-Dimethyl-1,1'-biphenyl		6 ± 1	5 ± 1	6 ± 2
1-Hexyl-4-methylbenzene		35 ± 1	36 ± 1	38 ± 2

Table E5. Products and yields from the Kumada cross-coupling reactions of *p*-iodotoluene and hexylMgBr catalyzed by 5 mol % (^{TsMe}N4)Ni^{II}Br₂.

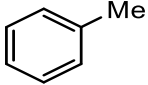

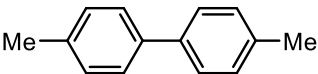
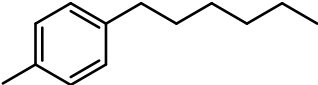
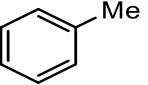
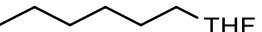
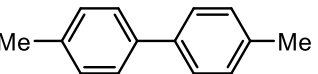
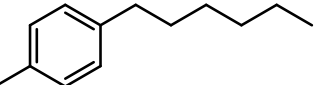
Product	Structure	Yield (%)		
		1 hour	2 hours	24 hours
Toluene		22 ± 1	22 ± 2	24 ± 2
Hexyl-THF		14 ± 1	13 ± 2	14 ± 1
Dodecane	C ₁₂ H ₂₆	7 ± 2	8 ± 1	9 ± 2
4,4'-Dimethyl-1,1'-biphenyl		2 ± 1	2 ± 1	2 ± 1
1-Hexyl-4-methylbenzene		37 ± 3	38 ± 2	40 ± 1

Table E6. Products and yields from the Kumada cross-coupling reactions of *p*-iodotoluene and hexylMgBr catalyzed by 5 mol % (^{Ts}N4)Ni^{II}Br₂.

Product	Structure	Yield (%)		
		1 hour	2 hours	24 hours
Toluene		22 ± 1	23 ± 1	23 ± 1
Hexyl-THF		13 ± 2	12 ± 2	13 ± 1
Dodecane	C ₁₂ H ₂₆	5 ± 1	5 ± 2	6 ± 1
4,4'-Dimethyl-1,1'-biphenyl		4 ± 1	4 ± 1	4 ± 1
1-Hexyl-4-methylbenzene		18 ± 1	17 ± 2	18 ± 1

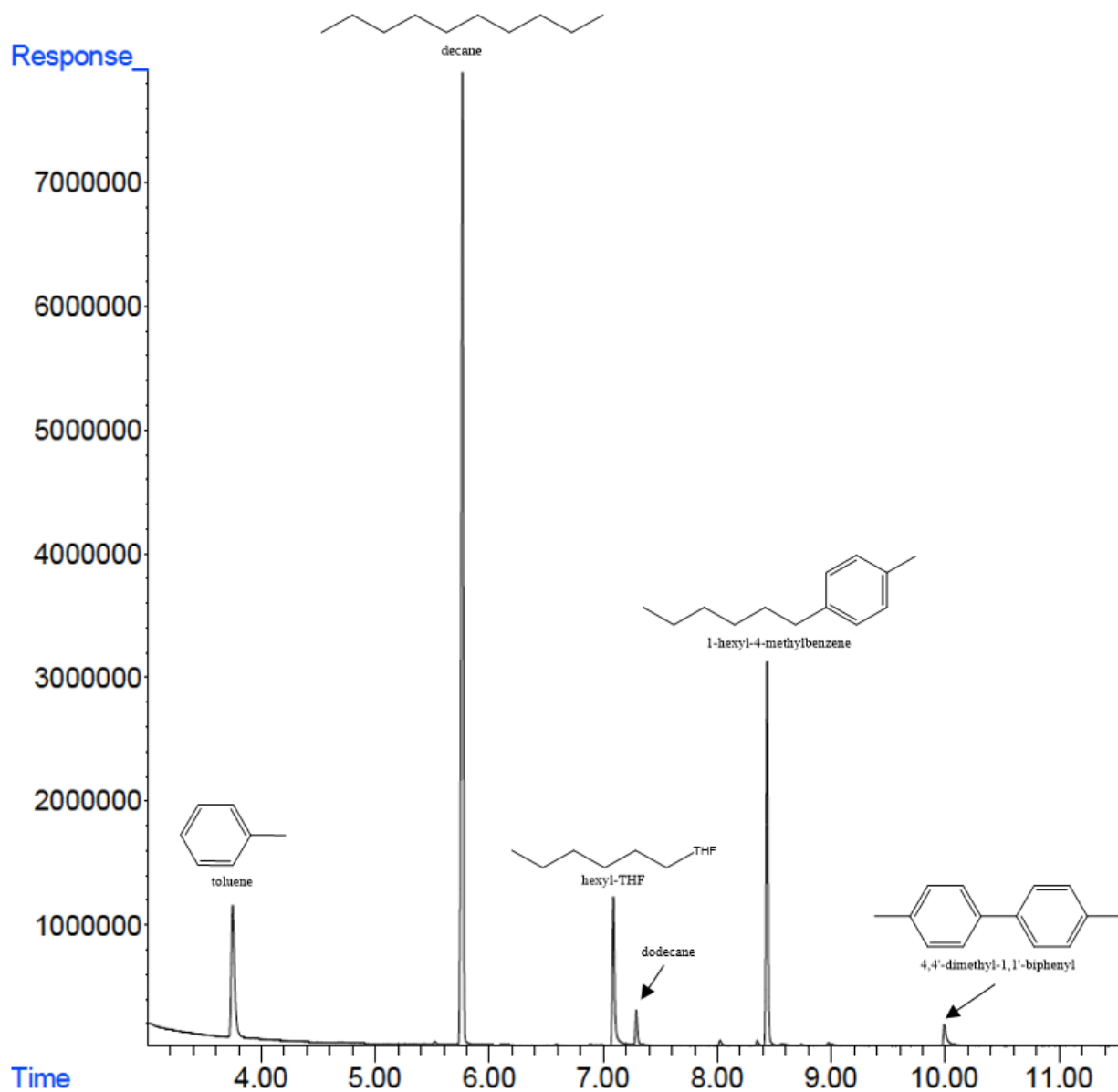


Figure E2. Representative GC chromatogram for the Kumada cross-coupling of *p*-iodotoluene with hexylMgBr catalyzed by 5 mol% $(^{\text{TsMe}}\text{N4})\text{Ni}^{\text{II}}\text{Br}_2$ at one hour.

Kumada Cross-Coupling of 1-Iodooctane and PhenylMgBr:

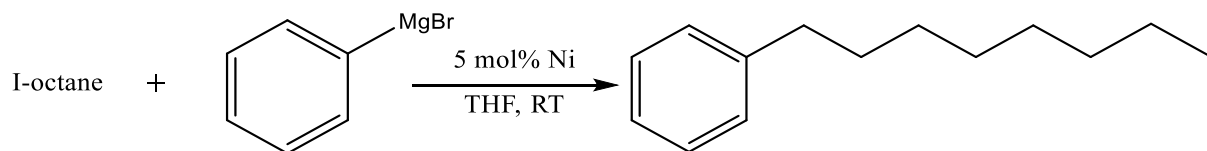


Table E7. Products and yields from the Kumada cross-coupling reactions of 1-iodooctane and phenylMgBr catalyzed by 5 mol % $(^{\text{Me}}\text{N4})\text{Ni}^{\text{II}}\text{Br}_2$.

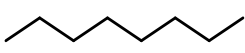
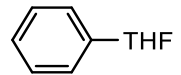
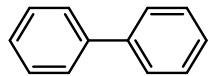
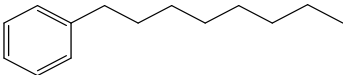
Product	Structure	Yield (%)		
		1 hour	2 hours	24 hours
Octane		51 ± 2	52 ± 3	54 ± 2
Phenyl-THF		5 ± 1	5 ± 2	5 ± 1
Biphenyl		37 ± 2	38 ± 1	37 ± 2
Octylbenzene		13 ± 2	14 ± 2	15 ± 1

Table E8. Products and yields from the Kumada cross-coupling reactions of 1-iodooctane and phenylMgBr catalyzed by 5 mol % (^{TsMe}N4)Ni^{II}Br₂.

Product	Structure	Yield (%)		
		1 hour	2 hours	24 hours
Octane		65 ± 4	64 ± 2	61 ± 2
Phenyl-THF		15 ± 3	15 ± 2	16 ± 1
Biphenyl		35 ± 2	36 ± 1	36 ± 1
Octylbenzene		14 ± 2	15 ± 2	15 ± 1

Table E9. Products and yields from the Kumada cross-coupling reactions of 1-iodooctane and phenylMgBr catalyzed by 5 mol % (^{Ts}N4)Ni^{II}Br₂.

Product	Structure	Yield (%)		
		1 hour	2 hours	24 hours
Octane		53 ± 3	52 ± 2	51 ± 2
Phenyl-THF		8 ± 1	8 ± 1	9 ± 1
Hexadecane	C ₁₆ H ₃₄	40 ± 5	41 ± 3	40 ± 2
Octylbenzene		4 ± 1	5 ± 1	5 ± 1

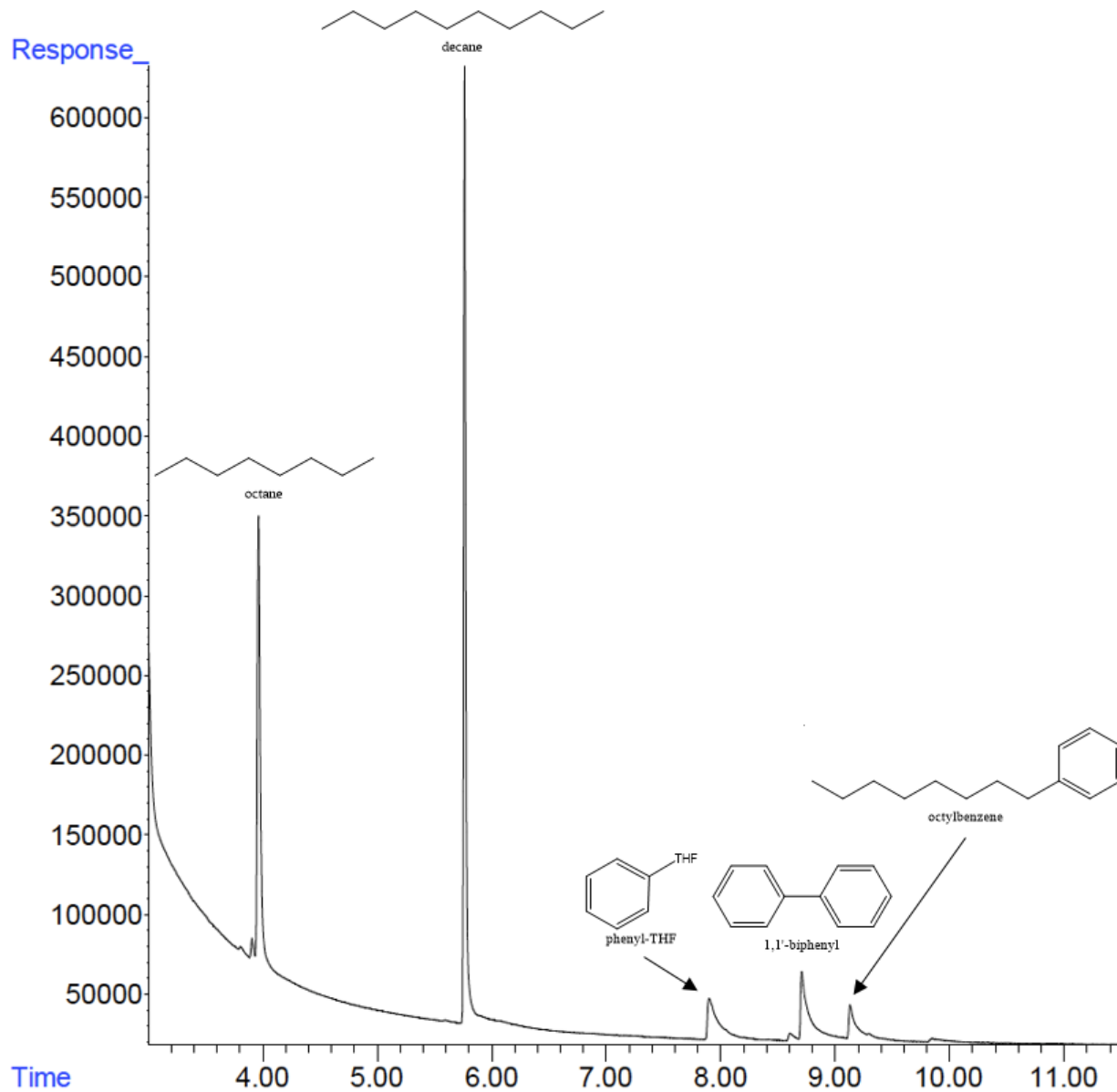


Figure E3. Representative GC chromatogram for the Kumada cross-coupling of 1-iodooctane with phenylMgBr catalyzed by 5 mol% $(^{\text{TSMc}}\text{N4})\text{Ni}^{\text{II}}\text{Br}_2$ at one hour.

Kumada Cross-Coupling of 1-Iodooctane and HexylMgBr:

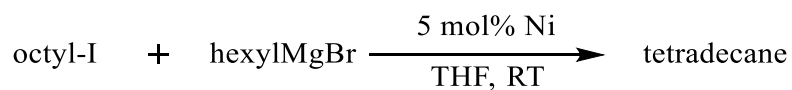


Table E10. Products and yields from the Kumada cross-coupling reactions of 1-iodooctane and hexylMgBr catalyzed by 5 mol % $(^{\text{Me}}\text{N4})\text{Ni}^{\text{II}}\text{Br}_2$.

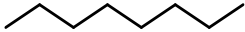

Product	Structure	Yield (%)		
		1 hour	2 hours	24 hours
Octane		55 ± 2	54 ± 2	55 ± 1
Dodecane	C ₁₂ H ₂₆	3 ± 2	3 ± 1	3 ± 2
1-Iodooctane		22 ± 2	21 ± 2	20 ± 1
Tetradecane	C ₁₄ H ₃₀	4 ± 1	4 ± 1	5 ± 2

Table E11. Products and yields from the Kumada cross-coupling reactions of 1-iodooctane and hexylMgBr catalyzed by 5 mol % $(^{\text{TSMe}}\text{N4})\text{Ni}^{\text{II}}\text{Br}_2$.

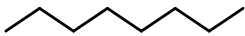

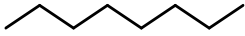

Product	Structure	Yield (%)		
		1 hour	2 hours	24 hours
Octane		47 ± 2	43 ± 2	44 ± 1
Dodecane	C ₁₂ H ₂₆	5 ± 1	5 ± 2	5 ± 1
1-Iodooctane		20 ± 1	19 ± 1	19 ± 1
Tetradecane	C ₁₄ H ₃₀	6 ± 1	6 ± 1	7 ± 1

Table E12. Products and yields from the Kumada cross-coupling reactions of 1-iodooctane and hexylMgBr catalyzed by 5 mol % $(^{\text{T3}}\text{N4})\text{Ni}^{\text{II}}\text{Br}_2$.

Product	Structure	Yield (%)		
		1 hour	2 hours	24 hours
Octane		43 ± 3	44 ± 2	44 ± 1
Dodecane	C ₁₂ H ₂₆	2 ± 1	2 ± 1	2 ± 1
1-Iodooctane		23 ± 2	22 ± 2	22 ± 1
Tetradecane	C ₁₄ H ₃₀	5 ± 1	5 ± 1	4 ± 2

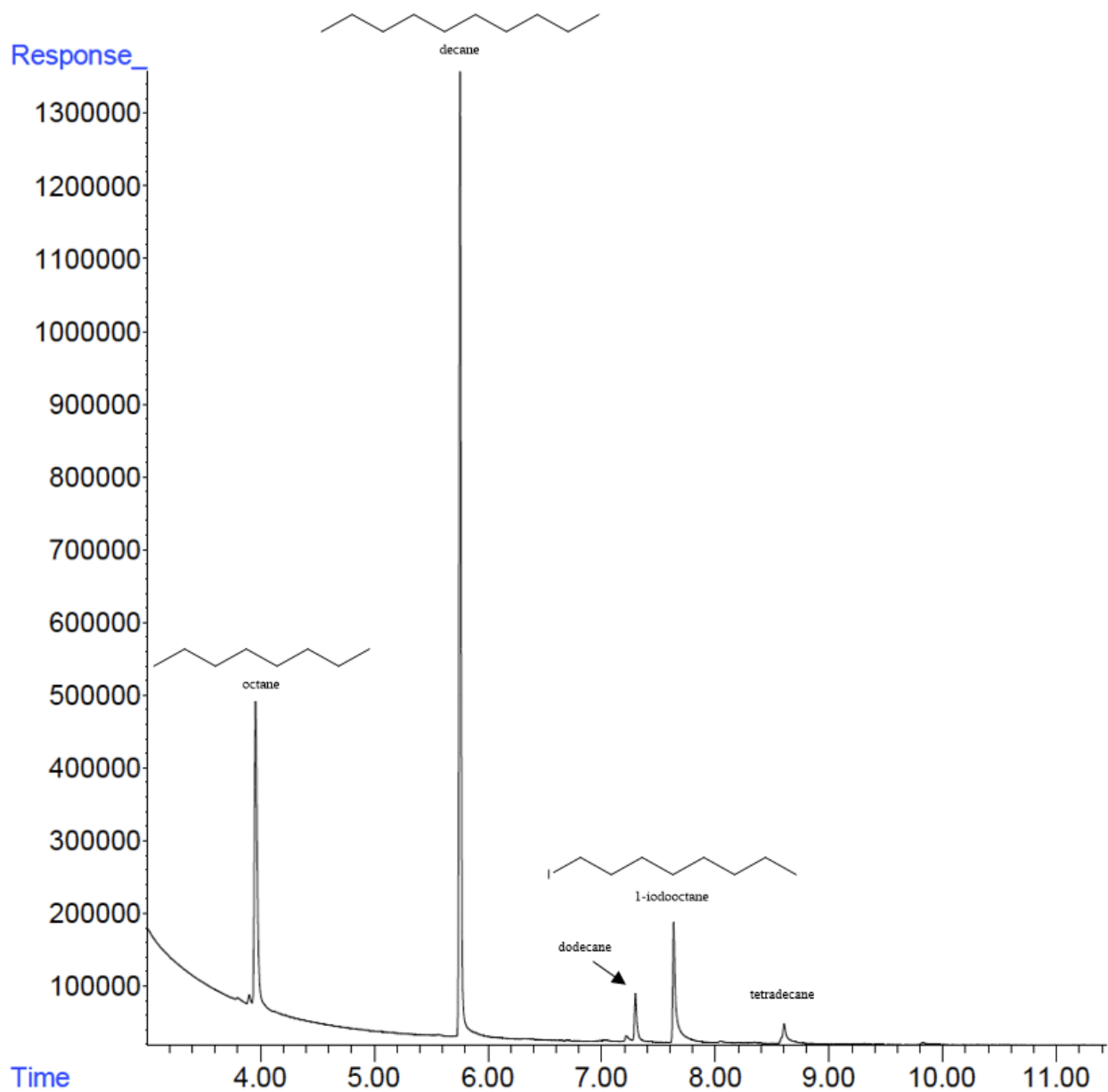
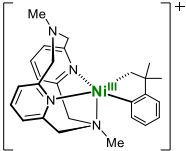
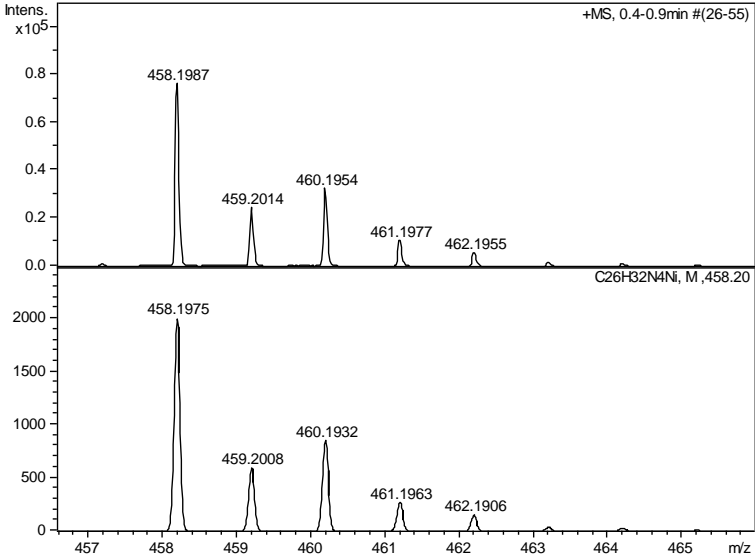
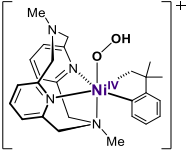
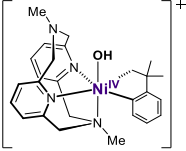
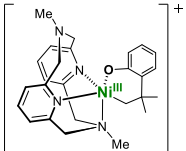
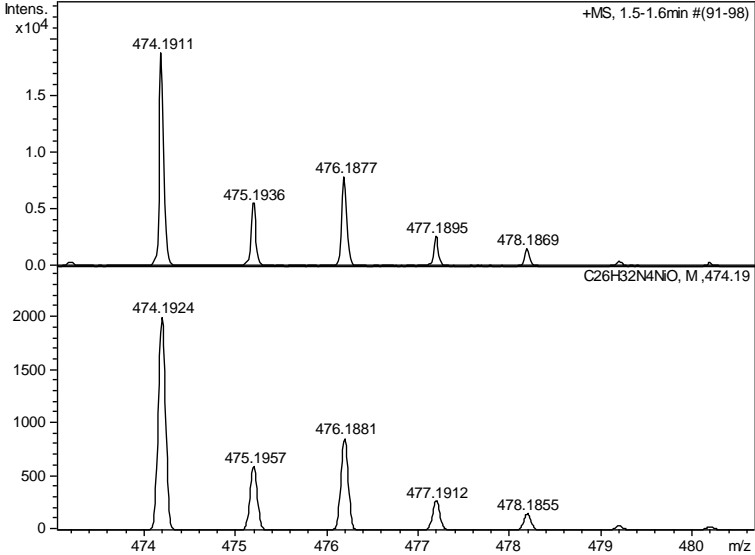


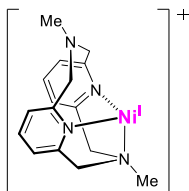
Figure E4. Representative GC chromatogram for the Kumada cross-coupling of 1-iodooctane with hexylMgBr catalyzed by 5 mol% $(^{\text{Tsm}}\text{MeN4})\text{Ni}^{\text{II}}\text{Br}_2$ at one hour.

Appendix F

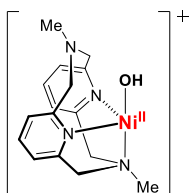
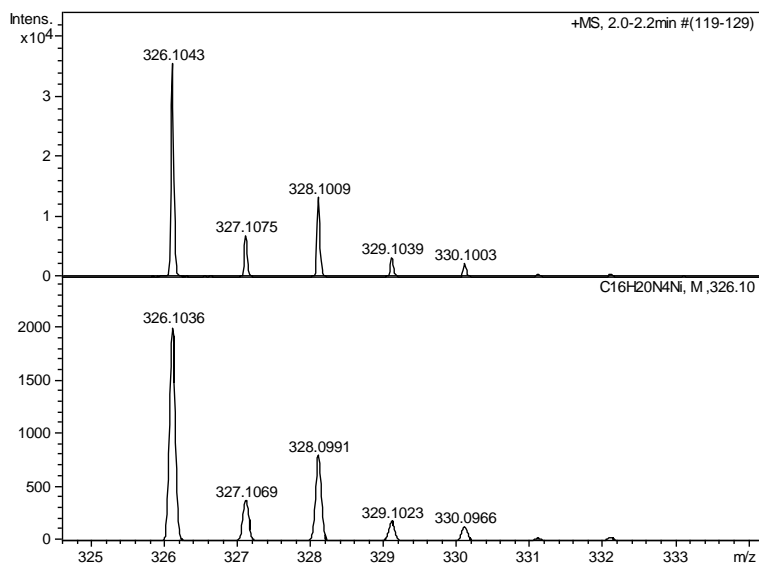
Supplemental Cryo-ESI-MS Data

Table F1. Cryo-ESI-MS results for the oxidation of (^{Me}N₄)Ni^{II}(cycloneophyl).

Intermediates	Chemical Formula and m/z	Spectra
	$C_{26}H_{32}N_4Ni$, 458.1975	
	$C_{26}H_{33}N_4NiO_2$, 491.1952	Not observed
	$C_{26}H_{33}N_4NiO$, 475.2002	Not observed
	$C_{26}H_{32}N_4NiO$, 474.1924	

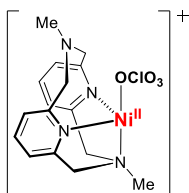


$C_{16}H_{20}N_4Ni$,
326.1036



$C_{16}H_{21}N_4NiO$,
343.1063

Not observed



$C_{16}H_{20}ClN_4NiO_4$,
425.0521

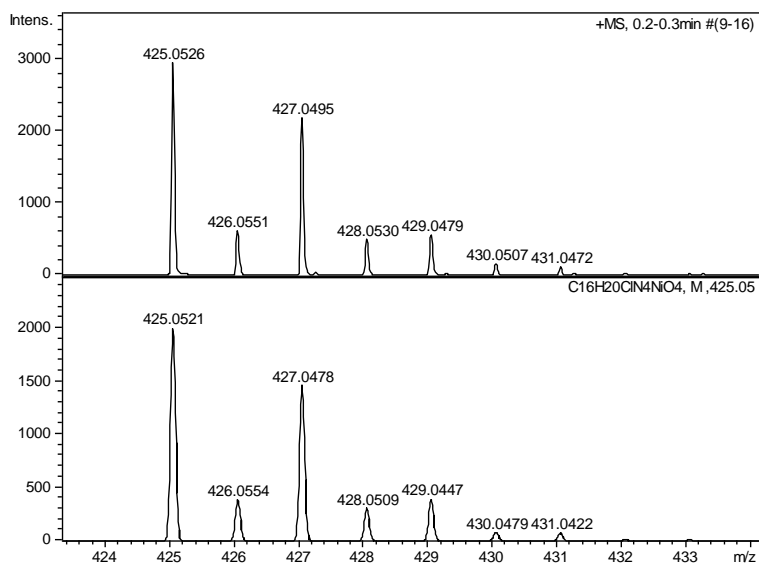
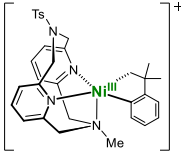
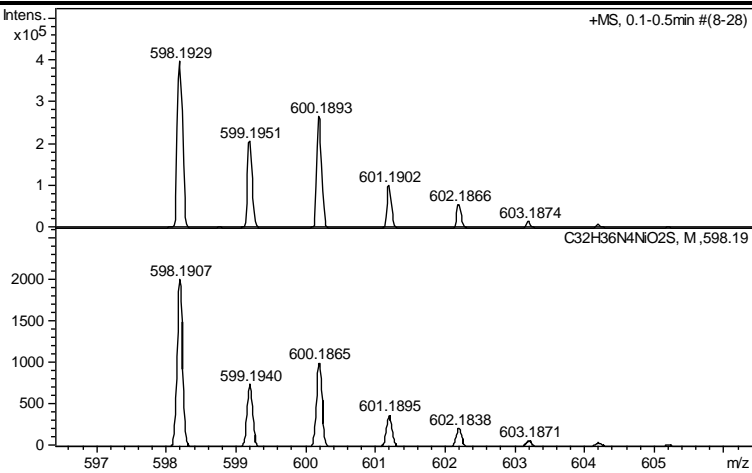
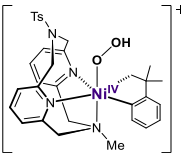
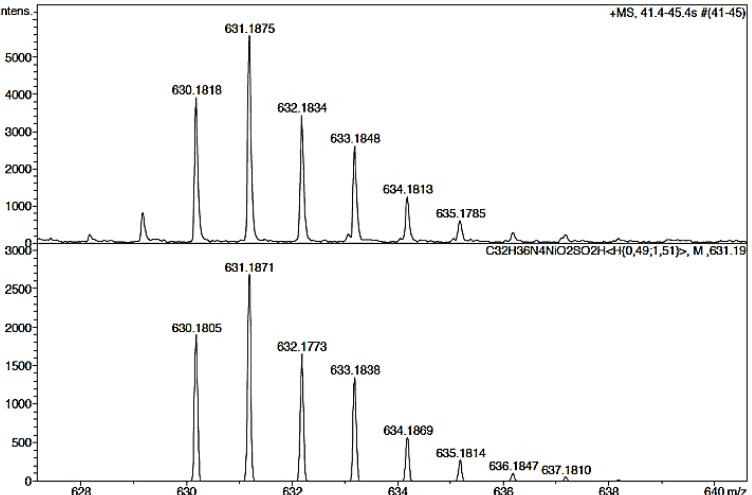
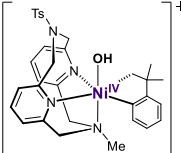
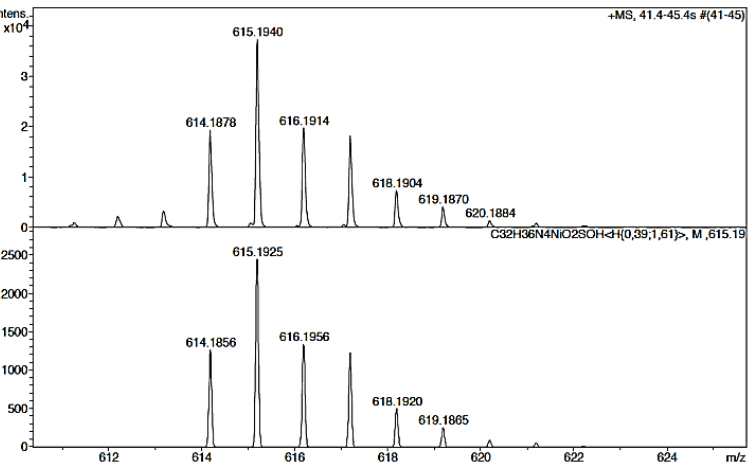
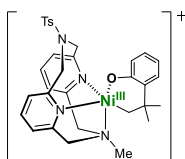
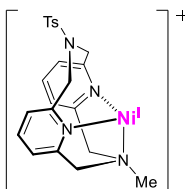
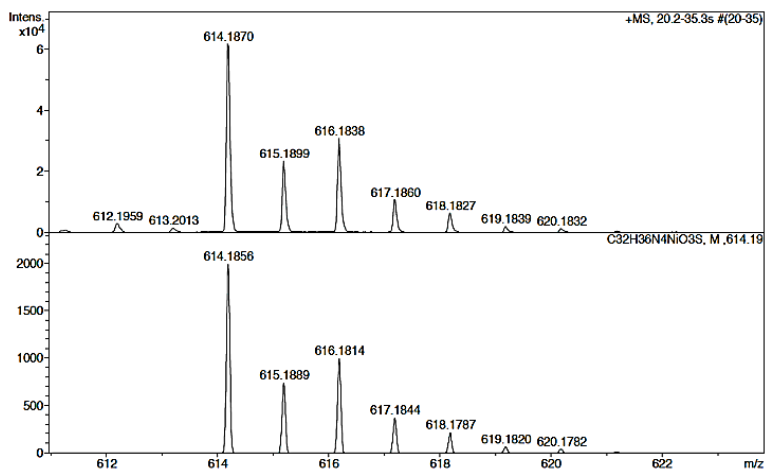


Table F2. Cryo-ESI-MS results for the oxidation of (^{TsMe}N₄)Ni^{II}(cycloneophyl).

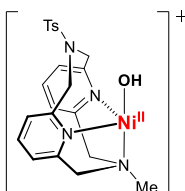
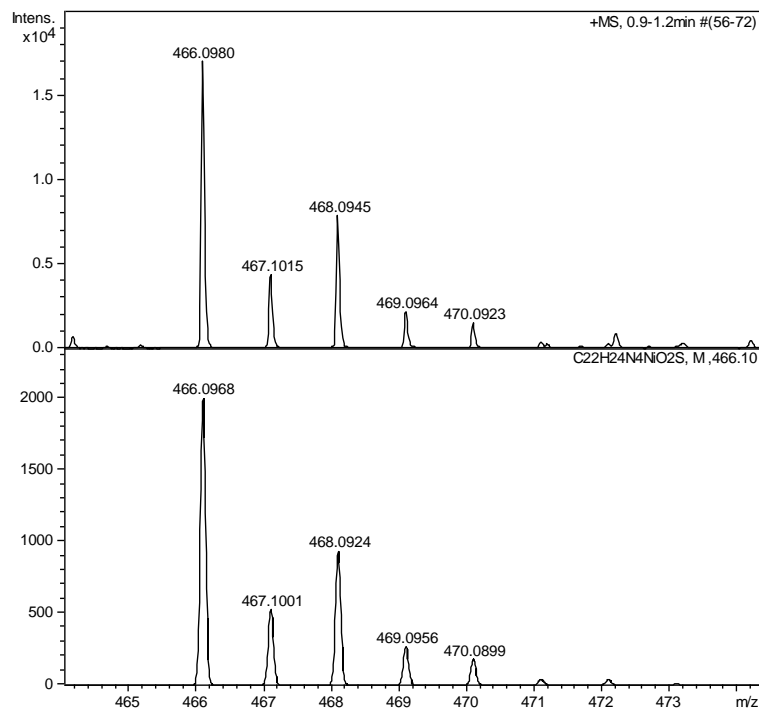
Intermediates	Chemical Formula and m/z	Spectra
	$C_{32}H_{36}N_4NiO_2S$, 598.1907	
	$C_{32}H_{37}N_4NiO_4S$, 631.1884	
	$C_{32}H_{37}N_4NiO_3S$, 615.1934	



$C_{32}H_{36}N_4NiO_3S$,
614.1856

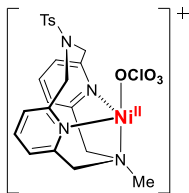


$C_{22}H_{24}N_4NiO_2S$,
466.0968



$C_{22}H_{25}N_4NiO_3S$,
483.0995

Not observed



$C_{22}H_{24}ClN_4NiO_6S$,
565.0453

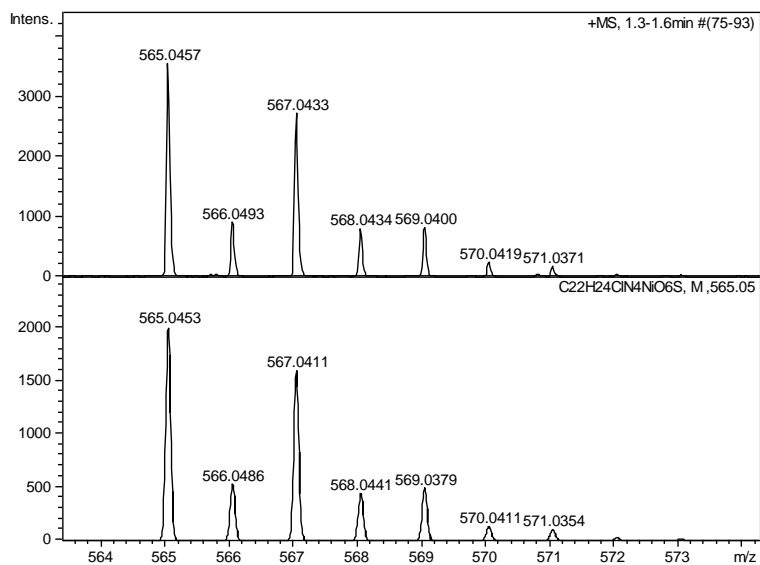
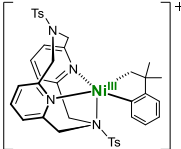
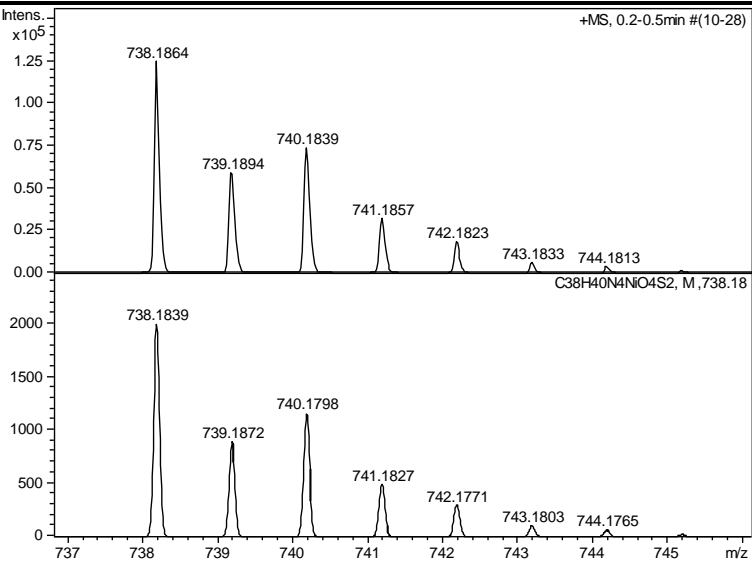
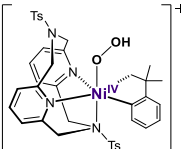
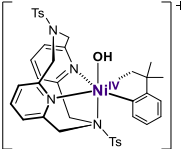
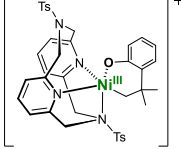
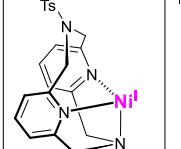
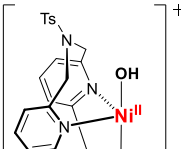
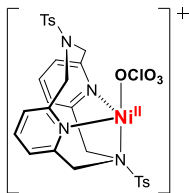
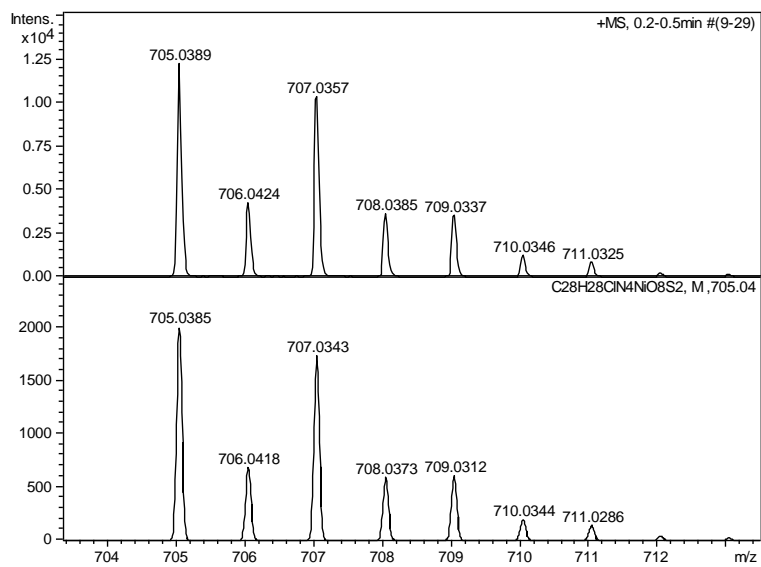


Table F3. Cryo-ESI-MS results for the oxidation of (^{Ts}N₄)Ni^{II}(cycloneophyl).

Intermediates	Chemical Formula and m/z	Spectra
	$C_{38}H_{40}N_4NiO_4S_2$, 738.1839	
	$C_{38}H_{31}N_4NiO_6S_2$, 771.1816	Not observed
	$C_{38}H_{41}N_4NiO_5S_2$, 755.1866	Not observed
	$C_{38}H_{40}N_4NiO_5S_2$, 754.1788	Not observed
	$C_{28}H_{28}N_4NiO_4S_2$, 606.0900	Not observed
	$C_{28}H_{29}N_4NiO_5S_2$, 623.0927	Not observed



$C_{28}H_{28}ClN_4NiO_8S_2$,
705.0385

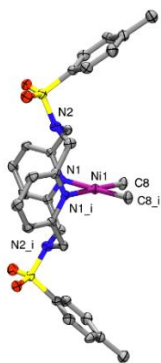
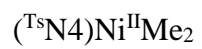
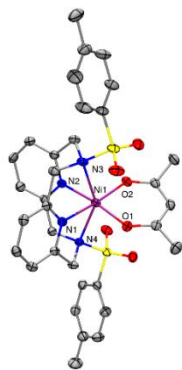
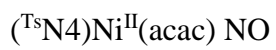
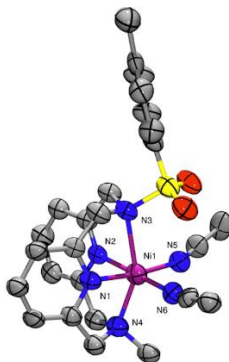
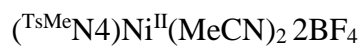
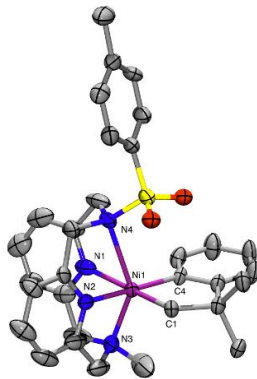
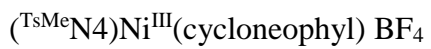


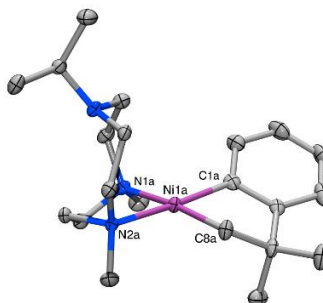
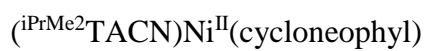
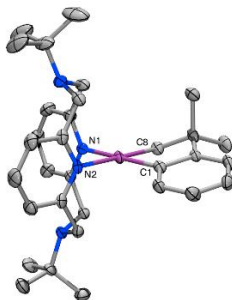
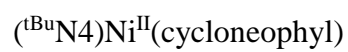
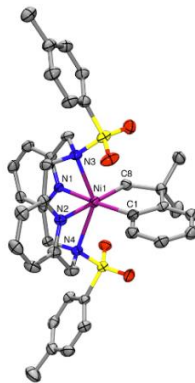
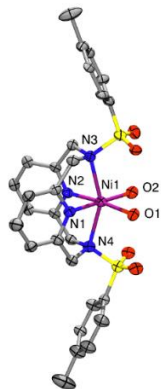
Appendix G

X-ray Crystal Structure Data

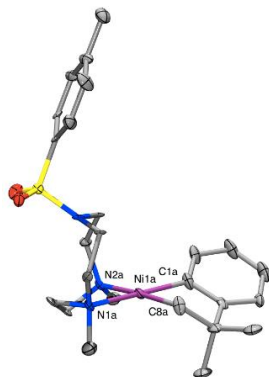
Table G1. ORTEP representation with 50% probability thermal ellipsoids.

Complex Name	Structure
$(\text{TsMeN4})\text{Ni}^{\text{II}}\text{Br}_2$	
$(\text{TsMeN4})\text{Ni}^{\text{II}}\text{Me}_2$	
$(\text{TsMeN4})\text{Ni}^{\text{III}}\text{Me}_2 \text{SbF}_6$	





(TsMe₂TACN)Ni^{II}(cycloneophyl)



(iPr³TACN)Ni^{II}(cycloneophyl)

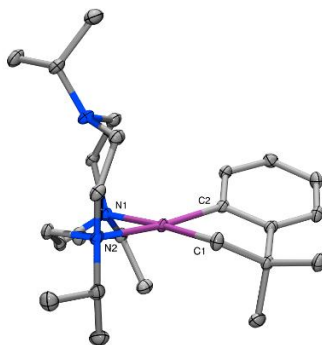


Table G2. Crystal data and structure refinement for Im614. (^{TsMe}N₄)Ni^{II}Br₂

Identification code	l614/lt/smart/SS101616	
Empirical formula	C ₂₄ H ₂₇ Br ₂ N ₅ Ni O ₂ S	
Formula weight	668.09	
Temperature	100(2) K	
Wavelength	0.71073 Å	
Crystal system	Orthorhombic	
Space group	P b c a	
Unit cell dimensions	a = 14.0788(15) Å	α = 90°.
	b = 14.3177(14) Å	β = 90°.
	c = 25.607(3) Å	γ = 90°.
Volume	5161.7(9) Å ³	
Z	8	
Density (calculated)	1.719 Mg/m ³	
Absorption coefficient	3.961 mm ⁻¹	
F(000)	2688	
Crystal size	0.138 x 0.127 x 0.068 mm ³	
Theta range for data collection	2.150 to 25.515°.	
Index ranges	-16 ≤ h ≤ 16, -17 ≤ k ≤ 16, -29 ≤ l ≤ 30	
Reflections collected	44975	
Independent reflections	4747 [R(int) = 0.0993]	
Completeness to theta = 25.242°	100.0 %	
Absorption correction	Semi-empirical from equivalents	
Max. and min. transmission	0.5619 and 0.4947	
Refinement method	Full-matrix least-squares on F ²	
Data / restraints / parameters	4747 / 0 / 319	
Goodness-of-fit on F ²	1.013	
Final R indices [I > 2σ(I)]	R1 = 0.0376, wR2 = 0.0695	
R indices (all data)	R1 = 0.0694, wR2 = 0.0799	
Extinction coefficient	n/a	
Largest diff. peak and hole	1.591 and -0.584 e.Å ⁻³	

Table G3. Select bond lengths [\AA] and angles [$^\circ$] for lm614.

Br(1)-Ni(1)	2.5203(7)
Br(2)-Ni(1)	2.4525(7)
Ni(1)-N(1)	2.010(3)
Ni(1)-N(2)	2.049(3)
Ni(1)-N(3)	2.125(4)
N(1)-Ni(1)-N(2)	83.01(13)
N(1)-Ni(1)-N(3)	82.40(14)
N(2)-Ni(1)-N(3)	81.36(14)
N(1)-Ni(1)-Br(2)	176.20(10)
N(2)-Ni(1)-Br(2)	93.34(10)
N(3)-Ni(1)-Br(2)	96.06(10)
N(1)-Ni(1)-Br(1)	87.55(9)
N(2)-Ni(1)-Br(1)	170.14(10)
N(3)-Ni(1)-Br(1)	100.25(9)
Br(2)-Ni(1)-Br(1)	96.15(2)

Projection view with 50% probability ellipsoids:

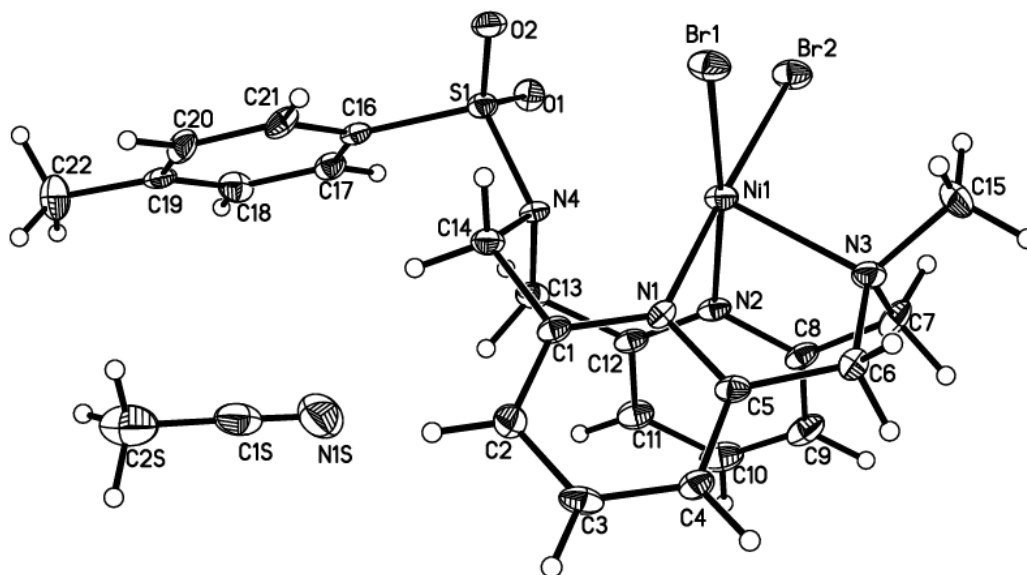


Table G4. Crystal data and structure refinement for lm9716. (^{TsMe}N₄)Ni^{II}Me₂

Identification code	19716/lt/x8/SS072616_2 (orange crystals)	
Empirical formula	C ₂₄ H ₃₀ N ₄ Ni O ₂ S	
Formula weight	497.29	
Temperature	100(2) K	
Wavelength	0.71073 Å	
Crystal system	Triclinic	
Space group	P $\bar{1}$	
Unit cell dimensions	a = 8.8474(4) Å	$\alpha = 89.114(3)^\circ$.
	b = 10.6903(5) Å	$\beta = 79.778(3)^\circ$.
	c = 12.7851(6) Å	$\gamma = 80.104(3)^\circ$.
Volume	1172.19(9) Å ³	
Z	2	
Density (calculated)	1.409 Mg/m ³	
Absorption coefficient	0.945 mm ⁻¹	
F(000)	524	
Crystal size	0.521 x 0.256 x 0.075 mm ³	
Theta range for data collection	1.619 to 27.680°.	
Index ranges	-7 ≤ h ≤ 11, -13 ≤ k ≤ 13, -16 ≤ l ≤ 16	
Reflections collected	17854	
Independent reflections	5277 [R(int) = 0.0416]	
Completeness to theta = 25.242°	97.1 %	
Absorption correction	Semi-empirical from equivalents	
Max. and min. transmission	0.6942 and 0.6092	
Refinement method	Full-matrix least-squares on F ²	
Data / restraints / parameters	5277 / 0 / 293	
Goodness-of-fit on F ²	1.007	
Final R indices [I > 2σ(I)]	R1 = 0.0406, wR2 = 0.0831	
R indices (all data)	R1 = 0.0690, wR2 = 0.0944	
Largest diff. peak and hole	0.747 and -0.514 e.Å ⁻³	

Table G5. Select bond lengths [\AA] and angles [$^\circ$] for lm9716.

Ni(1)-C(2)	1.925(3)
Ni(1)-C(1)	1.932(3)
Ni(1)-N(2)	1.965(2)
Ni(1)-N(1)	1.968(2)

C(2)-Ni(1)-C(1)	87.94(12)
C(2)-Ni(1)-N(2)	93.28(10)
C(1)-Ni(1)-N(2)	177.44(10)
C(2)-Ni(1)-N(1)	177.96(10)
C(1)-Ni(1)-N(1)	93.08(10)
N(2)-Ni(1)-N(1)	85.78(8)

Projection view with 50% probability ellipsoids:

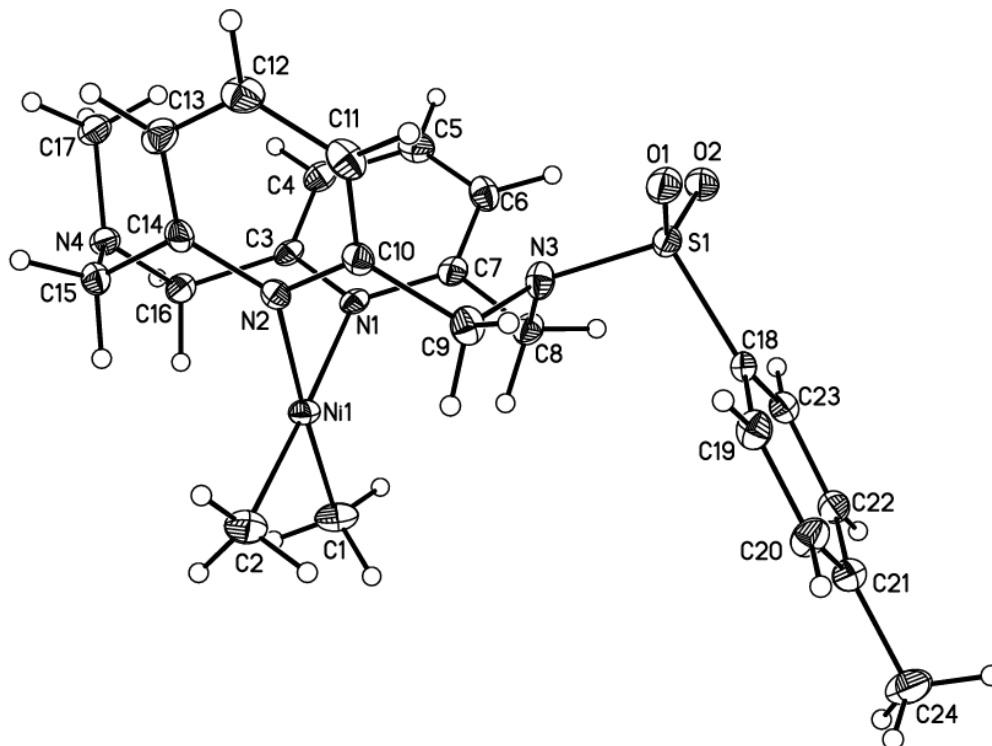


Table G6. Crystal data and structure refinement for 113816_sq. (^{TsMe}N₄)Ni^{III}Me₂⁺

Identification code	113816_sq/lt/x8/SS091616	
Empirical formula	C ₂₄ H ₃₀ F ₆ N ₄ Ni O ₂ S Sb	
Formula weight	733.04	
Temperature	100(2) K	
Wavelength	0.71073 Å	
Crystal system	Monoclinic	
Space group	C2/c	
Unit cell dimensions	a = 55.638(3) Å	α = 90°.
	b = 11.9611(7) Å	β = 100.254(3)°.
	c = 19.3634(10) Å	γ = 90°.
Volume	12680.5(12) Å ³	
Z	16	
Density (calculated)	1.536 Mg/m ³	
Absorption coefficient	1.573 mm ⁻¹	
F(000)	5872	
Crystal size	0.399 x 0.397 x 0.179 mm ³	
Theta range for data collection	1.743 to 26.519°.	
Index ranges	-69 ≤ h ≤ 69, -15 ≤ k ≤ 14, -24 ≤ l ≤ 21	
Reflections collected	63655	
Independent reflections	12987 [R(int) = 0.0611]	
Completeness to theta = 25.242°	99.6 %	
Absorption correction	Semi-empirical from equivalents	
Max. and min. transmission	0.6465 and 0.5415	
Refinement method	Full-matrix least-squares on F ²	
Data / restraints / parameters	12987 / 877 / 591	
Goodness-of-fit on F ²	1.228	
Final R indices [I > 2σ(I)]	R1 = 0.1342, wR2 = 0.3048	
R indices (all data)	R1 = 0.1522, wR2 = 0.3144	
Largest diff. peak and hole	3.302 and -2.518 e.Å ⁻³	

Table G7. Select bond lengths [\AA] and angles [$^\circ$] for 113816_sq.

Ni(1)-C(1)	1.956(13)
Ni(1)-C(2)	1.967(13)
Ni(1)-N(2)	1.983(12)
Ni(1)-N(1)	2.029(10)
Ni(1)-N(3)	2.154(11)

C(1)-Ni(1)-C(2)	86.0(6)
C(1)-Ni(1)-N(2)	93.3(5)
C(2)-Ni(1)-N(2)	177.1(6)
C(1)-Ni(1)-N(1)	176.1(5)
C(2)-Ni(1)-N(1)	97.4(5)
N(2)-Ni(1)-N(1)	83.2(4)
C(1)-Ni(1)-N(3)	98.3(5)
C(2)-Ni(1)-N(3)	99.5(5)
N(2)-Ni(1)-N(3)	83.4(5)
N(1)-Ni(1)-N(3)	83.1(4)

Projection view with 30% probability ellipsoids- H atoms omitted for clarity:

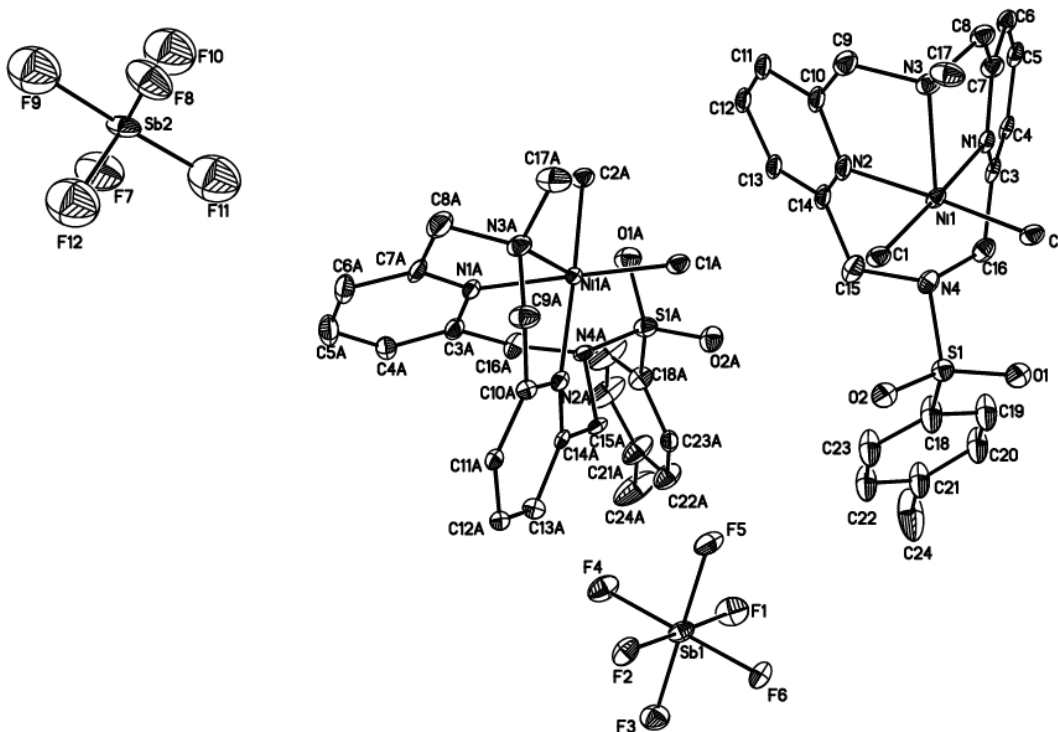


Table G8. Crystal data and structure refinement for Im9017. $(\text{TsMeN}_4)\text{Ni}^{\text{III}}(\text{cycloneophyl})^+$

Identification code	I9017/lt/SMS_TsMeN4Ni(Neophyl)_ThBF4	
Empirical formula	C32 H36 B F4 N4 Ni O2 S	
Formula weight	686.23	
Temperature	143(2) K	
Wavelength	0.71073 Å	
Crystal system	Monoclinic	
Space group	P2 ₁ /c	
Unit cell dimensions	a = 21.2777(18) Å	$\alpha = 90^\circ$.
	b = 8.9357(7) Å	$\beta = 112.115(4)^\circ$.
	c = 17.3493(15) Å	$\gamma = 90^\circ$.
Volume	3056.0(4) Å ³	
Z	4	
Density (calculated)	1.492 Mg/m ³	
Absorption coefficient	0.766 mm ⁻¹	
F(000)	1428	
Crystal size	0.593 x 0.251 x 0.104 mm ³	
Theta range for data collection	2.066 to 25.770°.	
Index ranges	-25 ≤ h ≤ 25, -10 ≤ k ≤ 10, -21 ≤ l ≤ 11	
Reflections collected	22586	
Independent reflections	5805 [R(int) = 0.0689]	
Completeness to theta = 25.242°	99.8 %	
Absorption correction	Semi-empirical from equivalents	
Max. and min. transmission	0.7453 and 0.6336	
Refinement method	Full-matrix least-squares on F ²	
Data / restraints / parameters	5805 / 183 / 513	
Goodness-of-fit on F ²	1.013	
Final R indices [I > 2σ(I)]	R1 = 0.0598, wR2 = 0.1125	
R indices (all data)	R1 = 0.1351, wR2 = 0.1415	
Largest diff. peak and hole	0.657 and -0.497 e.Å ⁻³	

Table G9. Select bond lengths [\AA] and angles [$^\circ$] for lm9017.

Ni(1)-N(2)	1.867(4)
Ni(1)-C(1)	1.938(9)
Ni(1)-C(4)	1.938(4)
Ni(1)-N(1)	2.182(5)
Ni(1)-N(3)	2.199(4)
Ni(1')-N(1)	1.683(5)
Ni(1')-C(4')	1.925(6)
Ni(1')-C(1')	1.947(12)
Ni(1')-N(3)	2.126(4)
Ni(1')-N(2)	2.217(5)
N(2)-Ni(1)-C(1)	93.7(3)
N(2)-Ni(1)-C(4)	175.0(2)
C(1)-Ni(1)-C(4)	82.2(3)
N(2)-Ni(1)-N(1)	82.71(15)
C(1)-Ni(1)-N(1)	175.6(3)
C(4)-Ni(1)-N(1)	101.3(2)
N(2)-Ni(1)-N(3)	81.54(16)
C(1)-Ni(1)-N(3)	105.0(3)
C(4)-Ni(1)-N(3)	102.2(2)
N(1)-Ni(1)-N(3)	77.08(17)
N(1)-Ni(1')-C(4')	170.4(3)
N(1)-Ni(1')-C(1')	91.5(4)
C(4')-Ni(1')-C(1')	81.5(4)
N(1)-Ni(1')-N(3)	90.8(2)
C(4')-Ni(1')-N(3)	97.5(3)
C(1')-Ni(1')-N(3)	107.0(4)
N(1)-Ni(1')-N(2)	85.90(17)
C(4')-Ni(1')-N(2)	100.7(3)
C(1')-Ni(1')-N(2)	176.3(4)
N(3)-Ni(1')-N(2)	75.75(16)

Projection view with 50% probability ellipsoids- disorder components omitted for clarity:

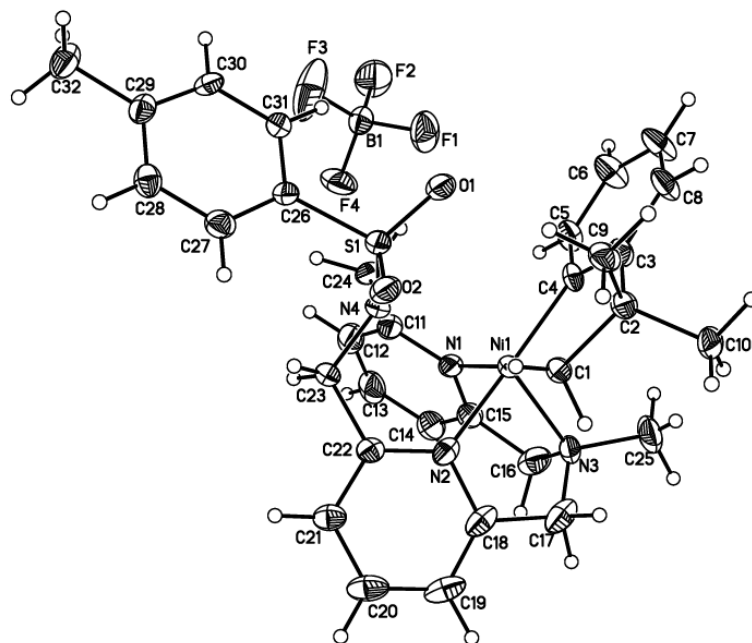


Table G10. Crystal data and structure refinement for lm11317. $(\text{TsMeN}_4)\text{Ni}^{\text{II}}(\text{MeCN})_2^{2+}$

Identification code	111317/lt/x8/SMS_TsMeN4Ni(Neophyl)_ThBF4	
Empirical formula	$\text{C}_{78} \text{H}_{94} \text{B}_6 \text{F}_{24} \text{N}_{18} \text{Ni}_3 \text{O}_8 \text{S}_3$	
Formula weight	2204.88	
Temperature	100(2) K	
Wavelength	0.71073 Å	
Crystal system	Orthorhombic	
Space group	Pnma	
Unit cell dimensions	$a = 12.4340(16) \text{ \AA}$	$\alpha = 90^\circ$.
	$b = 50.615(6) \text{ \AA}$	$\beta = 90^\circ$.
	$c = 15.0313(18) \text{ \AA}$	$\gamma = 90^\circ$.
Volume	9460(2) Å ³	
Z	4	
Density (calculated)	1.548 Mg/m ³	
Absorption coefficient	0.767 mm ⁻¹	
F(000)	4520	
Crystal size	0.288 x 0.228 x 0.169 mm ³	
Theta range for data collection	0.805 to 24.999°.	
Index ranges	-13 ≤ h ≤ 11, -60 ≤ k ≤ 58, -16 ≤ l ≤ 17	
Reflections collected	49988	
Independent reflections	7567 [R(int) = 0.305]	
Completeness to theta = 24.999°	89.7 %	
Absorption correction	Semi-empirical from equivalents	
Max. and min. transmission	0.8620 and 0.5919	
Refinement method	Full-matrix least-squares on F ²	
Data / restraints / parameters	7567 / 713 / 633	
Goodness-of-fit on F ²	0.850	
Final R indices [I > 2σ(I)]	R1 = 0.1034, wR2 = 0.2388	
R indices (all data)	R1 = 0.3772, wR2 = 0.3090	
Largest diff. peak and hole	0.972 and -0.616 e.Å ⁻³	

Table G11. Select bond lengths [\AA] and angles [$^\circ$] for Im11317.

Ni(1)-N(1)	1.991(12)
Ni(1)-N(6)	2.000(15)
Ni(1)-N(2)	2.035(13)
Ni(1)-N(5)	2.070(12)
Ni(1)-N(4)	2.093(13)
Ni(1)-N(3)	2.335(13)

N(1)-Ni(1)-N(6)	91.0(5)
N(1)-Ni(1)-N(2)	84.1(5)
N(6)-Ni(1)-N(2)	174.6(5)
N(1)-Ni(1)-N(5)	173.3(5)
N(6)-Ni(1)-N(5)	93.4(5)
N(2)-Ni(1)-N(5)	91.4(5)
N(1)-Ni(1)-N(4)	82.3(5)
N(6)-Ni(1)-N(4)	98.8(6)
N(2)-Ni(1)-N(4)	82.6(6)
N(5)-Ni(1)-N(4)	102.0(5)
N(1)-Ni(1)-N(3)	78.6(5)
N(6)-Ni(1)-N(3)	100.2(5)
N(2)-Ni(1)-N(3)	76.8(5)
N(5)-Ni(1)-N(3)	95.6(5)
N(4)-Ni(1)-N(3)	153.2(5)

Projection view with 50% probability ellipsoids- Only one of the Ni complexes shown for clarity:

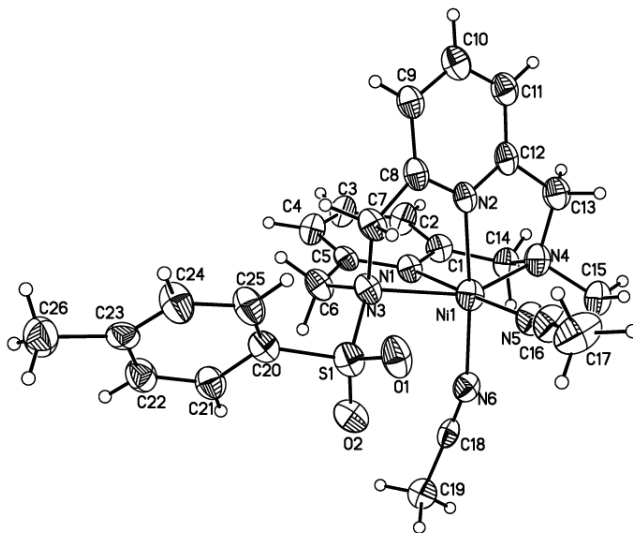


Table G12. Crystal data and structure refinement for lm2216. (^{Ts}N₄)Ni^{II}(acac)⁺

Identification code	l2216/lt/smart/SS020216-2	
Empirical formula	C ₃₄ H ₃₇ Cl ₂ N ₅ Ni O ₉ S ₂	
Formula weight	853.41	
Temperature	100(2) K	
Wavelength	0.71073 Å	
Crystal system	Monoclinic	
Space group	P2 ₁ /c	
Unit cell dimensions	a = 12.906(3) Å	α = 90°.
	b = 27.206(5) Å	β = 101.139(11)°.
	c = 10.785(2) Å	γ = 90°.
Volume	3715.5(12) Å ³	
Z	4	
Density (calculated)	1.526 Mg/m ³	
Absorption coefficient	0.839 mm ⁻¹	
F(000)	1768	
Crystal size	0.251 x 0.192 x 0.104 mm ³	
Theta range for data collection	1.497 to 27.588°.	
Index ranges	-15 ≤ h ≤ 16, -35 ≤ k ≤ 35, -13 ≤ l ≤ 13	
Reflections collected	47146	
Independent reflections	8521 [R(int) = 0.0544]	
Completeness to theta = 25.242°	100.0 %	
Absorption correction	Semi-empirical from equivalents	
Max. and min. transmission	0.8621 and 0.7900	
Refinement method	Full-matrix least-squares on F ²	
Data / restraints / parameters	8521 / 15 / 496	
Goodness-of-fit on F ²	1.028	
Final R indices [I > 2σ(I)]	R1 = 0.0418, wR2 = 0.0987	
R indices (all data)	R1 = 0.0569, wR2 = 0.1077	
Largest diff. peak and hole	0.602 and -0.441 e.Å ⁻³	

Table G13. Select bond lengths [Å] and angles [°] for Im2216.

Ni(1)-O(1)	1.9702(16)
Ni(1)-O(2)	1.9749(16)
Ni(1)-N(2)	2.0031(19)
Ni(1)-N(1)	2.0267(19)
Ni(1)-N(4)	2.307(2)
Ni(1)-N(3)	2.3427(18)

O(1)-Ni(1)-O(2)	92.90(7)
O(1)-Ni(1)-N(2)	175.46(7)
O(2)-Ni(1)-N(2)	89.57(7)
O(1)-Ni(1)-N(1)	92.59(7)
O(2)-Ni(1)-N(1)	173.46(7)
N(2)-Ni(1)-N(1)	85.19(8)
O(1)-Ni(1)-N(4)	96.55(7)
O(2)-Ni(1)-N(4)	105.08(7)
N(2)-Ni(1)-N(4)	79.12(7)
N(1)-Ni(1)-N(4)	77.80(7)
O(1)-Ni(1)-N(3)	106.39(7)
O(2)-Ni(1)-N(3)	97.06(7)
N(2)-Ni(1)-N(3)	77.05(7)
N(1)-Ni(1)-N(3)	77.96(7)
N(4)-Ni(1)-N(3)	147.15(7)

Projection view with 50% probability ellipsoids- disorder components omitted for clarity:

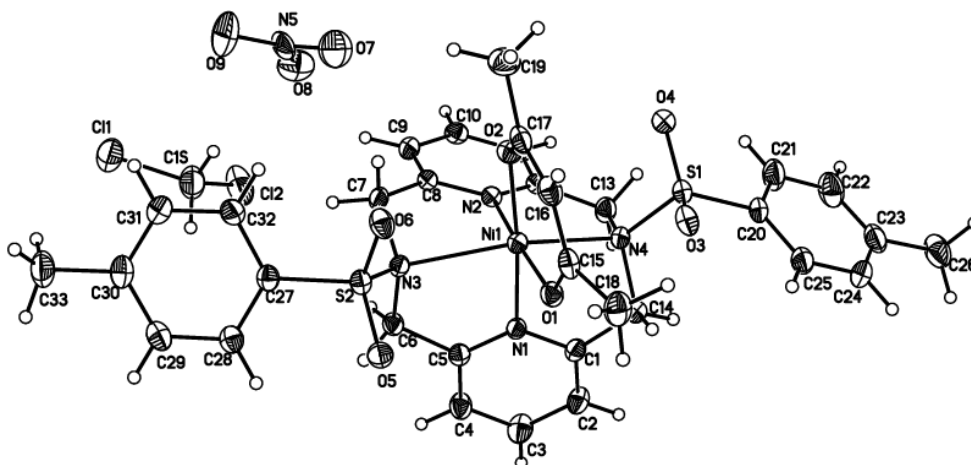


Table G14. Crystal data and structure refinement for lm1016. (^{Ts}N₄)Ni^{II}Me₂

Identification code	11016 /lt/X8/SS011916	
Empirical formula	C ₃₄ H ₄₄ N ₄ Ni O ₅ S ₂	
Formula weight	711.56	
Temperature	100(2) K	
Wavelength	0.71073 Å	
Crystal system	Orthorhombic	
Space group	C222 ₁	
Unit cell dimensions	a = 14.1011(16) Å	α = 90°.
	b = 14.7572(15) Å	β = 90°.
	c = 34.330(4) Å	γ = 90°.
Volume	7143.7(14) Å ³	
Z	8	
Density (calculated)	1.323 Mg/m ³	
Absorption coefficient	0.705 mm ⁻¹	
F(000)	3008	
Crystal size	0.195 x 0.177 x 0.113 mm ³	
Theta range for data collection	1.998 to 27.208°.	
Index ranges	-18 ≤ h ≤ 18, -18 ≤ k ≤ 18, -43 ≤ l ≤ 44	
Reflections collected	60612	
Independent reflections	7942 [R(int) = 0.085]	
Completeness to theta = 25.242°	100.0 %	
Absorption correction	Semi-empirical from equivalents	
Max. and min. transmission	0.8620 and 0.8185	
Refinement method	Full-matrix least-squares on F ²	
Data / restraints / parameters	7942 / 0 / 422	
Goodness-of-fit on F ²	1.023	
Final R indices [I > 2σ(I)]	R1 = 0.0411, wR2 = 0.0838	
R indices (all data)	R1 = 0.0662, wR2 = 0.0933	
Absolute structure parameter	-0.005(10)	
Largest diff. peak and hole	0.507 and -0.300 e.Å ⁻³	

Table G15. Select bond lengths [\AA] and angles [$^\circ$] for *lm1016*.

Ni(1)-C(8)	1.929(4)
Ni(1)-C(8)#1	1.929(4)
Ni(1)-N(1)	1.974(3)
Ni(1)-N(1)#1	1.974(3)
C(8)-Ni(1)-C(8)#1	87.3(2)
C(8)-Ni(1)-N(1)	177.0(3)
C(8)#1-Ni(1)-N(1)	93.24(13)
C(8)-Ni(1)-N(1)#1	93.24(13)
C(8)#1-Ni(1)-N(1)#1	177.0(3)
N(1)-Ni(1)-N(1)#1	86.35(16)

Projection view with 50% probability ellipsoids- H atoms omitted for clarity:

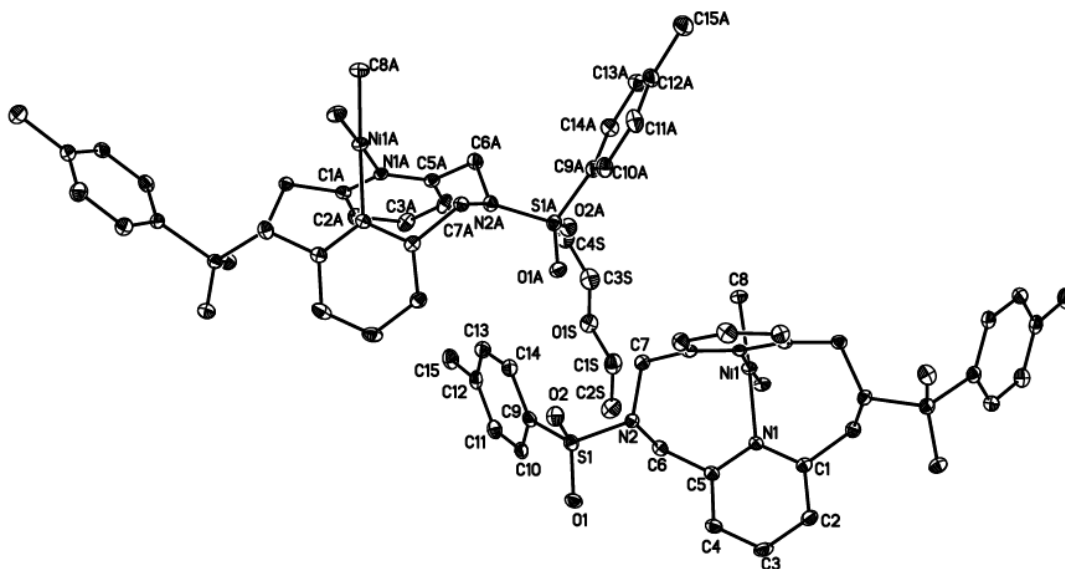


Table G16. Crystal data and structure refinement for 115316_sq. (^{Ts}N₄)Ni^{III}(OH)(H₂O)²⁺

Identification code	115316_sq/lt/x8/SS101816	
Empirical formula	C ₂₈ H ₃₁ F ₁₂ N ₄ Ni O ₆ S ₂ Sb ₂	
Formula weight	1113.90	
Temperature	100(2) K	
Wavelength	0.71073 Å	
Crystal system	Monoclinic	
Space group	P2 ₁ /n	
Unit cell dimensions	a = 13.982(8) Å	α = 90°.
	b = 28.040(16) Å	β = 111.763(16)°.
	c = 17.052(13) Å	γ = 90°.
Volume	6209(7) Å ³	
Z	4	
Density (calculated)	1.192 Mg/m ³	
Absorption coefficient	1.295 mm ⁻¹	
F(000)	2180	
Crystal size	0.346 x 0.275 x 0.258 mm ³	
Theta range for data collection	1.477 to 25.000°.	
Index ranges	-16 ≤ h ≤ 16, -33 ≤ k ≤ 33, -20 ≤ l ≤ 12	
Reflections collected	51162	
Independent reflections	10931 [R(int) = 0.311]	
Completeness to theta = 25.000°	99.9 %	
Absorption correction	Semi-empirical from equivalents	
Max. and min. transmission	0.8620 and 0.6061	
Refinement method	Full-matrix least-squares on F ²	
Data / restraints / parameters	10931 / 695 / 450	
Goodness-of-fit on F ²	1.278	
Final R indices [I > 2σ(I)]	R1 = 0.1702, wR2 = 0.4256	
R indices (all data)	R1 = 0.3306, wR2 = 0.5026	
Largest diff. peak and hole	1.710 and -1.172 e.Å ⁻³	

Table G17. Select bond lengths [Å] and angles [°] for I15316_sq.

Ni(1)-N(1)	1.908(12)
Ni(1)-O(2)	1.977(17)
Ni(1)-N(2)	2.03(2)
Ni(1)-O(1)	2.081(16)
Ni(1)-N(3)	2.25(2)
Ni(1)-N(4)	2.29(2)

N(1)-Ni(1)-O(2)	178.0(7)
N(1)-Ni(1)-N(2)	82.6(7)
O(2)-Ni(1)-N(2)	96.1(8)
N(1)-Ni(1)-O(1)	92.3(7)
O(2)-Ni(1)-O(1)	88.9(7)
N(2)-Ni(1)-O(1)	174.0(8)
N(1)-Ni(1)-N(3)	81.2(7)
O(2)-Ni(1)-N(3)	100.2(7)
N(2)-Ni(1)-N(3)	81.6(8)
O(1)-Ni(1)-N(3)	100.8(7)
N(1)-Ni(1)-N(4)	80.3(7)
O(2)-Ni(1)-N(4)	97.9(7)
N(2)-Ni(1)-N(4)	77.7(8)
O(1)-Ni(1)-N(4)	98.3(7)
N(3)-Ni(1)-N(4)	153.7(7)

Projection view with 50% probability ellipsoids:

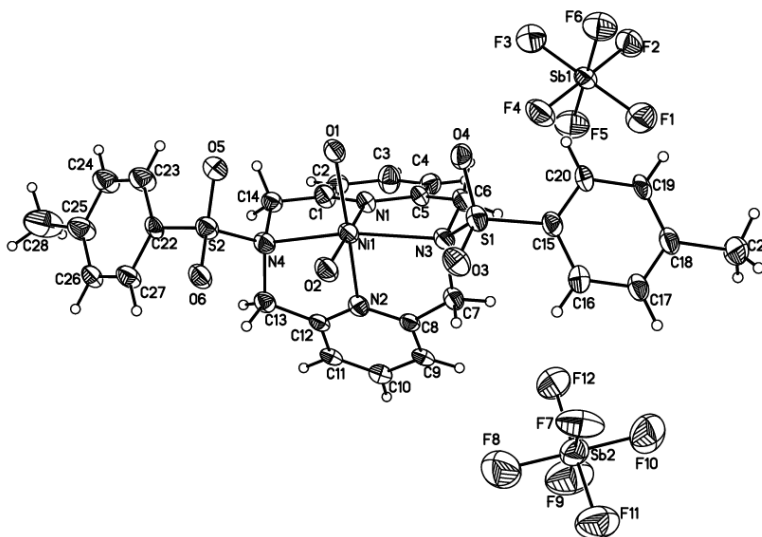


Table G18. Crystal data and structure refinement for lm8417. $(\text{TsN}_4)\text{Ni}^{\text{III}}(\text{cycloneophyl})^+$

Identification code	l8417/lt/x8/SMS_Ts2N4NiMe2-AgSbF6	
Empirical formula	C42 H46 F6 N6 Ni O4 S2 Sb	
Formula weight	1057.43	
Temperature	173(2) K	
Wavelength	0.71073 Å	
Crystal system	Monoclinic	
Space group	P2 ₁ /c	
Unit cell dimensions	a = 13.5650(6) Å	$\alpha = 90^\circ$.
	b = 16.4096(7) Å	$\beta = 93.577(2)^\circ$.
	c = 19.6099(10) Å	$\gamma = 90^\circ$.
Volume	4356.6(3) Å ³	
Z	4	
Density (calculated)	1.612 Mg/m ³	
Absorption coefficient	1.223 mm ⁻¹	
F(000)	2148	
Crystal size	0.444 x 0.247 x 0.219 mm ³	
Theta range for data collection	1.504 to 27.568°.	
Index ranges	-16 ≤ h ≤ 17, -21 ≤ k ≤ 21, -25 ≤ l ≤ 25	
Reflections collected	58394	
Independent reflections	10068 [R(int) = 0.0604]	
Completeness to theta = 25.242°	100.0 %	
Absorption correction	Semi-empirical from equivalents	
Max. and min. transmission	0.7041 and 0.6356	
Refinement method	Full-matrix least-squares on F ²	
Data / restraints / parameters	10068 / 162 / 596	
Goodness-of-fit on F ²	1.318	
Final R indices [I > 2σ(I)]	R1 = 0.0489, wR2 = 0.1138	
R indices (all data)	R1 = 0.0814, wR2 = 0.1262	
Largest diff. peak and hole	1.565 and -1.358 e.Å ⁻³	

Table G19. Select bond lengths [Å] and angles [°] for Im8417.

Ni(1)-C(1)	1.933(3)
Ni(1)-C(8)	1.982(3)
Ni(1)-N(1)	1.993(3)
Ni(1)-N(2)	2.010(3)
Ni(1)-N(3)	2.360(3)
Ni(1)-N(4)	2.436(3)

C(1)-Ni(1)-C(8)	80.86(14)
C(1)-Ni(1)-N(1)	174.20(12)
C(8)-Ni(1)-N(1)	93.35(12)
C(1)-Ni(1)-N(2)	99.71(13)
C(8)-Ni(1)-N(2)	179.42(13)
N(1)-Ni(1)-N(2)	86.08(11)
C(1)-Ni(1)-N(3)	105.67(12)
C(8)-Ni(1)-N(3)	101.66(12)
N(1)-Ni(1)-N(3)	75.73(10)
N(2)-Ni(1)-N(3)	78.29(10)
C(1)-Ni(1)-N(4)	102.89(12)
C(8)-Ni(1)-N(4)	105.30(12)
N(1)-Ni(1)-N(4)	78.20(10)
N(2)-Ni(1)-N(4)	74.50(10)
N(3)-Ni(1)-N(4)	143.25(9)

Projection view with 50% probability ellipsoids- disorder components of the anion omitted for clarity:

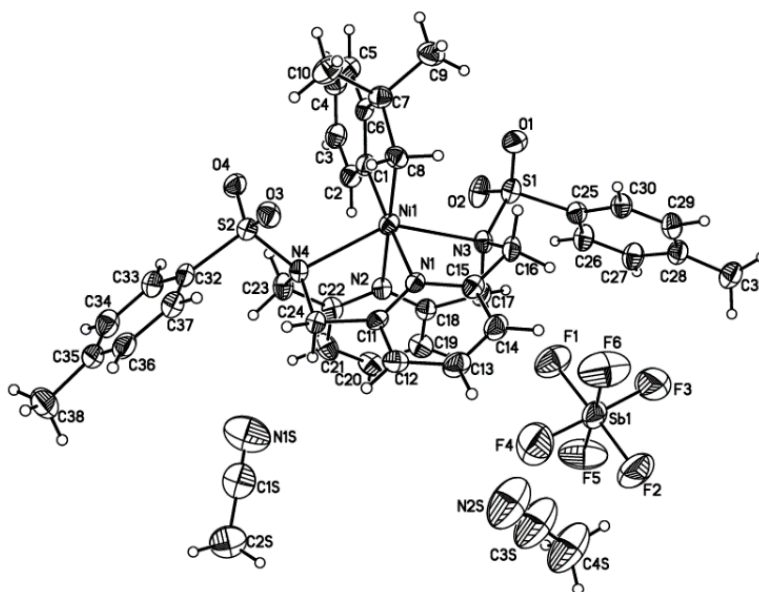


Table G20. Crystal data and structure refinement for lm2418. (^{tBu}N₄)Ni^{II}(cycloneophyl)

Identification code	l2418/lt/x8/3SMS117	
Empirical formula	C ₃₂ H ₄₄ N ₄ Ni	
Formula weight	543.42	
Temperature	100(2) K	
Wavelength	0.71073 Å	
Crystal system	Monoclinic	
Space group	P2 ₁ /c	
Unit cell dimensions	a = 9.4391(6) Å	α = 90°.
	b = 23.9058(13) Å	β = 92.174(4)°.
	c = 12.7167(8) Å	γ = 90°.
Volume	2867.4(3) Å ³	
Z	4	
Density (calculated)	1.259 Mg/m ³	
Absorption coefficient	0.704 mm ⁻¹	
F(000)	1168	
Crystal size	0.377 x 0.249 x 0.162 mm ³	
Theta range for data collection	1.704 to 30.631°.	
Index ranges	-12 ≤ h ≤ 13, -34 ≤ k ≤ 34, -14 ≤ l ≤ 18	
Reflections collected	49624	
Independent reflections	8789 [R(int) = 0.086]	
Completeness to theta = 25.242°	100.0 %	
Absorption correction	Semi-empirical from equivalents	
Max. and min. transmission	0.8253 and 0.7156	
Refinement method	Full-matrix least-squares on F ²	
Data / restraints / parameters	8789 / 0 / 342	
Goodness-of-fit on F ²	1.037	
Final R indices [I > 2σ(I)]	R1 = 0.0603, wR2 = 0.1255	
R indices (all data)	R1 = 0.1170, wR2 = 0.1477	
Largest diff. peak and hole	1.811 and -0.908 e.Å ⁻³	

Table G21. Select bond lengths [\AA] and angles [$^\circ$] for Im2418.

Ni(1)-C(1)	1.887(3)
Ni(1)-C(8)	1.938(3)
Ni(1)-N(1)	1.944(3)
Ni(1)-N(2)	1.976(2)

C(1)-Ni(1)-C(8)	82.44(12)
C(1)-Ni(1)-N(1)	173.36(10)
C(8)-Ni(1)-N(1)	91.31(11)
C(1)-Ni(1)-N(2)	98.51(11)
C(8)-Ni(1)-N(2)	179.05(12)
N(1)-Ni(1)-N(2)	87.74(9)

Projection view with 50% probability ellipsoids:

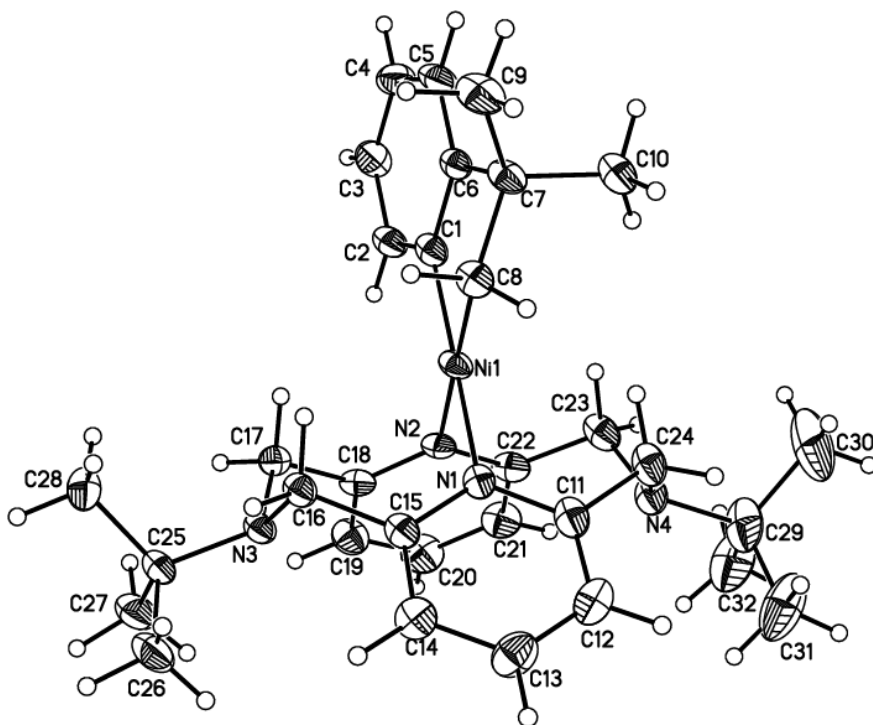


Table G22. Crystal data and structure refinement for lm15218. (ⁱPrMe₂TACN)Ni^{II}(cycloneophyl)

Identification code	115218/lt/x8/4SMS143-(yellow cryst)	
Empirical formula	C ₅₀ H ₉₀ N ₆ Ni ₂ O ₂	
Formula weight	924.69	
Temperature	100(2) K	
Wavelength	0.71073 Å	
Crystal system	Monoclinic	
Space group	P2 ₁ /c	
Unit cell dimensions	a = 26.171(3) Å	α = 90°.
	b = 10.6806(11) Å	β = 111.240(2)°.
	c = 19.0624(17) Å	γ = 90°.
Volume	4966.4(8) Å ³	
Z	4	
Density (calculated)	1.237 Mg/m ³	
Absorption coefficient	0.802 mm ⁻¹	
F(000)	2016	
Crystal size	0.371 x 0.233 x 0.186 mm ³	
Theta range for data collection	1.670 to 29.157°.	
Index ranges	-21 ≤ h ≤ 35, -14 ≤ k ≤ 14, -26 ≤ l ≤ 18	
Reflections collected	49178	
Independent reflections	13374 [R(int) = 0.106]	
Completeness to theta = 25.242°	99.9 %	
Absorption correction	Semi-empirical from equivalents	
Max. and min. transmission	0.8016 and 0.6840	
Refinement method	Full-matrix least-squares on F ²	
Data / restraints / parameters	13374 / 18 / 551	
Goodness-of-fit on F ²	0.982	
Final R indices [I > 2σ(I)]	R1 = 0.0574, wR2 = 0.1254	
R indices (all data)	R1 = 0.1112, wR2 = 0.1491	
Largest diff. peak and hole	0.912 and -0.969 e.Å ⁻³	

Table G23. Select bond lengths [Å] and angles [°] for Im15218.

Ni(1)-C(1)	1.909(3)
Ni(1)-C(8)	1.935(3)
Ni(1)-N(1)	2.052(2)
Ni(1)-N(2)	2.055(2)

C(1)-Ni(1)-C(8)	81.20(12)
C(1)-Ni(1)-N(1)	99.27(11)
C(8)-Ni(1)-N(1)	176.32(11)
C(1)-Ni(1)-N(2)	174.49(11)
C(8)-Ni(1)-N(2)	94.86(10)
N(1)-Ni(1)-N(2)	84.90(9)
C(17)-N(1)-C(16)	105.8(2)
C(17)-N(1)-C(11)	109.4(2)
C(16)-N(1)-C(11)	110.8(2)
C(17)-N(1)-Ni(1)	114.77(17)
C(16)-N(1)-Ni(1)	102.93(16)
C(11)-N(1)-Ni(1)	112.81(17)

Projection view with 50% probability ellipsoids- H atoms and disordered solvent components omitted for clarity:

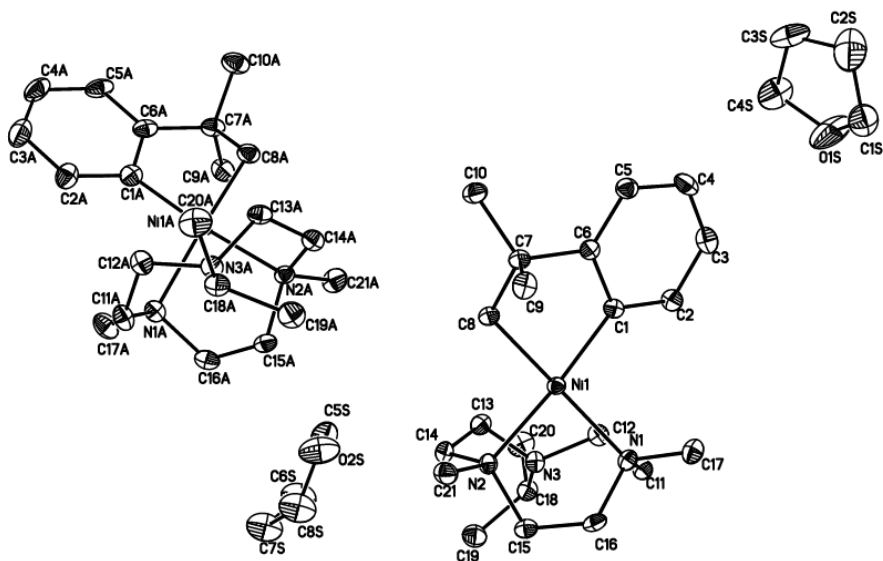


Table G24. Crystal data and structure refinement for 13118t5. (^{TsMe2}TACN)Ni^{II}(cycloneophyl)

Identification code	13118t5/lt/x8/3SMS116	
Empirical formula	C ₅₄ H ₈₂ N ₆ Ni ₂ O ₅ S ₂	
Formula weight	1076.79	
Temperature	100(2) K	
Wavelength	0.71073 Å	
Crystal system	Triclinic	
Space group	P-1	
Unit cell dimensions	a = 12.853(8) Å	α = 100.867(15)°.
	b = 14.259(9) Å	β = 97.294(16)°.
	c = 16.666(11) Å	γ = 111.946(16)°.
Volume	2716(3) Å ³	
Z	2	
Density (calculated)	1.317 Mg/m ³	
Absorption coefficient	0.821 mm ⁻¹	
F(000)	1152	
Crystal size	0.287 x 0.119 x 0.096 mm ³	
Theta range for data collection	1.593 to 24.999°.	
Index ranges	-15 ≤ h ≤ 15, -16 ≤ k ≤ 16, 0 ≤ l ≤ 19	
Reflections collected	10505	
Independent reflections	10505 [R(int) = 0.12]	
Completeness to theta = 24.999°	96.9 %	
Absorption correction	Semi-empirical from equivalents	
Max. and min. transmission	0.83707 and 0.49355	
Refinement method	Full-matrix least-squares on F ²	
Data / restraints / parameters	10505 / 607 / 531	
Goodness-of-fit on F ²	1.072	
Final R indices [I > 2σ(I)]	R1 = 0.0929, wR2 = 0.1938	
R indices (all data)	R1 = 0.1992, wR2 = 0.2377	
Largest diff. peak and hole	1.171 and -0.923 e.Å ⁻³	

Table G25. Select bond lengths [\AA] and angles [$^\circ$] for I3118t5.

Ni(1)-C(1)	1.920(13)
Ni(1)-C(8)	1.944(12)
Ni(1)-N(2)	2.075(10)
Ni(1)-N(1)	2.077(10)

C(1)-Ni(1)-C(8)	81.3(5)
C(1)-Ni(1)-N(2)	175.1(5)
C(8)-Ni(1)-N(2)	93.8(5)
C(1)-Ni(1)-N(1)	99.9(5)
C(8)-Ni(1)-N(1)	175.4(5)
N(2)-Ni(1)-N(1)	85.0(4)

Projection view with 50% probability ellipsoids: one of the two unique molecules and solvent THF omitted for clarity:

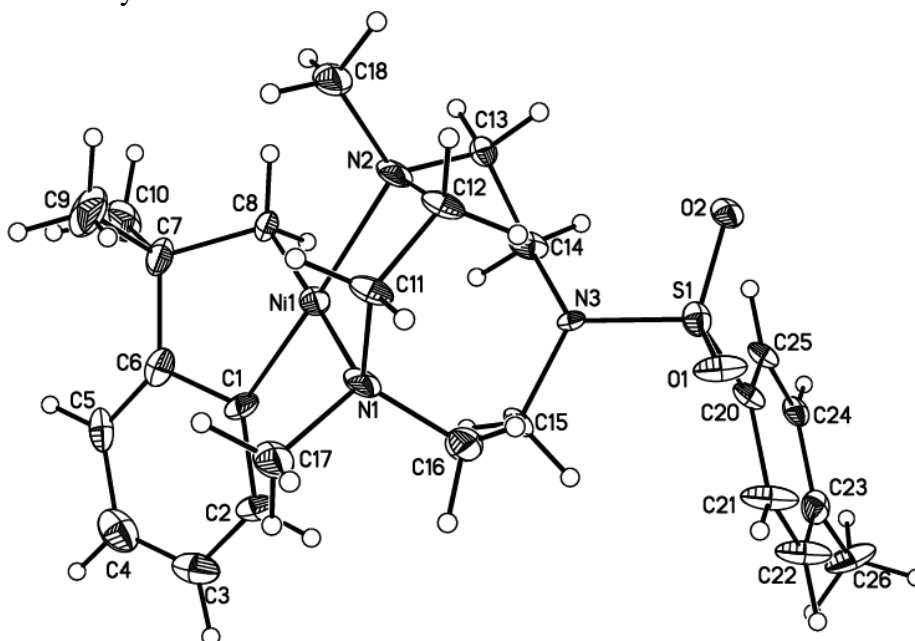


Table G26. Crystal data and structure refinement for $\text{Im20417} \cdot (\text{Me}_4\text{N})\text{Ni}^{\text{II}}(\text{MeCN})_2^{2+}$

Identification code	I20417/It/x8/3SMS92	
Empirical formula	$\text{C}_{137} \text{H}_{138} \text{B}_4 \text{N}_{12} \text{Ni}_2 \text{O}_2$	
Formula weight	2145.25	
Temperature	100(2) K	
Wavelength	0.71073 Å	
Crystal system	Monoclinic	
Space group	P2 ₁ /c	
Unit cell dimensions	$a = 17.7048(10) \text{ Å}$	$\alpha = 90^\circ$.
	$b = 17.7252(10) \text{ Å}$	$\beta = 91.858(3)^\circ$.
	$c = 17.7287(10) \text{ Å}$	$\gamma = 90^\circ$.
Volume	5560.7(5) Å ³	
Z	2	
Density (calculated)	1.281 Mg/m ³	
Absorption coefficient	0.400 mm ⁻¹	
F(000)	2272	
Crystal size	0.384 x 0.228 x 0.169 mm ³	
Theta range for data collection	1.970 to 27.581°.	
Index ranges	$-23 \leq h \leq 23, -23 \leq k \leq 18, -23 \leq l \leq 23$	
Reflections collected	54965	
Independent reflections	12841 [R(int) = 0.117]	
Completeness to theta = 25.242°	99.9 %	
Absorption correction	Semi-empirical from equivalents	
Max. and min. transmission	0.8621 and 0.8032	
Refinement method	Full-matrix least-squares on F ²	
Data / restraints / parameters	12841 / 2 / 713	
Goodness-of-fit on F ²	1.404	
Final R indices [I > 2σ(I)]	R1 = 0.1015, wR2 = 0.2487	
R indices (all data)	R1 = 0.1909, wR2 = 0.2895	
Largest diff. peak and hole	3.540 and -1.833 e.Å ⁻³	

Table G27. Select bond lengths [\AA] and angles [$^\circ$] for Im20417.

Ni(1)-N(2)	1.983(4)
Ni(1)-N(6)	2.010(7)
Ni(1)-N(1)	2.014(5)
Ni(1)-N(5)	2.041(4)
Ni(1)-N(4)	2.142(5)
Ni(1)-N(3)	2.174(4)
N(2)-Ni(1)-N(6)	93.7(2)
N(2)-Ni(1)-N(1)	84.53(17)
N(6)-Ni(1)-N(1)	177.9(2)
N(2)-Ni(1)-N(5)	178.85(18)
N(6)-Ni(1)-N(5)	86.9(2)
N(1)-Ni(1)-N(5)	94.82(17)
N(2)-Ni(1)-N(4)	82.10(17)
N(6)-Ni(1)-N(4)	97.1(3)
N(1)-Ni(1)-N(4)	81.54(18)
N(5)-Ni(1)-N(4)	98.75(18)
N(2)-Ni(1)-N(3)	82.01(17)
N(6)-Ni(1)-N(3)	99.1(3)
N(1)-Ni(1)-N(3)	81.87(18)
N(5)-Ni(1)-N(3)	96.96(17)
N(4)-Ni(1)-N(3)	157.99(18)

Projection view with 50% probability ellipsoids- solvents omitted for clarity:

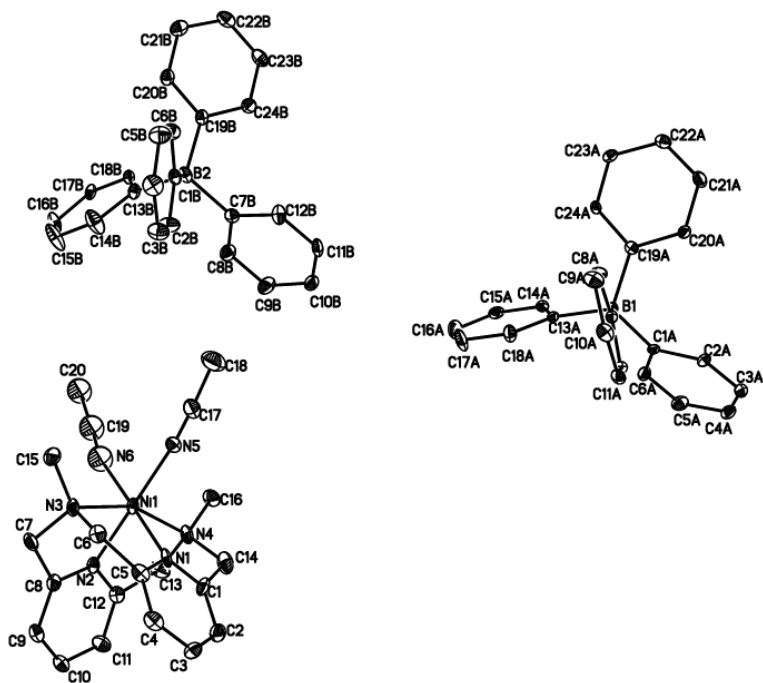


Table G28. Crystal data and structure refinement for (^{iPr}3TACN)Ni^{II}(cycloneophyl).

Identification code	iPrTACNNiCycloneophyl	
Empirical formula	C ₂₅ H ₄₅ N ₃ Ni	
Formula weight	446.35	
Temperature	100(2) K	
Crystal system	monoclinic	
Space group	C2/c	
Unit cell dimensions	a = 17.8116(5) Å	α = 90°.
	b = 15.0289(4) Å	β = 113.6290(10)°.
	c = 19.3936(7) Å	γ = 90°.
Volume	4756.3(3) Å ³	
Z	8	
Density (calculated)	1.247 Mg/m ³	
Absorption coefficient	0.832 mm ⁻¹	
F(000)	1952	
Crystal size	0.417 x 0.16 x 0.06 mm ³	
Radiation	MoKα (λ = 0.71073)	
Theta range for data collection	4.84 to 54.242°.	
Index ranges	-22 ≤ h ≤ 22, -19 ≤ k ≤ 19, -24 ≤ l ≤ 24	
Reflections collected	32600	
Independent reflections	5237 [R _{int} = 0.0512, R _{sigma} = 0.0314]	
Data / restraints / parameters	5237/0/270	
Goodness-of-fit on F ²	1.047	
Final R indices [I > 2σ(I)]	R1 = 0.0315, wR2 = 0.0769	
R indices (all data)	R1 = 0.0373, wR2 = 0.0798	
Largest diff. peak and hole	0.53 and -0.39 e.Å ⁻³	

Table G29. Select bond lengths [\AA] and angles [$^\circ$] for ($i\text{Pr}^3\text{TACN}$)Ni^{II}(cycloneophyl).

Ni(1)-N(2)	2.0977(13)
Ni(1)-N(1)	2.1019(13)
Ni(1)-C(2)	1.9194(15)
Ni(1)-C(1)	1.9329(15)

N(2)-Ni(1)-N(1)	85.18(5)
C(2)-Ni(1)-N(1)	99.85(6)
C(2)-Ni(1)-N(2)	170.79(6)
C(2)-Ni(1)-N(1)	81.06(6)
C(1)-Ni(1)-N(1)	176.17(6)
C(1)-Ni(1)-N(2)	94.43(6)

SOFIA M. SMITH

Department of Chemistry
Washington University in St. Louis
One Brooking Drive, St. Louis, MO 63130

Phone: +1 (314) 800-8032
Email: smsmith@wustl.edu
www.linkedin.com/in/sofia-m-smith/

PROFESSIONAL SUMMARY

Ph.D. in chemistry with extensive knowledge and experience in organometallic synthesis and characterization. Supervisory experience as senior laboratory safety officer responsible for optimizing safety protocols and conducting safety inspections. Received the WUSTL Chemistry Department Teaching Assistant Award. Diverse leadership experience in university committees and participation in recruitment, onboarding, and mentoring of new students in chemistry. Fluent in English, Dutch and Italian.

EDUCATION

Ph.D. in Chemistry, Washington University in St. Louis, USA *May 2019*
Dissertation: Oxidative C–C and C–heteroatom Reactivity of High-Valent Nickel Complexes.
B.A.Sc. in Chemistry, Rotterdam University of Applied Sciences, NL *2014*

RESEARCH EXPERIENCE

Graduate Research Assistant, Washington University in St. Louis, USA *2014 – May 2019*
Advisor: Professor Liviu M. Mirica

- Discovered and characterized rare high-valent organometallic nickel complexes.
- Explored the oxidative reactivity of organometallic nickel complexes towards C–C and C–heteroatom bond formation.
- Investigated ligand modifications on nickel centers to observe changes in reactivity.
- Performed catalytic oxidation studies on unactivated alkanes using hypohalites as the oxidant.

Internship, Washington University in St. Louis, USA (6 months) *2014*
Advisor: Professor Vladimir B. Birman

- Explored asymmetric catalytic approaches to axially chiral N-aryl-thiazoline-2-thiones.

Internship, SABIC, Bergen op Zoom, NL (6 months) *2012*
Advisors: Dr. Cristian Wold and Dr. Elena Uliyanchenko

- Development and optimization of separation methods for analysis of novel polymeric materials for anti-fog applications. Techniques used include, Size Exclusion Chromatography (SEC), Gradient Polymer Elution Chromatography (GPEC), Two-dimensional Liquid Chromatography (2D LC) and Fourier Transform Infrared (FTIR).

SKILLS AND INTERESTS

Laboratory

- Inorganic and organic synthesis, NMR (^1H , ^{13}C , ^{19}F , 2D), GC-MS, ESI-MS, HPLC, electrochemistry, Electron Paramagnetic Resonance (EPR) spectroscopy and UV-vis.

Programs

- Microsoft Office, OriginLab Graphing and Analysis, Chemdraw, MestReNova, Mercury and POV-Ray.

HONORS AND AWARDS

WUSTL Chemistry Department Teaching Assistant Award *2015*
Lieberman Leadership Award – Trailblazer (WUSTL Ballroom Club) *2018*

LEADERSHIP

Senior Laboratory Safety Officer 2015 – 2019

- Directed regular safety checks and all necessary safety procedures.
- Improved lab safety by creating new organizational methods.
- Trained all new incoming students on the safety regulations required in lab.

Mentor for “Catalysts for Change: Women in STEM” 2014 – 2019

- Catalyst for Change is an outreach program for St. Louis high-school girls, organized by the Women, Gender, and Sexuality Studies (WGSS) Program, the Teaching Center and the Department of Chemistry at Washington University in St. Louis.

Chair, Marcus Lecture Committee 2015 – 2017

- Led the committee organizing the Marcus Lecture Series, with visiting Prof. Richard Eisenberg (2016) and Prof. Jennifer A. Lewis (2017). The Marcus Lecture committee is a student governed lecture series at Washington University in St. Louis.

Teaching Assistant 2014 – 2017

Courses: General Chemistry Laboratory I and II (80 students), General Chemistry I and II (90 students) and Organic Chemistry (60 students) at Washington University in St. Louis.

- Organized recitation sections, covered lecture material, facilitated discussions, graded exams and quizzes in General Chemistry and Organic Chemistry.
- Facilitated POGIL (Process-Oriented Guided Inquiry Learning) sessions designed to teach challenging concepts through social learning styles in General Chemistry.
- Supervised individual General Chemistry Laboratories insuring a safe environment, demonstrating relevant techniques and providing trouble shooting.

Co-president and Treasurer, WUSTL Ballroom Club 2017 – 2019

- Initiated the WUSTL ballroom club in August 2017 at Washington University in St. Louis. Providing ballroom lessons in many styles including Waltz, Tango, Cha Cha and Rumba. Now the club has expanded to approximately 50 members.

PUBLICATIONS

1. **Sofia M. Smith**, Nigam P. Rath, and Liviu M. Mirica* “High-Valent Organometallic Nickel Complexes Relevant to Carbon–Carbon Bond Formation Reactions.” *Organometallics To be submitted*
2. **Sofia M. Smith**, Oriol Planas, Laura Gómez, Nigam P. Rath, Xavi Ribas, and Liviu M. Mirica* “Aerobic C–C and C–O Bond Formation Reactions Mediated by High-Valent Organometallic Nickel Species.” *J. Am. Chem. Soc. To be submitted*
3. **Sofia M. Smith** and Liviu M. Mirica* “Catalytic Oxidation Studies for Unactivated Alkanes Using Hypohalites as the Oxidant.” *To be submitted*
4. **Sofia M. Smith**, Leonel Griego and Liviu M. Mirica* “High-Valent Ni(III/IV) Chemistry.” Book chapter. *To be submitted*

PRESENTATIONS

1. **Sofia. M. Smith**, Nigam P. Rath and Liviu M. Mirica* “Synthesis and Reactivity of Organometallic Ni^{II} and Ni^{III} Compounds”, 30th Missouri Inorganic Day, St. Louis, MO, May 2017. (Oral)
2. **Sofia. M. Smith** and Liviu M. Mirica* “Aerobic C–C and C–O Bond Formation Reactions Mediated by High-Valent Organometallic Nickel(III/IV) Species”, 256th ACS National Meeting & Exposition, Boston, MA, August 2018. (Oral)
3. **Sofia. M. Smith** and Liviu M. Mirica* “Bioinspired Aerobic Oxidation Chemistry using High-Valent Nickel Species” Graduate Research Symposium at Washington University in St. Louis, St. Louis, Missouri, March 2019. (Poster)